Hydrogen Assisted Cracking of High Strength Alloys

Richard P. Gangloff

R.P. Gangloff, "Hydrogen Assisted Cracking of High Strength Alloys", in Comprehensive Structural Integrity, I. Milne, R.O. Ritchie and B. Karihaloo, Editors-in-Chief, J. Petit and P. Scott, Volume Editors, Vol. 6, Elsevier Science, New York, NY, pp. 31-101 (2003).

HYDROGEN ASSISTED CRACKING OF HIGH STRENGTH ALLOYS

Richard P. Gangloff

6.03.1 INTRODUCTION

6.03.2 HYDROGEN EFFECTS ON CRACK PROPAGATION
- 6.03.2.1 Internal Hydrogen Assisted Cracking
- 6.03.2.2 Hydrogen Environment Assisted Cracking
- 6.03.2.3 Commonalities and Differences

6.03.3 HYDROGEN CRACKING IN DAMAGE TOLERANT STRUCTURAL INTEGRITY
- 6.03.3.1 Fracture Mechanics Similitude and Subcritical Crack Growth
- 6.03.3.2 Fracture Toughness
- 6.03.3.3 Standard Laboratory Test Methods
- 6.03.3.4 Data Bases and Terminology
- 6.03.3.5 Complications
  - 6.03.3.5.1 Loading Format and Rate

6.03.4 TECHNOLOGICAL IMPORTANCE OF HYDROGEN CRACKING IN HIGH STRENGTH COMPONENTS

6.03.5 PHENOMENOLOGY OF HYDROGEN CRACKING
- 6.03.5.1 High Strength Steels
- 6.03.5.2 Superalloys
- 6.03.5.3 7000 Series Aluminum Alloys
- 6.03.5.4 Beta Titanium Alloys

6.03.6 IMPORTANT VARIABLES AFFECTING HYDROGEN CRACKING
- 6.03.6.1 Fracture Mechanics Variables
- 6.03.6.2 Metallurgical Variables
  - 6.03.6.2.1 Alloy Strength
  - 6.03.6.2.2 Alloy Composition and Microstructure
- 6.03.6.3 Chemical Variables
  - 6.03.6.3.1 Hydrogen Concentration in IHAC
  - 6.03.6.3.2 Environmental Hydrogen Activity in HEAC
  - 6.03.6.3.3 Temperature

6.03.7 MECHANISTIC BASIS FOR HYDROGEN ASSISTED CRACK GROWTH
- 6.03.7.1 Role of Hydrogen Assisted Damage in Stress Corrosion Cracking
  - 6.03.7.1.1 Example Experiments for 7000 Series Aluminum Alloys
  - 6.03.7.1.2 Crack Chemistry Advances
- 6.03.7.2 Hydrogen Assisted Damage Mechanisms
  - 6.03.7.2.1 Hydrogen Enhanced Decohesion
  - 6.03.7.2.2 Hydrogen Affected Localized Plasticity

6.03.8 MECHANISM-BASED MICROMECHANICAL-CHEMICAL MODELING OF HYDROGEN ASSISTED CRACKING
- 6.03.8.1 Crack Tip Mechanics
- 6.03.8.2 Crack Tip Hydrogen Accumulation
- 6.03.8.3 Threshold Stress Intensity Modeling
  - 6.03.8.3.1 HEAC
  - 6.03.8.3.2 IHAC
  - 6.03.8.3.3 Temperature Dependence
- 6.03.8.4 Crack Growth Rate Modeling
  - 6.03.8.4.1 IHAC
  - 6.03.8.4.2 HEAC
  - 6.03.8.4.3 Location of H Damage Sites in FPZ

6.03.9 UNCERTAINTIES AND NEEDS
- 6.03.9.1 Fracture Mechanics Issues
  - 6.03.9.1.1 Specimen Constraint
  - 6.03.9.1.2 Small Crack Size
  - 6.03.9.1.3 Precrack Path
  - 6.03.9.1.4 Mixed Mode Hydrogen Assisted Cracking
  - 6.03.9.1.5 Transient Exposure
  - 6.03.9.1.6 Interacting Cracks
  - 6.03.9.1.7 Distribution of Material-Cracking Properties
- 6.03.9.2 Research Needs
  - 6.03.9.2.1 Hydrogen Damage Mechanism
  - 6.03.9.2.2 Crack Chemistry and H Production
  - 6.03.9.2.3 Crack Tip Mechanics
  - 6.03.9.2.4 Hydrogen Trapping

6.03.10 CONCLUSIONS

6.03.11 ACKNOWLEDGEMENT

6.03.12 REFERENCES

6.03.1 INTRODUCTION

Two important advances over the past 40 years enable the optimization and effective management of the structural integrity of components in high performance applications. First, the solid mechanics community established linear elastic fracture mechanics as the premier framework for modeling the damage tolerance of fracture critical components (Irwin and Wells, 1997; Paris, 1998). Second, materials scientists developed metals with outstanding balances of high tensile strength and high fracture toughness (Garrison, 1990; Wells, 1993; Boyer, 1993; Starke and Staley, 1995; Olson, 1997; Kolts, 1996). An example of achievable strength-toughness properties is provided in Fig. 1, a plot of plane strain fracture toughness (K_{IC}) *vs.* tensile yield strength (σ_{YS}) for ultra-high strength steels (UHSS) and β-Ti alloys precipitation hardened with α phase (Gangloff, 2001). New nano-scale characterization and high performance computational methods provide for additional advances in the mechanical performance properties of structural metals. These modern alloys and analysis tools satisfy technological needs for optimization and management of component performance in demanding fatigue and fracture critical applications in the aerospace, marine, energy, transportation, and defense sectors.

Counter to these successes, hydrogen broadly and severely degrades the fracture resistance of high strength metallic alloys. The Mode I stress intensity factor (K) levels that produce subcritical-hydrogen cracking are low, of order 5 to 25% of K_{IC}, as indicated by the shaded areas in Fig. 1. In essence the toughness gains from decades of metallurgical research are compromised by so-called hydrogen embrittlement. In response a massive literature on H effects in metals has evolved, as represented by important archival

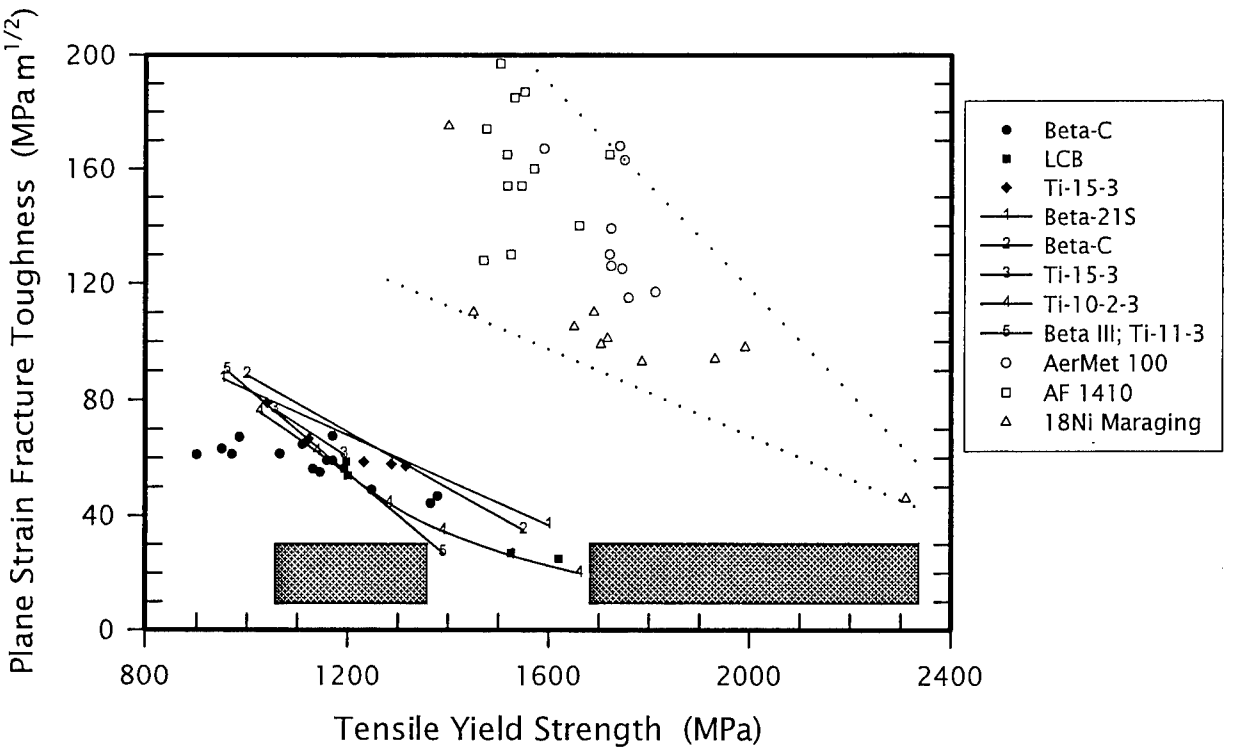

Figure 1. The yield strength dependence of plane strain fracture toughness for high strength α-precipitation hardened β-Ti alloys and tempered martensitic alloy steels fractured in moist air at 25°C. The shaded areas generally represent the lower bound stress intensity regime for severe IHAC and HEAC.

proceedings (Scully, 1971; Raymond, 1972, 1988; Bernstein and Thompson, 1974, 1981; Swann, et al., 1977; Louthan and McNitt, 1977; Alefeld and Völkl, 1978, 1997; Staehle et al., 1977; Louthan, et al., 1981; Azou, 1982; Interrante and Pressouyre, 1982; Gangloff, 1984; Oriani et al., 1985; Jones and Gerberich, 1986; Praeger, 1989, 1994; Gangloff and Ives, 1990; Lisagor et al., 1990; Moody and Thompson, 1990a; Turnbull, 1995; Thompson and Moody, 1996; Moody and Thompson 2003) and 100s of journal papers. In spite of these efforts, hydrogen embrittlement continues to plague applications of high strength metals.

The objective of this chapter is to establish the foundation necessary to control hydrogen assisted subcritical cracking in high strength metals by quantitative structural integrity assessment. The elements of this foundation include: (a) definition of the forms of hydrogen cracking in 6.03.2, (b) the role of fracture mechanics-similitude scaling of laboratory data to enable component prediction, 6.03.3, (c) the technological importance of hydrogen cracking in 6.03.4, (d) a summary of data that describe hydrogen degradation phenomena, 6.03.5, and the effects of important variables, 6.03.6, (e) assessment of the state-of-the-art in basic mechanistic understanding, 6.03.7, (f) micromechanical and chemical modeling to predict material properties, 6.03.8, and (g) critical uncertainties that hinder life prediction, 6.03.9.

This chapter concentrates mainly on high and ultra-high strength metals with tensile yield strength/elastic modulus ratio above about 0.005 and that exhibit hydrogen assisted crack propagation in the absence of metal hydride formation. Alloy families include tempered martensitic low alloy and stainless steels, precipitation hardened aluminum alloys, precipitation hardened body-centered cubic titanium (β-Ti) alloys, and precipitation hardened austenitic superalloys. Hydride-based embrittlement of hexagonally closed packed

Ti and Zr alloys is discussed elsewhere in Volume 6. All forms of hydrogen damage, except hydride cracking, that occur in the temperature range within $\pm 150^{o}C$ of ambient are considered here. Hydrogen effects on fatigue crack propagation are reviewed elsewhere (Gangloff, 1990, 1990a, 2002). The linear elastic fracture mechanics framework provides the effective basis for each aspect of this review and only crack propagation is considered. This chapter builds on previous reviews of hydrogen embrittlement of high strength alloys (Louthan et al., 1972; Blackburn et al., 1972; Speidel and Hyatt, 1972; Speidel, 1975; Wanhill, 1975; Kerns, et al., 1977; Dautovich and Floreen, 1977; Sandoz, 1977; Oriani, 1978; Hirth, 1980; Thompson and Bernstein, 1980; Nelson, 1983; Vehoff and Rothe, 1983; Gruhl, 1984; Lynch, 1988, 2003; McIntyre, 1985; Gangloff, 1986, 2003; Moody et al., 1990; Holroyd, 1990; Marsh and Gerberich, 1992; Interrante and Raymond, 1995; Vehoff, 1997; McMahon, 2001).

6.03.2 HYDROGEN EFFECTS ON CRACK PROPAGATION

Hydrogen degradation of the crack propagation resistance of high strength alloys is categorized as either *Internal Hydrogen Assisted Cracking* (IHAC) or *Hydrogen Environment Assisted Cracking* (HEAC). These phenomena are also called *Internal Hydrogen Embrittlement* (IHE) and *Hydrogen Environment Embrittlement* (HEE), respectively. The former designations are favored since H clearly degrades crack propagation resistance by assisting the microscopic processes that constitute crack tip advance, while embrittlement restricts the perception of the precise nature of the H-damage mechanism as detailed in 6.03.7. In high strength alloys, H effects are invariably localized

to the crack tip. IHAC and HEAC are distinguished by the source of the offending H supplied to the crack tip fracture process zone (FPZ), but otherwise share common aspects. This view is summarized in Fig. 2.

6.03.2.1 Internal Hydrogen Assisted Cracking—*IHAC*

Atomic hydrogen can be introduced globally throughout the microstructure by manufacturing operations (e.g., casting, welding, surface-chemical cleaning, electrochemical machining, electroplating, and heat treatment) as well as by environmental exposure (e.g., cathodic electrochemical reactions at low temperatures and gaseous hydrogen exposure at elevated temperatures). Subcritical crack growth occurs when the hydrogen "charged" metal is subsequently stressed, as shown in the right-portion of Fig. 2. Loading causes a redistribution of dissolved hydrogen from the surrounding microstructure to the crack tip process zone to promote crack growth. Stress is not necessary during hydrogen uptake, and environmental hydrogen production at the crack tip during stressing is not significant since the loading environment is typically benign.

6.03.2.2 Hydrogen Environment Assisted Cracking--*HEAC*

HEAC involves the conjoint action of mechanical loading and chemical reaction. Atomic hydrogen is produced predominantly on clean crack surfaces localized near to the tip, followed by H uptake into the crack tip FPZ and subsequent embrittlement as shown in the left and bottom portions of Fig. 2. Mass transport of elements of the surrounding environment is unique to the occluded crack volume and supplies crack tip surface reactions,

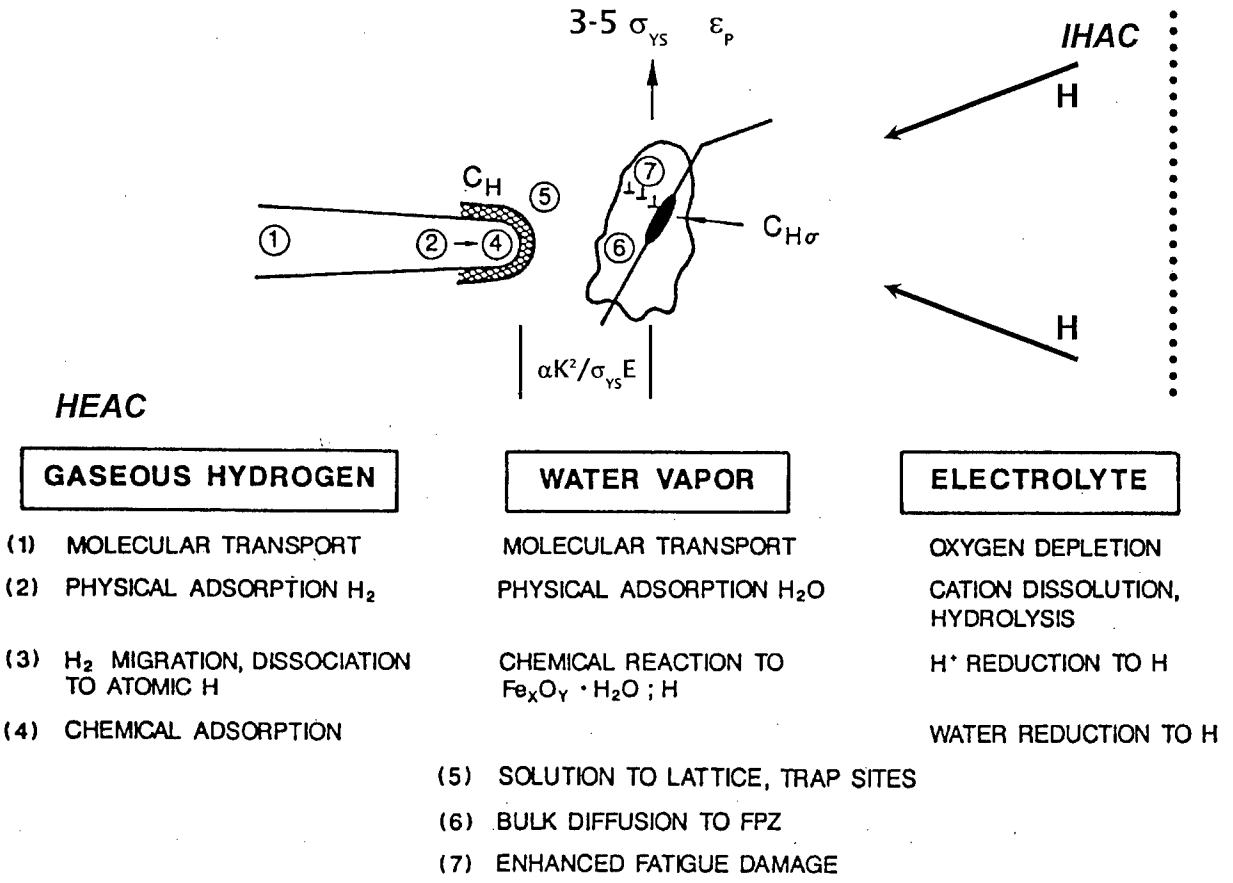

Figure 2. The sequence of elemental processes that supply damaging H to the crack tip fracture process zone during either HEAC for gaseous hydrogen, water vapor or an electrolyte, or IHAC for a H precharged microstructure. The dotted line indicates the outer boundary of the plastic zone. Crack tip tensile stresses are maximized at some distance ahead of the tip, proportional to $K^2/\sigma_{YS}E$ (see 6.03.8.1).

as illustrated for three environments. From left to right, atomic hydrogen (H) is produced by dissociative chemical adsorption for H_2, by chemical reactions for gases such as water vapor or H_2S, or by electrochemical cathodic reactions for acidic or alkaline electrolytes. Once produced, the H diffuses ahead of the crack tip into the FPZ to affect damage. This scenario provides the hydrogen mechanism for stress corrosion cracking (SCC) and sulfide stress cracking for alloys in aqueous H_2S-bearing electrolytes. Electrochemical reactions leading to metal dissolution and passive film formation can occur at the crack tip, concurrent with H production, to affect crack growth. The extent to which hydrogen dominates damage is controversial, but the HEAC mechanism for SCC is accepted broadly for high strength metals as summarized in 6.03.7.1.

6.03.2.3 Commonalities and Differences

IHAC and HEAC share common features for high strength metals. Each damage mode occurs subcritically at stress intensity levels well below K_{IC}. IHAC and HEAC proceed by similar microscopic crack paths; typically either intergranular, interfacial, or along crystallographically defined planes through grains; in sharp contrast to the microvoid-based morphology typical of ductile fracture in high strength alloys (Shipley and Becker, 2002). Both IHAC and HEAC are affected similarly by variables such as applied K level, loading rate (dK/dt), alloy σ_{YS}, grain boundary impurity composition, temperature, and FPZ H concentration, as detailed in 6.03.6. One or more common atomistic embrittlement mechanisms are probably responsible for both IHAC and HEAC, as detailed in 6.03.7. In each case, strong gradients in H concentration and stress about the crack tip govern crack

growth, and challenge damage characterization and modeling work. Both IHAC and HEAC operate if a precharged steel is stressed in a H-producing environment,.

The differences between internal and hydrogen environment assisted cracking are associated with the kinetics of crack growth (Sandoz, 1977), and are not intrinsic (Walter et al., 1969). Each mode is time dependent, governed by mobile-H diffusion (Gangloff, 2003). The kinetics of the environmental-mass transport and H production steps illustrated in Fig. 2 may alternately control rates of HEAC depending on specific cracking conditions. The details of FPZ damage, and particularly the location of damage processes ahead of the crack tip, differ for IHAC *vs.* HEAC (Page and Gerberich, 1982). Factors that control the precise damage location include the tensile stress distribution maximized at some distance ahead of the crack tip, the plastic strain (ε_P) and associated dislocation density profile about the crack tip, the distribution of H trap sites, and the concentration of environmentally produced H on the crack tip surface, as amplified in 6.03.8 (Gangloff, 1988, 2003).

6.03.3 HAC IN DAMAGE TOLERANT STRUCTURAL INTEGRITY

6.03.3.1 Fracture Mechanics Similitude and Subcritical Crack Growth

Linear elastic fracture mechanics provides the well established basis for incorporating hydrogen cracking into structural integrity management methods (Barsom, 1987; Barsom and Rolfe, 1987). The governing role of K, as the single-parameter descriptor of loading and crack geometry effects on the rate of subcritical hydrogen crack propagation (da/dt), was established by pioneering experimental work at the Naval Research Laboratory (Brown and Beachem, 1965, 1966), and confirmed by many others over the ensuing decades (Smith

et al., 1968; Novak and Rolfe, 1969, 1970; Wei, et al., 1972; Wei and Novak, 1987). The central importance of K is cemented by micromechanical modeling of the local stresses and strains that fundamentally affect crack tip damage, as developed in 6.03.8. The high strength levels of the alloys under review minimize the need for more complex elastic-plastic analysis (Hackett, et al., 1986; Anderson, 1995).

Since hydrogen promotes subcritical crack propagation at stress intensities below K_{IC}, it is necessary for a structural integrity model to predict: (a) the threshold loading and crack size conditions below which IHAC and HEAC are not likely to occur, and/or (b) the remaining life of a component based on rates of hydrogen assisted crack propagation. Stress intensity similitude provides the foundation for such modeling; that is, da/dt depends uniquely on K for a given alloy and hydrogen exposure condition, independent of loading and crack geometry. Crack growth threshold and kinetics are measured in the laboratory with a fracture mechanics specimen. Threshold stress and crack size are predicted using the measured crack growth threshold. The functional relationship between da/dt and K is integrated in conjunction with the stress intensity solution for a cracked component, and from the initial existing to target-final crack size, to predict component propagation life. The principle of this approach has been in place for 30-40 years and parallels fatigue crack propagation life prediction (Wei et al., 1972; Barsom and Rolfe, 1987; Anderson, 1995; Hertzberg, 1996).

The K dependence of da/dt is common for a wide range of IHAC and HEAC in high strength alloys; the specific form is illustrated in Figs. 3 and 4 for an 18Ni Maraging steel cracked in low pressure H_2 as well as a quenched and tempered martensitic steel in three H-

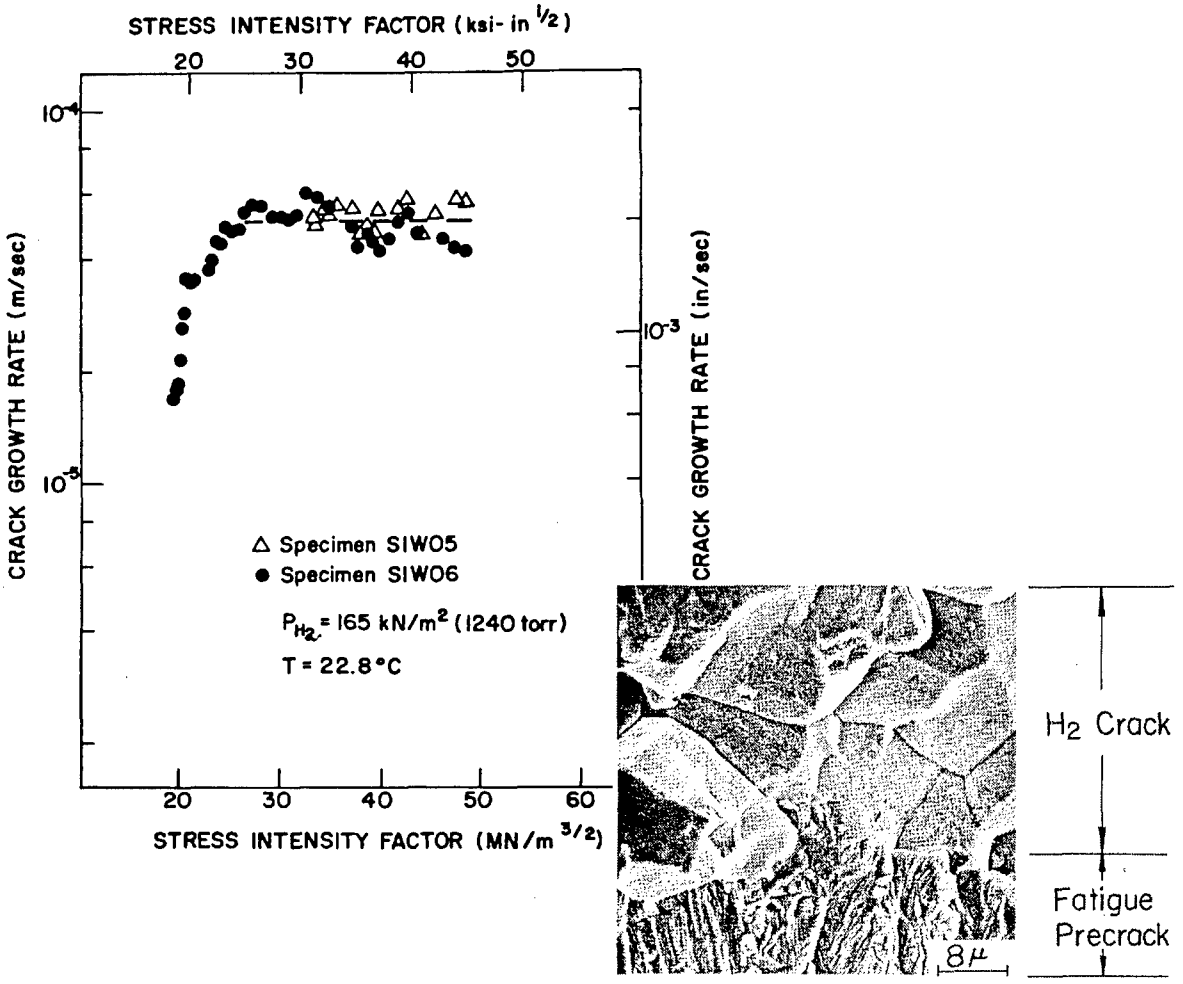

Figure 3. The stress intensity dependence of subcritical crack growth rate produced in 18Ni Maraging steel by concurrent exposure to low pressure purified hydrogen gas at 23°C and stressing at constant load. HEAC is predominantly along prior austenite grain boundaries. (Gangloff and Wei, 1977, 1978)

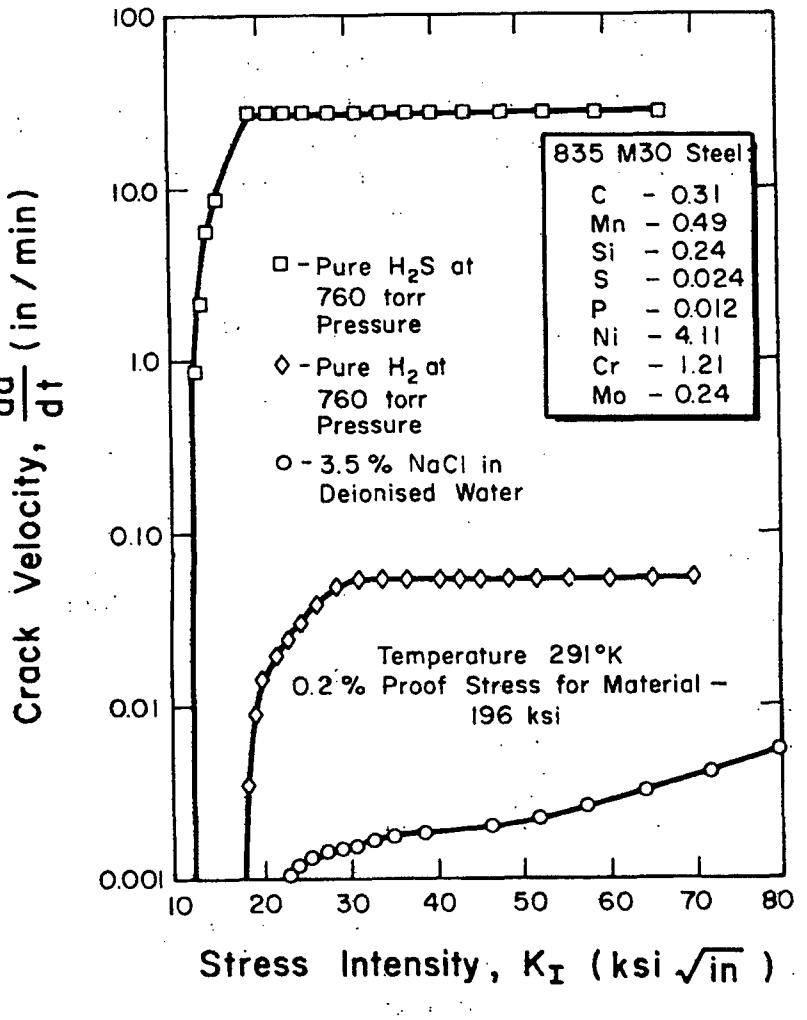

Figure 4. The stress intensity dependence of subcritical crack growth rate produced in a tempered martensitic steel during exposure in three separate environments that produce atomic hydrogen at the crack tip during stressing under slow-rising CMOD producing dK/dt = 0.18 MPa$\sqrt{m}$/s. (1 ksi$\sqrt{in}$ = 1.098 MPa$\sqrt{m}$, 1 in/min = 0.423 mm/s, 1 ksi = 6.89 MPa, and 1 torr = 133.3 Pa.) (McIntyre and Priest, 1972; plotted by Kerns et al., 1977: Copyright NACE International, reprinted with permission.)

producing environments, respectively. For these steels, the K_{IC} exceeds 100 MPa$\sqrt{m}$ (Fig. 1), while HEAC occurs at K levels above 15 to 40 MPa$\sqrt{m}$. The crack growth behavior is defined by four features: (a) a threshold K, K_{TH} (or other terminology), below which stable crack growth is not resolved, (b) Stage I just above K_{TH} where da/dt rises sharply with increasing K due to presumed mechanical control of crack tip damage, (c) Stage II where crack growth rate (da/dt_{II}) is independent of K due to reaction rate/H diffusion control, and (d) Stage III where da/dt increases with rising K approaching K_{IC} due to superposition of ductile fracture damage. In some instances, Stage II crack growth rate depends on a power-law function of K, with the exponent substantially reduced compared to Stage I cracking but greater than 0 (Nelson, 1983). The precise relationship between da/dt and K depends on a wide variety of test method, environmental exposure, H concentration, temperature, alloy strength and metallurgical variables (6.03.5 and 6.03.6).

6.03.3.2 Fracture Toughness

In addition to promoting subcritical crack growth in high strength alloys, H distributed throughout the crack tip FPZ can reduce plane strain fracture toughness. This mode of H degradation has not been studied broadly for high strength alloys, but results show that it can occur. For example, the K_{IC} of ~140 MPa$\sqrt{m}$ for microvoid fracture in an ultra-high strength steel (AerMet®100) was reduced to levels in the range from 50 to 90 MPa$\sqrt{m}$ due to predissolved H, as shown in 6.03.5 (Thomas et al., 2003). This form of H damage is promoted by loading rates that are sufficiently rapid to preclude time dependent IHAC or HEAC, and does not involve a change in the microscopic fracture mode. Rather, one or

more aspects of the ductile fracture process is promoted by dissolved H. This H enhanced ductile fracture was studied for lower strength alloy and stainless steels (Thompson and Bernstein, 1981; Hirth, 1996; McMahon, 2001), and is not considered further in this chapter. Additionally, H has been claimed to promote cleavage cracking in low strength Cr-Mo steels and raise the ductile-to-brittle transitions temperature under impact loading (Sakai, et al., 1997). This failure mode is not typically relevant to high strength alloys.

6.03.3.3 Standard Laboratory Test Methods

Laboratory experimentation to characterize the threshold and kinetics for hydrogen assisted cracking is substantially more complex than methods dealing with fracture toughness or fatigue crack propagation. Only limited standards exist (ASTM Standard E1681-99: *Standard Test Method for Determining a Threshold Stress Intensity Factor for Environment-Assisted Cracking of Metallic Materials*; ISO Standard 7539-6: *Corrosion of Metals and Alloys-Stress Corrosion Testing with Precracked Specimens*; NACE Standard Test Method TM 0177-90: *Method for Laboratory Testing of Metals for Resistance to Sulfide Stress Cracking in H_2S Environments*). Standard E1681 is being enhanced to guide experimental measurement of K_{TH} and da/dt (Vigilante et al., 2000). Alternately, the experimentalist can follow procedures outlined in compilations (ASM International, 1985; Sedriks, 1990; Baboian, 1995) or reported in specific papers.

IHAC and HEAC experiments involve several important elements. A standard fracture mechanics specimen is fatigue precracked and stressed under either constant or programmed-rising load, constant or rising crack mouth opening displacement (CMOD), or constant K. Constant load is typically achieved using a cantilever beam and constant

weight, constant CMOD is achieved by a self-stressing bolt, and programmed-rising load/CMOD or constant K are achieved using a closed loop servo-electric or servo-hydraulic machine. Crack length, load, CMOD and time are measured typically during subcritical crack propagation to define data of the sort shown in Figs. 3 and 4. Crack length can be measured automatically with either the direct current electrical potential or elastic compliance method. For IHAC, the precracked specimen is exposed to the environment prior to loading to enable H charging by electrochemical or gaseous hydrogen reaction with bulk and crack tip surfaces. The H-precharged specimen is then loaded in ambient-moist air to produce internal hydrogen cracking. For HEAC, a chamber is affixed to the fatigue cracked area and the crack tip plus external surfaces are exposed to the H producing environment coincident with stressing. For IHAC, a calibration is required to relate environmental exposure to the hydrogen concentration. For HEAC, environment chemistry must be controlled during crack growth.

6.03.3.4 Databases and Terminology

Formal databases for IHAC and HEAC of high strength alloys are not established, but data compilations exist (Carter, not dated; Gangloff, 1986; McEvily, 1990). In the initial development of a structural integrity model, literature data on crack growth thresholds and rates should be sufficient to enable calculations of various H cracking scenarios. As the method is developed, or if the problem is sufficiently important, then published data must be augmented by experiments that incorporate the specific environment/H concentration, metallurgical, and loading variables. The resources required may be substantial.

The terminology of hydrogen cracking is diverse, particularly for threshold quantities, but common terms are emerging. The ASTM standard aims to yield a specimen-size-independent threshold K for environment assisted cracking (EAC), K_{IEAC}, using constant load or constant displacement (ASTM, 2000). This terminology is equivalent to the predecessor term, K_{ISCC}, (Brown and Beachem, 1965; Barsom and Rolfe, 1987), and is reasonably extended to K_{IHEAC} or K_{IIHAC} for situations where the damage mechanism is hydrogen based. The term, K_{IH}, describes the threshold for the onset of resolvable hydrogen cracking under rising CMOD (Gangloff, 1986; Gangloff et al., 1996). Often, K_{TH} is used to describe the threshold property for IHAC or HEAC, and either a crack arrest or crack-growth initiation experiment, provided that the context is clearly stated. The K_{IC-H} is used to designate H reduction in K_{IC} that is not associated with subcritical crack propagation.

6.03.3.5 Complications

In addition to the complexity of experiments and lack of databases, incorporating hydrogen cracking in structural integrity modeling is challenged by important complications and uncertainties (NMAB, 1982). IHAC and HEAC are affected by a number of variables that interact (6.03.6) and require a substantial number of experiments that may be of prolonged duration. Additional factors that could complicate K-similitude have not been resolved, but must be considered in structure-life modeling. The importance of loading rate and loading format are considered here. The effects of specimen size, small crack size, precrack path, mixed mode loading, interacting cracks, and statistical distribution of H cracking properties are discussed in 6.03.9.

6.03.3.5.1 Loading Rate and Format

Loading format and loading rate affect the threshold and kinetics of IHAC and HEAC. Early research employed either constant load (rising K) or fixed CMOD (falling K) experiments to define the threshold (K_{IHEAC} or K_{ISCC}) and da/dt for hydrogen assisted subcritical cracking. It is critical to load for a sufficiently long time to allow H to accumulate and stimulate damage in the FPZ. The ASTM standard focuses on the fixed CMOD method and suggests that threshold measurement requires a 1,000 h exposure for titanium alloys, 5000 h for UHSS, and 10,000 h for aluminum alloys (ASTM, 2000). In laboratory testing, it is important to avoid the complicating influence of transient-loading (Wei et al., 1972). For example, substantial incubation times and crack growth rate transients were observed immediately after a load change applied to high strength 4340 steel in distilled water (Hudak and Wei, 1981). The K_{IHEAC} for high strength steel in H_2 and NaCl solution increased monotonically with increasing level of a single prestress applied to a fatigue precracked specimen before testing at increasing low-load steps in the environment (Jonas, 1973).

A rising load or rising displacement method was advocated to accelerate determination of the kinetics of IHAC and HEAC (McIntyre and Priest, 1972; Clarke and Landes, 1976; Hirano et al., 1985; Crumly, 1988; Dietzel et al., 1989; Mayville, et al., 1989; Tyler et al., 1991; Dietzel and Ghosal, 1998; Somerday, et al., 2000; Dietzel and Mueller-Roos, 2001). For high strength alloys, this acceleration produces da/dt data (see Fig. 4) that are analogous to the K_{TH}-Stage I-Stage II response achieved by long term constant load or constant CMOD testing (Fig. 3). The rising CMOD method successfully produces lower-bound threshold

values, provided that the loading rate (best expressed as dK/dt) is sufficiently slow, as shown for a single high strength steel and purified H_2 environment in Fig. 5. Here, the critical K level for the onset of resolvable crack growth (K_{IH}) decreases with decreasing dK/dt, as expected since HEAC in this high strength steel in NaCl solution requires time for the reaction steps (Fig. 2) to produce embrittling H in the FPZ. Notably, this critical K_{IH} approaches the K_{IHEAC}; but the time for the rising load measurement, ~6 h, is up to several orders of magnitude shorter than the prolonged times typically used for the constant load or constant CMOD measurement of K_{TH}. Similar results were reported for high strength steel and aluminum alloys in chloride solutions (Hirano, et al., 1985; Crumly, 1988; Dietzel et al., 1989; Dieztel and Ghosal, 1998; Dietzel and Mueller-Roos, 2001; Thomas et al., 2003).

The loading rate necessary to achieve a lower bound threshold depends on the material and environment. Lower applied dK/dt are required to resolve a lower bound threshold as the susceptibility to IHAC or HEAC declines, for example due to reduced environmental hydrogen production. The necessary dK/dt is directly proportional to the Stage II da/dt (Dietzel and Mueller-Roos, 2001). For example, high strength β-Ti alloys exhibit very high da/dt_{II} for HEAC in chloride solution and K_{IH} values are independent of loading rate ($d\delta_m/dt$ in Fig. 6 = dCMOD/dt) for dK/dt at least as high as 30 MPa$\sqrt{m}$/s, as shown in Fig. 6 (Somerday et al., 2000). A less susceptible (lower da/dt_{II}) high strength steel required a displacement rate of 0.8 nm/s or slower to measure a lower bound K_{IH} (Dietzel and Mueller-Roos, 2001). Crack growth rate generally increases with increasing dK/dt, but understanding is limited (Mayville, et al., 1989; Dietzel and Ghosal, 1998; Somerday, et al., 2000).

The rising CMOD method is particularly important for hydrogen cracking in lower

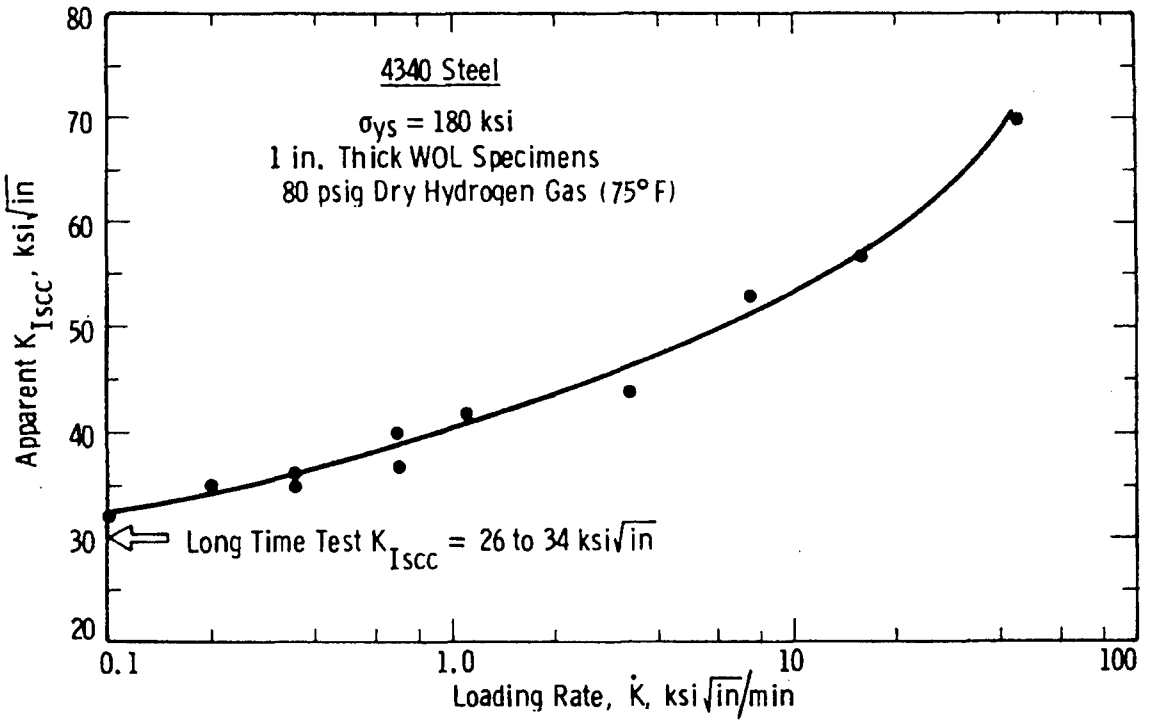

Figure 5. The effect of rising-K rate on the threshold stress intensity factor for the onset of resolvable HEAC in high strength steel stressed actively in purified hydrogen gas. (1.0 ksi√in = 1.098 MPa√m, 1.0 ksi√in/min = 0.0183 MPa√m/s, 1 psig = 6.89 kPa.) (Clark and Landes, 1976: Copyright ASTM International, reprinted with permission.)

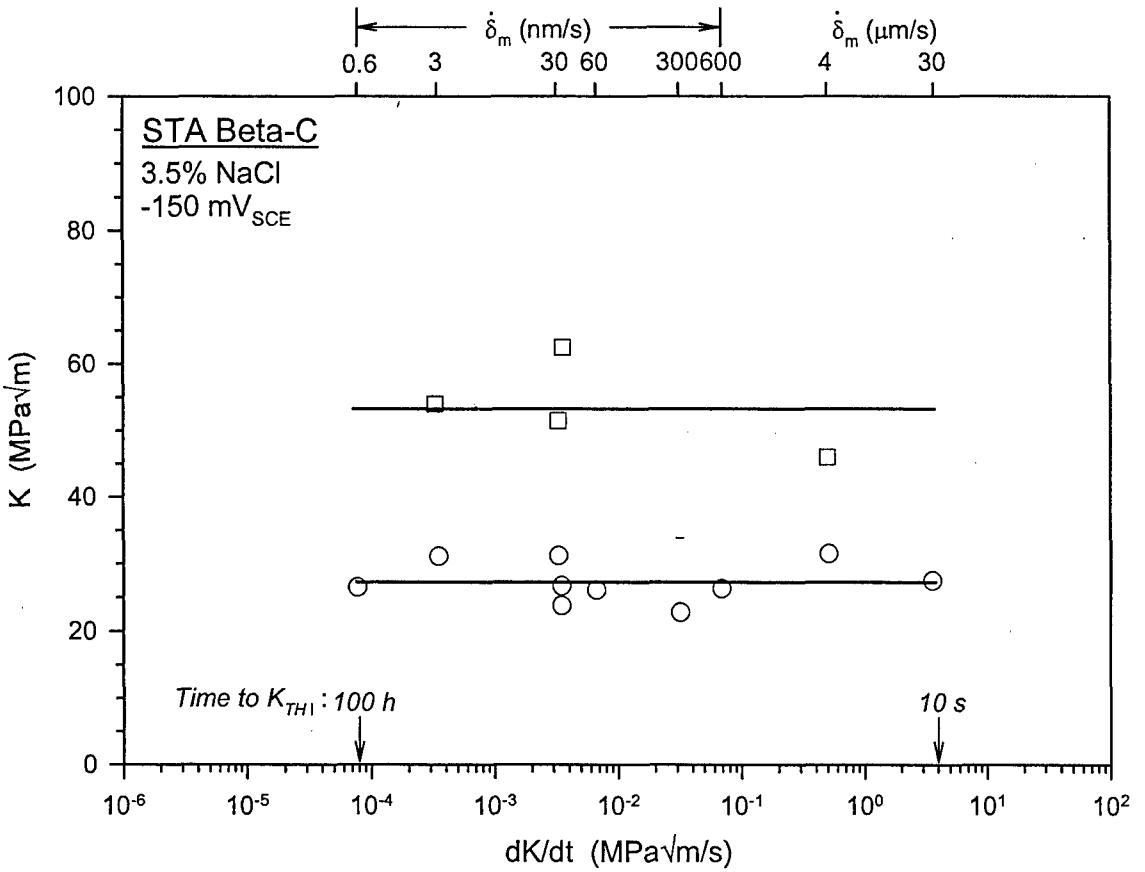

Figure 6. The effect of rising-K rate on the threshold stress intensity factor (K_{IH}, O) for the onset of resolvable HEAC in a high strength α-precipitation hardened β-Ti alloy stressed actively in aqueous chloride solution. Plane strain initiation-fracture toughness data are shown for similar loading in moist air (K_{JIC}, 9). (Somerday et al., 2000)

strength alloys. In this case, substantial data show that K_{IH} for rising CMOD is several times less than K_{TH} defined by long term fixed CMOD experiments for IHAC in lower strength alloy steels (Gangloff, 1986). Specific data are presented in Fig. 7 for a quenched-bainitic microstructure in 2¼ Cr-1Mo steel tempered to achieve various strengths, precharged by elevated temperature exposure to H_2, quenched to 23°C, then cracked under either rising-CMOD (□, rising K) or fixed CMOD (9, falling K) (Gangloff, et al., 1996; Gangloff, 1998). The K_{IH} for the rising CMOD case is substantially lower than K_{IIHAC} defined by crack arrest under falling K, provided that the steel strength is less than about 1000 MPa. The explanation for this effect is unclear, but may involve the damaging role of active crack tip plasticity in H cracking, and/or H loss from the laboratory specimen during long term fixed CMOD testing. Fortunately, the data in Fig. 7 suggest that the difference in K_{TH} for rising *vs.* falling K conditions is small when steel yield strength exceeds about 1000 MPa. Either loading method provides reasonable values of the crack growth threshold (and perhaps kinetics) for IHAC and HEAC in the high strength alloys pertinent to this chapter.

6.03.4 TECHNOLOGICAL IMPORTANCE OF HYDROGEN CRACKING IN HIGH STRENGTH COMPONENTS

Hydrogen assisted crack propagation should be considered in a comprehensive structural integrity management methodology. First, high strength alloys based on Fe, Ni, Ti and Al are highly susceptible to hydrogen cracking. As illustrated in Fig. 1, high levels of plane strain fracture toughness that are typical of such alloys are reduced by up to an order of magnitude by hydrogen exposure. Hydrogen cracking degrades critical crack size, operating stress level, and damage tolerant life.

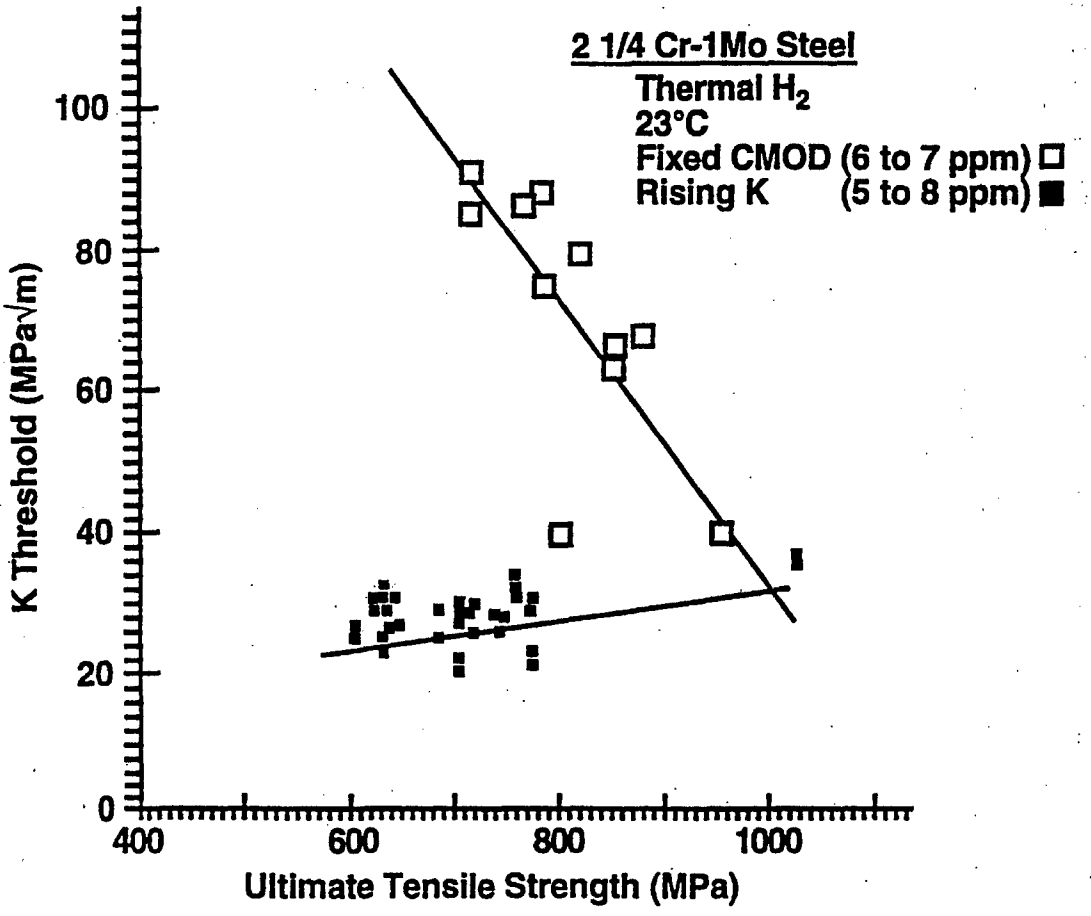

Figure 7. The effect of loading format, including fixed CMOD yielding crack arrest under falling K (9) and rising CMOD causing crack growth initiation under rising K (□), on IHAC of a tempered bainitic alloy steel containing a claimed-constant amount of precharged H. (Gangloff, 1998)

The breadth of the hydrogen cracking problem is significant due to the ubiquity of H. Hydrogen is readily introduced into alloys during both manufacturing and service exposure and promotes IHAC. A wide range of environments; from gases such as H_2, H_2S and C_XH_Y to aqueous electrolytes over the range of pH from 0 to 14 and applied electrode potentials above and below the free corrosion state; are capable of producing atomic H at a straining crack tip. Specific examples from failure analyses demonstrate the importance of IHAC (Baggerly, 1996; Mukhopadhyay, et al., 1999; Schmidt, et al., 2000; Reddy, et al., 2001) and HEAC (Speidel and Fourt, 1977; Whelan, 1981; Akhurst and Baker, 1981; Fritzemeier et al., 1990; Lynch, 1994; Chen et al., 1996; Vehovar, 1998; Woodtli and Kieselbach, 2000; Carter and Cornish, 2001; Troiano et al., 2002). Many other case studies are likely to exist, but are not reported in the open literature due to proprietary considerations. These examples include electroplated high strength steels for fastener and landing gear applications, pearlitic steels for concrete prestressing, precipitation hardened stainless steels and nickel based alloys for deep oil and gas well casings as well as aerospace piping and nuclear applications, forged or rolled precipitation hardened Al-Zn-Mg-Cu alloys for airframe construction, and precipitation hardened β-Ti alloys for marine and aerospace uses.

An alternate representation of the importance of IHAC and HEAC to structural integrity is provided by the results of a computer search of literature databases, Table 1. For example, the Metadex database contains almost 1000 publications since 1990 that included the four key words of hydrogen, embrittlement, high and strength. An additional 1000 papers were published between 1980 and 1990. In spite of this extensive research, the hydrogen cracking problem is not solved to the point where this failure mode can be

precluded from structural integrity management. As amplified in 6.03.5, most modern alloys based on Fe, Ni, Ti and Al continue to be susceptible to substantial hydrogen cracking. Materials scientists have not produced high strength alloys that are truly immune to H cracking. Unexpected manufacturing and service environment conditions often promote hydrogen cracking. Mechanisms of IHAC and HEAC are uncertain and controversial (6.03.7). The micromechanical/microchemical models that are necessary to augment laboratory data for life prediction are semiquantitative at best, as shown in 6.03.8

Table 1. Citations in the materials science literature since 1990 for key words relevant to IHAC and HEAC

Hydrogen Embrittlement +	Metadex	Corrosion Abstracts
Plating	159	49
Aircraft	61	25
Fastener	37	15
Landing Gear	10	3
Turbine	43	9
Concrete	54	47
High Strength	960	307
High Strength (from 1980)	2,033	479
High Strength (from 1970)	2,417	498

Hydrogen cracking in high performance components is controlled by one or more approaches, including: (1) alloy substitution, (2) metallurgical change often leading to reduced alloy strength or improved alloy purity with increased cost, (3) environment inhibition for HEAC, (4) manufacturing-environment change or improved H-outgassing treatment for IHAC, (5) reduced applied or residual stress through design and fabrication modifications, and (6) improved inspection to detect existing cracks. A comprehensive structural integrity plan should quantify and facilitate such improvements.

6.03.5 PHENOMENOLOGY OF HYDROGEN CRACKING

Laboratory data that describe the stress intensity dependencies of the subcritical rates of IHAC and HEAC, as well as microscopic crack paths, are centrally important to structural integrity modeling to control hydrogen cracking in high strength alloys. These same data provide a basis for understanding crack tip damage mechanisms (6.03.7) and micromechanical-chemical modeling of K_{TH} and da/dt (6.03.8). Extensive da/dt *vs.* K data are available in the literature. New results from experiments conducted at the University of Virginia are emphasized in this review, and demonstrate that hydrogen assisted cracking continues to degrade the most modern high strength alloys.

6.03.5.1 High Strength Steels

High and ultra-high strength alloy steels with tempered martensitic microstructure and σ_{YS} from 1200 to 2200 MPa are embrittled severely by hydrogen. (Carter, not dated; Kerns, et al., 1977; Dautovich and Floreen, 1977; Nelson, 1983; Gangloff, 1986, 2003; Moody et al., 1990; McEvily, 1990; Interrante and Raymond, 1995; McMahon, 2001).

The pioneering work of Troiano and coworkers demonstrated severe internal hydrogen assisted cracking in low alloy steels such as AISI 4340 (Johnson et al., 1958; Steigerwald et al., 1960; Troiano, 1960), and this behavior was amplified by subsequent research using fracture mechanics (Dautovich and Floreen, 1973; Gerberich et al., 1988). Here, 1-5 parts-per-million by weight (ppm) of predissolved H promoted subcritical crack growth at K levels as low as 10 MPa$\sqrt{m}$ and da/dt values up to 20 μm/s for high strength steels with σ_{YS} of 1400-2000 MPa and H-free K_{IC} levels of 60-150 MPa$\sqrt{m}$.

Considering HEAC, the da/dt *vs.* K data in Figs. 3 and 4 illustrate that a wide variety of environments produce severe subcritical crack growth in tempered martensitic steels. Specific environments include gaseous H_2, H_2S, and water vapor; while electrolytes include solutions with or without chloride and spanning the range of pH from highly acidic to highly alkaline. Each is capable of producing atomic H at the crack tip through the scenario in Fig. 2. The da/dt depends on environmental variables that govern this amount of H adsorbed on the crack tip surface, and even relatively benign environments such as low pressure H_2 or H_2O, moist air, and pure-liquid water are severely embrittling (Fig. 4) (Charbonnier and Margot-Marette, 1982).

Subcritical IHAC and HEAC each occur along prior austenite grain boundaries in typical quenched and tempered martensitic steels such as AISI 4340, not processed for impurity control, as well as in higher purity maraging steels (Fig. 3) (McMahon, 2001; Eliaz et al., 2002). Such cracking can also occur along transgranular (TG) paths associated with either crystallographic planes or interfaces in the tempered martensitic structure (Gangloff and Wei, 1978; Gao and Wei, 1984; Gao, et al., 1984). The dominant morphology depends on variables such as steel purity, environment chemistry, crack tip FPZ hydrogen content, stress intensity, and temperature.

Modern ultra-high strength steels continue to be embrittled severely by predissolved or environmental hydrogen, as illustrated by the behavior of AerMet®100 steel. Here, ultra-high strength is developed through nano-scale metal carbide precipitation in unrecovered martensite, and high fracture toughness is achieved by impurity control and temper optimization (Olson, 1997). This modern steel is susceptible to severe HEAC and IHAC

that progresses largely along transgranular paths through the lath-martensite microstructure. For example, Figure 8 shows the deleterious effect of H predissolved electrochemically from $Ca(OH)_2$ solution on the threshold K for the onset of subcritical crack growth under slow-rising CMOD at various rates (Thomas, 2000; Thomas et al., 2003). For this diffusible H content (4.6 ppm), brittle subcritical cracking was produced at a K_{TH} equal to 10-15% of K_{IC} over a wide range of applied dK/dt from 0.0002 to 0.3 MPa$\sqrt{m}$/s. At higher loading rates, the threshold K rose monotonically, but never reached K_{IC} even for dK/dt levels as high as 2,000 MPa$\sqrt{m}$/s. Dissolved H affected a fracture mode transition from microvoid-based processes without H (top-right fractograph), to essentially all-brittle transgranular (TG) cracking associated with lath martensite interfaces for the low-K_{TH} plateau (bottom-left insert). A dimpled morphology correlated with the rising K_{TH} at higher loading rates for H-charged AerMet®100, but dimple size was substantially smaller compared to the H-free fracture surface. Reduced dimple size was reported for IHAC in high strength maraging steel (Tiwari et al., 2000), and more broadly for H-assisted ductile fracture in lower strength steels (Thompson and Brooks, 1975; Thompson and Bernstein, 1981; Hirth, 1996).

The IHAC of high strength martensitic steels is generally reversible if dissolved H is removed by outgassing at elevated temperature (Johnson et al., 1958; Barth and Steigerwald, 1970). For maraging steel, the low K_{TH}/K_{IC} of 0.3 after H charging was increased to 1.0 by baking for several hours at 150°C (Dautovich and Floreen, 1973). For AerMet®100, heating in moist air at 190°C for 24 h eliminated all diffusible H from the prior electrochemical charging and restored the ductile fracture resistance; K_{TH} of 16 MPa$\sqrt{m}$ for a charged-diffusible H content of 4.0 wppm was increased by baking to about 140 MPa$\sqrt{m}$, equal to

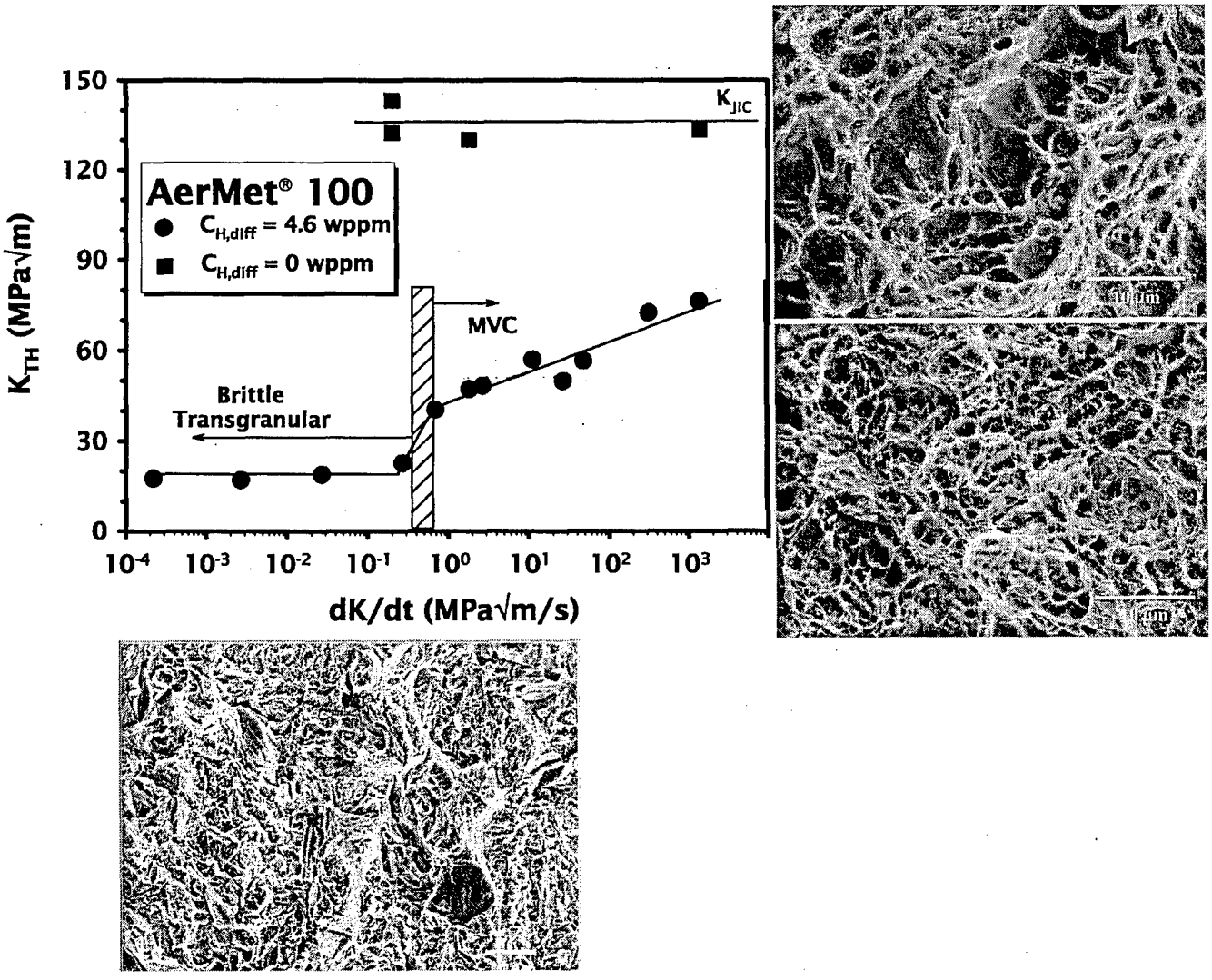

Figure 8. Rising CMOD threshold stress intensity *vs.* applied-initial dK/dt for AerMet®100 precharged to $C_{H\text{-}DIFF}$ = 4.6 wppm. At dK/dt less than 0.3 MPa√ms, brittle-TG fracture occurs at K_{TH} < 20 MPa√m. At dK/dt greater than 0.7 MPa√m/s, fracture occurs by MVC at K_{TH} < 60 MPa√m. The H-free plane strain elastic-plastic fracture toughness of AerMet®100 is 132-143 MPa√m. (Thomas, 2000; Thomas et al. 2003; Gangloff and George, 2002a)

the K_{IC} of H-free steel (Thomas et al., 2003). Similarly severe transgranular HEAC was reported for AerMet®100 stressed during exposure to several acidic environments (Buckley et al., 1993; Buckley et al., 1994; Oehlert and Atrens, 1998; Lee et al., 2000; Vigilante et al., 2000).

Martensitic stainless steels with 10-20% Cr, up to 10% Ni, perhaps Mo, and low C as well as precipitation hardening elements (Al, Ti, and Cu) are susceptible to severe HEAC even at strength levels that are less than those of ultra-high strength alloy steels such as AISI 4340 and AerMet®100. This behavior is illustrated by the threshold stress intensity data in Fig. 9 for aged hardened PH 13-8 Mo, 17-4 PH and PH 15-5 steels, each stressed during exposure in electrolytes with cathodic polarization (Scully, 2002). The open symbols were reported in early studies (Carter, not dated; Fujii, 1976; various internal reports), while the closed data are more recent (Thompson, 1978; Tyler, Levy and Raymond, 1991; Young et al., 1995; Vigilante, et al., 1997). Cracking was either IG (Young et al., 1995) or brittle TG (Thompson, 1978), depending on steel heat treatment and strength. Progressively less severe HEAC was reported for these martensitic stainless steels stressed in neutral NaCl solution or seawater as cathodic polarization was reduced towards the open circuit corrosion condition (Tyler et al., 1991; Scully, 2002).

6.03.5.2 Superalloys

Iron and nickel-based superalloys; with a face-centered cubic austenite matrix that is precipitation hardened by intermetallic phases based on Ti, Al, and Nb; are prone to severe hydrogen cracking as revealed by initial studies involving high pressure H_2 exposure (Jewett

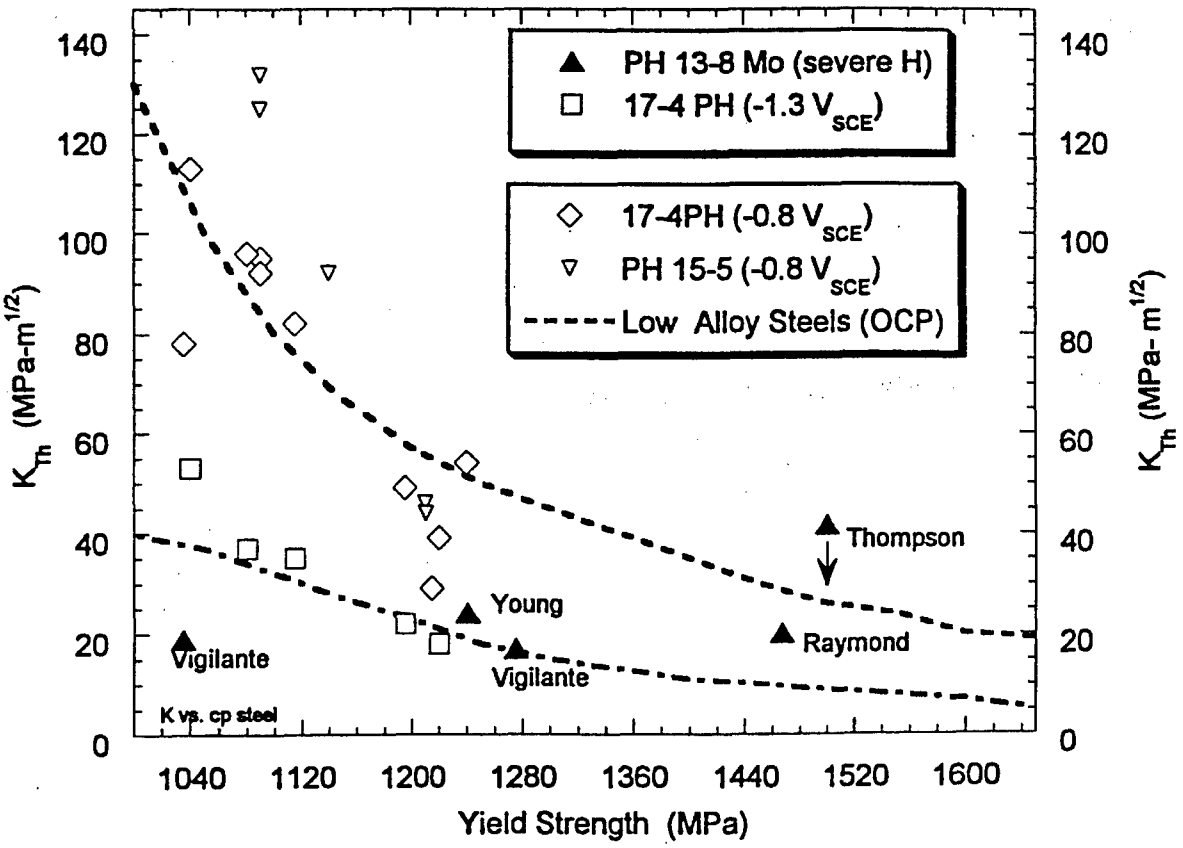

Figure 9. The yield strength dependence of the threshold stress intensity for HEAC of precipitation hardened martensitic stainless steels stressed in neutral to acidic H-producing electrolytes with substantial-applied cathodic polarization.. (Scully, 2002) The dashed trend lines reflect the bounds on σ_{YS} dependent K_{TH} for quenched and tempered low alloy steels tested at the open circuit potential (OCP). (Gangloff, 1986)

et al., 1973; Fritzemeier, 1990). Ensuing results have shown that iron-based alloys such as A286 and IN903 are susceptible to both IHAC and HEAC in high pressure H_2 (Perra and Stoltz, 1981; Moody et al., 1986; Moody et al., 1987; Moody et al., 1988; Moody et al., 1990; Moody et al., 1990b; Moody et al., 1991; Hicks and Altstetter, 1992; Moody et al., 2001). Other studies demonstrate that nickel-based superalloys IN718 and X-750 are prone to H-assisted cracking (Walter and Chandler, 1974, 1977; Hicks and Altstetter, 1992; Symons and Thompson, 1997; Symons, 1998, 2001; Hall and Symons, 2001). The tensile yield strengths of these materials were in the range from 800 to 1100 MPa when examined with regard to H cracking; however, yield strengths approaching 1400 MPa are possible. Hydrogen free superalloys crack by microvoid processes at high K_{IC}, but IHAC and HEAC progress by a mixture of IG separation and TG cracking associated with {111} slip planes in austenite (Moody et al., 1986; Moody et al., 1988; Moody et al., 1990b; Moody et al., 2001, Symons, 2001). The proportion of each mode depends on metallurgical variables such as grain size, as well as on H concentration, temperature, and CMOD-control mode. The IG cracking dominates for conditions that produce threshold stress intensity levels below about 50 MPa$\sqrt{m}$, while TG slip plane cracking is favored at lower H contents and higher thresholds.

As an example, H introduced to the crack tip process zone reduces substantially the stress intensity for H cracking in Fe-based alloy IN903 at 23°C, as established in Fig. 10 (Moody et al., 1988, 1990b). Considering IHAC, K_{IC} is lowered to $K_{IC\text{-}H}$ due to predissolved H interacting with relatively rapidly rising CMOD (□), and the threshold K at crack arrest during fixed CMOD loading (K_{IIHAC}, •) is also lowered by H precharging. Considering

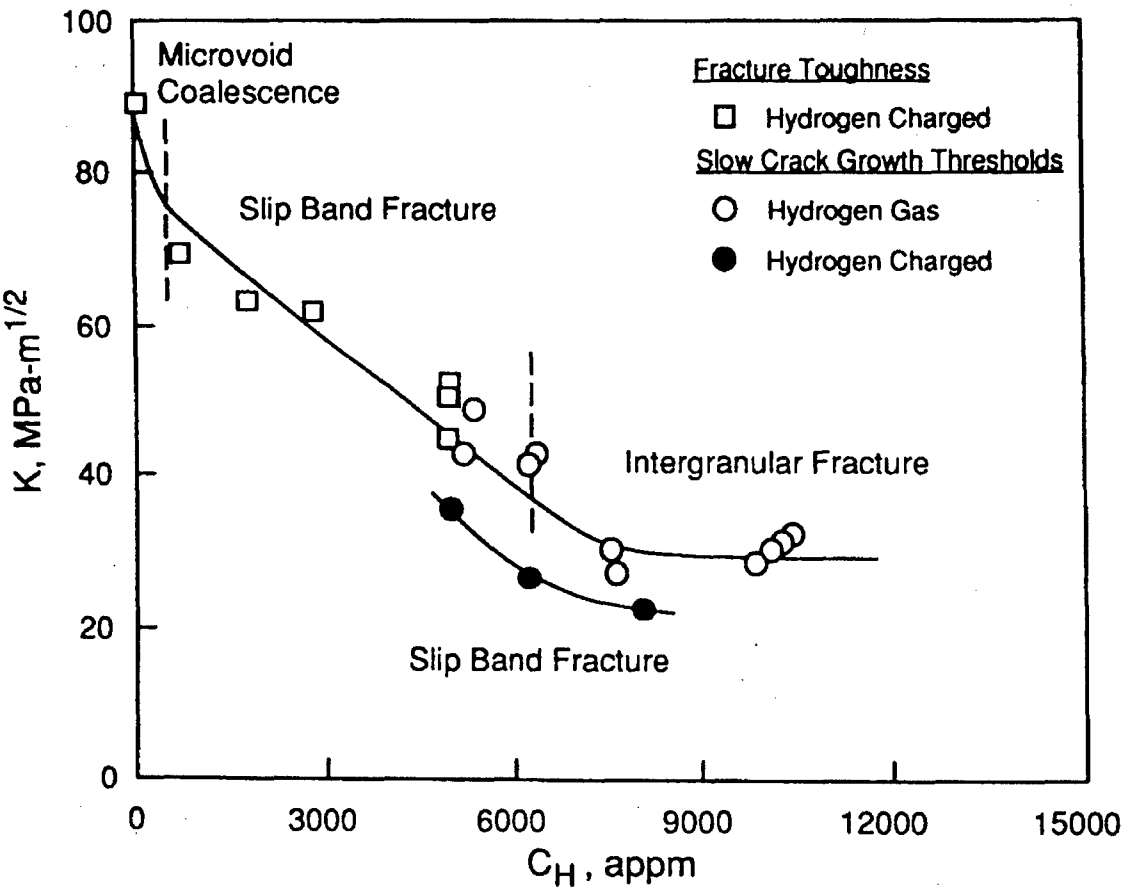

Figure 10. The crack tip total hydrogen concentration dependence of the threshold stress intensity for H-assisted cracking in precipitation hardened IN903 (σ_{YS} = 1080 MPa): (a) stressed with precharged H in moist air for either rising CMOD (9, $K_{IC\text{-}H}$ at dK/dt = 0.7 MPa$\sqrt{m}$/s) or fixed CMOD (•, K_{IIHAC}) loading conditions, and (b) stressed at fixed CMOD (o, K_{IHEAC}) in high pressure (20.7 MPa to 207 MPa) H_2 without precharging. All experiments were conducted at 23°C. The H concentration was calculated according to the method described in the text and amplified in 6.03.8. (Moody, Perra and Robinson, 1988, 1990b: Copyright The Minerals, Metals and Materials Society, reprinted with permission.)

HEAC in high pressure H_2 without H precharging, K_{IHEAC} (o) is well below K_{IC} and declines with increasing crack tip H content. In each case the concentration of atomic H at the crack tip was calculated based on experimental determination of the equilibrium H content for unstressed exposure of the superalloy in a given H_2 pressure (P_{H2}) and temperature (T) environment, coupled with enhancement due to crack tip hydrostatic stresses, as detailed in 6.03.8. The microscopic fracture path, be it microvoid cracking, slip plane cracking or IG cracking, is noted for each test condition. Symons reported identical fracture mechanics and fractographic results for IHAC and HEAC in a high strength Ni-based superalloy (X-750) (Symons, 2001).

While results are less extensive, precipitation hardened Fe and Ni-based austenitic superalloys are sensitive to HEAC when stressed during exposure to electrolytes that are capable of producing H on crack tip surfaces. Underwood and coworkers confirmed that IN718 (σ_{YS} = 1115 MPa) suffers IG subcritical cracking during fixed CMOD stressing in NaCl solution with As_2O_3 addition and cathodic polarization to stimulate H entry into the metal at 23°C; K_{IHEAC} is less than 13 MPa$\sqrt{m}$ (Vigilante et al., 1997). Two other alloys, IN706 (σ_{YS} = 1110 MPa) and Fe-based A286 (σ_{YS} = 760 MPa) were not susceptible to HEAC during 2,000 h exposure in this environment.

Lillard confirmed the HEAC susceptibility of precipitation hardened superalloys, particularly IN718, stressed under slow-rising CMOD in aqueous-acidified chloride solution at 23°C (Lillard, 1998). The results in Fig. 11 show that K_{IH} is well below the plane strain fracture toughness of each of two microstructures for a wide range of applied electrode potentials that are cathodic relative to the free corrosion potentials. The STA microstructure

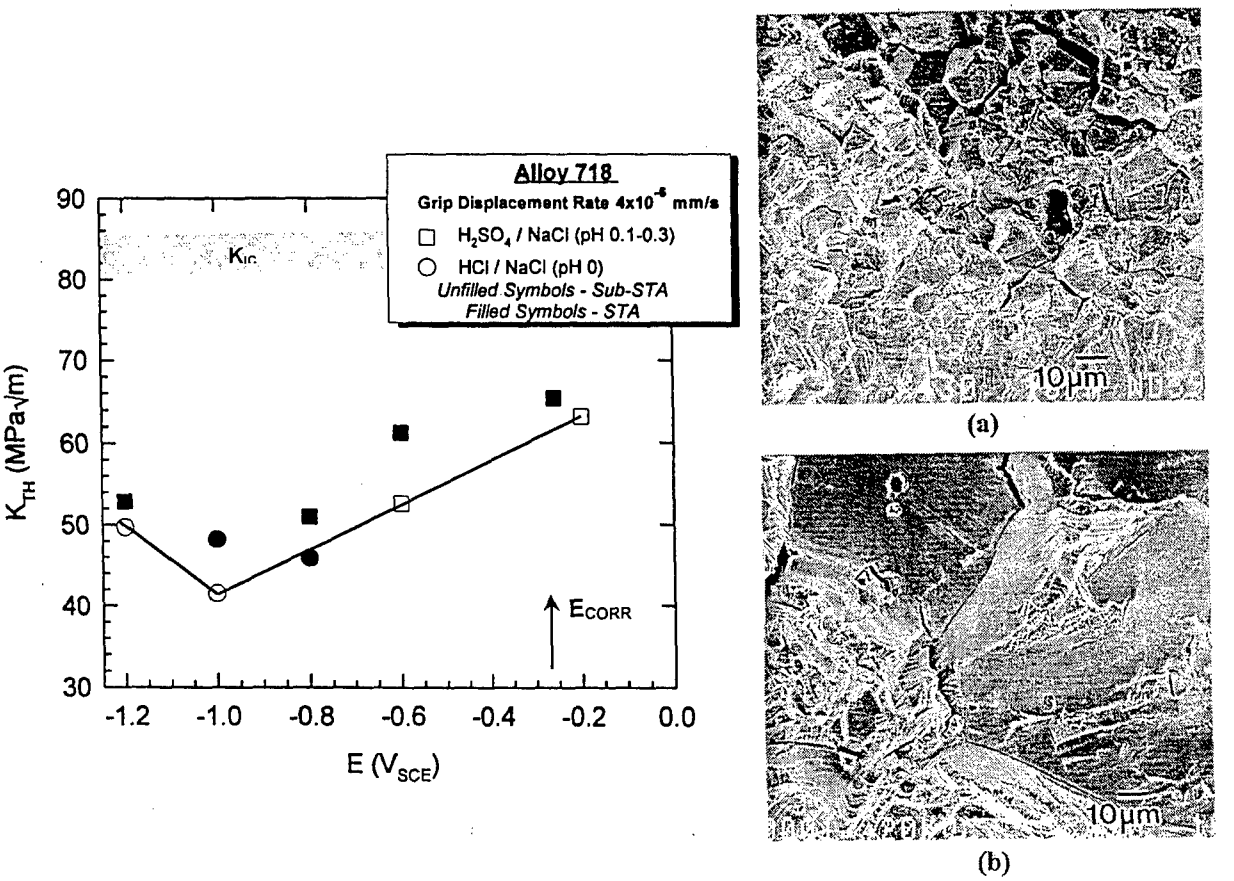

Figure 11. Threshold stress intensity for HEAC in peak aged IN718, stressed in acidified chloride solution with varying cathodic polarization and rising CMOD at a constant grip displacement rate of 4 x 10^{-6} mm/s yielding dK/dt = 6 x 10^{-4} MPa$\sqrt{m}$/s prior to the onset of subcritical crack growth. The free corrosion potential for this alloy and solutions is between –0.25 and –0.35 V_{SCE}. HEAC produced a mixture of intergranular and transgranular slip-plane based cracking, as shown by the SEM fractographs for: (a) Sub-STA with K_{IH} = 50 MPa$\sqrt{m}$ and (b) STA with K_{IH} = 53 MPa$\sqrt{m}$. (Lillard, 1998)

was solution treated above the δ-phase solvus then aged isothermally, resulting in large grain size characterized by a yield strength of 840 MPa and K_{IC} of 85 MPa$\sqrt{m}$. The Sub-STA microstructure was solution treated below this solvus for smaller grain size and higher precipitation-hardened strength (σ_{YS} = 990 MPa and K_{IC} = 81 MPa$\sqrt{m}$). The HEAC susceptibility is similar for each of these two metallurgical conditions; however, the finer grain size microstructure is more prone to subcritical cracking at somewhat lower thresholds for each level of cathodic polarization. The IN 718 cracked by microvoid processes in air, while HEAC produced a mixture of intergranular and TG slip-plane based cracking, with the proportions dependent on H content and grain size. IG cracking dominated for K_{TH} below 55 MPa$\sqrt{m}$, as illustrated by the SEM fractographic inserts in Fig. 11.

6.03.5.3 7000 Series Aluminum Alloys

High strength aluminum alloys; particularly the 7000 series that are precipitation hardened through addition of Zn, Mg, and Cu; are susceptible to severe intergranular and transgranular subcritical cracking in moist gaseous and electrolytic environments. Internal H-assisted cracking occurs as a result of unstressed preexposure to water vapor or moist air, typically at elevated temperatures (~100°C), and followed by stressing at ambient temperature (Scamans et al., 1976; Christodoulou and Flower, 1980; Tuck, 1985). This IHAC is also produced by electrochemical precharging of H (Gest and Troiano, 1974; Albrecht et al., 1977). Alternately, 7000 series aluminum alloys crack subcritically when stressed in water vapor or aqueous solutions typically containing chloride ions (Speidel and Hyatt, 1972; Speidel, 1975; Gruhl, 1984; Holroyd, 1990; Young and Scully, 2002).

Typical subcritical crack growth kinetics are presented in Fig. 12 for two peak aged 7000 series Al alloys (σ_{YS} ~ 500 MPa) stressed in either distilled water or aqueous chloride solution at the free corrosion potential and 23°C. This figure shows the variability in crack growth rate data for multiple-replicate experiments. The 7079 composition exhibits the fastest environment-assisted crack growth kinetics of all aluminum alloys examined to date. For both alloys, the stress intensity dependence of da/dt includes an apparent K_{IHEAC} between 3 and 7 MPa$\sqrt{m}$, strongly K-dependent Stage I cracking, and K-independent Stage II growth. The fracture toughness is likely above 25 MPa$\sqrt{m}$ for these alloys and crack orientation, and Stage III HEAC is not observed in Fig. 12.

A central feature of 7000 series aluminum alloys is that HEAC is mitigated and perhaps eliminated by overaging, provided that the alloy contains Cu (Sarkar et al., 1981; Holroyd, 1990). This behavior is illustrated for aluminum alloy (AA) 7050 in Fig. 13, where the extent of isothermal aging is indicated by electrical conductivity (Young, 1999; Young and Gangloff, 2001). (Specimens were solution treated, water quenched, and aged at 154°C or 163°C for times between 1 h and 30 h. The conductivity, as %IACS, increases monotonically with the evolution of precipitate nucleation and growth as solute is removed progressively from the aluminum lattice.) The crack orientation in Fig. 13 is the susceptible SL case, the solution is acidified chloride with chromate inhibitor at a fixed electrode potential, and the da/dt levels are typical of fixed-CMOD loading at Stage II K levels between 12 and 18 MPa$\sqrt{m}$. For commercial unrecrystallized AA7050, the da/dt decreases by over 5 orders of magnitude due to increased isothermal aging from the under to peak to overaged conditions. No crack growth was resolved for the overaged condition in the S

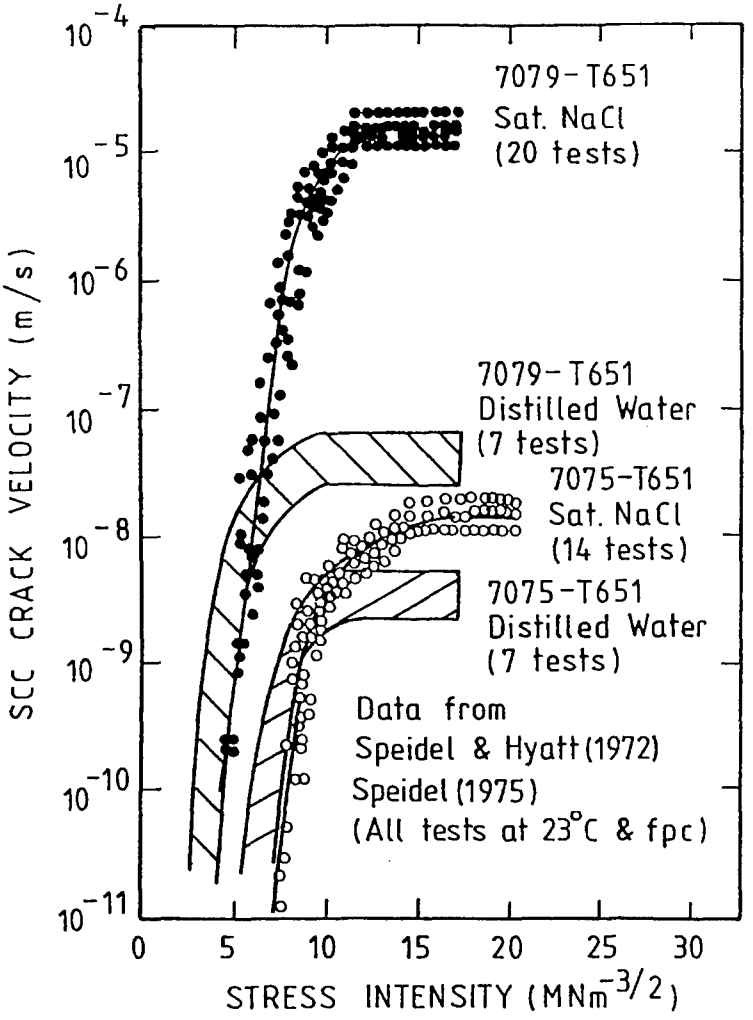

Figure 12. The stress intensity dependence of subcritical crack growth rate for two peak aged 7000 series aluminum alloys stressed in either distilled water or aqueous chloride solution at the free corrosion potential and 23°C. The crack orientation is TL (stress parallel to the transverse (T) direction and crack growth in the longitudinal or rolling (L) direction). (Holroyd, 1990; reproduced from Speidel and Hyatt, 1972; Speidel, 1975: Copyright NACE International, reprinted with permission.)

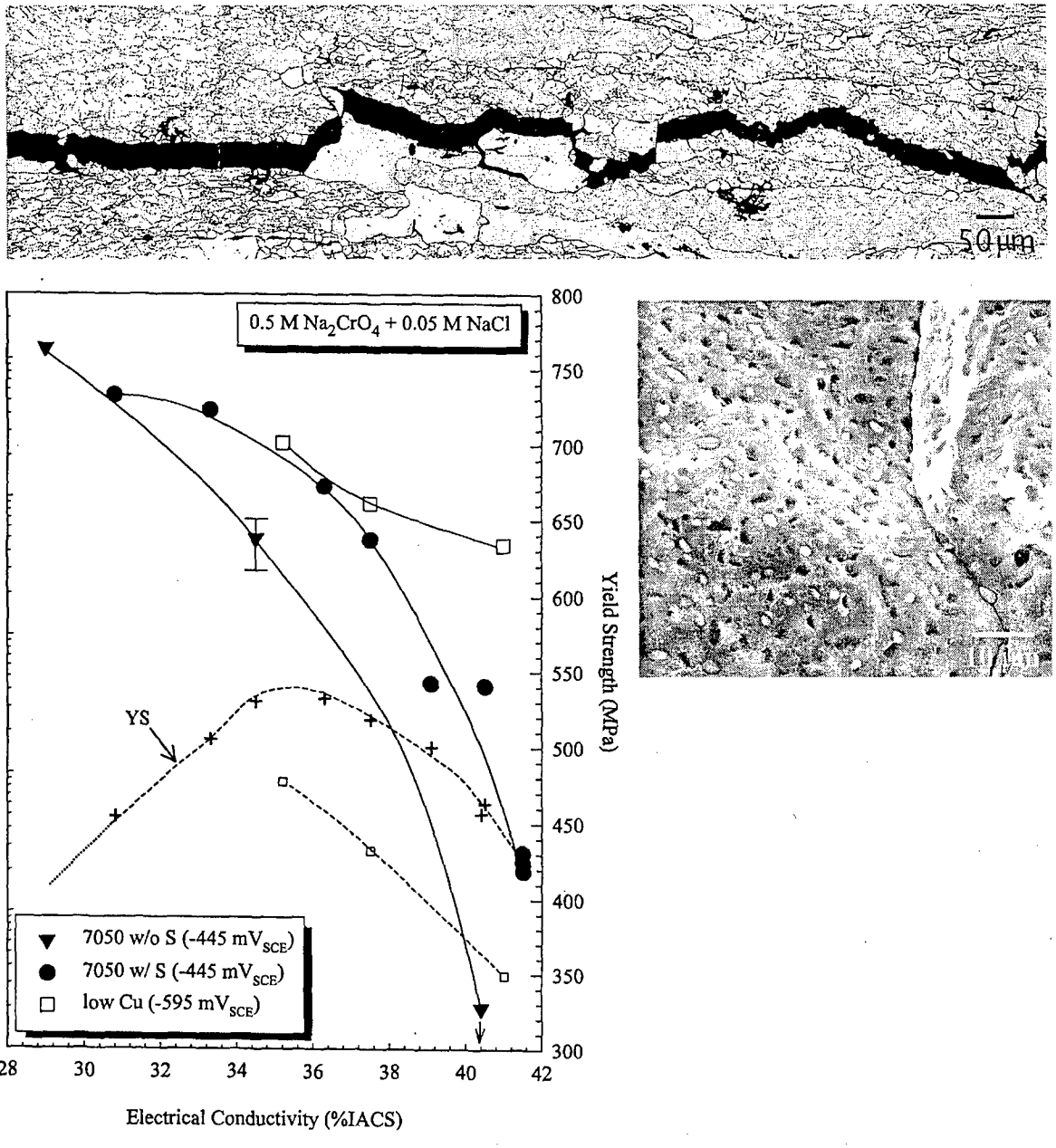

Figure 13. The effect of temper on steady state HEAC rate at fixed CMOD ($20 > K > 10$ MPa$\sqrt{m}$) and electrochemical conditions for S-free (□) and S-bearing (●) AA7050, as well as for low-Cu (□) AA7050. The aging dependence of yield strength is presented for S-bearing (+) AA7050 and low-Cu AA;7050 (□). The crack orientation is SL (stress parallel to the short transverse (S) direction and crack growth in the longitudinal or rolling (L) direction). The metallographic section (S-direction is vertical and L direction is horizontal) and fractograph show intergranular cracking in the T6 temper of S-bearing AA7050. (Young, 1999; Young and Gangloff, 2001)

phase (Al_2CuMg) free microstructure stressed in the environment for 30 days. The presence of S reduced the amount of Cu available to enable the beneficial effect of aging in AA7050. The severe HEAC produced in a Cu-free model composition is apparent, even for the overaged microstructure.

6.03.5.4 Beta Titanium Alloys

Body-centered cubic β-titanium alloys, hardened by fine precipitates of the hexagonally-close packed α phase, exhibit high strength-to-weight and corrosion resistance, but are susceptible to severe hydrogen assisted cracking (Feeney and Blackburn, 1970; Wanhill, 1975; Young et al., 1995). This cracking differs from the behavior of α and α + β titanium alloys discussed elsewhere in this volume (Chapter 6.3b) because the solubility of H in β is large and the brittle hydride phase is almost certain not to form or participate in H cracking (Gaudett and Scully, 2000; Teter et al., 2001). Two factors are necessary requisites for subcritical hydrogen cracking to occur in β/α-Ti alloys; a fatigue precrack, as well as a threshold amount of aging and/or the associated α must be present in the β matrix.

The occurrence of transgranular IHAC in a H-precharged peak aged β-Ti alloy is illustrated in Fig. 14 (Hayes, 2000; Gangloff, 2001). Fracture mechanics specimens of Ti-15V-3Cr-3Al-3Sn (weight pct) were solution treated and aged isothermally to produce increasing amounts of α precipitation and increased tensile strength. Specimens were then fatigue precracked, H charged to a level of 1300 ppm by an electrochemical method, and cracked under slow-rising CMOD in moist air. Surface oxide precluded significant H loss from the specimen during this testing. The critical stress intensity for the onset of stable

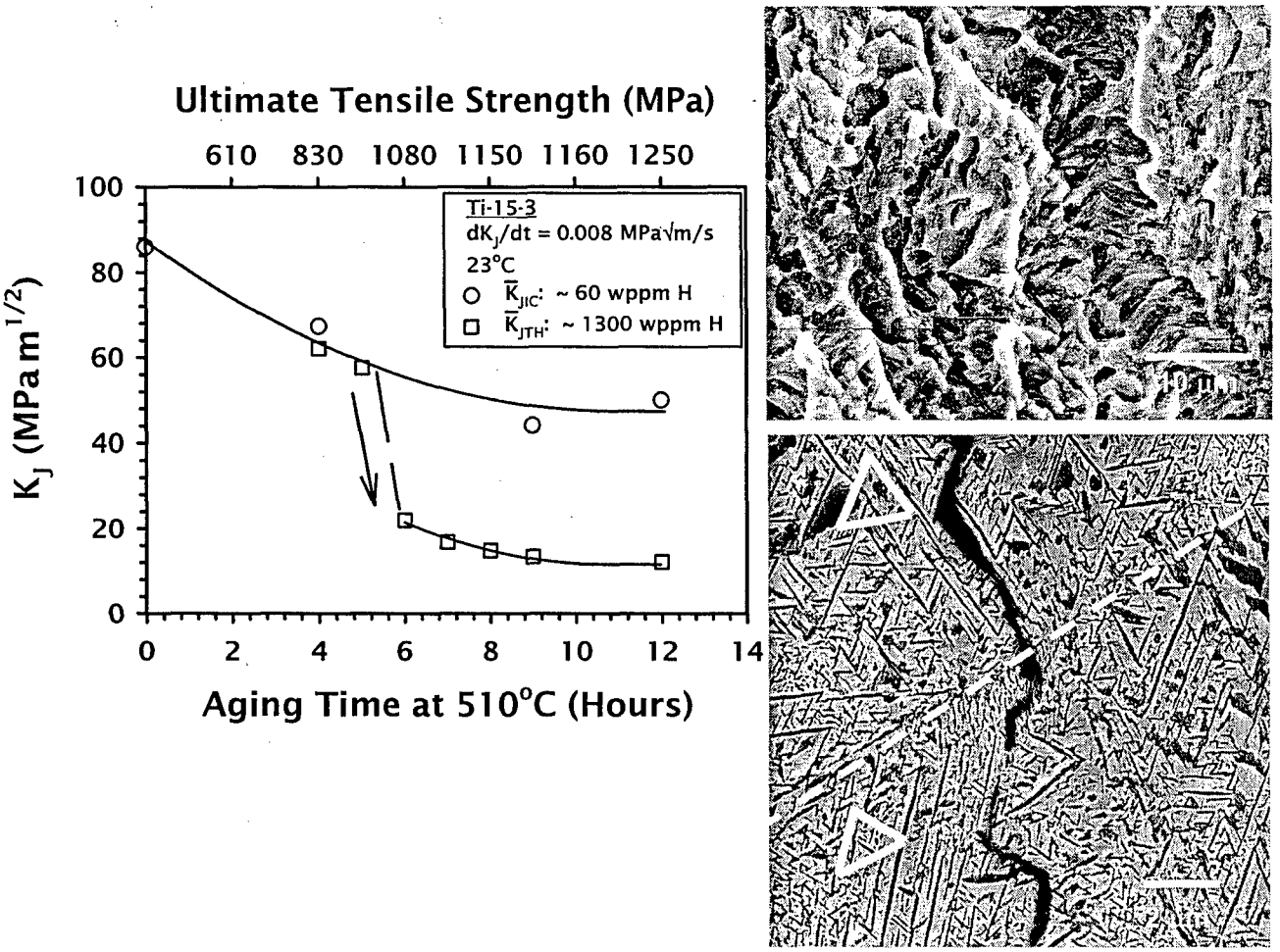

Figure 14. The isothermal-aging time and yield strength dependencies of plane strain fracture toughness at the as-processed H content of 60 ppm and threshold stress intensity for IHAC in H-precharged ($C_{H\text{-}TOT}$ = 1300 ppm) Ti-15V-3Al-3Sn stressed in moist air at 25°C. The SEM fractograph shows the morphology of transgranular IHAC for the 12 h age case and the metallographic cross-section shows that H-cracking progresses along β/α interfaces, with the α needles (dark phase) present in three variants shown by the triangles on either side of a high angle grain boundary (dashed line). The subscript, J, denotes elastic K calculated from the elastic-plastic J-integral, and the bar indicates the average of 1st initiation and blunting-line offset definitions of crack growth. (Hayes, 2000; Gangloff, 2001)

cracking in the H-charged microstructures equals the H-free fracture toughness, but only for aging times less than about 4 h. Specimens aged for longer times exhibit substantial IHAC. The short-term aged specimens that were immune to H cracking failed by microvoid processes, while a brittle TG morphology was produced where K_{IIHAC} was less than K_{IC}, as illustrated by the fractographic insert. This H cracking progressed along β/α interfaces, as shown in the metallographic section where the α needles (dark phase) are present in 3 variants shown by the white triangles on either side of a high angle grain boundary (dashed line). Similarly severe IHAC was reported for other β/α-Ti alloys, including Ti-3Al-8V-6Cr-4Mo-4Zr (Beta-C) and Ti-15Mo-3Nb-3Al (Gaudett and Scully, 1999, 2000; Young and Scully, 1994).

The HEAC behavior of aged β-Ti alloys is both similar and strikingly different from IHAC. Figure 15 shows that the all-β-phase microstructure of Beta-C, produced by solution treatment without aging, is immune to HEAC during rising-CMOD loading in neutral chloride solution. This immunity persists for the initial stage of α-precipitation hardening (Somerday, 1998b; Gangloff, 2001; Somerday et al., 2003). Continued aging and increased amount of α precipitation results in severe environment assisted cracking with K_{IHEAC} substantially less than K_{IC}. In contrast to IHAC of these alloys, subcritical cracking in chloride solution is essentially fully intergranular, as shown by the fractographic insert in Fig. 15. Similarly severe cracking was reported for the α-precipitation hardened β-Ti alloy, Beta-21S (Young et al., 1995).

The HEAC in β/α-Ti alloys stressed in neutral-aqueous chloride solution is notable in that the kinetics are rapid. The results in Fig. 6 show that the rising-CMOD K_{IH} is low for

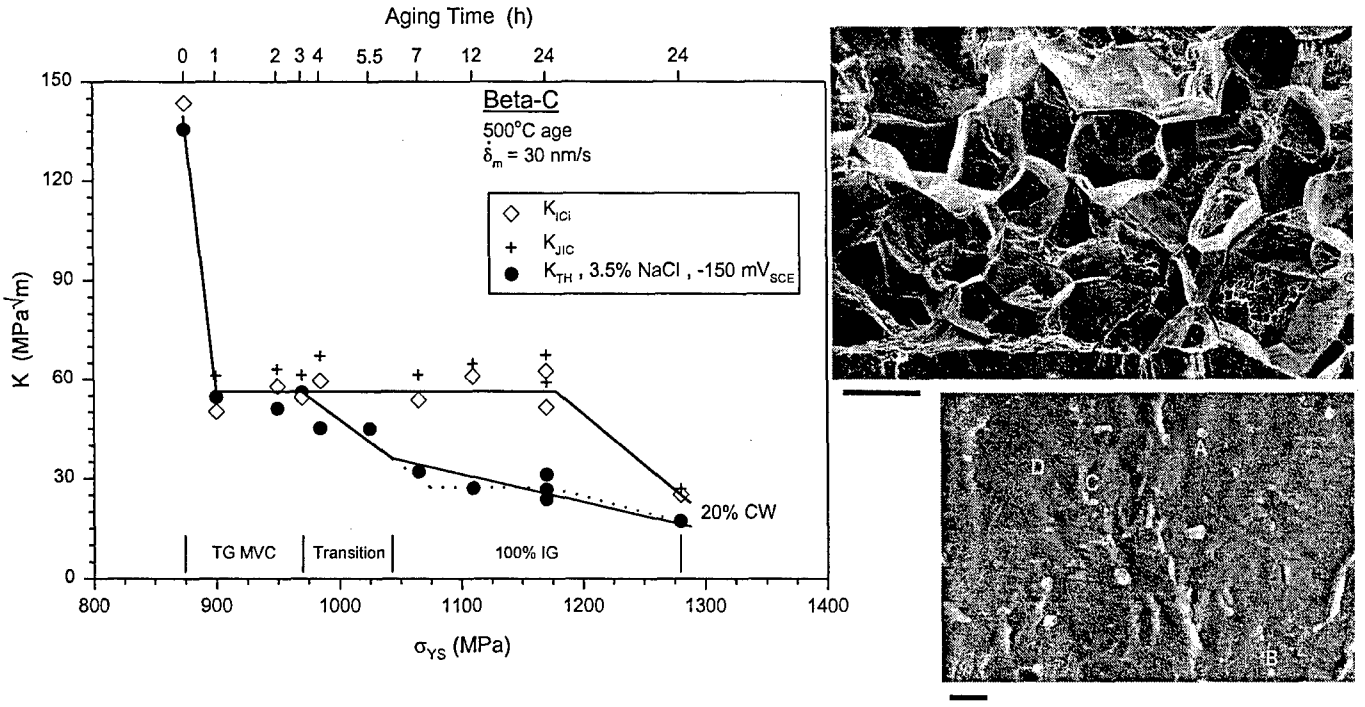

Figure 15. The strength and isothermal-aging time dependencies of fracture toughness and threshold K for the onset of HEAC in solution treated Beta-C (Ti-3Al-8V-6Cr-4Mo-4Zr) stressed under slow-rising CMOD (or δ_m) loading in moist air and aqueous-chloride solution at constant applied electrode potential of –150 mV_{SCE} and 25°C. The highest strength and lowest cracking resistances were achieved by 20% cold work (CW) prior to aging to stimulate fine-α precipitation. SEM fractographs show the morphology of 100% intergranular HEAC for the 6 to 24 h age cases (top, 100 μm bar) and the high magnification view of an IG facet surface in these STA microstructures (bottom, 250 nm bar), as amplified in Fig. 43. (Somerday, 1998; Somerday et al., 2002)

24h aged Beta-C and independent of loading rate for applied dK/dt between 0.0001 and 4 MPa$\sqrt{m}$/s; severe IG cracking can propagate under loading that rises over a period of less than 10 s (Somerday et al., 2000). Paralleling this behavior, subcritical rates of HEAC in these alloys are very fast, on the order of 10 to 40 μm/s, and independent of applied K as shown in Fig. 16.

6.03.6 IMPORTANT VARIABLES AFFECTING HYDROGEN CRACKING

The rate of subcritical H cracking is governed by K, as given by threshold and da/dt *vs.* K properties. However, a large number of mechanical, metallurgical, and environment chemical variables affect the kinetics of IHAC and HEAC. The more important effects of these variables are summarized. Mechanism-based explanations and quantitative model predictions of these effects are discussed in 6.03.8. The implementation of a fracture mechanics based structural integrity model requires that the variables relevant to the application be incorporated into the basic materials properties that define crack propagation threshold and rates.

6.03.6.1 Fracture Mechanics Variables

The mechanical variables that affect threshold and growth rate properties pertinent to IHAC and HEAC include loading format (fixed CMOD, rising CMOD or constant load) and rate (dK/dt) as discussed in 6.03.3.5. Data showing the effect of applied dK/dt on the threshold for HEAC were presented in Fig. 5 for a low alloy steel in pure H_2 and in Fig. 6 for a high strength β/α-Ti alloy in aqueous NaCl solution. The effect of loading rate on the

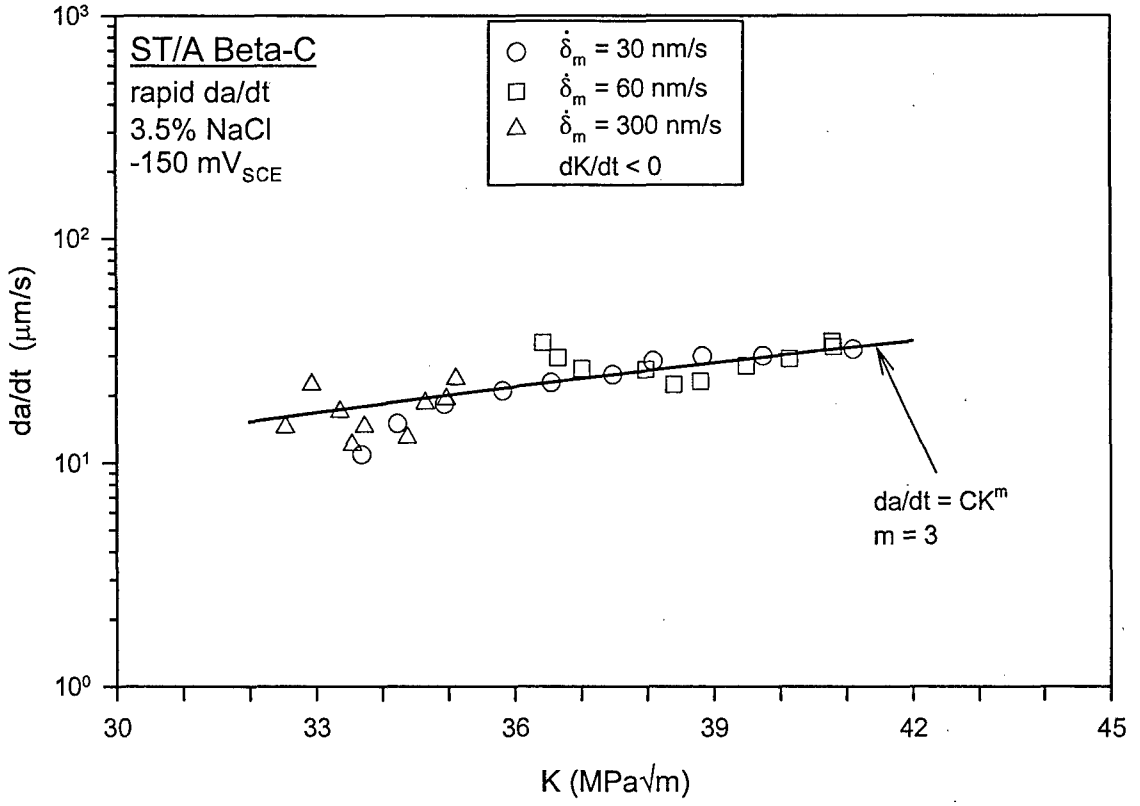

Figure 16. The stress intensity dependence of subcritical crack growth rate for intergranular HEAC in 24 h aged Beta-C stressed under slow-rising CMOD (or δ_m) loading in aqueous-chloride solution at a constant applied electrode potential of –150 mV_{SCE} and 25°C. The crack growth rates are independent of the applied loading rate between 30 and 300 nm/s (Somerday et al., 2000).

threshold stress intensity for IHAC in ultra-high strength steel is shown in Fig. 8. Additionally, loading mode (I, II or III, as well as mixed modes), cracked body constraint, small crack size, and load transients can affect crack propagation. These variables have not been studied broadly, as discussed in 6.03.9.1 on the issues that hinder the fracture mechanics prediction of H cracking life.

Researchers at the Naval Research Laboratory contended that the threshold stress intensity for HEAC is reduced by superposition of a small-amplitude cyclic (or ripple) load on a fixed or rising K (Bayles et al., 1993). Specific data were presented to show a strong reduction in the K_{IHEAC}, due to a cyclic K range ($\Delta K = K_{IHEAC} - 0.90$ to $0.95K_{IHEAC}$) for high strength steels (Pao, et al., 1991), a β/α-Ti alloy (Yoder et al., 1990; Pao, et al., 1996) and AA7075 (Pao, Gill and Bayles, 1991a). The reduction in the K_{IHEAC} in chloride solutions was substantial for alloys that otherwise resisted environmental cracking and exhibited a relatively high K_{IHEAC} from quasi-static loading experiments, including overaged AA7075 compared to AA7075-T6 and lower strength martensitic steel compared to higher strength 4340 (Pao et al., 1991, 1991a). The results of the experiments presented to date are best interpreted as high mean stress environmental fatigue crack growth (Gangloff, 1990; Horstmann and Gregory, 1991). A material that resists quasi-static HEAC will exhibit a large ripple load effect if the alloy is susceptible to high mean stress environmental fatigue at low stress intensity amplitudes and a maximum K level that is below the static K_{IHEAC}. In this interpretation, ripple loading is not an intrinsic aspect of quasi-static load HEAC, and correlation of H-assisted quasi-static and fatigue crack propagation data on a single plot of maximum K levels *vs.* time to failure is misleading (Bayles et al., 1993). For example, a

ripple load will cause stable cracking at maximum K levels below K_{IC} for an alloy in ultra-high vacuum. The toughest alloys will show the largest effect of the ripple load. However, there is no novel environmental damage involved, but only crack tip fatigue and the problem is best viewed in this context.

Cyclic loading at low stress intensity amplitudes and a wide range of maximum K levels should exacerbate H assisted cracking in high strength alloys (Gangloff, 1990). Whether this is claimed as a novel ripple load effect in H cracking, or environment assisted fatigue crack growth is unimportant. The key is to explain the effect of K variation on crack tip H production, uptake and damage in the context of a micromechanical-chemical model (6.03.8). No definitive results have been reported to explain a unique small-amplitude cyclic load effect on a basic element of the HEAC scenario (Fig. 2) and H damage mechanism (6.03.7). The fertile area for such study is at very low ΔK, below 0.5-1 MPa$\sqrt{m}$. For example, cracking in AA7075-T6 in chromate-chloride solution progressed at a da/dt_{II} level of 4×10^{-6} mm/s for a constant K of 13 MPa$\sqrt{m}$ (Mason and Gangloff, 1994). This da/dt did not increase when K was cycled from 13 to 12.3 MPa$\sqrt{m}$ at frequencies of 5 Hz or 30 Hz, demonstrating the lack of an effect for a system where ripple plasticity could destabilize the crack tip passive film from chromate addition. Rather, this time-based rate is consistent with the expected-small effect of cyclic loading from superposition of a corrosion fatigue growth rate and the quasi-static da/dt. Additional work is required to explore the interface between monotonic and cyclic loading effects in H cracking of high strength alloys. Ripple loading critically influences environment-sensitive crack propagation in low strength alloys through film rupture considerations (Parkins, 1990, 1991).

6.03.6.2 Metallurgical Variables

A broad literature exists describing the effects of metallurgical variables on IHAC and HEAC, as reviewed elsewhere (Bernstein and Thompson, 1976; Thompson and Bernstein, 1980). Fundamental interpretation and application of such results to structural integrity modeling is compromised by three factors: (a) yield strength varies concurrently with one or more microstructure changes to affect crack tip mechanics, (b) a metallurgical effect on H cracking can vary in different regimes of chemical and mechanical variables, and (c) mechanisms of H production, uptake and damage are controversial. Examples of recent results are reviewed to amplify the data presented in previous sections. These findings represent improved attempts to account for these important interactions.

6.03.6.2.1 Alloy Strength

Invariably, IHAC and HEAC are exacerbated by increased yield strength, as manifest by decreased K_{TH} and increased da/dt. The largest body of data on the strength dependence of H cracking exists for steels, as illustrated in Fig. 17. Lower bound trend lines represent over 400 measurements of the threshold stress intensity factors for IHAC and HEAC in C-Mn ferrite-pearlite and martensitic alloy steels exposed to a variety of IHAC and HEAC environmental conditions at 23°C (Gangloff, 1986, 1988). The trend lines marked "JSW" and "Thermally Charged Hydrogen" represent the data base for IHAC in tempered bainitic Cr-Mo steels, with a portion of these data shown previously in Fig. 7, as well as limited results for low alloy martensitic steels at higher strengths. The JSW line from Fig. 7 illustrates the strong effect of rising-CMOD loading on K_{TH}, mainly for lower strength steels

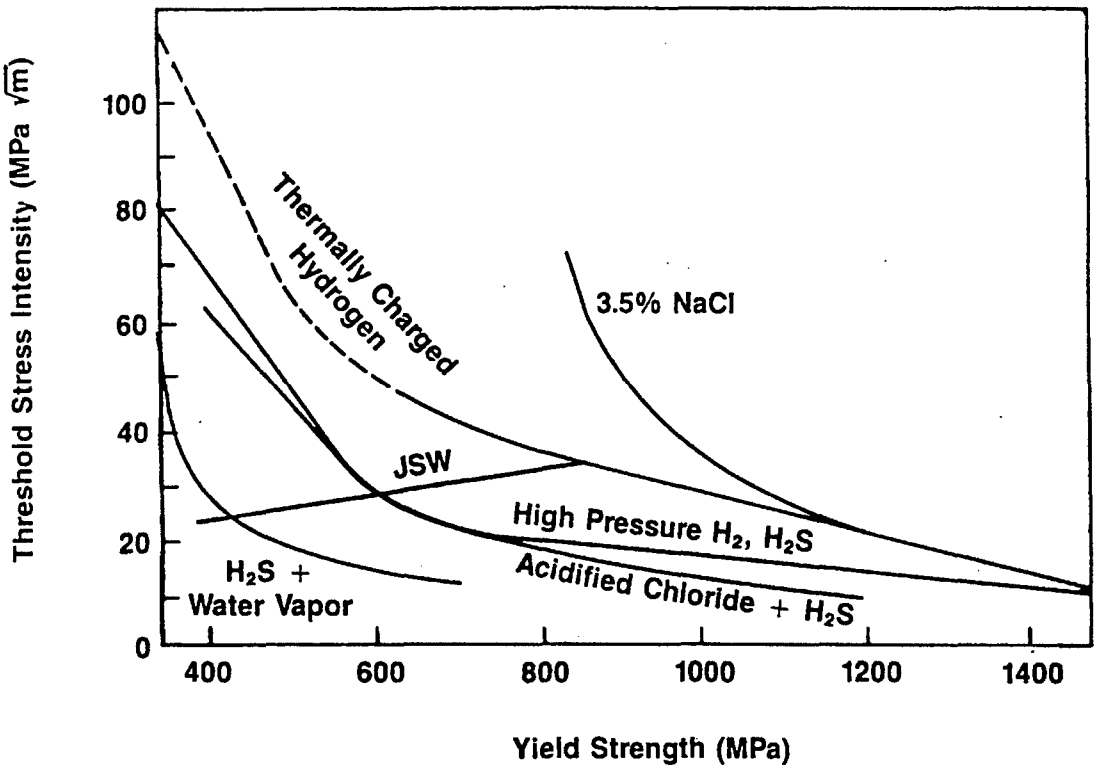

Figure 17. Lower bound trend lines drawn to represent the results of over 400 measurements of the threshold stress intensity factor for IHAC and HEAC in C-Mn and alloys steels exposed to a variety of IHAC and HEAC environmental conditions at 23°C. JSW refers to results reported by the Japan Steel Works in the early 1980s, specific to rising CMOD loading (see Fig. 7). Most other thresholds were measured for quasi-static loading, typically involving crack arrest. (Gangloff, 1986, 1988).

and compared to the standard quasi-static crack arrest thresholds that was measured for the other trend lines in Fig. 17 (see 6.03.3.5.1). The remaining curves describe HEAC in several environments including 3.5% NaCl solution at free corrosion, high pressure H_2 and H_2S gases, acid-chloride solution saturated with H_2S gas, and a mixture of water vapor and H_2S.

For each environment, the strength dependence of the threshold stress intensity exhibits two regimes of behavior; K_{TH} decreases with increasing steel yield strength, sharply at the lower strengths and more gradually in the high to ultra-high strength regime. The location of this transition shifts to lower σ_{YS} as the hydrogen-producing activity of the environment increases. Specific data are presented in Fig. 18 for martensitic low alloy steels in near-neutral NaCl solution, with the mild strength dependence suggested for σ_{YS} exceeding about 1350 MPa. A similar result was reported for 4340 steel in low pressure H_2 (Moody et al, 1990). A second result is shown in Fig. 9 for martensitic stainless steels tested under HEAC conditions (Scully, 2002). The K_{TH} declines strongly with increasing strength in the lower strength regime, with a reduced dependence on strength, or perhaps a plateau, at σ_{YS} above about 1300 MPa. The data in Figs. 9, 17 and 18 establish that steel strength is particularly important for lower strength alloys and/or mildly aggressive environments where immunity to hydrogen cracking may be observed. However, aggressive H production or rising-CMOD loading promote embrittlement in the lowest strength alloys. Increasing steel strength from 1300 to 2000 MPa and above does little to exacerbate already severe embrittlement.

The influence of strength on IHAC and HEAC in Ni, Ti and Al alloy systems is not clearly defined, in part because strong and concurrent microstructure effects complicate the

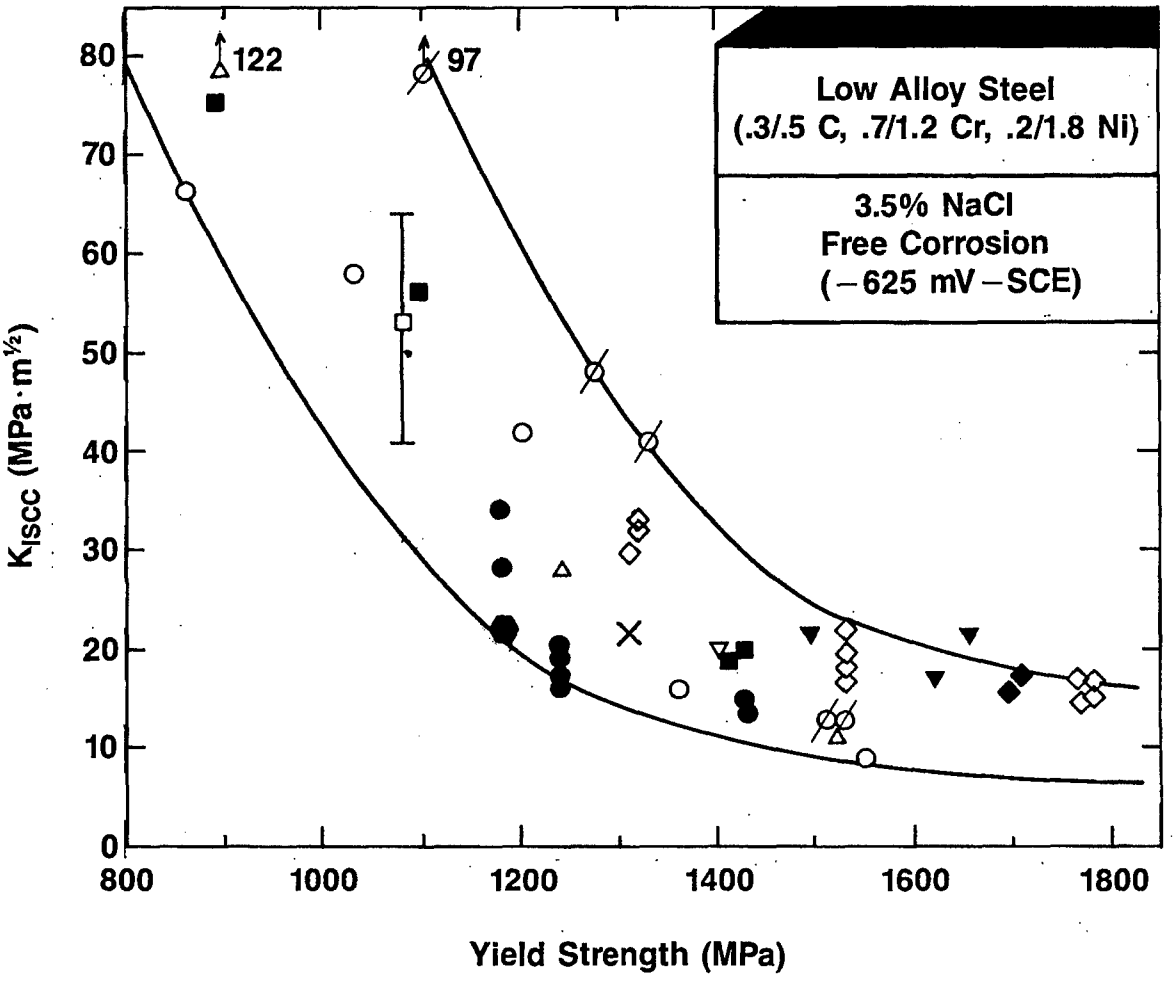

Figure 18. The yield strength dependence of the threshold stress intensity factor for HEAC in tempered martensitic steels cracked quasi-statically during stressed exposure in near-neutral NaCl solution at free corrosion potentials and 23°C. (Gangloff, 1986).

intrinsic strength effect.

6.03.6.2.2 Alloy Composition and Microstructure

6.03.6.2.2.1 7000-series Al alloys: Cu Content and Precipitate Condition

Alloy composition and microstructure dominate the IHAC and HEAC resistance of precipitation hardened 7000 series aluminum alloys (Holroyd, 1990; Burleigh, 1991; Starke and Staley, 1995). Examples include the effect of aging on HEAC in Cu-bearing AA7050 stressed in either chromate-chloride solution, Fig. 13 (Young, 1999; Young and Gangloff, 2001), or water vapor saturated air, Fig. 19 (Young and Scully, 2002). For all cases in Figs. 13 and 19, the H-assisted subcritical crack growth rate declines monotonically with increasing aging time, while tensile yield strength exhibits the expected maximum at an intermediate aging time. All cracking in Figs. 13 and 19 is intergranular for the susceptible SL crack orientation. While strength should play a role in HEAC susceptibility (6.03.8), changes in solute content and precipitate microstructure dominate the cracking response in these Al alloys. This conclusion is supported by the fact that the Cu free alloy in Figs. 13 and 19 exhibits the lowest strengths but highest rates of da/dt for HEAC at each aging time.

The mechanism for the aging dependence of HEAC in 7000 series aluminum alloys is unclear in spite of 40 years of research (Speidel, 1975; Thompson and Bernstein, 1980; Pickens et al., 1987; Holroyd, 1990; Burleigh, 1991; Young, 1999; Young and Scully, 2002). The problem is complex since several aspects of the precipitate-matrix microstructure likely affect one or more of the elements involved in HEAC, including crack chemistry evolution, H production at the crack tip, H uptake into the FPZ, H transport to damage sites,

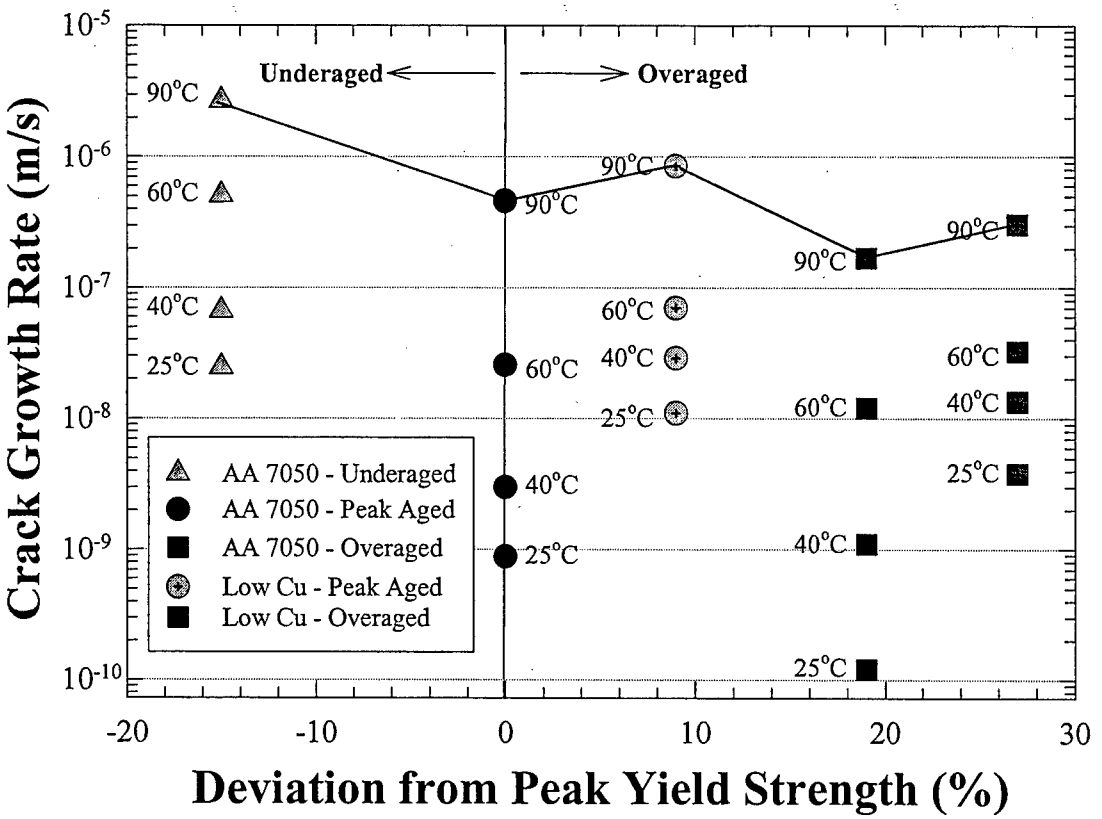

Figure 19. The yield strength, precipitate microstructure, and temperature dependencies of the subcritical HEAC growth rate in AA7050 and a low-Cu model alloy stressed in water vapor saturated moist air. (Scully and Young, 2002: Copyright The Minerals, Metals and Materials Society, reprinted with permission.)

and the H embrittlement mechanism (Fig. 2). These microstructural factors change concurrently during aging, and direct observation of such changes interacting with H damage in the crack tip FPZ is hindered by the sub-micrometer scale and highly gradated-transient character of these processes. For example, changes during under through peak to overaging aging include: (a) increasing amount and changing Al/Zn/Mg/Cu content of grain boundary precipitates that affect local electrochemical reactions and act as trap sites for H, (b) increasing thickness and changing composition of soft precipitate free zones adjacent to grain boundary precipitates that affect strain localization and electrochemical reaction kinetics, (c) increasing and/or decreasing amounts of grain boundary segregation of elements such as Zn, Mg and Cu, and (d) planar-heterogeneously localized to homogeneous slip transition due to changing interaction of dislocations with intragranular precipitates that evolve from solute zones through coherent then incoherent particles. Given these complex interactions, it is no wonder that the governing mechanisms for the aging dependence of HEAC in 7000 series alloys remain elusive.

The composition and heat treatment of modern 7000 series alloys are tailored for strength and H cracking resistance (Starke and Staley, 1995). Heat treatment focuses on controlled solution treatment temperature plus heating/cooling rates, followed by multi-step aging (Holroyd, 1990). For example, the retrogression and reaging process couples short-term high temperature aging of under or peak aged alloy to achieve HEAC resistance with a subsequent low temperature-aging step for high strength (Thompson, et al., 1987).

6.03.6.2.2.2 Beta-Ti Alloys: Alpha Precipitation

The opposite situation exists for the age hardened β-Ti alloys, where susceptibility to transgranular IHAC and intergranular HEAC increases with increasing isothermal aging. For the two alloys represented in Figs. 14 and 15, the thresholds for IHAC and HEAC decline monotonically with increased precipitation of fine α particles and the associated increase in yield strength (Somerday, 1998b; Hayes, 2000; Gangloff, 2001; Somerday et al., 2003). Neither strength nor H cracking susceptibility decrease for the increasing isothermal aging times examined. In this case H cracking is likely to be exacerbated by an interaction of increasing amount of the deformable α phase in the microstructure, as well as increasing macroscopic strength without overaging.

Experiments were conducted to separate these contributions to HEAC by cold working the single-β phase microstructure to various levels and thus yield strengths. The all-β microstructure of Beta-C was immune to both IHAC and HEAC for cold work levels from 0 to 80 pct, suggesting that IG cracking is promoted primarily by a metallurgical property associated with aging and not by increased yield strength or decreased work hardening (Somerday and Gangloff, 1998, 1998a; Gaudett and Scully, 2000). The precise mechanism for the effect of aging on H cracking susceptibility of β/α-Ti alloys was not established, but may involve elemental segregation to β/α interfaces during aging, as well as the micromechanics of plastic deformation in the β/α mixture where each phase is capable of plastic deformation with the possibility of microscopic constraint (Somerday et al., 2003).

6.03.6.2.2.3 Nickel Superalloys and Steels: Grain Size

Austenite grain size affects the H cracking resistance of precipitation hardened superalloys, as well as high strength martensitic steels (Bernstein and Thompson, 1976; Moody et al., 1990). The results (•) in Fig. 20 show that the threshold stress intensity for HEAC in Fe-based IN903 stressed during exposure in high pressure (207 MPa) H_2 increases with increasing grain size, d, following a relationship of the form $K_{IHEAC} \alpha \sqrt{d}$ (Moody and Robinson, 1990; Somerday and Moody, 2001). A similar grain size effect is shown by the K_{IHEAC} data in Fig. 11 for IN718 stressed in acidic solutions (Lillard, 1998).

A compilation of data for H-cracking in high strength martensitic 4340 steels showed a similar-strong grain size effect on K_{TH} for a single study involving IHAC (o in Fig. 20) (Lessar and Gerberich, 1976), but only a mild to nil dependence on $\sqrt{d}$ for two heats of commercial 4340 steel tested in aqueous environments constituting HEAC (□ and ∀ in Fig. 20) (Procter and Paxton, 1962; Carter, 1969). Kameda showed that K_{TH} was independent of prior austenite grain size, from 40 to 500 μm, for H_2-assisted cracking in two high purity laboratory heats of Fe-3.5Ni-1.7Cr-0.3C (Kameda, 1986). The threshold for cracking declined modestly for the largest grain size when the steel was doped with P impurity. With increasing grain size, da/dt decreased for the pure steel and increased for the impure alloy. For each grain size and purity, HEAC was severe and intergranular.

Interpreting the effect of grain size on H cracking is complicated since several microstructural factors change as grain size increases. For example, the results in Fig. 20 for IN903 reflect an intrinsic grain size dependence since σ_{YS} did not vary significantly with grain size in this precipitation hardened alloy. In contrast, strength decreased with

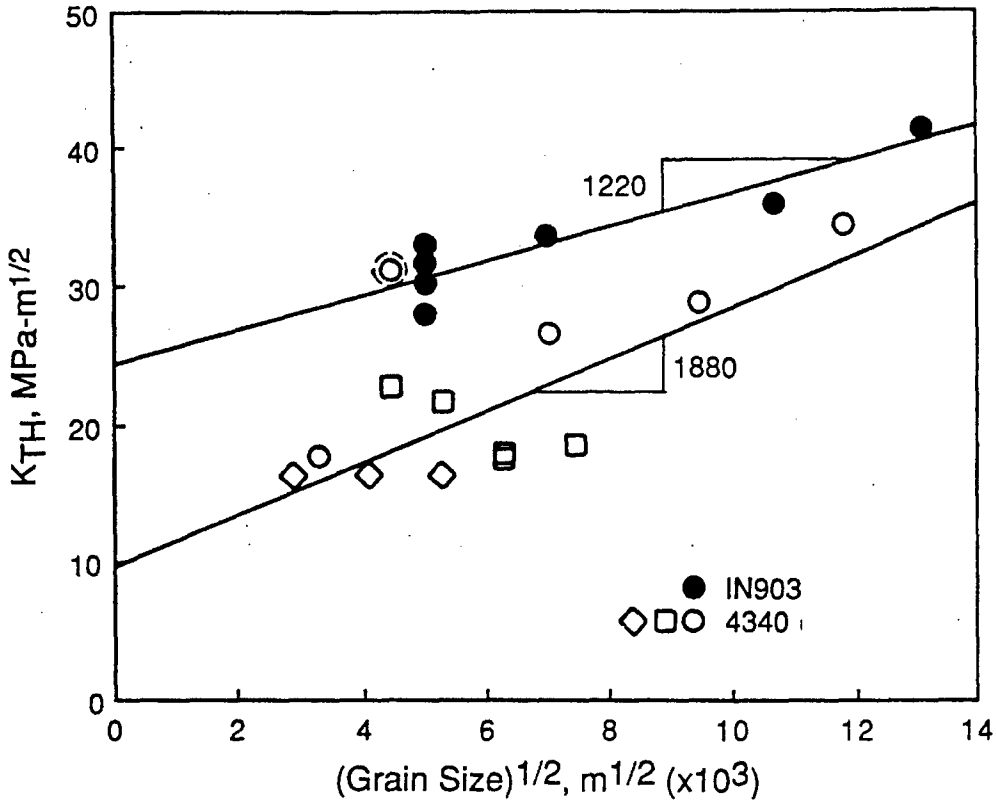

Figure 20. The austenite grain size dependence of the threshold stress intensity factor for subcritical HEAC in iron-based superalloy IN903 in high pressure H_2 (•), as well as for HEAC (∀ and 9) and IHAC (o) in tempered martensitic AISI 4340 steel, all at 23°C. (Moody, Robinson and Garrison, 1990: Reprinted with permission from Elsevier.)

increasing grain size for 4340 steel, and to some extent for the IN718 data in Fig. 11. Additionally, the amount of impurity segregation (see 6.03.6.2.2.4) may decrease as grain size increases for Fe and Ni-based alloys, since higher temperatures in the austenite phase field are employed to achieve increased grain size (Kameda, 1986). These factors should reduce susceptibility to H cracking with increasing grain size. Understanding the grain size effect in the superalloy is further complicated by a change in H-crack path, from IG for fine grain size to TG for large grain sizes (Somerday and Moody, 2001). This behavior was interpreted based on a fundamental change in the governing-H cracking mechanism, from grain size sensitive crack tip stress-based damage in fine grain size microstructures, to grain size independent damage governed by plastic strain in the large grain size conditions.

6.03.6.2.2.4 Steels: Purity

Metalloid impurity elements affect the intergranular H cracking resistance of martensitic steels. Elements such as P, S, Sn, As, or Sb segregate to and embrittle prior austenite grain boundaries in martensitic microstructures in the absence of hydrogen (Briant and Banerji, 1978, 1983), and moreover, interact with H to promote intergranular IHAC and HEAC. The literature on impurity effects on H cracking in low alloy steels is broad (McMahon, 2001) and this issue is particularly important for moderate strength steels with $\sigma_{YS} < 1000$ MPa (Yoshino and McMahon, 1974; Viswanathan and Hudak, 1977). Boundary segregation effects have been considered as a factor in the H cracking of β/α-Ti alloys (Somerday et al., 2003), 7000 series Al alloys (Pickens, et al., 1987; Holroyd, 1990) and superalloys (Moody et al., 1990), although systematic studies are lacking for these nonferrous alloys.

Two important correlations, reproduced in Figs. 21 and 22, establish the effect of purity on H cracking in high strength steels (Bandyopadhyay et al., 1983). Tempered martensitic 4340-type steels were processed for varying P, S, Si and Mn; tempered to vary σ_{YS} between 1200 and 1900 MPa, and cracked subcritically by stressed exposure in pure H_2 at pressures between 30 and 200 kPa and 23°C. Considering these data *in toto*, Fig. 21 shows that K_{IHEAC} declines from the H-free K_{IC} of about 130 MPa$\sqrt{m}$ to 15-20 MPa$\sqrt{m}$, correlating with the increase in percentage of IG cracking from 0 to 100%. The K_{IHEAC} decreases uniquely with increasing composition parameter, Ψ, as established in Fig. 22. This parameter is the sum of the bulk amounts of impurity (S and P), Mn and Si that promote segregation of impurities to austenite boundaries, and the H present in the crack tip FPZ. This H content was computed based on H solubility from H_2 (proportional to $\sqrt{P_{H2}}$ at constant T) and enhanced by crack tip hydrostatic stress (6.03.8). These correlations demonstrate that the deleterious effects of hydrogen and impurity elements are additive since a single trend represents the range of H contents from varying H_2 pressure, as well as different impurity contents from steel processing. This impurity parameter, without the H contribution, correlated the relatively low K_{IHEAC} values (15-25 MPa$\sqrt{m}$) for AISI 4340 steel stressed during exposure to aqueous NaCl solution (Moody et al., 1990). In this view, H affects grain boundary fracture resistance analogous to other impurity elements, consistent with the decohesion theory summarized in 6.03.7.

The practical implication is that production of high strength martenstic steels of high purity substantially eliminates IHAC and HEAC. For example considering high and ultra-high strength steels, Olson speculated that IG hydrogen cracking is eliminated by rare-earth

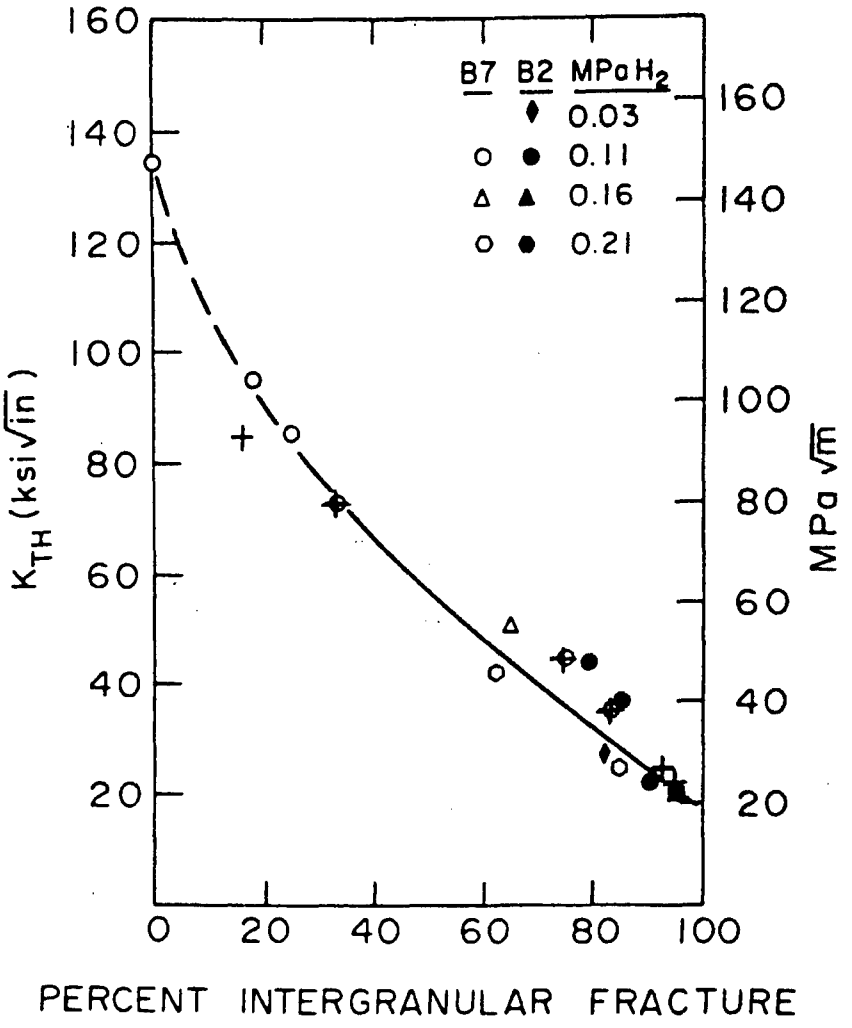

Figure 21. The correlation between the amount of IG cracking and K_{IHEAC} for tempered martensitic low alloy steels of the AISI 4340 base composition stressed during exposure in moderate pressure H_2 at 23°C. (McMahon, 2001; Bandyopadhyay et al., 1983: Reprinted with permission from Elsevier.)

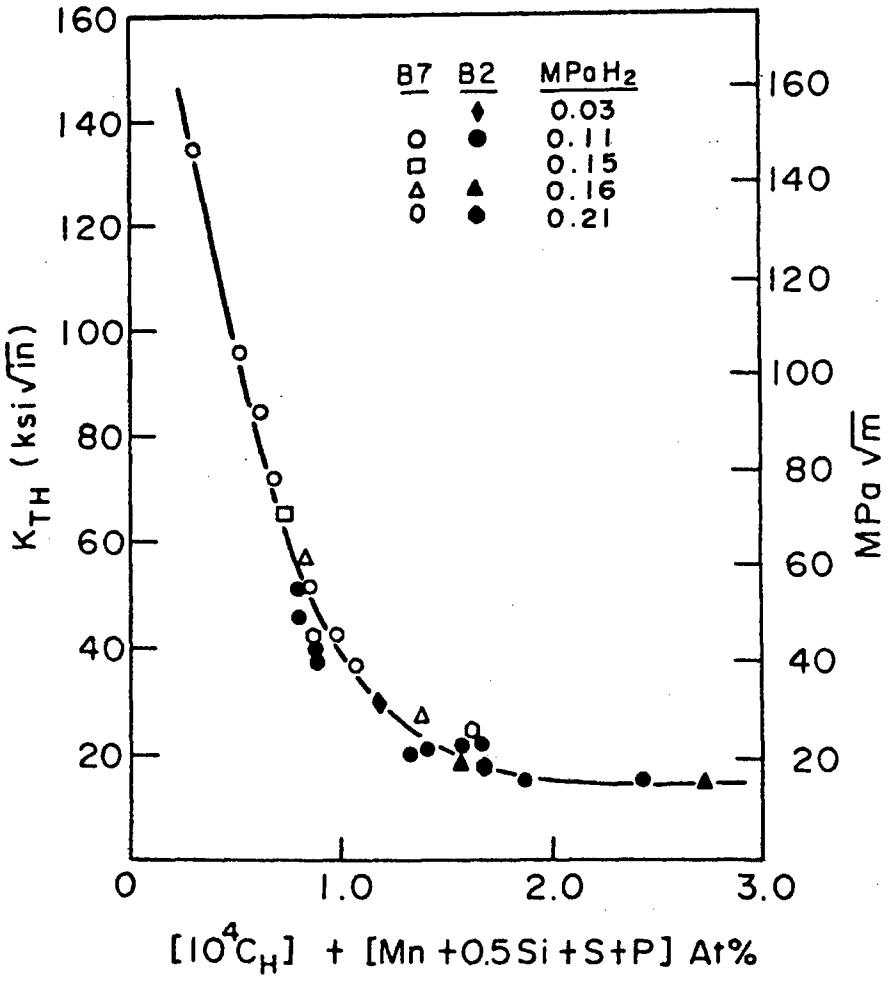

Figure 22. The H and metalloid impurity concentration dependence of the K_{IHEAC} in tempered martensitic low alloy steels of the AISI 4340 base composition stressed during exposure in moderate pressure H_2 at 23°C. (McMahon, 2001; Bandyopadhyay et al., 1983: Reprinted with permission from Elsevier.)

addition that reduces grain boundary impurity segregation (Olson, 1987, 1997). Unfortunately, severe embrittlement is encountered in modern steels that are processed for high purity and ultra-high strength. High strength 18Ni Maraging steels contain only trace levels of P, S, Si and Mn, but are susceptible to severe intergranular IHAC and HEAC as illustrated in Fig. 3 (Dautovich and Floreen, 1977). Severe embrittlement is produced in high purity martensitic stainless steels at high strength levels, Fig. 9 (Scully, 2002). AerMet®100 is produced by double-vacuum melting to yield ultra-low S and P levels, and neither Mn nor Si are added. However, this UHSS is prone to IG HEAC in acids and near-neutral chloride solutions with cathodic polarization, but less so than less pure steels (Buckley et al., 1993; Buckley et al., 1994; Oehlert and Atrens, 1998; Vigilante et al., 2000).

Approaches to produce H-cracking resistant high strength steels by improving the purity of prior austenite grain boundaries are ineffective for two reasons. First, micromechanical models of interface decohesion suggest that H trapping and very high stress at a crack tip are sufficient to promote hydrogen embrittlement without a dominant impurity contribution (6.03.8). Second, high strength steels are susceptible to severe transgranular H cracking, as illustrated by the low K_{IIHAC} results for AerMet®100 steel (Fig. 8). Grain boundary composition is not therefore a primary factor in the H cracking of high strength alloys.

6.03.6.3 Chemical Variables

6.03.6.3.1 Hydrogen Concentration in IHAC

Hydrogen is trapped at various microstructural features in a complex alloy, and this behavior critically affects H solubility and diffusion, as well as IHAC and HEAC (Oriani,

1970; Kumnick and Johnson, 1970; Pressouyre and Bernstein, 1978; Pressouyre, 1979, 1983; Hirth, 1980; LeBlond and Dubois, 1983; Krom and Bakker, 2000; Scully, et al., 2000; Moody et al., 2001; Thomas, et al. 2002). High tensile strength and strong H-trapping frequently correlate because nano-scale features that strengthen an alloy often provide effective sites for H segregation. When trapping occurs, it is necessary to specify the H content in the alloy as either total H concentration ($C_{H\text{-}TOT}$) or diffusible H concentration ($C_{H\text{-}DIFF}$). The former represents the sum of: (a) H dissolved in the alloy lattice, (b) H in dynamic equilibrium with 1 or more reversible trap states, and (c) H trapped strongly in irreversible sites (Pressouyre, 1979, 1983). The $C_{H\text{-}DIFF}$ is that H dissolved in the lattice plus trapped at reversible sites, and depends on temperature exponentially through the energies of H-lattice solution (H_S) and H-trap binding, E_B (Hirth, 1980).

The concentration of H, predissolved in a high strength alloy microstructure, affects both the threshold stress intensity and subcritical crack growth rates for IHAC. Extensive data show that K_{IIHAC} decreases as $C_{H\text{-}TOT}$ increases for low alloy steels such as 4340 and 300M, as well as precipitation hardened maraging steels (Dautovich and Floreen, 1973, 1977; Gerberich et al., 1988; Yamaguchi, et al., 1997). This behavior is typically described by a relationship of the form:

$$K_{IIHAC} = \alpha(C_{H\text{-}TOT})^{-\beta} \quad (1)$$

where α and β are fitting constants determined from the experimental data (Gangloff, 1986). $C_{H\text{-}TOT}$ is typically measured by hot vacuum or inert gas extraction of H at a sufficiently high temperature where trapping does not occur.

Yamakawa and coworkers suggested that the threshold stress intensity for H cracking

correlates with $C_{H\text{-}DIFF}$ determined from H permeation experiments with an unstressed membrane (Yamakawa et al., 1984, 1986). Results for high strength quenched and tempered AISI 4135 steel were well described by:

$$K_{TH}\ (MPa\sqrt{m}) = 16.1\ (C_{H\text{-}DIFF})^{-0.10} \quad (ppm) \qquad (2)$$

This result is not relevant to IHAC or HEAC *per se* because the correlation was based on K_{TH} for specimens that were H precharged and stressed in the charging solution, constituting a worst-case combination of the two forms of H cracking. Experiments systematically characterized H trapping and the cracking threshold for AerMet®100 steel stressed in moist air (Thomas, 2000, Thomas et al., 2002, 2003). The K_{IIHAC} decreased with increasing diffusible and total H concentrations, according to regression-based relationships of the data in Fig 23:

$$K_{IIHAC}\ (MPa\sqrt{m}) = 40\ C_{H\text{-}DIFF}^{-0.54} \quad (ppm)$$

$$K_{IIHAC}\ (MPa\sqrt{m}) = 100\ C_{H\text{-}TOT}^{-0.49} \quad (ppm) \qquad (3)$$

Similar H-concentration dependences were reported for other high strength alloys. Results in Fig. 10 show the deleterious effect of increased precharged-H content on K_{IIHAC} as well as $K_{IC\text{-}H}$ for IHAC of an Fe-based precipitation hardened superalloy (Moody, Perra and Robinson, 1988, 1990b). IHAC in high strength β/α-Ti alloys is exacerbated by increasing H concentration, as illustrated by the data contained in Fig. 24, extending the findings shown in Fig. 14. The threshold stress intensity for IHAC in α-precipitation hardened Ti-15-3 sheet is plotted as a function of $C_{H\text{-}TOT}$ for specimens that were H-charged electrochemically then stressed at constant dK/dt and 23°C in moist air (Hayes, 2000). Results suggest that the alloy is toughened somewhat by H addition up to about 400 ppm,

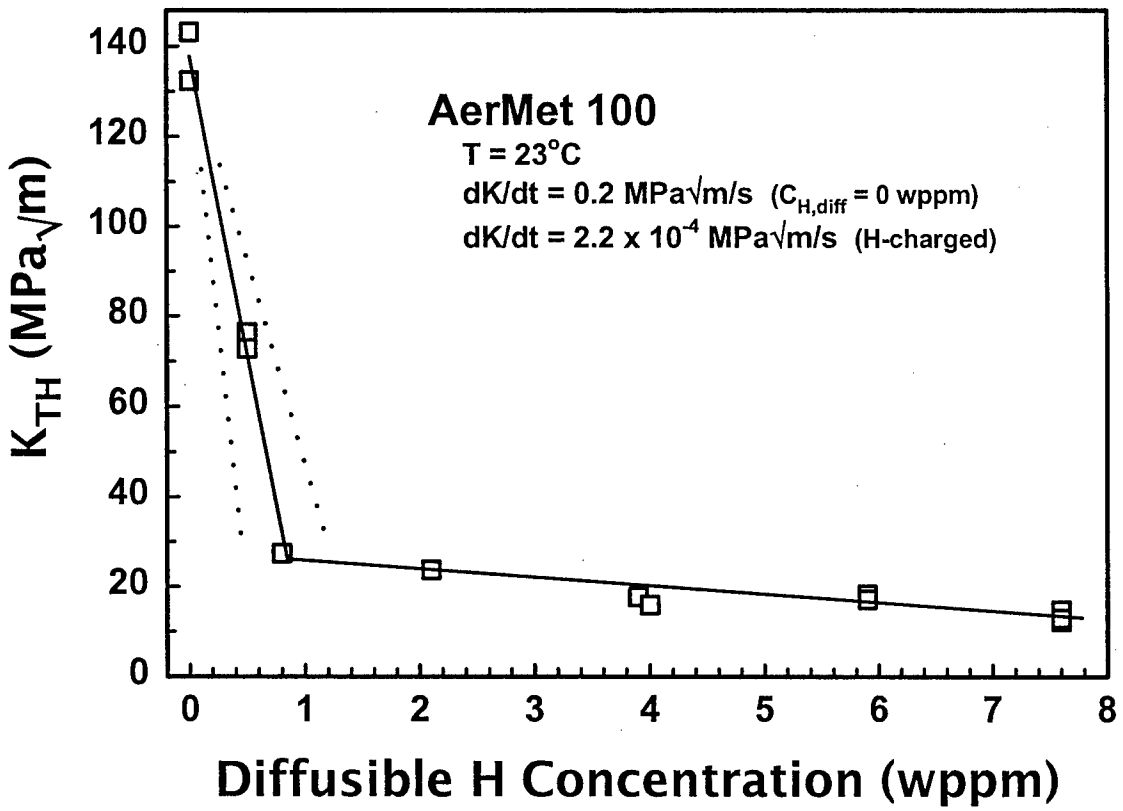

Figure 23. Threshold stress intensity for IHAC in peak aged AerMet®100, containing varying diffusible H concentration dissolved electrochemically, and stressed at constant dK/dt of 2.2 x 10^{-4} MPa√m/s. (Thomas, 2000; Thomas et al. 2002, 2003)

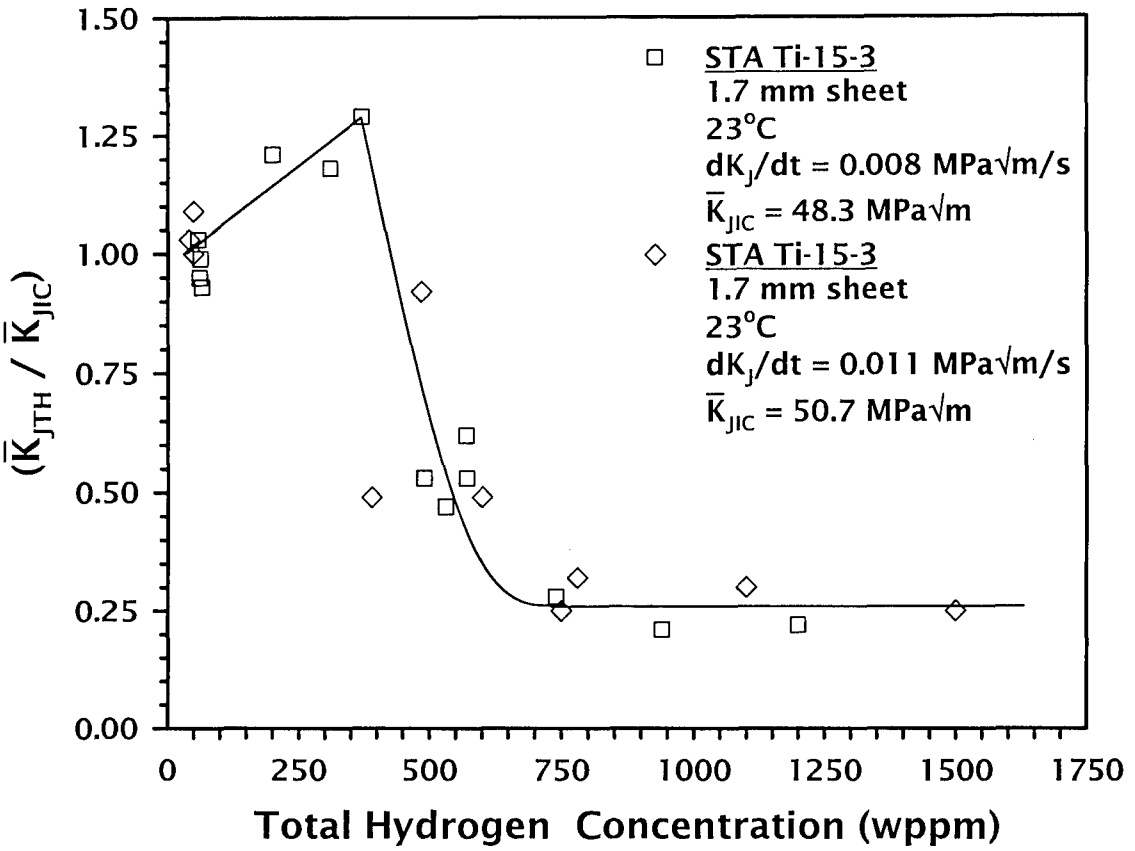

Figure 24. Threshold stress intensity for IHAC in α-precipitation hardened Ti-15-3 sheet, containing varying total H concentration dissolved electrochemically, and stressed at constant dK/dt of either 0.011 or 0.008 MPa√m/s. The threshold K in this plot was determined by an elastic-plastic J-integral analysis and normalized by the average plane strain fracture toughness for this alloy containing 60 ppm H. (Hayes, 2000).

followed by a precipitous decrease in K_{IH} for increasing $C_{H\text{-}TOT}$ from 400 to 700 ppm. Additional increase in H content did not affect the low threshold for IHAC in this alloy. Analogous results were reported for a second high strength β/α-Ti alloy, Ti-7Mo-4.5Fe-1.5Al (Hayes, 2000). For both β/α-Ti alloys, IHAC progressed along a brittle transgranular crack path, (e.g., Fig. 14) for all H concentrations examined (Hayes, 2000).

Extensive H trapping can increase or decrease the hydrogen embrittlement susceptibility of an alloy (Pressouyre and Bernstein, 1979, 1981; Pressouyre, 1980; Morgan and McMahon 1985). A homogeneous distribution of strong (irreversible) traps increases resistance to cracking by preventing (or shielding) H segregation to the crack tip FPZ containing lower H-binding energy sites that are interconnected and susceptible to decohesion. This is particularly true if a finite quantity of H is available, as typical of IHAC (Coudreuse and Bocquet, 1995). Embrittlement was reduced by strong H trapping at TiC particles in HSLA steel (Stevens and Bernstein, 1985), VC in 2¼-1Mo-0.3V (Coudreuse and Bocquet, 1995) and PdAl in PH 13-8 Mo stainless steel (Scully, et al., 1991). In contrast weak (reversible) traps provide a reservoir of diffusible H to supply the crack tip fracture process zone and decrease resistance to IHAC (Thomas, et al., 2002, 2003). Both beneficial and detrimental effects of H trapping are likely in high strength alloys due to the number and variety of trap sites in such complex microstructures.

6.03.6.3.2 Environmental H-Producing Activity in HEAC

The amount of atomic hydrogen, absorbed on crack surfaces in close proximity to the tip, critically affects HEAC in high strength alloys, analogous to the influence of

predissolved H concentration in IHAC. This uptake of H is controlled by environmental variables for gases and electrolytic solutions.

6.03.6.3.2.1 Gaseous Environments

Increasing H_2 pressure promotes HEAC in high strength alloys, as manifest by decreasing K_{IHEAC} and increasing da/dt. The P_{H2} dependence of K_{IHEAC} is presented in Fig. 25 for high and ultra-high strength steels with σ_{YS} between 1350 and 1650 MPa (Gangloff, 1986). This pressure dependence is observed broadly for steels (Oriani and Josephic, 1974; Clarke, 1979; Bandyopadhyay, 1983; Moody et al., 1990) as well as Fe and Ni based superalloys (Moody et al., 1990); however, the slope of the dependence declines sharply as alloy strength increases. For example, steels with $\sigma_{YS} < 1200$ MPa exhibit an extremely strong P_{H2} dependence of K_{IHEAC}, while very high strength steels with $\sigma_{YS} > 1700$ MPa do not (Akhurst and Baker, 1981; Moody et al., 1990). The H_2 pressure dependence of K_{TH} is affected by steel impurity content (Bandyopadhyay, 1983) and temperature, but data for the latter are limited. Clarke reported that K_{IHEAC} for 4140 steel is independent of the pressure of H_2S from 100 to 2000 kPa; however, an effect is likely at lower P_{H2S} (Clarke, 1979).

The H_2 pressure dependence of subcritical crack growth rate likely reflects the dependence of the threshold. For example, the Stage II da/dt increases with increasing P_{H2} raised to a power less than 1.0 for ultra-high strength 18Ni Maraging steel. The precise power law depends on gas temperature as illustrated in Fig. 26, and determined by both equilibrium and kinetic considerations (6.03.8) (Gangloff and Wei, 1977). The pressure dependence of da/dt_{II} also depends on steel strength (Nelson and Williams, 1977).

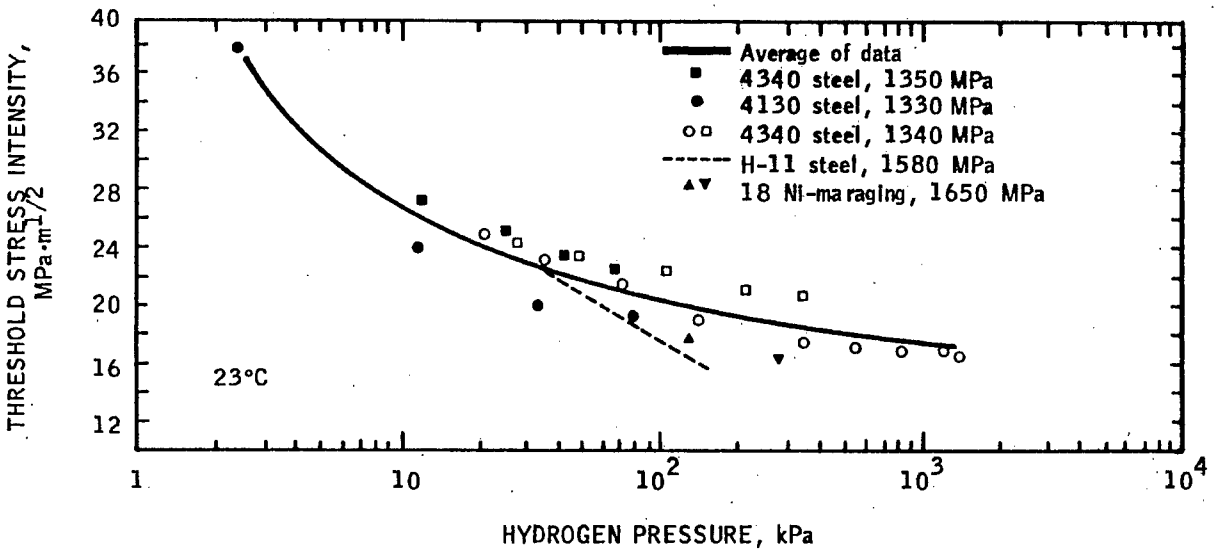

Figure 25. The effect of H_2 pressure on the threshold stress intensity factor for HEAC of several high and ultra-high strength steels stressed in this environment at 23°C. (Gangloff, 1986)

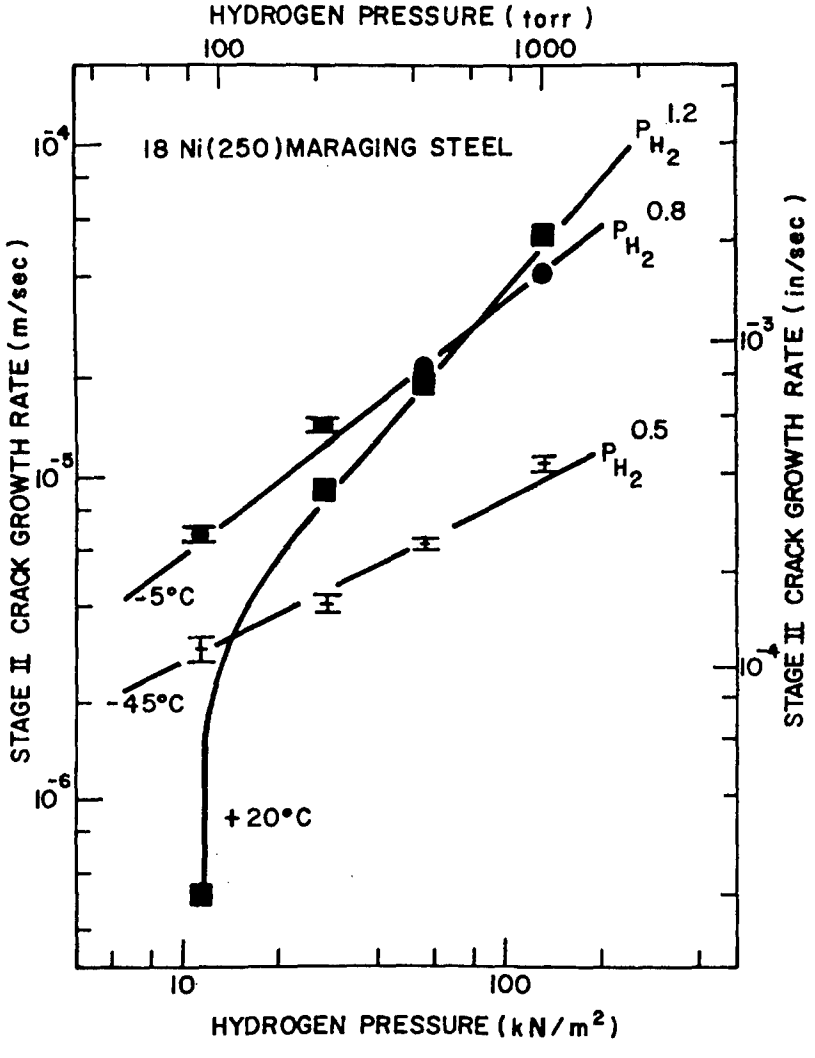

Figure 26. The effect of H_2 pressure on the HEAC growth rate for ultra-high strength 18Ni Maraging steel stressed in a highly purified hydrogen environment at three temperatures. (Gangloff and Wei, 1977)

The composition of the gas environment affects susceptibility to HEAC. Nelson and coworkers reported astonishingly fast rates of subcritical HEAC when AISI 4130 steel (σ_{YS} = 1344 MPa) was stressed in an H_2-H gas mixture produced by thermal dissociation of the hydrogen molecule (Nelson et al., 1971). High rates of subcritical HEAC were reported for ultra-high strength steel stressed during exposure to gaseous HCl, HBr and H_2S (Kerns et al., 1977; Opoku and Clark, 1980). This work also evidenced significant crack growth in Cl_2, suggesting either a residual impurity effect or a damage mechanism other than HEAC (Sieradzki and Ficalora, 1979).

Gas addition can inhibit rates of HEAC. For example, substantial subcritical crack growth that occurs in a high strength martensitic steel stressed in pure water vapor or H_2 was arrested by small addition of O_2 (Hancock and Johnson, 1966; Sawicki, 1971; Kerns et al., 1977). Hydrocarbon molecules such as ethylene (C_2H_4) and acetylene (C_2H_2) react with an iron surface to consume adsorbed H and thus inhibit HEAC when added to H_2 (Gangloff, 1988). The key is the number of unsaturated C-C bonds available to react with surface H to inhibit HEAC; C_2H_4 addition to pure H_2 reduced rates of HEAC in high strength AISI 4130 steel (σ_{YS} = 1330 MPa) but CH_4 with saturated C bonds did not. When present in pure form, hydrocarbon molecules may be catalytically dissociated to produce surface H and HEAC; however, rates of cracking are substantially less than those produced by H_2 (Kerns, et al., 1977; Opoku and Clark, 1980; Gangloff, 1988).

6.03.6.3.2.2 Aqueous Electrolytic Environments

Substantial data show the generally deleterious effects of cathodic polarization,

decreasing pH, H_2S addition, temperature, and other chemical variables on the susceptibility of high strength alloys to HEAC in electrolytes. Extensive reviews document such environmental effects on subcritical crack growth in steels (Carter, not dated; Kerns et al., 1977). Holroyd reviewed the substantial amount of data that pertain to environment chemistry effects on cracking in high strength 7000 series Al alloys (Holroyd, 1990). Those aqueous environmental conditions that promote increased H production and uptake into the crack tip FPZ reduce K_{IHEAC} and increase da/dt, analogous to the deleterious effect of increasing $C_{H\text{-}DIFF}$ in IHAC.

Permeation-Based Correlation: A first step in correlating a range of environmental effects on HEAC employed the permeation experiment to determine the $C_{H\text{-}DIFF}$ produced in a high strength alloy in equilibrium with a gas or electrolyte (Yamakawa et al., 1984, 1986; Gangloff, 1986). Permeation experiments have not generally included stress or occluded-crack chemistry effects; however, such issues can be incorporated by using specialized specimens or an environment that simulates the occluded crack situation (Scully and Moran, 1988; Kolman and Scully, 1997).

The permeation-based approach without considering crack chemistry is illustrated in Fig. 27 for martensitic 4340-type steels ($1300 < \sigma_{YS} < 1500$ MPa). For gaseous hydrogen, K_{IHEAC} is plotted (including data similar to those presented in Fig. 25) *vs.* $C_{H\text{-}DIFF}$ estimated from permeation experiments and corrected to a yield strength of 1400 MPa using an elastic analysis with crack tip hydrostatic stress of $2.4\sigma_{YS}$ (6.03.8). For reference, *log H solubility* of –0.1 ppm ($C_{H\text{-}DIFF}$ = 0.3 ppm) corresponds to P_{H2} = 7 kPa and *log H solubility* of 1.8 ($C_{H\text{-}DIFF}$ = 63 ppm) corresponds to P_{H2} = 11.4 MPa at 23°C. The data (□) are well fit by:

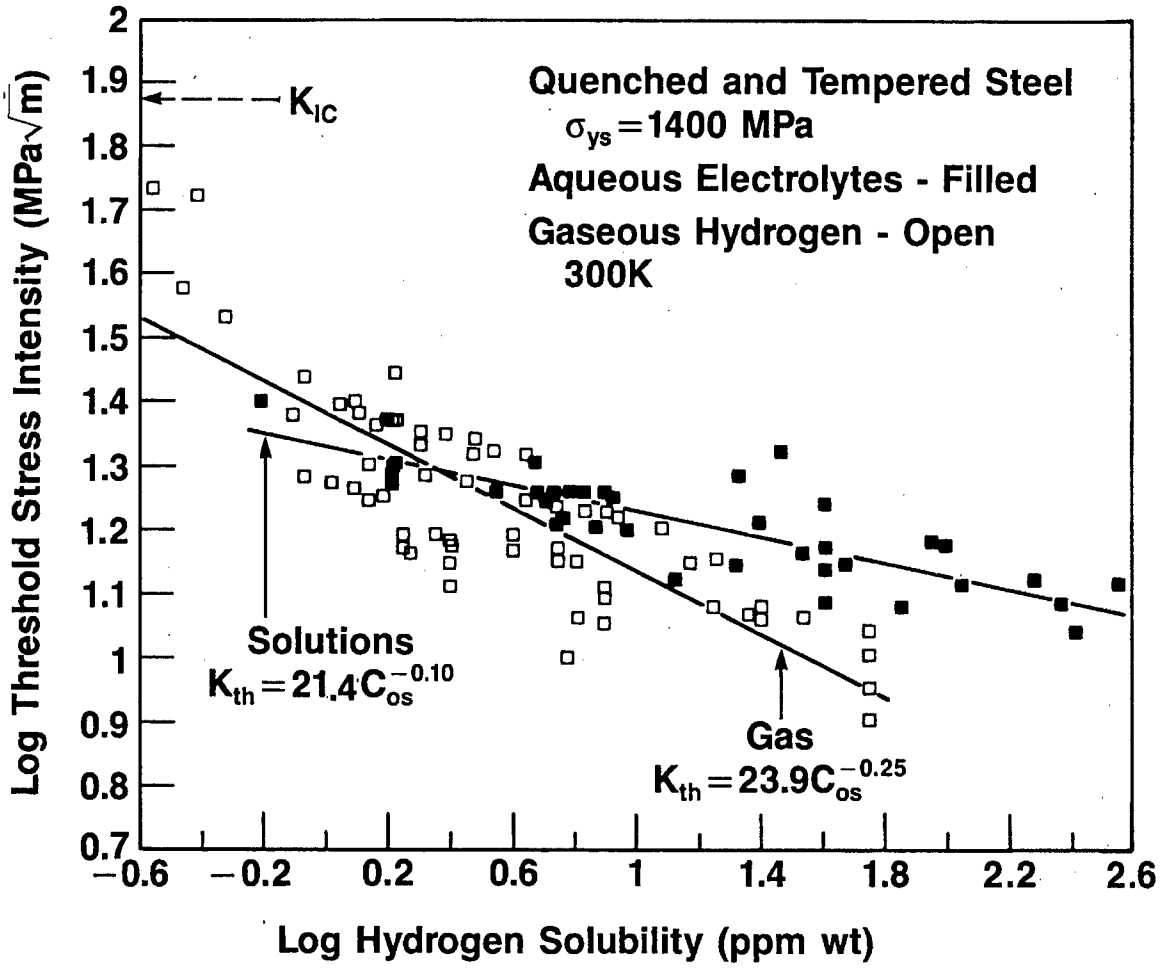

Figure 27. The correlation between crack tip H concentration and the threshold stress intensity for HEAC in tempered martensitic steels of the 4340 type (σ_{YS} = 1400 ± 100 MPa) stressed in various gaseous and electrolytic environments at 23°C. (Gangloff, 1986)

$$K_{IHEAC}\ (MPa\sqrt{m}) = 23.9\ (C_{H\text{-}DIFF})^{-0.25}\ \ (ppm) \qquad (4)$$

with a regression coefficient of 0.84 and 95% confidence interval estimate of the slope as 0.246 $\pm$ 0.040. The filled data points represent a similar analysis performed on data for cracking of this steel class in various electrolytes. For reference, *log H solubility* of 0.2 ppm ($C_{H\text{-}DIFF}$ = 1.6 ppm) corresponds to neutral 3.5% NaCl solution at the free corrosion potential and *log H solubility* of 2.2 ($C_{H\text{-}DIFF}$ = 160 ppm) corresponds to acidified NaCl solution saturated with H_2S gas. The data for HEAC in these electrolytes (□) are well fit by:

$$K_{IHEAC}\ (MPa\sqrt{m}) = 21.4\ (C_{H\text{-}DIFF})^{-0.10}\ \ (ppm) \qquad (5)$$

with a regression coefficient of 0.83 and 95% confidence interval estimate of the slope as 0.100 $\pm$ 0.023. Statistically equivalent trend lines at the 95% confidence level do not fit the populations of K_{IHEAC} data for H_2 and the electrolytes. Bulk pH, electrode potential, and solution composition are easily matched for permeation and cracking experiments. However, consistent with the statistically distinct trends in Fig. 27, crack solution pH and near tip electrode potential differ from bulk conditions and govern H uptake near the crack tip to predominantly drive cracking in high strength metals.

Effect of Applied Electrode Potential: The effect of applied electrode potential on HEAC in high strength alloys is important from engineering and mechanistic perspectives. Considering steel, the general view is that K_{IHEAC} is reduced with increasing cathodic polarization, as illustrated for 17-4 PH stainless steel (Fig. 9) in chloride solution and coupled with Mg or Zn, or polarized potentiostatically (Fujii, 1976). Increasing anodic polarization also exacerbates HEAC in high strength steels; that is, cracking resistance can

be highest in the vicinity of the free corrosion potential, and decrease with both anodic and cathodic polarization (Brown, 1971, 1977; Sandoz, 1977; Dautovich and Floreen, 1977; Tyler et al., 1991; Buckley, et al., 1993; Lee et al., 2000). An example is provided by the data in Fig. 28 for AerMet®100 where H cracking is transgranular. A similar maximum in IG cracking susceptibility near the free corrosion potential was reported for 18Ni Maraging steel in neutral NaCl solution (Dautovich and Floreen, 1977). The K_{IH} for the AISI 4340 steel in Fig. 28 is low and independent of cathodic or anodic polarization. A similar nil to mild maximum in HEAC susceptibility, just anodic of the free corrosion potential, was reported for five strengths of AISI 4340 steel ($1250 < \sigma_{YS} < 2200$ MPa) in NaCl solution (Sandoz, 1977).

Anodic polarization exacerbates environmental cracking in 7000-series aluminum alloys exposed to chloride solution. The da/dt increases with increasing anodic polarization at levels above the free corrosion range and until a plateau crack growth rate is achieved near the bold-surface pitting potential (Speidel and Hyatt, 1972; Speidel, 1975; Holroyd, 1990). (Bold in this usage refers to a surface that is exposed to a bulk electrolyte and not occluded compared to a crack or crevice). This electrode potential dependence is confirmed for a modern alloy, AA7050, as shown in Fig. 29 building on the data in Fig. 13 (Young, 1999). The rate of subcritical cracking in the susceptible peak aged microstructure increases with increasing applied electrode potential. Notably, the cracking resistant overaged temper does not exhibit subcritical HEAC over a wide range of applied potential. Results in Fig. 29 were developed for steady-state cracking conditions; however, substantial and potential dependent

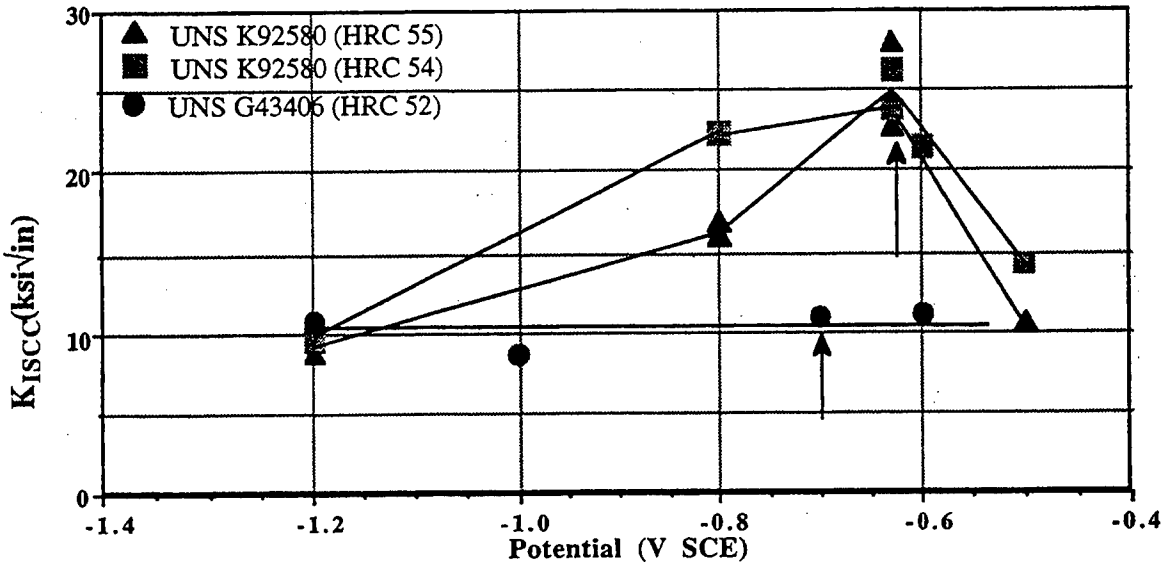

Figure 28. The applied electrode potential dependence of the threshold stress intensity for HEAC in two ultra-high strength steels, AerMet®100 (UNS K92580) and ESR 4340 (UNS G43406), each stressed in neutral chloride solution under slow-rising CMOD at 23°C. The free corrosion potential for each steel is between –600 and –700 mV_{SCE}, as shown by the vertical arrows, and K_{IC} is about 130 MPa√m for AerMet®100 and 80 MPa√m for ESR 4340 steel. (Buckley et al., 1993: Publication permission requested from US Army Research Laboratory.)

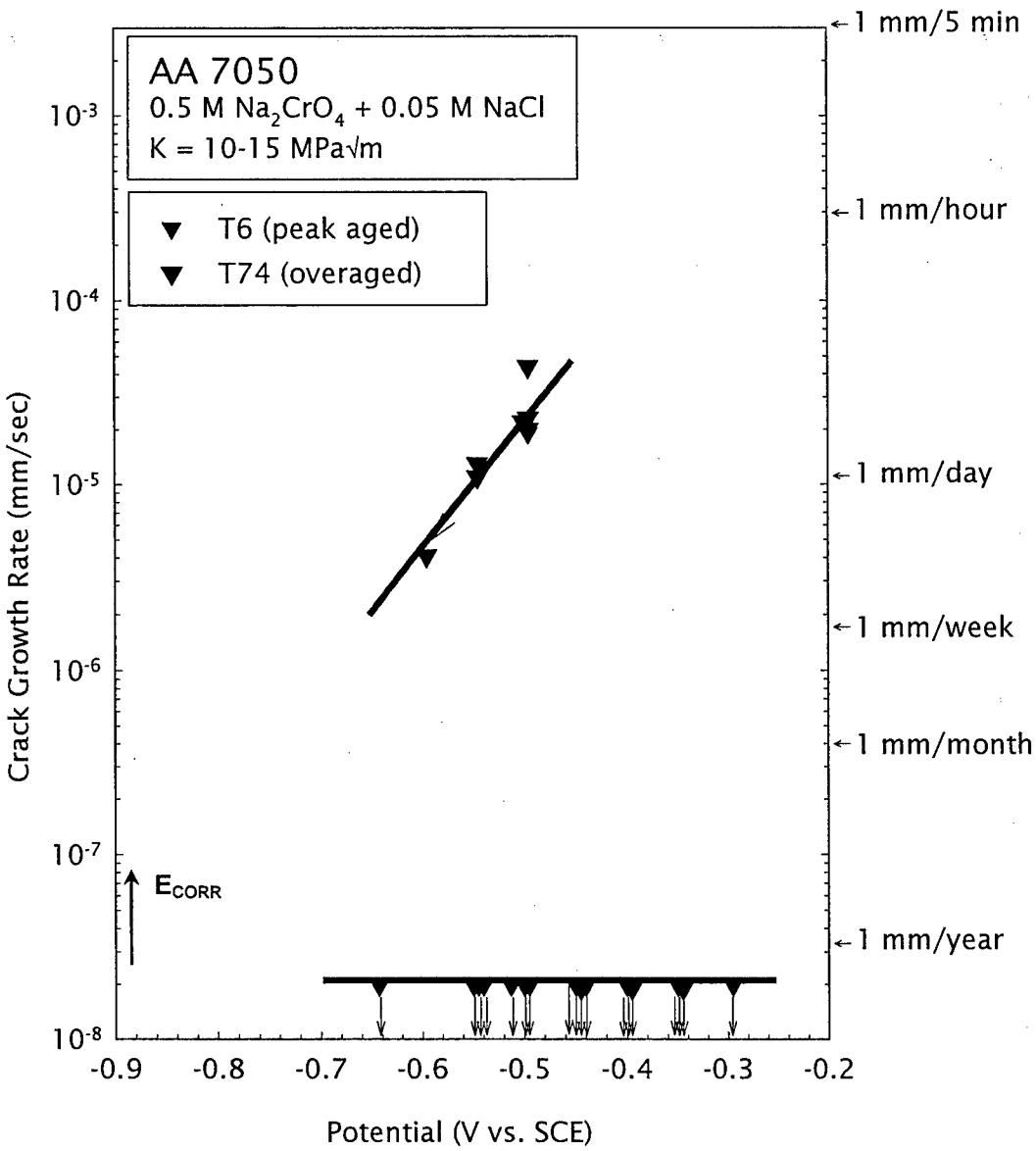

Figure 29. The effect of applied electrode potential on the steady state subcritical crack growth rate for two tempers of AA7050 stressed at fixed CMOD ($20 > K > 10$ MPa$\sqrt{m}$) in acidified chloride-chromate solution. The free corrosion potential was between –935 and –890 mV_{SCE} during 48 h immersion in quiescent solution and the pitting potential was -230 mV_{SCE}. The vertical arrows indicate that environment-assisted crack growth was not observed after a 20 day exposure and hence da/dt is less than the resolution limit of the compliance-based crack length measurement system. The peak aged microstructure was tempered at 118°C for 20 h plus 154°C for 12 h. The overaged condition was produced for the same solution treatment condition, but with aging at 163°C for 27 h. The crack orientation was SL. (Young, 1999)

incubation occurred prior to this steady-state (Young, 1999). For example, the precrack was stagnant for up to several days of stressed exposure, prior to acceleration to the growth rates shown. This incubation was attributed to time-dependent crack chemistry development and was minimized by anodic polarization to affect high da/dt, followed by reduced potential to develop the data in Fig. 29.

The applied electrode potential dependence of environmental cracking in high strength Ni and β-Ti alloys introduces a new behavior; HEAC mitigation by polarization away from free corrosion. For the superalloy represented in Fig. 11, IN718 stressed in two acidic solutions, cathodic polarization from the free corrosion range reduced the threshold stress intensity for subcritical cracking for acidic solution conditions (Lillard et al., 1997; Lillard, 1998), analogous to the behavior of high strength steels in Fig. 28. However, there is the suggestion in Fig. 12 that highly cathodic polarization improves resistance to environmental cracking. The effect of anodic polarization has not been reported for this class of superalloys. The data for β/α-Ti alloys stressed in near-neutral NaCl solution, Fig. 30, amplifies the occurrence of a strong cathodic inhibition of environmental cracking and show that the threshold stress intensity also rises toward K_{IC} with increasing anodic potential.

These complex electrode potential dependencies shown in Figs. 11 and 28-30 are explained within the HEAC framework of Fig. 2 by considerations of crack tip H production and uptake resulting from local-occluded chemistry and crack tip potential changes upon bold surface polarization, as discussed in 6.03.7.1.2.

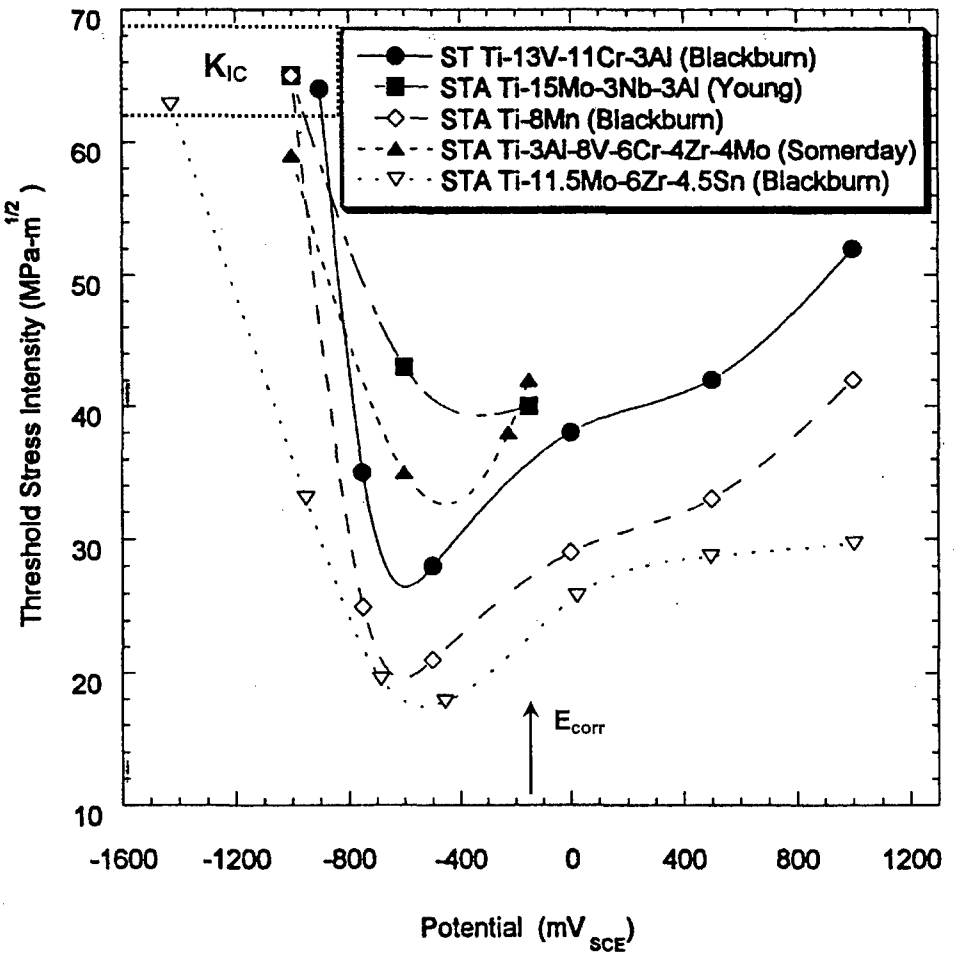

Figure 30. The applied electrode potential dependence of the threshold stress intensity for HEAC in five α-precipitation hardened β-Ti alloys, each stressed in chloride solution under slow-rising CMOD at 23°C. The free corrosion potential for this class of alloys and neutral chloride solution is –100 to –200 mV_{SCE}. The H-free plane strain fracture toughness for this strength level of β/α-Ti alloy is 60-75 MPa√m. (Blackburn et al., 1972; Grandle et al., 1994; Young et al., 1995; as presented in Kolman and Scully, 1997: Reprinted with permission from Elsevier.)

6.03.6.3.3 Temperature

The severity of both IHAC and HEAC in high strength alloys is maximized at a temperature within $\pm$ 150°C of ambient. The precise relationship depends on H content, alloy strength, and environment chemistry. The temperature dependence of cracking is understood qualitatively by the temperature dependencies of the elemental processes shown in Fig. 2 and modeled quantitatively in 6.03.8.

6.03.6.3.3.1 Internal Hydrogen Assisted Cracking

Temperature affects both the threshold and kinetics for IHAC in high strength alloys, due to the temperature dependencies of H trapping and diffusion. The results presented in Fig. 31 show that K_{IIHAC} is a minimum and da/dt is maximized near 25°C for H precharged IN903 (Moody et al., 2001). A similar trend is illustrated in Fig. 32 for Stage II da/dt measured for ultra-high strength AISI 4340 steel containing 3 ppm of predissolved H (Gerberich et al., 1988). In this case, da/dt is maximized at 50-100°C. For both alloys at temperatures below the maximum, da/dt depends on 1/T according to an Arrhenius relationship with activation energies of 69 kJ/mol and 27 kJ/mole for the superalloy and martensitic steel, respectively. For temperatures above the maximum, da/dt declines sharply for the steel and somewhat less so for the Fe-based austenitic superalloy. The loss of H from the fracture mechanics specimen, and specifically the fracture process zone, must be considered when selecting data for structural integrity modeling and mechanistic interpretation (Thomas, et al., 2003). Since the diffusivity of H in high strength alloys is low ($< 10^{-7} cm^2/s$) below 200°C (Gangloff, 2003), this problem is often not limiting.

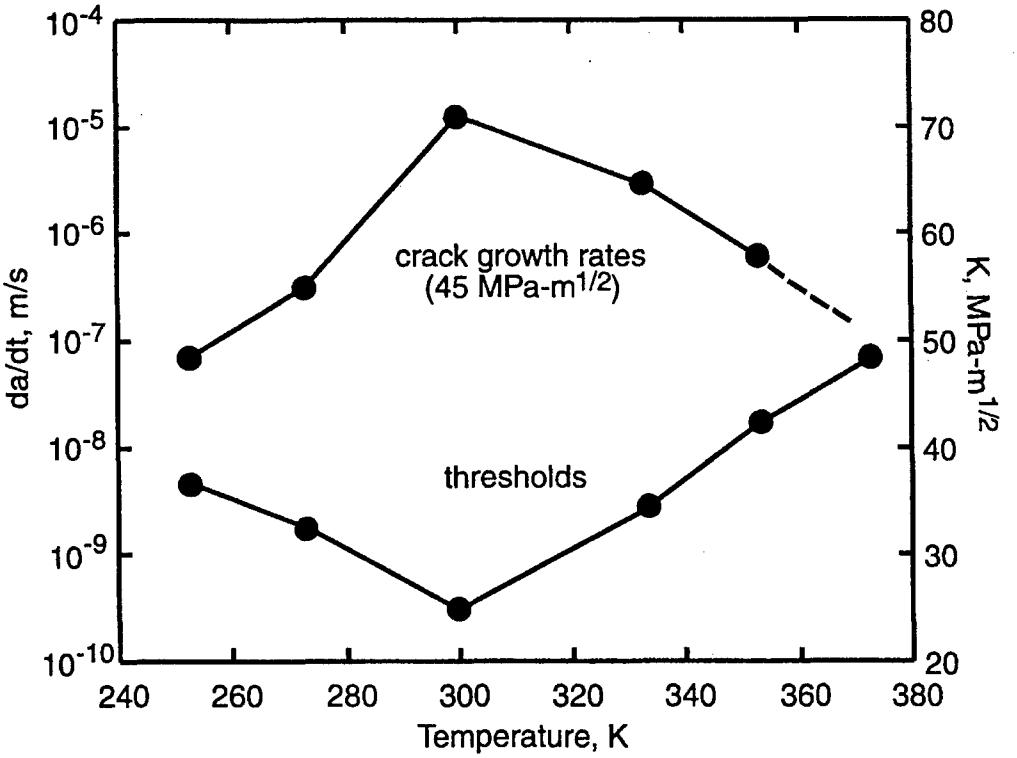

Figure 31. The temperature dependence of the threshold stress intensity and subcritical crack growth rate for IHAC in precipitation hardened IN903 (σ_{YS} = 1080 MPa and K_{IC} = 90 MPa$\sqrt{m}$), H-precharged ($C_{H\text{-}TOT}$ = 2900 ppm), and tested at fixed CMOD in moist air. (Moody, Robinson and Garrison, 1990: Reprinted with permission from Elsevier.)

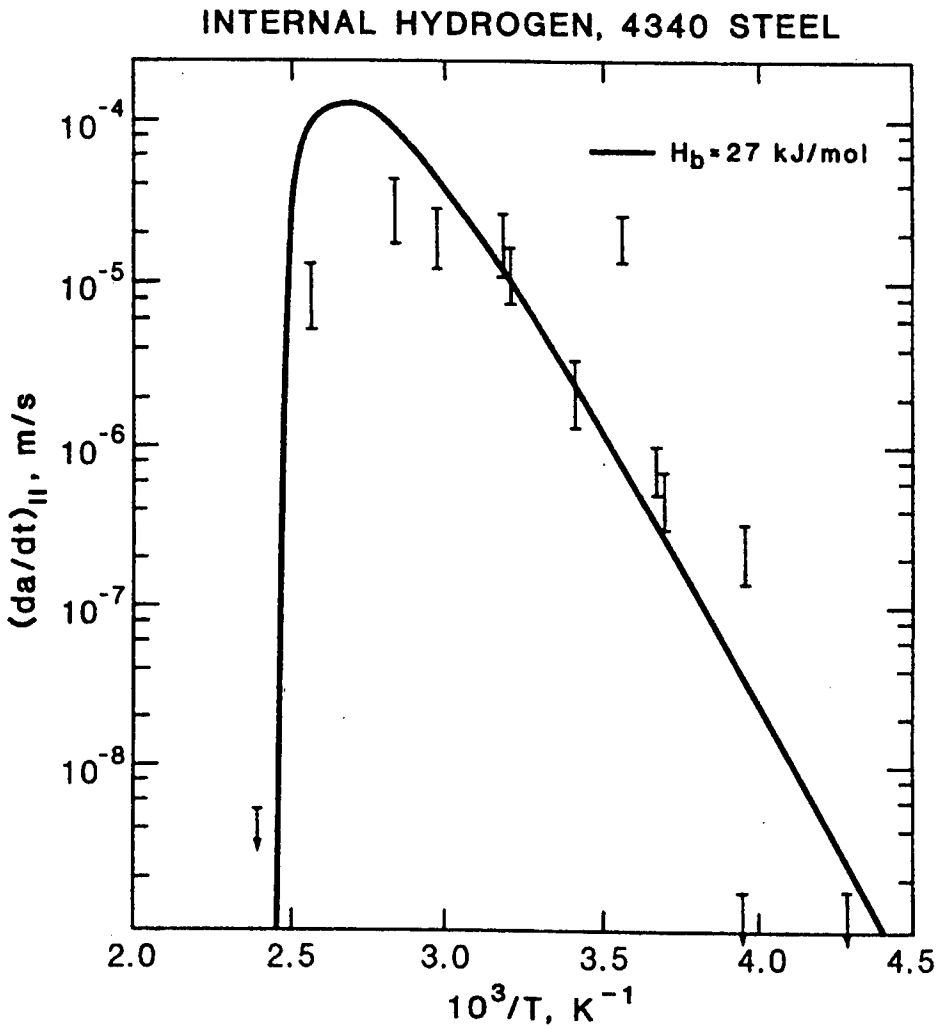

Figure 32. The temperature dependence of the Stage II K-independent subcritical crack growth rate for IHAC in tempered martensitic 4340 steel (σ_{YS} = 1660 MPa), H-precharged ($C_{H\text{-}TOT}$ = 3 ppm or more) and tested at fixed load in moist air. The bars represent experimental measurements and the solid line is the model prediction using a H-trap binding energy of H_b = E_B = 27 kJ/mol. (Gerberich et al., 1988: Reprinted with permission from Elsevier.)

Fracture mechanics based data have not been reported to define the temperature dependencies of K_{IIHAC} and da/dt for IHAC of high strength β-Ti and 7000 series aluminum alloys.

6.03.6.3.3.2 Hydrogen Environment Assisted Cracking

Temperature affects both the threshold and kinetics for HEAC in high strength alloys, with the effect complicated by the temperature dependencies of crack-environment chemistry, H production, and H uptake; as well as H trapping and diffusion (Fig. 2).

Threshold Stress Intensity: The threshold stress intensity for HEAC increases monotonically with rising temperature, as illustrated by the data in Fig. 33 for several high strength steels stressed during exposure in pure H_2 (Moody et al., 1990 as first reported by Gangloff and Wei, 1977; Nelson and Williams, 1977; Clark, 1979). This is consistent with the results for IHAC in Fig. 31. Low temperature threshold behavior must be considered with caution since slower reaction and mass transport kinetics could prolong the testing time required to achieve a true near-equilibrium condition. In this regard, the rise in K_{IIHAC} in Fig. 31, and the suggestion of such an increase for the 18Ni (200) Maraging steel in Fig. 33 may reflect artificially high threshold values from insufficient duration experiments. The intrinsic threshold for IHAC and HEAC may be temperature independent or fall mildly with decreasing temperature in the low-T regime.

Subcritical Crack Growth Rate: Substantial data describe the temperature dependence of the Stage II da/dt for HEAC in high strength alloys. The specific behavior is different for pure H_2 compared to water vapor environments, particularly in the high temperature regime.

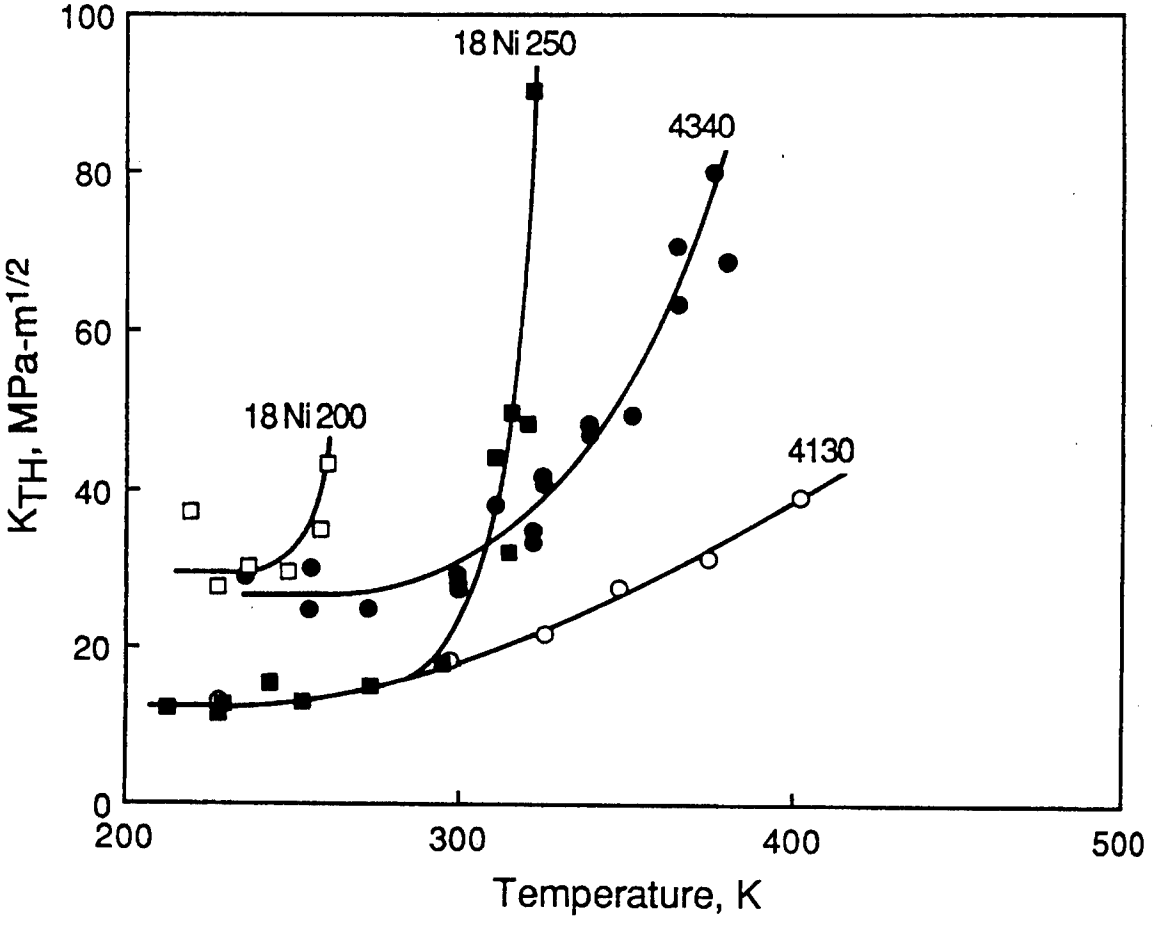

Figure 33. The temperature dependence of the threshold stress intensity for HEAC in several high and ultra-high strength martensitic steels tested in purified H_2 at either constant or rising load (Moody et al., 1990). Tensile yield strength levels are: 18 Ni (200) = 1270 MPa and 18 Ni (250) = 1650 MPa (Gangloff and Wei, 1977); 4340 = 1235 MPa (Clark, 1979); 4130 = 1330 MPa (Nelson and Williams, 1977. (Reprinted with permission from Elsevier.)

HEAC in the high strength steel/H_2 system parallels the temperature dependence of IHAC in such alloys, as illustrated by the data in Fig. 34 for ultra-high strength 18Ni (250) Maraging steel in pure H_2 at two pressures (Gangloff and Wei, 1977, 1978). Based on more extensive data, the maximum in da/dt_{II} occurs at about 25°C for the higher P_{H2} and 0°C for the lower pressure; in general, the temperature for maximum da/dt increases with increasing H_2 pressure and increasing steel strength (Gangloff and Wei, 1977). At lower temperatures, H cracking is thermally activated, with activation energy of 18 kJ/mole. At higher temperatures, da/dt declines precipitously by several orders of magnitude for a 1-3°C temperature increase. This growth rate decrease is reversed essentially immediately by a 1-3°C temperature reduction. The scanning electron fractographs in Fig. 34 show that HEAC is fully intergranular in the low temperature regime and transitions with increasing temperature to brittle TG cracking through the martensitic microstructure. Similar temperature dependent da/dt data were reported for AISI 4130 steel (σ_{YS} = 1344 MPa), with a low temperature activation energy of 16-17 kJ/mole for IG H cracking, but a less steep decline in da/dt in the high temperature regime and a transition from IG to transgranular microvoid-based cracking (Williams and Nelson, 1970, 1970a; Nelson and Williams, 1977). In novel experiments Nelson and coworkers showed that the maximum in da/dt was eliminated for the AISI 4130 steel in thermally dissociated H_2/H gas mixture; simple Arrhenius behavior was reported for $-20°C < T < 40°C$ with an activation energy of 29 kJ/mol and HEAC appeared to occur for temperatures as high as 160°C (Nelson, et al., 1971). Older data suggested low temperature activation energy for IG H_2 cracking of ultra-high strength steels in the range from 9 to 12 kJ/mol (Sawicki, 1971; McIntyre et al., 1972a).

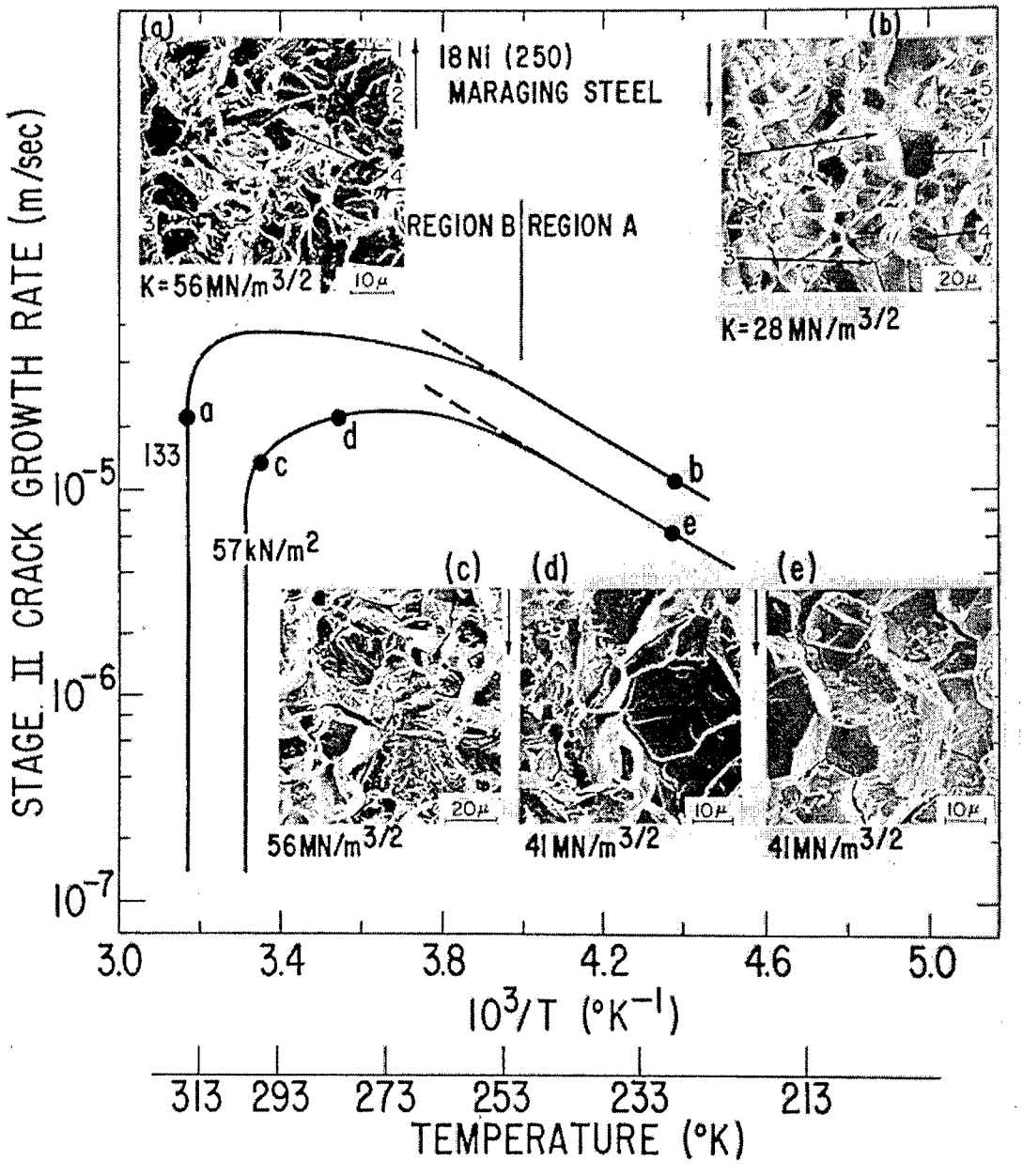

Figure 34. The temperature dependence of the Stage II subcritical crack growth rate for HEAC in ultra-high strength 18Ni (250) Maraging steel (σ_{YS} = 1650 MPa), stressed at fixed load in highly purified H_2. (Gangloff and Wei, 1977, 1978)

Chen and Gerberich reported thermally activated Stage II cracking in Fe-Si single crystals in 100 kPa H_2, with a low temperature activation energy of 25 kJ/mol, a maximum in crack growth rate at about 125°C, and a 100-fold decrease in da/dt between 105°C and 160°C (Chen and Gerberich, 1991). This result is notable since HEAC was by transgranular cleavage along {100} planes in the Fe-Si single crystal at all temperatures.

The composition of the environment affects the temperature dependence of HEAC. This result is illustrated by the data collected in Fig. 35 for tempered martensitic AISI 4340 steel (σ_{YS} = 1345 MPa) stressed during exposure in several environments (Wei, 1981; Wei and Gao, 1985). The temperature dependence of this steel in 133 kPa pure H_2 parallels the behavior of AISI 4340 and the 18 Ni maraging steels, particularly in terms of a low temperature activation energy of 15 kJ/mol and maximum da/dt at 80°C. Different behavior is noted for H_2S, where the low temperature activation energy is lower, equaling either 5 kJ/mol or 0 kJ/mol for higher and lower H_2S pressures, respectively. In these two cases, da/dt_{II} appears to decline with increasing temperatures above 25°C. A similar result of nearly temperature independent da/dt_{II} was reported for AISI 4130 steel in low pressure (0.2 kPa) H_2S (–40°C < T < 50°C) (Nelson, 1983), with a higher activation energy of 8 kJ/mol reported for the steel of Fig. 4 in 13 kPa H_2S (-75°C < T < 130°C) (McIntyre et al., 1972a).

The temperature dependence of HEAC in high strength 4130 and 4340 steels in pure-liquid water is unique. As shown in Fig. 35, da/dt_{II} increases monotonically with increasing T up to 80°C for AISI 4340 steel, with higher activation energy of 34 kJ/mol. The identical result was reported for lower strength AISI 4130 steel, with a monotonic da/dt increase for 0°C < T < 90°C and activation energy of 80 kJ/mol (Nelson, 1983). The da/dt for 4130

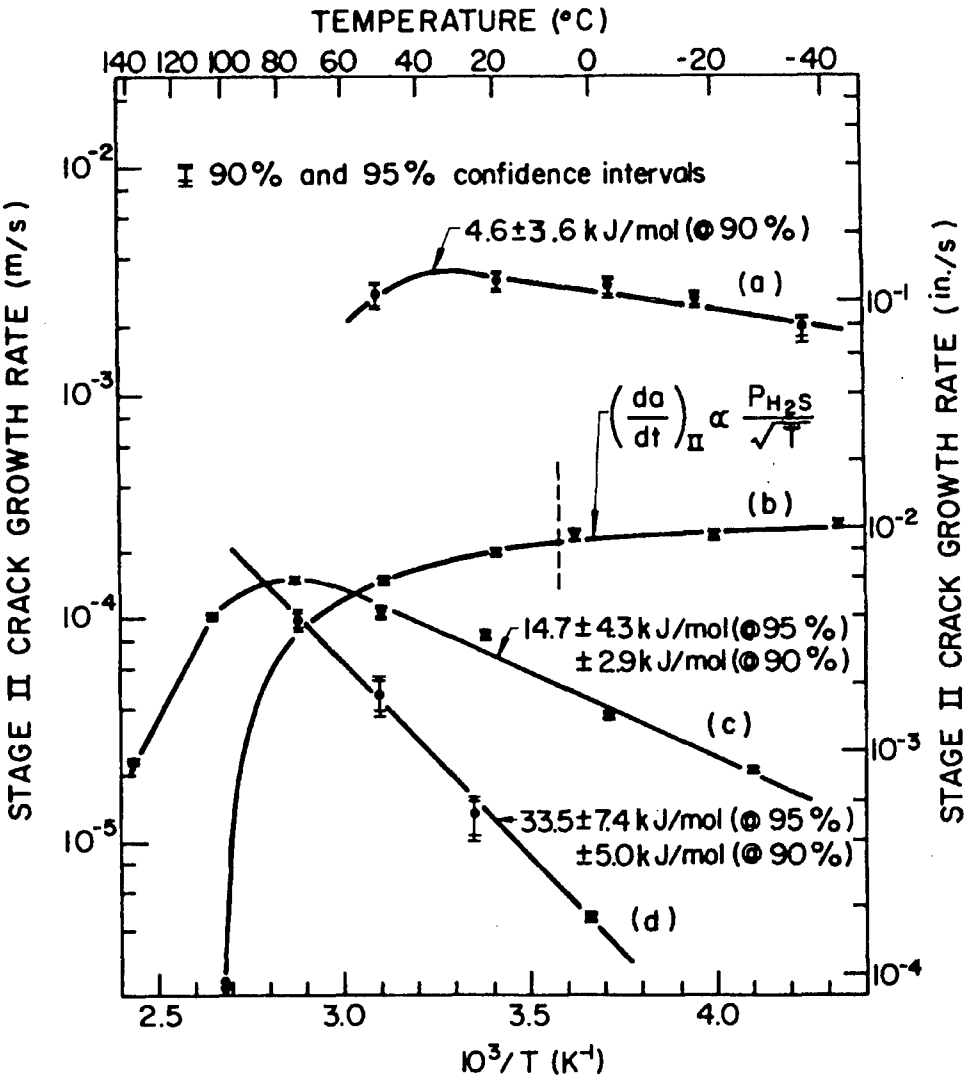

Figure 35. The temperature dependence of the Stage II subcritical crack growth rate for HEAC in high strength 4340 steel (σ_{YS} = 1345 MPa), stressed at fixed load in several highly purified environments. (a) 2.7 kPa H_2S, (b) 0.13 kPa H_2S, (c) 133 kPa H_2, and (d) liquid water. (Wei, 1981; Wei and Gao, 1985: Copyright The Minerals, Metals and Materials Society, reprinted with permission.)

began to decline, below the Arrhenius line, suggesting a maximum growth rate at 70-80°C or higher, but the high temperature regime was not well characterized. Older data for other martensitic steels in distilled water are consistent with the lower activation energy of 30-40 kJ/mol for $0°C < T < 100°C$ (Johnson and Willner, 1965; Van der Sluys, 1969; Speidel, 1974). McIntyre and coworkers reported that the temperature dependence of HEAC in the steel of Fig. 4, stressed in aqueous NaCl solution, was defined by a single Arrhenius relationship with an activation energy of 36 kJ/mol (McIntyre et al., 1972a).

While data are limited, precipitation hardened Ni-based superalloys and 7000 series aluminum alloys exhibit temperature dependent crack growth rates that parallel the behavior of high strength steels. The temperature dependence of the subcritical crack growth rate in Ni-based alloy X-750 (σ_{YS} = 800 to 1000 MPa, depending on precise heat treatment) stressed in pure water is shown in Fig. 36; da/dt_{II} for H cracking is a maximum at 100-125°C and eliminated at 150°C (Mills et al., 1999; Hall and Symons, 2001). Crack growth at lower temperatures obeys an Arrhenius relationship with activation energy of 40-48 kJ/mol from straight line approximation to the log da/dt *vs.* 1/T data. Speidel reported simple Arrhenius behavior for lower strength Nimonic 105 (σ_{YS} = 825 MPa) for $0°C < T < 100°C$ (Speidel, 1974). The very high temperature crack growth behavior in Fig. 36 (Shen and Shewmon, 1991), labeled *Creep Limited*, is not considered, as it is outside the scope of this chapter on H cracking of high strength alloys within $\pm$150°C of ambient.

Arrhenius behavior described the temperature dependence of da/dt_{II} for 7000 series aluminum alloys in moist environments generally below 100°C, without evidence of reduced crack growth rate at higher temperatures. Specific activation energies are 40 kJ/mole for

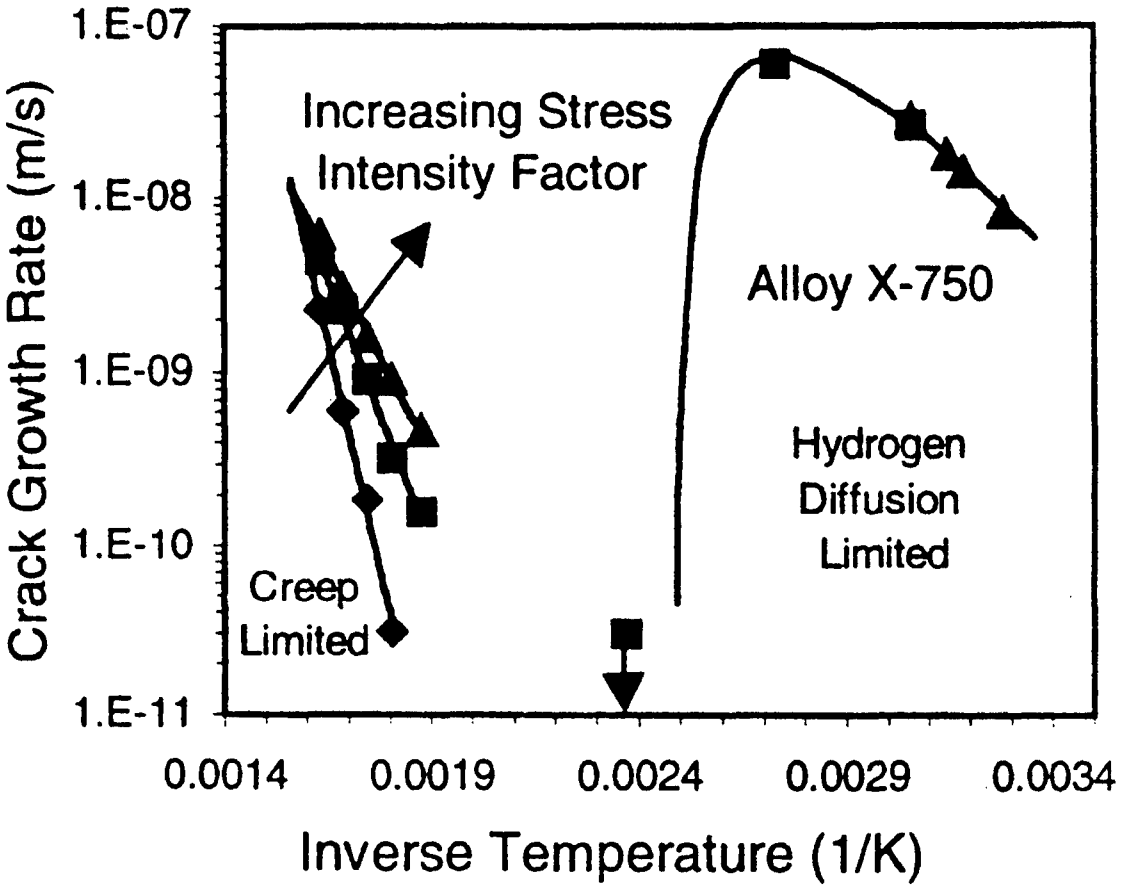

Figure 36. The temperature dependence of the Stage II K-independent subcritical crack growth rate for HEAC in precipitation hardened superalloy X-750 (σ_{YS} = 800 to 1000 MPa) stressed in high purity pressurized water. Only the low temperature regime, between 30 and 150°C, is relevant to the present review of H cracking in high strength alloys. (Hall and Symons, 2001; using low temperature data (□) by Mills et al., 1999; low temperature data (□) by Symons; and high temperature data (□, □, □) at several K levels (15, 32, and 61 MPa√m) by Shen and Shewmon, 1991.) (Copyright The Minerals, Metals and Materials Society, reprinted with permission.)

AA 7039-T6 in distilled water ($0^{\circ}C < T < 100^{\circ}C$) (Speidel, 1974), 60 kJ/mol for AA7022-T6 in high purity water ($0^{\circ}C < T < 140^{\circ}C$) (Vogt and Speidel, 1998), 85 kJ/mol for AA7039-T6 in aqueous KI electrolyte ($20^{\circ}C < T < 110^{\circ}C$) (Speidel and Hyatt, 1972), and 82 kJ/mol for AA7050-T6 in water vapor ($25^{\circ}C < T < 90^{\circ}C$) (Young and Scully, 2002). The study by Vogt and Speidel is unique in suggesting a maximum da/dt_{II} in this 7000 series aluminum alloy at about 30°C, with subsequent sharp decline in da/dt, followed by a 2nd rise, as shown in Fig. 37. The mechanistic explanation for the low temperature trend and da/dt_{II} maximum followed by further increase in crack growth rate at very high temperatures approaching the aging temperature is summarized in 6.03.8.4.2. In work by Young and Scully summarized in Fig. 19, the activation energy increased from 66 to 98 kJ/mol as AA7050 was aged from under to overaged conditions, consistent with an earlier result by Lee and coworkers (Lee et al., 1991; Young and Scully, 2002). The activation energy for Cu-free AA7050 was 59 kJ/mol for peak and overaged microstructures.

The activation energy computed by curve fitting a simple Arrhenius relationship to log da/dt *vs.* 1/T data is useful for engineering algorithms that describe temperature dependent cracking in structural integrity modeling. Fundamental mechanistic interpretation is; however, complicated because each of the fast and slow steps in the HEAC scenario shown in Fig. 2 is temperature dependent. A mechanism-based model for da/dt is required to explain an observed temperature dependence by establishing the precise combination of elemental-process activation energies that constitute the overall activation energy computed from crack growth rate measurements. Modeling in this regard is presented in 6.03.8.4.

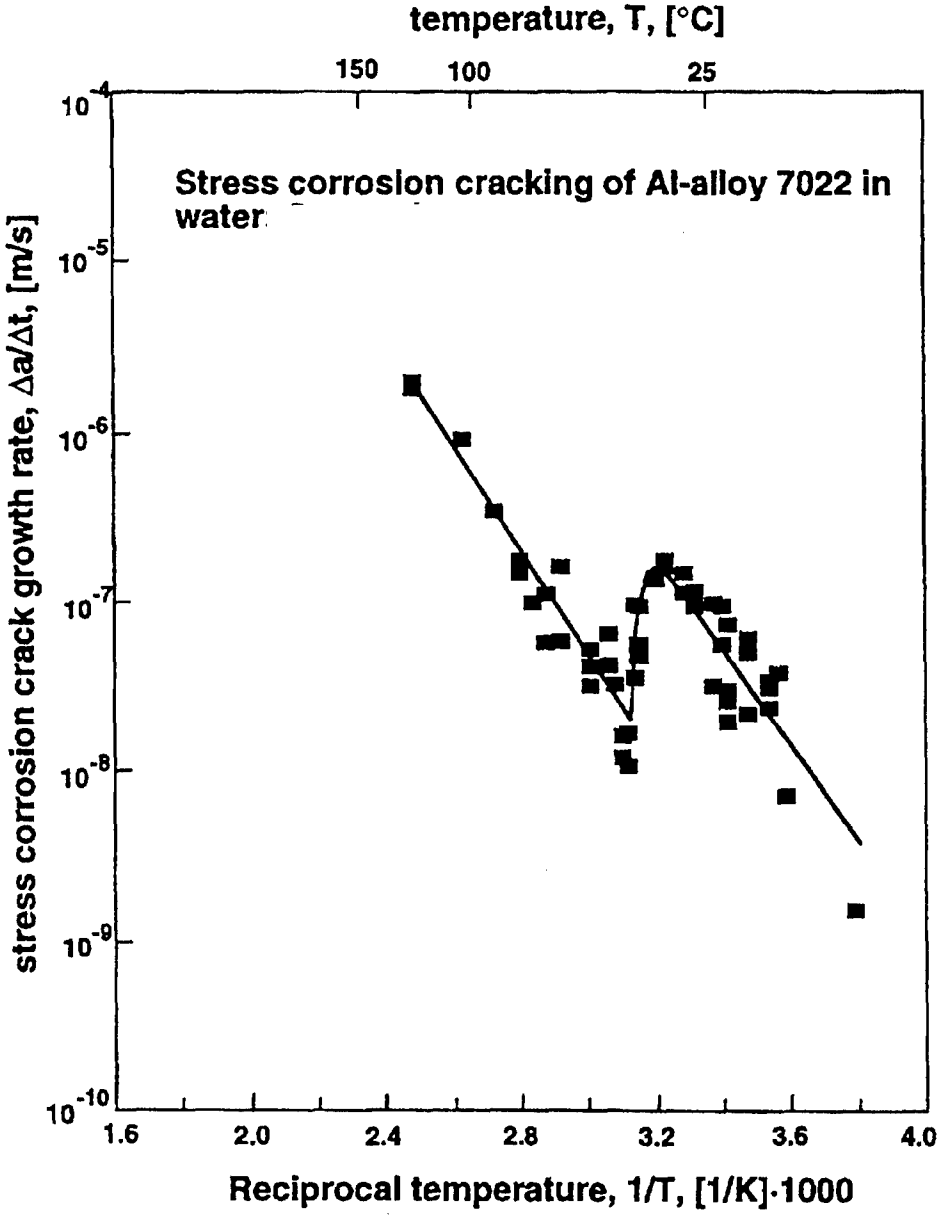

Figure 37. The temperature dependence of the Stage II crack growth rate in peak aged AA7022 (σ_{YS} = 495 MPa) stressed in high purity water. The solid line represents a crack growth rate prediction by the surface mobility model of Galvele, modified to include the effect of H from environmental reaction at the crack tip (6.03.8.4.2). (Vogt and Speidel, 1998: Publication permission requested from Elsevier Science.)

6.03.7 MECHANISTIC BASIS FOR HYDROGEN ASSISTED CRACK GROWTH

Mechanistic understanding of H cracking is essential to develop micromechanical-chemical models that predict threshold and growth rate properties for use in structural integrity modeling. Two mechanistic issues have dominated scientific discussions over the past several decades: (1) *Does the HEAC mechanism explain stress corrosion crack growth in high strength alloys in moist environments?* and (2) *What is the basic mechanism by which hydrogen causes crack tip damage leading to subcritical crack growth?*

6.03.7.1 Role of Hydrogen Assisted Damage in Stress Corrosion Cracking

Controversy has centered on the ability of the HEAC mechanism (Fig. 2) to explain subcritical crack growth in alloys stressed in environments that support concurrent crack tip dissolution, passive film formation, and atomic hydrogen production. A strong consensus has emerged that H provides the dominant damage mechanism for most high strength alloys stressed in moist environments.

6.03.7.1.1 Example of Experimental Support for HEAC: *7000-series Al Alloys*

Most reviews have concluded that hydrogen causes significant intergranular cracking in 7000-series aluminum alloys stressed in chloride solutions and moist gases (see Figs. 12 and 13) (Speidel and Hyatt, 1972; Gest and Troiano, 1974; Speidel, 1974, 1975; Thompson and Bernstein, 1980; Gruhl, 1984; Nguyen, 1987; Pickens et al., 1987; Burleigh, 1991; Lee et al., 1991;). However, supporting evidence is circumstantial (Holroyd, 1990). The nature of this experimental support is typical of that advanced to identify the HEAC mechanism for

stress corrosion cracking of other high strength alloy systems based on Fe, Ni and Ti.

The 7000 series aluminum alloys that are not susceptible to HEAC in dry gases including H_2 (Speidel and Hyatt, 1972; Speidel, 1974) do crack in H_2 that is ionized to produce atomic H, as well as in water vapor at pressures that are sufficiently low to preclude condensation and electrochemical reaction at the crack tip, but not H production through oxidation (Speidel, 1974; Koch, 1979; Wei and Gangloff, 1989). Similar IG fracture surface features were observed for cracking in atomic H and aqueous environments (Koch, 1979). The 7000-series alloys are susceptible to IG IHAC, similar to cracking in the external environment, and this IHAC is reversible when the H is removed by thermal treatment (Gest and Troiano, 1974; Montgrain and Swan, 1974; Scamans et al., 1976; Albrecht et al., 1979, 1982; Holroyd and Hardie, 1981; Tuck, 1985). Subcritical IG cracking was produced by H that was charged electrochemically during stressing, but on surfaces removed from the crack tip to separate H damage from dissolution and film formation (Ratke and Gruhl, 1980).

Environmental cracking in AA7075 in NaCl is substantial in Mode I, but greatly reduced for Mode III loading (Swanson, et al., 1981; Pickens et al., 1983), consistent with the dominant role of hydrostatic stress in HEAC (see 6.03.8.1 and 6.03.9.1.4). Atomic Mg and Zn segregate to grain boundaries in 7000 series alloys and there contribute, with H from environmental reaction, to decohesion analogous to temper embrittled steels (Pickens et al., 1983; Schmiedel and Gruhl, 1983). Subcritical crack growth in AA7075 stressed during exposure in a chloride environment was discontinuous, as evidenced by acoustic emission measurements and fracture surface crack arrest markings, consistent with repeated H accumulation within the crack tip FPZ as opposed to continuous crack advance by a

dissolution-based mechanism (Scamans, 1980; Martin et al., 1985). Discontinuous crack advance can be explained reasonably by mechanisms for environmental cracking that do not involved H (Parkins, 1990).

6.03.7.1.2 Crack Chemistry Advances

Stemming from the seminal work of Brown and coworkers (Sandoz et al., 1970; Smith et al., 1970; Brown, 1977), modern considerations of occluded crack electrochemistry more firmly establish the contributing roles of H production, dissolution and passive film formation in environment-assisted cracking (Gangloff, 1984; Turnbull, 1984; Turnbull and Ferriss, 1987). This recent work supports the HEAC mechanism as governing subcritical crack growth in high strength alloys. A critical accomplishment was a demonstration that the effects of various environmental variables on K_{TH} and da/dt (6.03.6.3.2) are described by the amount of atomic hydrogen produced locally at the straining crack tip.

6.03.7.1.2.1 Superalloys

Subcritical environment-assisted cracking in high strength superalloys is described by HEAC for gases and electrolytes, and using occluded-crack chemistry analysis for the latter situation. In separate studies the threshold for IN718 was measured to decrease with increasing P_{H2} (Moody et al., 1986; Moody et al., 1988) or decreasing electrolyte pH (Lillard, 1998), with regression analyses giving:

$$K_{IHEAC}\ (MPa\sqrt{m}) = 110\ P_{H2}^{-0.25}\quad (MPa)$$

$$K_{IH}\ (MPa\sqrt{m}) = 46.8\ exp(0.311\ pH) \qquad (6)$$

The microscopic cracking modes were similar for each environment and involved a mixture of IG and TG slip-plane based cracking. Figure 38 shows that these thresholds are defined by a single function of the crack tip H concentration for IN718 stressed in aqueous-acidified chloride solution (•) as well as high pressure H_2 (o) (Lillard, 1998). The K_{TH} declines with increasing crack tip H concentration, above 20 ppm and independent of the crack tip environment that produced this H. The specific regression result for these data in Fig. 38 is:

$$K_{IHEAC}\ (MPa\sqrt{m}) = 345\ (C_{H\text{-}TOT})^{-0.53} \quad (ppm) \tag{7}$$

This single correlation for gas and aqueous environment-assisted cracking supports the HEAC mechanism.

For the H_2 results in Fig. 38, the H content of the FPZ, in equilibrium with P_{H2} that is everywhere equal, was estimated using lattice-H solubility from Sievert's law, extrapolated from elevated temperature and increased to account for trapping using results for a similar superalloy microstructure (Moody et al., 1989). For IN718 in acid, the H concentration at the crack tip was estimated considering crack chemistry change. First, crack tip pH was estimated *vs.* bulk solution pH. The cathodic current density at this crack tip pH was determined experimentally from current density *vs.* applied potential data for IN718 exposed boldly in acid at several pH levels. Local H content was related to cathodic current density by hot extraction measurements of boldly preexposed specimens. With these estimates of $C_{H\text{-}TOT}$ in Fig. 38, the resulting correlation with K_{IHEAC} is identical for the acid and gas environments. This correlation is based on two assumptions. Since the strengths of these two lots of IN 718 were equal, the H contents in Fig. 38 were not increased to reflect crack

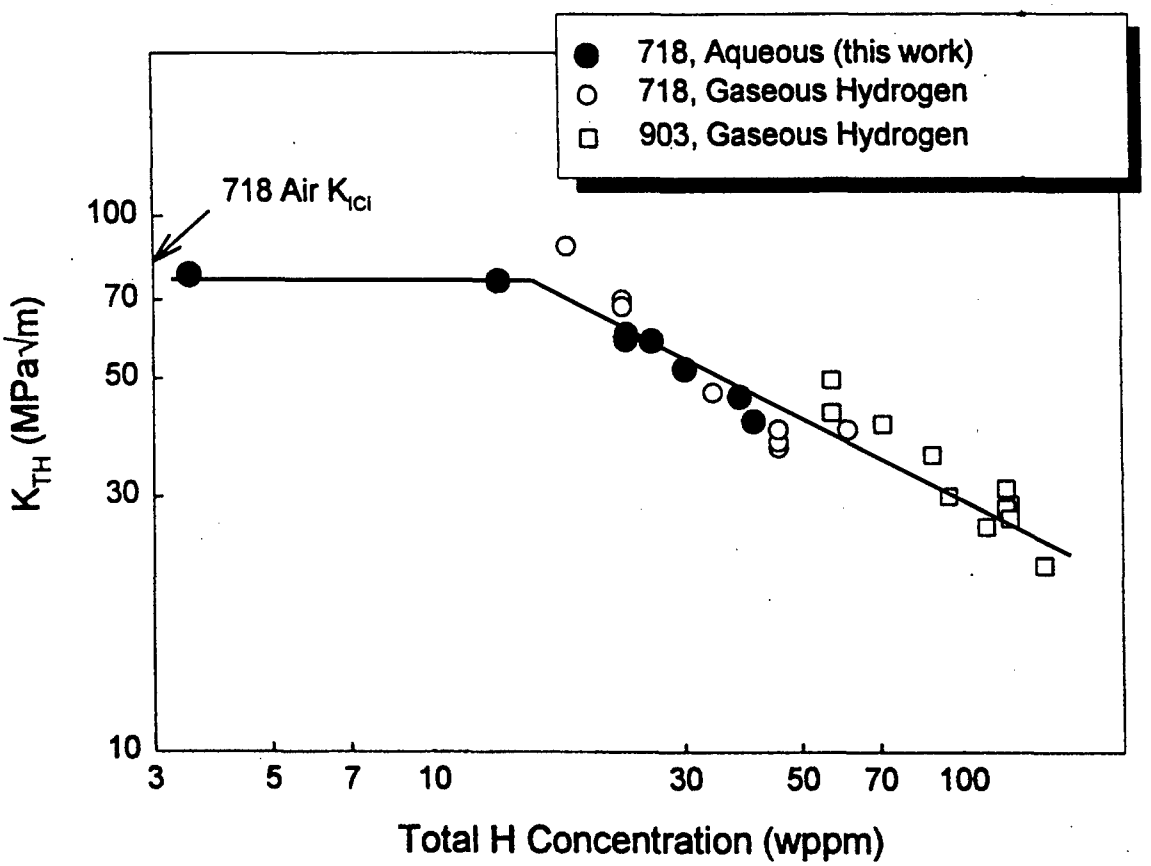

Figure 38. Threshold stress intensity for HEAC in peak aged IN718 and IN903, stressed in either high pressure H_2 (9, O), or acidified chloride solution with cathodic polarization at –1.0 V_{SCE} (•), *vs.* calculated H content produced at the crack tip. H-free superalloys cracked by microvoid processes at high K_{IC}, while HEAC in each environment produced a mixture of intergranular and transgranular slip-plane based cracking. IG cracking dominated at K_{TH} below about 50 MPa√m. (Lillard, 1998; Moody et al., 1986; Moody et al., 1988)

tip hydrostatic stress enhancement. The electrode potential gradient along the crack tip was judged to be sufficiently small so as not to affect crack tip H uptake.

6.03.7.1.2.2 Electrode Potential Dependence

Crack electrochemistry studies establish that the electrode potential dependence of environmental cracking in high strength metallic alloys is explained within the HEAC scenario. Applied potential affects both crack pH and tip electrode potential. The key parameter is the overpotential (η_H) that governs H production, equaling the difference between the pH dependent reversible potential for H production (E_H^o) and crack tip potential. For fixed surface film and microstructure, H content increases as η_H becomes more negative.

Steel: The deleterious effects of both anodic and cathodic polarization on subcritical crack growth thresholds for high strength steel in neutral chloride solution (Fig. 28) are explainable by crack chemistry considerations, strengthening the HEAC argument for these alloys (Smith et al., 1970; Sandoz et al., 1970; Brown, 1977). As potential is made more anodic, crack pH decreases due to increased cation dissolution and hydrolytic acidification (e.g., $Fe^{+2} + H_2O = H^+ + FeOH^+$ and $Cr^{+3} + H_2O = H^+ + CrOH^{+2}$) and E_H^o becomes more noble. Crack IR tends to depress the crack tip potential to values more negative than those applied to the external surface, near or above the free corrosion potential. The result of these two contributions from anodic polarization is that η_H becomes more negative and H concentration is intensified at the crack tip; K_{TH} decreases.

Increasing cathodic polarization promotes H uptake and lower threshold, provided that

the crack tip is polarized proportionate to the boldly exposed surface. Local polarization is required to maintain a favorable-negative overpotential for H production since E_H^o is progressively more negative as the crack pH becomes more alkaline. With this chemistry change, bold-surface H production could become the dominant supply of H to the crack tip FPZ provided there is sufficient time for H diffusion (Turnbull and deSanta Maria, 1990).

The sum of these behaviors explains the electrode potential dependence of a maximum in HEAC resistance for high strength steels (Fig. 28); however, the contributions of crack tip and bold-surface H are not defined and may vary with exposure time, specimen size and geometry, and H diffusivity. This analysis was quantified by extensive crack chemistry modeling by Turnbull and coworkers (Turnbull, 1984; Turnbull and Ferriss, 1987, 1987a; Turnbull, 2001, 2001a). Crack tip pH and electrode potential were modeled, and the amount of crack tip H was predicted. This approach is capable of predicting the effects of a wide range of environmental, crack geometry, and loading variables on crack tip H production. An example is provided by the results shown in Fig. 39, where the effect of crack depth on the threshold K_{IH} is modeled for high strength AISI 4130 steel in neutral NaCl solution and measured with short crack fracture mechanics experiments; agreement between theory and experiment is good (Gangloff and Turnbull, 1986).

7000-series Aluminum Alloys: The results in Fig.29, showing that Stage II crack growth rate increases with increasing anodic polarization for AA7050 in acidic chloride solution are consistent with HEAC. This hypothesis is confirmed directly by the data in Fig. 40, a plot of da/dt_{II} for peak aged AA7050 *vs.* the concentration of H measured local to the cracking process (Young, 1999; Cooper, et al., 2000). A 1 mm-thick specimen was cut from

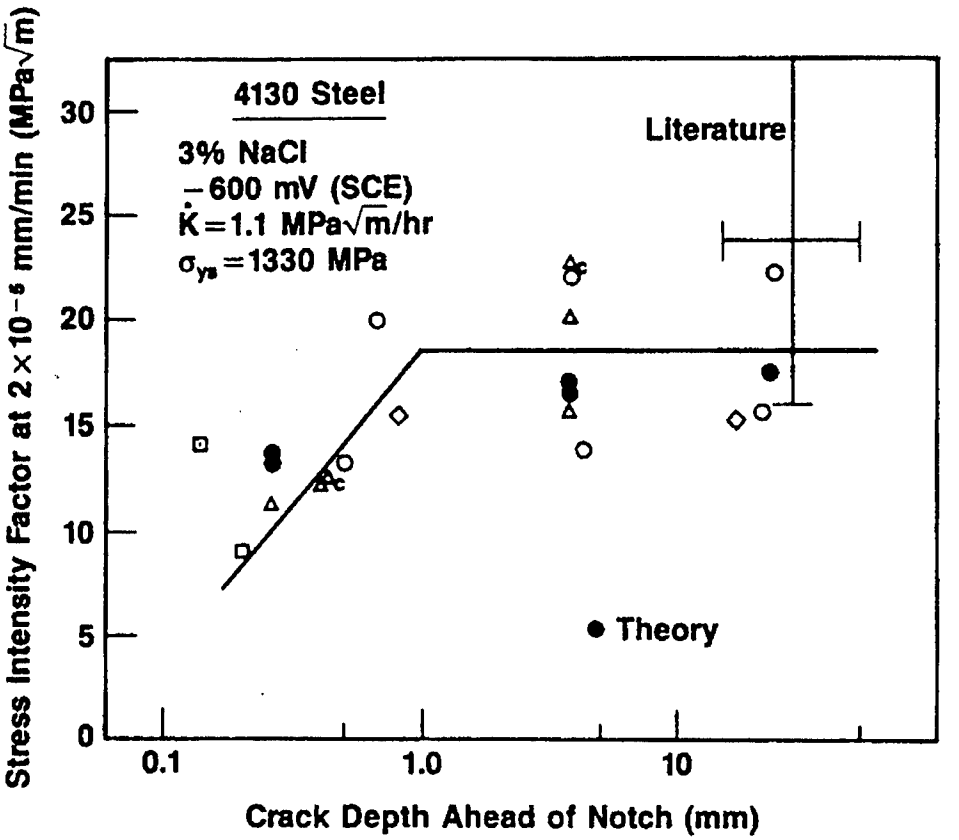

Figure 39. The model predicted (•) and measured (open symbols) crack depth dependence of the threshold stress intensity factor for subcritical crack growth in high strength AISI 4130 steel stressed under slow-rising CMOD ($dK/dt = 3 \times 10^{-4}$ MPa$\sqrt{m}$/s) in neutral NaCl solution at fixed electrode potential in the free corrosion regime. (Gangloff and Turnbull, 1986)

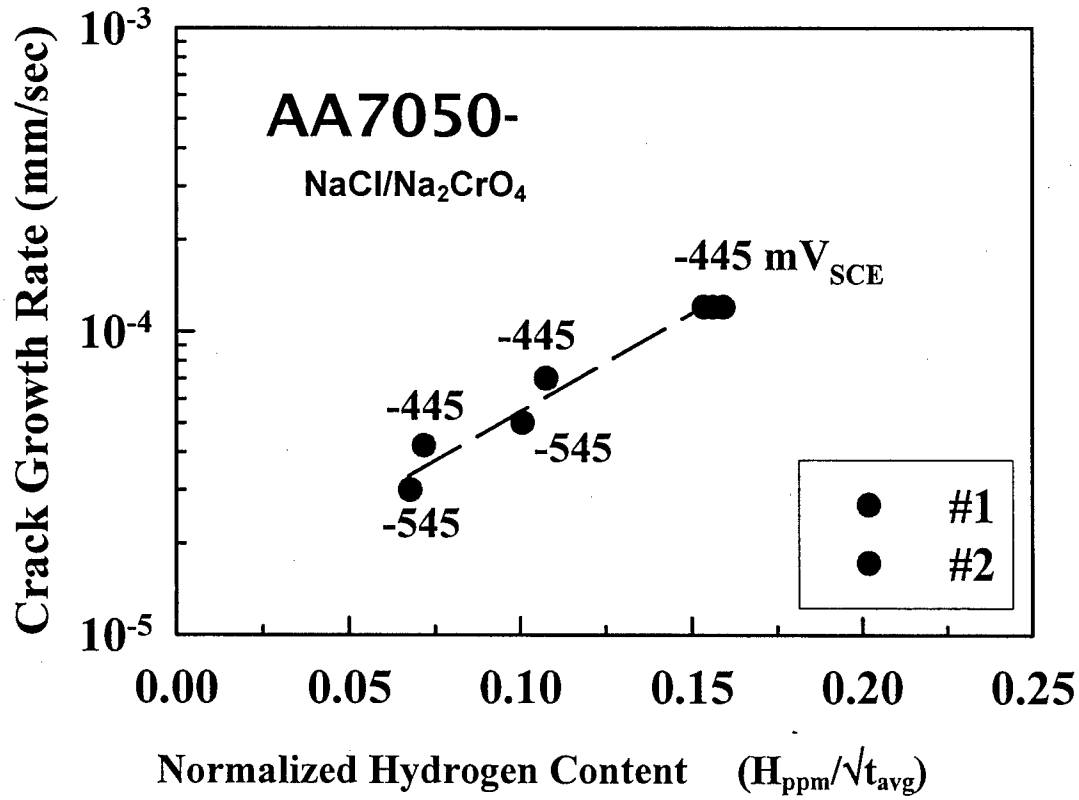

Figure 40. The dependence of da/dt on crack wake H content measured by thermal desorption spectroscopy and normalized by the average wake exposure time for two AA7050-T651 specimens cracked in acidic chloride-chromate solution at either –445 or –545 mV_{SCE}, corresponding to the conditions shown in Fig. 29. (Cooper et al., 2000:)

the wake of a crack grown in acidic chloride solution, processed to retain H, and subjected to thermal desorption spectroscopy to yield the H content that was presumably within the crack tip FPZ during subcritical crack growth. Crack growth rate is directly proportional to H concentration, normalized by the square root of the average time that the crack wake was exposed to solution. This normalization provides a speculative means to account for H uptake during crack surface corrosion well behind the growing crack tip. The most anodic polarization produced the highest-normalized H content and higher da/dt_{II}. Polarization to –545 mV_{SCE} produced less H and lower da/dt_{II}, while subsequent polarization to –445 mV_{SCE} produced the same low H content due to a complex hysteresis effect and da/dt_{II} remained low. These average H concentrations were confirmed by nuclear reaction analysis that showed a very large amount of H, of order 0.01 to 0.1 atom pct, localized within the first micrometer of the crack surface (Young, 1999; Cooper et al., 2000).

The presence of very high H in the FPZ, as well as enhanced H content due to anodic polarization that correlates with da/dt_{II}, each support the HEAC mechanism. Enriched H with anodic polarization is consistent with hydrolytic acidification (e.g., $Al^{+3} + H_2O = H^+ + AlOH^{+2}$). Moreover for AA7050, direct measurements showed that the crack tip potential is relatively insensitive to applied-anodic potentials in the range of Fig. 29, with the net result that η_H becomes more negative and H content on the crack tip surfaces increases with increasing anodic polarization (Cooper et al., 2000; Cooper and Kelly, 2001). These recent results strengthen the older evidence for predominant HEAC in 7000 series Al alloys, as summarized in 6.03.7.1.1.

Considering cathodic polarization, the situation is less clear and additional work is

required. Enhanced H production under both anodic and cathodic polarization of 7000 series aluminum alloys was inferred from permeation data (Gest and Troiano, 1974). There are; however, only limited data on crack growth rate under cathodic polarization and there is no evidence to support increased da/dt_{II} at potentials below those shown in Fig. 29 (Speidel and Hyatt, 1972; Holroyd, 1990). Increased growth rates are expected since the crack tip in AA7075 is polarized in the active sense in response to applied cathodic polarization (Edwards, 1985; Turnbull, 1984). The Al_2O_3 passive film dissolves under alkaline conditions and H uptake should occur in the crack with $\eta_H < 0$, as well as on bold surfaces if transient alkalinity is present.

Superalloys: The potential dependence of cracking in this class of alloys in strong acid solutions is consistent with the arguments developed for steels and aluminum alloys. The reduction in K_{IH} with increasing cathodic polarization (Fig. 11) is consistent with increasingly negative η_H because the crack tip potential parallels the applied values and E_H^o is unlikely to decrease since the solutions are highly acidic. Anodic polarization effects have not been reported and may not be significant since enhanced crack tip acidification is not likely in acidic-bulk solution. The data in Fig. 11 suggest that HEAC is mitigated at high-cathodic potentials. The reason for this is considered in the next section.

β/α-Ti: Extensive research established that severe intergranular environmental cracking in β-Ti alloys in neutral chloride solution (Figs. 6, 15 and 16) was by HEAC (Kolman and Scully, 1997, 1998, 2000). This work ruled out the formation of brittle hydride phase, as well as crack advance due to film rupture and dissolution. Rather, the scenario for cracking for this alloy class in the free corrosion regime in neutral chloride

solution followed that discussed previously: (1) crack tip passive film rupture from dislocation plasticity, (2) local dissolution of the exposed titanium and repassivation, (3) hydrolytic acidification of dissolved cations to lower crack tip pH, (4) H^+ reduction to form adsorbed H, and (5) H diffusion into the FPZ to nucleate damage (Kolman and Scully, 1997). Kolman and Scully performed electrochemical measurements to establish that elements (1) through (4) are valid and sufficient to enable H-assisted cracking. The passive film that forms on Ti crack and boldly exposed surfaces is stable for all chemical conditions typical of the results in Fig. 30. This behavior is unique compared to the Fe, Ni and Al-based alloy cases, and is critical to the cracking mechanism.

From this scenario, the applied potential dependence of K_{TH} (Fig. 30) is explained by H production at $\eta_H < 0$ governed by the hydrolysis reaction and crack IR in the free corrosion regime. Initial cathodic polarization exacerbates this cracking to a minimum K_{TH}, but polarization to more cathodic levels inhibits HEAC. This initial increase in cracking susceptibility should correspond to increasingly negative η_H, but this detail was not modeled. Cathodic inhibition was explained based on reduced η_H towards 0 as the crack tip electrode potential shifted in the negative sense less strongly compared to the reduction in E_H° as the crack chemistry became increasingly alkaline. Bulk surface H production never contributed to cracking due to the stable TiO_2 passive film that blocked H uptake. The benefit of anodic polarization, shown by the data for the older alloys in Fig. 30 (Blackburn et al., 1972), was explained speculatively by anodic polarization of the crack tip to above E_H° even with this reversible potential increased from hydrolytic acidification.

Local electrochemistry and HEAC explain two aspects of crack growth in β/α-Ti alloys.

Environmental cracking requires a preexisting crack. This is explained because crack tip acidification and IR polarization necessary for H production require a tight-occluded crack geometry (Kolman and Scully, 1997, 1998). Hydrogen production is nil on a surface that is exposed boldly to near-neutral chloride solution in the free corrosion regime. Second, the stable TiO_2 film at the crack tip must be ruptured to enable H production and uptake. Mechanical destabilization of this film was attributed to intersection of superdislocations with the crack front, followed by transients in anodic current as the Ti repassivated (Kolman and Scully, 1999). This behavior suggests that the rate of crack tip straining relative to Ti repassivation is an important variable.

An experimental study confirmed that intergranular HEAC was exacerbated by loading conditions that promoted increased crack tip strain rate ($\dot{\varepsilon}_{CT}$) to levels sufficient to destabilize the crack tip passive film and permit H entry to the FPZ(Somerday et al., 2000). $\dot{\varepsilon}_{CT}$ depends on dK/dt and da/dt, as well as crack tip creep deformation. The severe cracking susceptibility represented in Fig. 6 was produced by rising-K loading over a range of dK/dt, as well as during quasi-static loading where dK/dt ~ 0 but da/dt was high. In contrast IG HEAC was mitigated at low $\dot{\varepsilon}_{CT}$, insufficient to destabilize the crack tip passive film that remains in tact and thus is capable of blocking hydrogen uptake and subsequent embrittlement. For example, a stationary crack under slow dK/dt or fixed CMOD loading, or prolonged air preexposure at fixed K to reduce the primary creep strain rate, caused low $\dot{\varepsilon}_{CT}$ and eliminated IG cracking. Crack tip strain rate formulations have not been developed sufficiently from either continuum or dislocation mechanics modeling to reconcile these results quantitatively.

6.03.7.2 Hydrogen Assisted Damage Mechanisms

The fundamental mechanisms for hydrogen-assisted damage in metals have been reviewed extensively (Troiano, 1960, 1974; Lynch, 1988, 1997, 2003; Oriani, 1978, 1987, 1990; Hirth, 1980; Nelson, 1983; Birnbaum, 1990; Gerberich et al., 1996; Birnbaum et al., 1996; McMahon, 2001). Apart from cracking due to hydride formation, discussed elsewhere in this volume, the atomistic mechanism for hydrogen embrittlement is controversial with three major candidates advanced: Hydrogen Enhanced Decohesion (HEDE), Hydrogen Enhanced Localized Plasticity (HELP), and Adsorption Induced Dislocation Emission (AIDE). Each of these mechanisms is summarized, and the supporting theoretical and experimental evidence is noted. An additional and controversial mechanism based on surface diffusion of corrosion-induced vacancies to the crack tip (6.03.8) has not been applied extensively to H cracking in high strength alloys (Galvele, 1987; Parkins, 1990).

6.03.7.2.1 Hydrogen Enhanced Decohesion

The HEDE mechanism was first suggested by Troiano, and developed in detail by Oriani and coworkers (Fromberg, Barnett and Troiano, 1955; Troiano, 1960, 1974; Oriani, 1972, 1977, 1987, 1990; Oriani and Josephic, 1974, 1977; Gerberich et al., 1991). In this model, H accumulates within the crack tip FPZ and there reduces the cohesive bonding strength between metal atoms. Initially, H accumulation above the unstressed-lattice solubility was driven by lattice dilation due to elastic hydrostatic stresses (Li et al., 1966), while later work recognized that trapping is a potent mechanism for H segregation (Pressouyre, 1980). McMahon and coworkers advanced the view that impurity elements segregated to grain

boundaries similarly reduced host-metal bond cohesion, adding to the embrittling effect of H (Bandyopadhyay, et al., 1983; Briant and Banerji, 1983; McMahon, 2001). The HEDE provides the basic notion that H damage occurs in the FPZ when the local crack tip opening tensile stress exceeds the maximum-local atomic cohesion strength, lowered by the presence of H (Oriani, 1972). In the HEDE scenario, H damage sites are located at a distance ahead of the crack tip surface where tensile stresses are maximized. Predictions are derived from knowledge of crack tip stress, H concentration at damage sites, and its relationship with the interatomic bonding force vs. atom displacement law.

A consensus is emerging that HEDE is the dominant mechanism for IHAC and HEAC in high strength alloys that do not form hydrides (Oriani, 1987, 1990). HEDE is likely for several reasons. First, large concentrations of H should accumulate in the FPZ due to very high crack tip stresses plus H trapping along a crack path, as suggested by Oriani (1987) and supported by modern considerations of crack tip mechanics and trapping (see 6.03.8.1 and 6.03.8.2) (Gangloff, 2003). For example, the model calculations in Fig. 41 show that substantial levels of H, approaching full interface coverage at 100 atomic pct, can in principle accumulate along grain boundaries in a Ni-based superalloy undergoing HEAC. The higher H contents shown in Fig. 41, achieved during stressing at 54°C in H_2, are particularly relevant to this discussion of HEDE. The data points for cracking at 260 and 338°C may be pertinent to a creep based damage mechanism rather than decohesion, as suggested by the crack growth rate data in Fig. 36 (Hall and Symons, 2001). Figure 36 also reflects the temperature dependence of H production from electrochemical reactions of Ni with water, while Fig. 41 relates to temperature dependent dissociative chemisorption of H_2

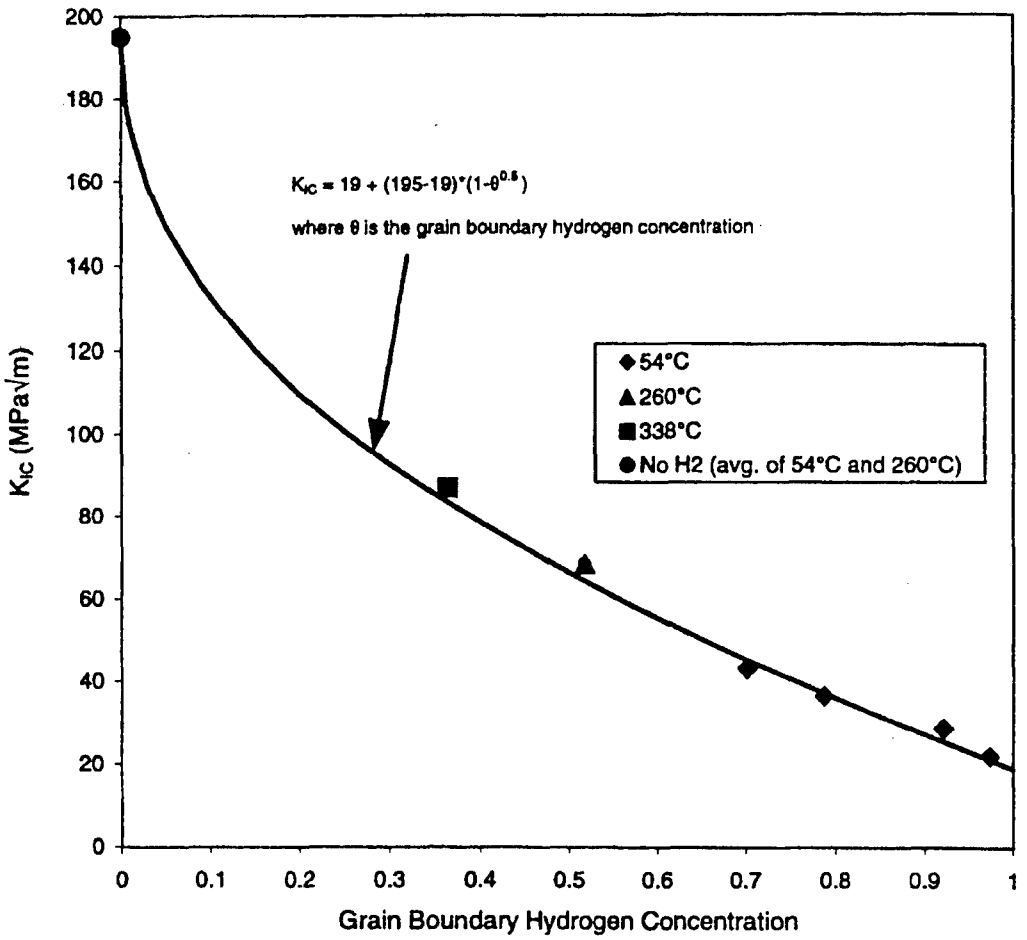

Figure 41. The localized-H concentration dependence of the threshold stress intensity for HEAC of high strength superalloy X-750 (σ_{YS} = 800 MPa) tested in H_2 at several pressures and temperatures under rising CMOD at dK/dt = 0.0012 MPa√m/s. The plotted H concentration (atom fraction of H in Ni) was calculated as localized at grain boundaries due to H trapping at boundary carbides (E_B = 26 kJ/mol) coupled with crack tip hydrostatic stress estimated from conventional plasticity theory as $\sigma_H = 4.5\sigma_{YS}$, see 6.03.8.1 and 6.03.8.2. Tests at 260 and 338°C were conducted in 13.8 MPa H_2, while those at 54°C were conducted at several P_{H2} levels between 0.14 and 34.5 MPa. (Symons, 2001: Reprinted with permission from Elsevier.)

to H, coupled with H trapping in both cases (6.03.8.4). Similarly high crack tip hydrogen concentrations, approaching many atomic pct, were predicted for IHAC in AerMet®100 UHSS due to very high-local tensile stress and H trapping (Thomas et al., 2003).

Second, experiments show directly that the sharpness of a crack tip in stressed Fe-3%Si single crystal increases progressively with increasing H_2 pressure and decreasing temperature; shown by decreasing crack tip angle (α) in Fig. 42 (Vehoff and Rothe, 1983; Vehoff and Neumann, 1985). In this figure, the horizontal-dashed line represents crack growth by slip only, at a crack tip opening angle, α, of 70° that equals the angle between active slip planes in the single crystal. This angle will decrease as a second mechanism of crack growth becomes increasingly important. Since the crack planes in Fe-3Si were always parallel to {100} and dimples were not resolved on these crack surfaces (see ensuing discussion of AIDE), the results in Fig. 42 were interpreted to prove that the decohesion mechanism progressively replaced crack tip slip as the advance process, as least for this case of transgranular HEAC and with increasing P_{H2}. The temperature and P_{H2} dependencies were argued to be consistent with the amount of H expected to adsorb on an Fe surface.

Third, atomistic simulations suggest that H can reduce atomic cohesion (Oriani, 1987, 1990; Gerberich, et al., 1991). Finally, a wide range of micromechanical models have been derived from the decohesion principle and effectively fit experimental values of K_{TH} and da/dt_{II} for IHAC and HEAC. These models span the range from continuum fracture mechanics to crack tip dislocation mechanics (Gerberich et al., 1991). The effects of P_{H2} and T, including rapid pressure or temperature-change experiments, as well as the effects of H concentration and σ_{YS}, have been predicted reasonably as summarized in 6.03.8.

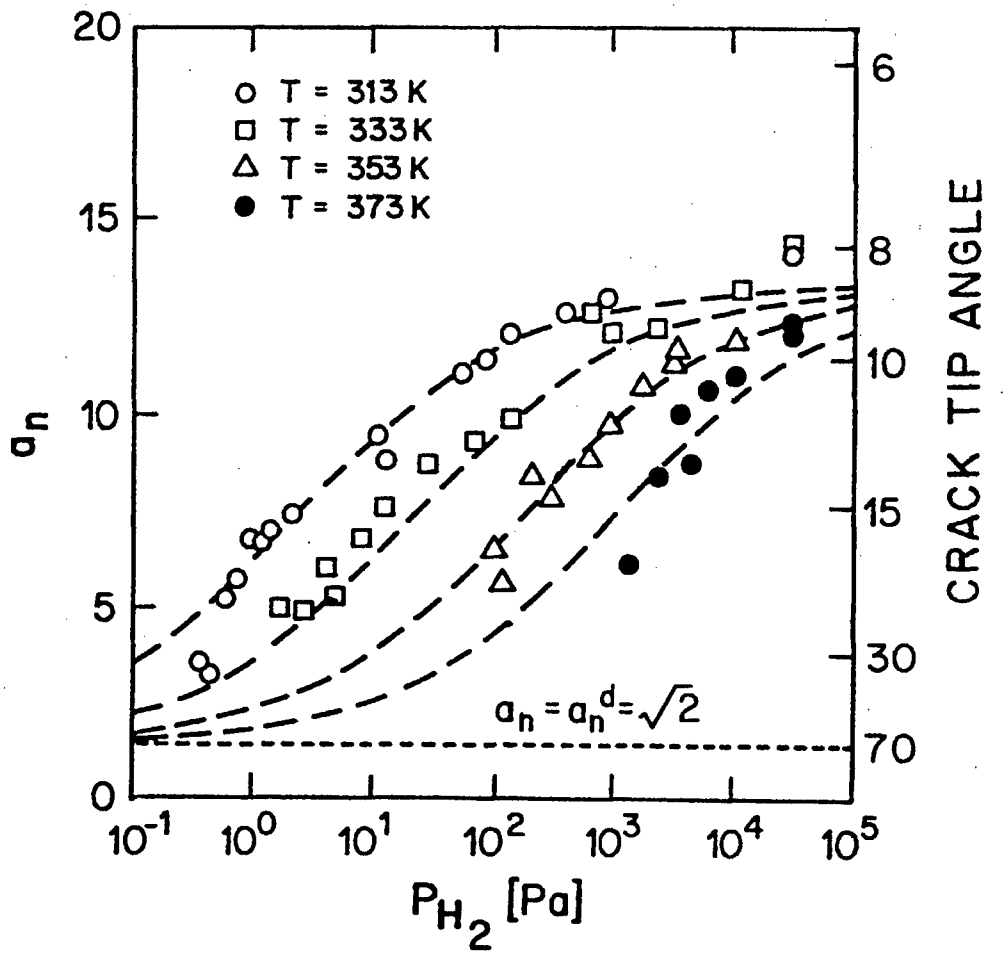

Figure 42. The dependence of *in situ* measured crack tip opening angle, α, on H_2 pressure for Fe-3%Si single crystals stressed at several temperatures. The parameter a_n represents the ratio of incremental crack extension to crack mouth opening; a_n = cot (α/2). The horizontal-dashed line represents crack growth exclusively by crack tip slip, with α as the angle between active slip planes in the single crystal. As decohesion-based growth becomes increasingly important, α decreases. (Oriani, 1990. After data from Vehoff and Rothe, 1983 as well as Vehoff and Neumann, 1985: Copyright NACE International, reprinted with permission.)

The HEDE mechanism is debated because of weaknesses in the supporting evidence. Foremost, there is no direct experimental demonstration that atomic H dissolved in a metal lowers the interatomic force-displacement relationship, or alters elastic properties or surface energy that are derived from such bonding. The primary problem is that the amount of H that can be dissolved in a specimen for bulk-property measurement is orders of magnitude less than that projected to accumulate locally within the crack tip FPZ. While theory suggests effects of H on metal bonding, results are limited by the capabilities of such modeling and necessary assumptions. The theoretical demonstration of H-sensitive bond strength can similarly support HEDE, HELP and AIDE (Daw and Baskes, 1987). Finally, all HEDE-based models of macroscopic K_{TH} and da/dt properties contain one or more adjustable parameters due to uncertain features of the crack tip problem, as outlined in 6.03.8. As such, good predictions of IHAC and HEAC data are tempered.

6.03.7.2.2 Hydrogen Affected Localized Plasticity

Beachem first suggested that H stimulates dislocation processes that localize plastic deformation sufficiently to result in subcritical crack growth with brittle characteristics on the macroscopic scale (Beachem, 1972). Two variations of this notion have been advanced as the AIDE and HELP mechanisms.

6.03.7.2.2.1 Adsorption Induced Dislocation Emission

Lynch argued that H-induced weakening of metal-atom bond strength results in enhanced emission of dislocations from crack tip surfaces where H is absorbed (Lynch,

1977, 1988, 1997, 2003). AIDE attributes H-enhanced crack growth as predominantly due to this focused emission of dislocations, exactly from the crack front and along intersecting planes that geometrically favor sharp-crack opening and advance rather than crack tip blunting in the absence of H. During loading, plastic deformation is also triggered within the crack tip plastic zone; and microvoid formation, with or without an assist from dissolved H, could occur. The linkup of voids adds a component to crack advance and maintains a sharp crack tip by interacting with the intense slip bands from crack tip dislocation emission.

The crack surface should reflect this advance process and contain facet-like features parallel to the plane that bisects crack tip slip planes, as well as a high density of microvoids if this latter feature occurs. Voids should occur on a size scale that is substantially less than those formed about inclusions and larger dispersoids or precipitate particles during fracture without H and AIDE. Facets may be parallel to low index planes for certain symmetric slip plane configurations, but also along higher index planes if the crack tip slip state is unbalanced. Intergranular cracking in the AIDE formulation reflects preferential adsorption of H along the line of intersection between the grain boundary plane and crack front, and perhaps a higher density of precipitates that may form preferentially along grain boundaries (Lynch, 1988). This mechanism is best suited for HEAC; however, H localization to a crack tip during IHAC could also be result in AIDE.

The main evidence for the AIDE mechanism is fractographic (Beachem, 1972; Lynch, 1977, 1988). Specifically, the geometry of transgranular cracking, largely along low index planes that intersect active slip systems intersecting a crack front in single crystals of Al alloys and Fe-Si, was claimed to support AIDE. A high density of very small dimples

populated IG facet surfaces produced by HEAC in several alloy systems and polycrystalline microstructures. Critically, these features were reported to be similar for HEAC and liquid metal embrittlement (LME). Cracking by LME is clearly restricted to a crack surface mechanism, consistent with AIDE. Since similar fracture surface features are reported for HEAC and LME, logic suggests that the AIDE mechanism is similarly operative at the crack surface only (Lynch, 1997, 2003). Third, Lynch argued that the very fast da/dt reported for HEAC in high strength alloys is only explained by surface embrittlement, as envisioned in the AIDE mechanism and counter to HEDE where H damage sites are within the crack tip FPZ. Atomistic calculations that suggest H-reduced atomic cohesion can be invoked to support AIDE as well as HEDE (Daw and Baskes, 1987).

The AIDE mechanism is debated because of weaknesses in the supporting evidence. The structure of slip about a crack tip in a hydrogen exposed metal has never been characterized sufficiently to show H stimulated dislocation emission and associated geometric crack extension. High strength polycrystalline alloys are strengthened by a complex array of finely spaced barriers to dislocation motion that should provide significant back-stress to stifle dislocation emission from a crack tip. Intergranular cracking is predominant in IHAC and HEAC, but AIDE does not provide a clear explanation of why this is prevalent, apart from enhanced fine-scale voiding. The presence of very small voids on intergranular facets from HEAC and LME is controversial. Those who favor HEDE tend to not observe an organized void-like structure on facet surfaces. The initial argument that small-shallow voids are only resolved by careful transmission electron microscopy of low-angle shadowed replicas viewed at high tilt was reasonable (Lynch, 1977), but has been diluted by modern

SEM methods. An example of a modern-SEM analysis is summarized in Fig. 43, where an IG facet from HEAC in α precipitation hardened β-Ti was examined with a high brightness electron source, multiple detectors to change surface topography, high magnification, and matching surface stereographic analysis (Somerday, 1998b; Somerday et al., 2003). Shallow microvoids as small as 0.02-0.04 μm in diameter should be resolvable with this method; however, there was no evidence of an organized surface structure indicative of shallow microvoiding. Rather, the features were undulations with occasional matching ridges and protrusion-cavity pairs, each consistent with decohesion of β-Ti grain boundaries that are impacted by α precipitates in the complex-underlying microstructure. While there is need for systematic observations, surface features typical of AIDE have not been reported widely. The argument that only AIDE can explain rapid rates of crack growth is refuted by the analysis of H diffusion from the crack tip surface to damage sites in the FPZ, as presented in 6.03.8.4.2 (Gangloff, 2003). Finally, the AIDE mechanism has not been developed to yield semi-quantitative predictions of K_{TH} or da/dt_{II} for subcritical IHAC and HEAC. As such, this model has not been tested and the AIDE perspective is to date not useful for supporting structural integrity analysis.

6.03.7.2.2.2 Hydrogen Enhanced Localized Plasticity

Birnbaum and coworkers proposed that dissolved H enhances the mobility of dislocations, resulting in extreme localization of plastic deformation sufficient to enable

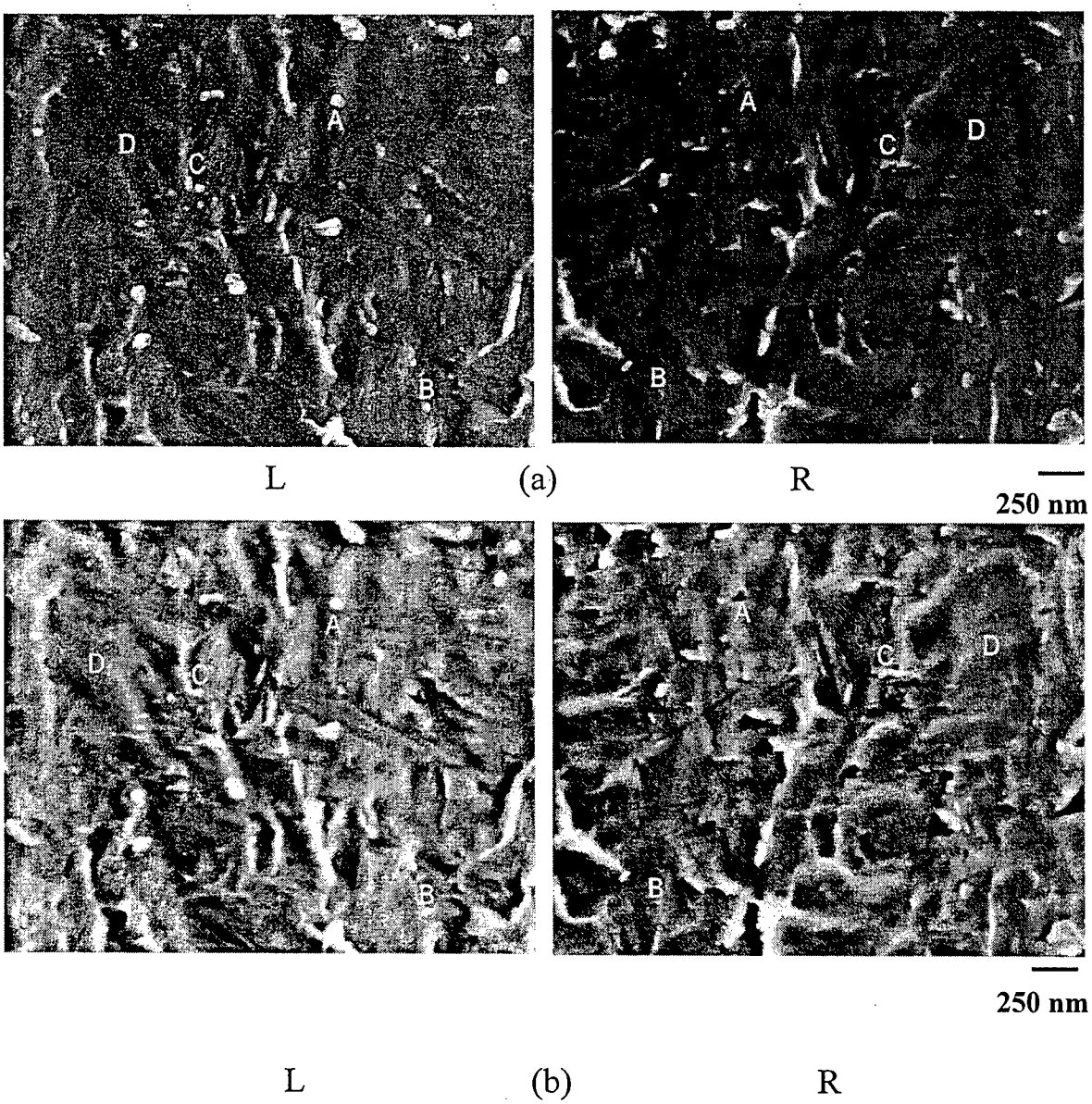

Figure 43: Matching field emission SEM images of an IG facet in α-hardened β-Ti (Beta-C) cracked in aqueous NaCl following the conditions illustrated in Fig. 15. These high magnification images were formed with the signal accumulated from: (a) the secondary electron detector immediately above the specimen, and (b) dual secondary electron detectors. The images marked "L" and "R" were obtained from the matching-opposite areas of the fracture surface. The features marked A, B, and C are matching protrusion/cavity pairs; D shows subtle undulations on the fracture surface. (Somerday, et al., 2003)

subcritical crack growth that is macroscopically brittle (Birnbaum, 1990; Birnbaum et al., 1997, Robertson, 2001). This effect was reported for high strength Al alloys (Bond et al., 1987), pure Ni (Robertson and Birnbaum, 1986), pure Fe (Tabata and Birnbaum, 1984), austenitic stainless steel (Rozenak et al., 1990), and single phase α-Ti (Shih et al., 1988). The HELP mechanism differs from AIDE in that dislocation mobility is enhanced due to H accumulation about dislocation cores, resulting in reduced elastic energies of interaction between moving dislocations and a variety of obstacles (Birnbaum and Sofronis, 1993; Robertson, 2001). Since H reduces interaction energy, the stress required for dislocation motion is decreased and plasticity is enhanced.

The primary evidence for HELP is *in situ* high voltage electron microscopy of thinned specimens subjected to plastic deformation during exposure to either vacuum or H_2 (Robertson, 2001). Such observations revealed an increased number of dislocations in a pileup, as well as initiation of dislocation motion, due to H_2 introduction to the electron microscope. Similar plastic deformation accompanies crack growth in the TEM; however, such growth occurred at lower-applied stresses in the presence of H. For example, a stationary crack formed in vacuum began to propagate after introduction of H_2 to the microscope. Such cracks propagated along a grain boundary and in the matrix volume adjacent to a boundary; with the interface mode prevalent when impurities such as S in Ni were present to augment H damage.

Studies of H effects on bulk specimens show decreased flow stress, increased stress relaxation, and altered strain rate sensitivity due to dissolved-bulk H (Robertson, 2001). However, H effects on hardening/softening are controversial, with diametrically opposed

results reported for the same alloy and debate on experimental differences or artifacts possibly responsible for each trend (Robertson, 2001; Birnbaum, 1990). While such information can confirm that H interacts with dislocations to affect plastic flow, the point is moot since the high hydrogen content, highly triaxial stress state, and gradated character of the crack tip FPZ are not represented by bulk crystal uniaxial deformation experiments.

The HELP mechanism is debated because of additional weaknesses in the supporting evidence. The TEM studies use a thin foil (< 200 nm) with at best a two-dimensional stress state and substantial possibility for surface effects on dislocation motion. Surface issues may be exacerbated by the high fugacity H, produced by H_2 dissociation in the electron beam and capable of reducing surface oxide and oxidizing hardening solute such as carbon or oxygen. These changes, rather than a core-H interaction could cause the observed plasticity and thus be unique to the thinned foil. Studies have not been extensive for complex microstructures with multiple obstacles and very short slip distances typical of high strength alloys. The geometry of localized flow in such high strength microstructures has not been developed. Modeling of dislocation mobility has not included H drag on the moving-dislocation line. Finally, the HELP mechanism has not been developed to yield semi-quantitative predictions of K_{TH} or da/dt_{II}. As such, the HELP model does not support structural integrity analysis.

6.03.8 MECHANISM-BASED MICROMECHANICAL-CHEMICAL MODELING OF HYDROGEN ASSISTED CRACKING

The goal of micromechanical-chemical modeling of IHAC and HEAC is to predict the dependencies of the threshold stress intensity and subcritical crack growth rate on

environmental, material and loading variables. This is accomplished by focusing on the crack tip FPZ shown in Fig.2 and developing relationships that describe:

- *Crack tip stress and plastic strain distributions*
- *Crack tip H concentration localization*
- *Location of H-damage sites at a critical distance (χ_{CRIT}) into the crack tip FPZ*
- *Failure criterion involving a critical H content-local stress combination*

Modeling must include the key factors that govern IHAC and HEAC, including: (a) H production by occluded crack electrochemistry, (b) trap-sensitive H solubility and mobility, (c) specific microscopic crack path, (d) coupling of continuum and dislocation-based crack mechanics over multiple length scales, and (e) the mechanism of H damage, either decohesion or plasticity based. Models of the threshold assume an equilibrium perspective, while da/dt formulations must include kinetics.

Three complications hinder modeling. First, it is necessary to integrate the mass transport and reaction processes that drive crack growth. Second, these factors change sharply over distances on the order of 0.05-10 μm in the FPZ, and finally, the location of H-damage ahead of a crack tip is controversial. All models developed to date contain one or more unknown parameters that are adjusted to fit experimental data. As such, the best of models are informative but not fully predictive for use in structural integrity analysis.

6.03.8.1 Crack Tip Mechanics

Quantitative descriptions of crack tip stress and strain distributions are central to micromechanical models of H cracking. The singularity and (distance, x)$^{-1/2}$ dependence are

central features of the elastic tensile stresses about the crack tip. The correct plasticity treatment to predict actual opening direction (σ_{YY}) and hydrostatic (σ_H) tensile stresses, as well as the tensile-plastic strain (ε_P), is critically important. Three approaches have been taken, including: (a) elastic-plastic fracture mechanics with finite element analysis, (b), strain gradient plasticity, and (c) dislocation-configuration shielding.

Rice proposed the basic elastic-plastic fracture mechanics approach that has provided the foundation for IHAC and HEAC modeling over the past two decades (Rice, 1977). The Hutchinson-Rice-Rosengren (HRR) field describes stresses and strains within the crack tip plastic zone, based on the J-integral and augmented by large strain finite element analysis by McMeeking and others (Anderson, 1995). The critical features of this formulation are illustrated schematically by the curve labeled *Conventional J_2 Plasticity* in Fig. 44. The σ_{YY} increases from near the uniaxial σ_{YS} at the crack tip surface, through a maximum at a distance ahead of the crack tip given by $x \sim J/\sigma_{flow} \sim K^2/\sigma_{flow}E$, and merges with the HRR and elastic stress distributions that decay as $1/x^{(1/1+n)}$ where n is a hardening exponent that equals 1 for elastic deformation and 10 to 20 for plasticity in high strength alloys. The hydrostatic stress distribution mirrors the σ_{YY} trend, with the maximum level of each equaling a multiple of σ_{YS} and the exact value depending on work hardening. For the high strength and low work hardening alloys relevant to this chapter, the maximum levels of σ_{YY} and σ_H are $3.5\sigma_{YS}$ and $2.5\sigma_{YS}$, respectively (Akhurst and Baker, 1981; Anderson, 1995). The crack tip is modeled to blunt in this formulation to an opening, δ_T, equaling $K^2/2\sigma_{YS}E$ where $\sigma_{YS} \sim \sigma_{flow}$ for high strength alloys, and crack tip tensile stresses are maximum at

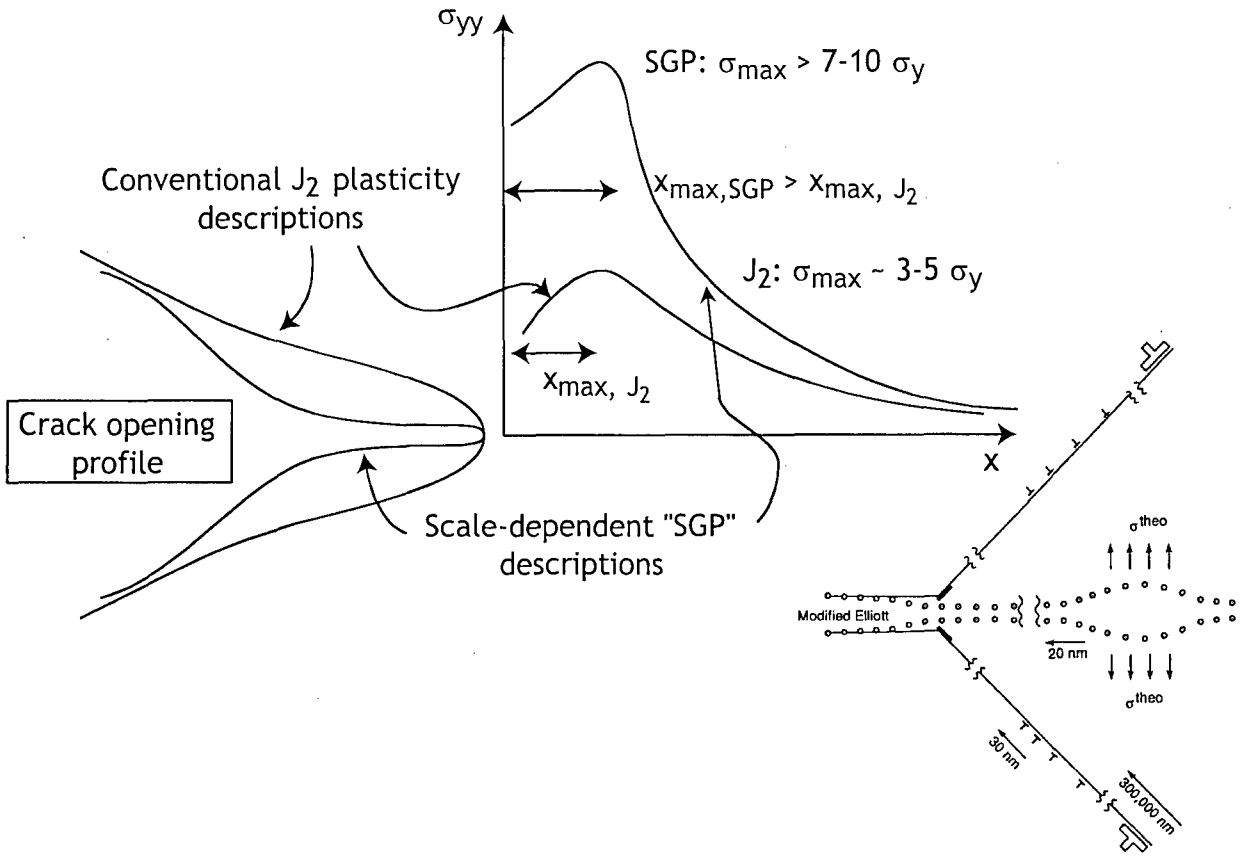

Figure 44. Schematic diagrams of: (top) the distributions of crack tip tensile stress reflecting either conventional plasticity description of elastic-plastic deformation, or a length-scale dependent hardening description of near-crack tip deformation in the presence of a strong strain gradient (Wei and Hutchinson, 1997; Jiang et al., 2001), and (bottom-right) the discrete dislocation model of crack tip mechanics from Gerberich and coworkers (Gerberich et al., 1991). SGP refers to strain gradient plasticity. (Publication permission requested from Taylor and Francis Group.)

about $2\delta_T$ ahead of the crack tip surface. Typical distances are shown in Table 2.

Table 2. Calculated maximum stress distances for high strength alloys at low applied K

Alloy	σ_{YS} (MPa)	Applied K (MPa $\sqrt{m}$)	$2\delta_T = K^2/\sigma_{YS}E$ (μm)
Fe-3%Si Single Crystal	300	30	20
Precipitation Hardened Austenitic Steel	850	90	48
Nickel Based Superalloy	1125	50	12
Precipitation Hardened Aluminum	500	15	6
18Ni Maraging Steel	1700	30	4
Tempered Martensitic Steel	1600	40	6
$\beta + \alpha$ Ti Alloy	1150	30	8

The blunt crack solution may not be relevant to H cracking in high strength alloys. Recent attention focused on strain gradient plasticity (SGP) as a mechanism to produce a very sharp crack tip and extraordinary stress elevation just ahead of the tip, as shown schematically by the higher trend in Fig. 44 (Hutchinson, 2000; Fleck and Hutchinson, 2001; Needleman and Sevillano, 2003). Geometrically necessary dislocations form to accommodate a high gradient in strain, as exists at a crack tip, and provide an additional hardening source to augment work hardening. This behavior persists at a crack tip if the size of plasticity is on the order of the material length scale that defines the gradient hardening response; of order 0.5-5 μm.

IHAC and HEAC in high strength alloys at low applied K levels are within the crack tip deformation regime where gradient plasticity effects must be considered. Hutchinson and others applied this plasticity description to the crack tip problem, and predicted a factor of 3 reduction in the blunted δ_T, increases in σ_{YY} to as high as $10\sigma_{YS}$, and increased σ_H to $8\sigma_{YS}$

(Wei and Hutchinson, 1997; Jiang et al., 2001). As strain gradient based descriptions of crack tip plasticity are emerging rapidly, these results are approximate and require verification for various crack tip boundary conditions. None-the-less, the possibility for stress elevation of the sort shown in Fig. 44 must be incorporated in micromechanical models of crack tip IHAC and HEAC. To date, this had not been accomplished formally (Thomas et al., 2003). The location of the maximum stresses in an SGP affected FPZ is not clear, but is certainly no larger than the values indicated in Table 2 from J_2 plasticity theory.

As a third approach, dislocation considerations have been employed to determine an elastic-plastic crack tip stress distribution for input to H damage modeling. Thompson and latter Kameda described the stresses adjacent to the tip of an atomistically sharp intergranular crack pertinent to hydrogen embrittlement (Thomson, 1978; Kameda, 1986a). A very small dislocation-free zone between the crack tip and dislocation pileup that screened the elastic crack tip singularity guaranteed this sharpness in the Mode I opening direction. The crack opening-direction stress in the dislocation free zone was estimated to equal between 6.5 and 9 GPa for a high strength material (σ_{YS} = 1,500 MPa and $0.08 < n < 0.10$) and subjected to applied K levels typical of IG hydrogen cracking thresholds (Kameda, 1986a).

Gerberich and coworkers extended this approach by modeling the interaction of elastic stress fields associated with a sharp crack tip under remote loading, as well as a distribution of discrete-shielding dislocations that dominate very-near tip stresses and a superdislocation that is removed from the tip and defines global crack tip plasticity with work hardening (Gerberich et al., 1991; Gerberich et al., 1996; Katz et al., 2001). This situation is shown

schematically in the lower portion of Fig. 44. The aim is to connect the local crack tip driving force, as stress or the crack tip stress intensity (k_{tip}) with the standard far-field stress intensity factor, K, used to correlate H cracking properties for structural integrity applications. This dislocation model, applied to understand HEAC in an Fe-Si single crystal (σ_{YS} = 300 MPa), predicted crack tip σ_H of 15 to 25 GPa, maximized 20 nm ahead of a sharp crack tip (Chen and Gerberich, 1991). These very near tip stresses are substantially higher than those associated with the continuum plasticity solution pertinent to the relatively large crack tip plastic zone. Away from the crack tip, into the plastic zone and beyond, the dislocation simulation is consistent with the HRR and elastic stresses (Huang and Gerberich, 1992). Notably, the existence of a dislocation free zone and morphology of slip about the crack tip have not been determined experimentally for high strength alloys with complex microstructures.

Plastic strain-based models have also been proposed to describe H-assisted threshold and crack growth rate properties, particularly in austenitic superalloys that exhibit a substantial amount of H-assisted transgranular cracking associated with slip bands (Moody et al., 1990b, 2001; Somerday and Moody, 2001). These models are not reviewed here as they are specific to IHAC and HEAC in lower strength alloys.

6.03.8.2 Crack Tip Hydrogen Accumulation

Hydrogen accumulates in the crack tip FPZ under the influence of two driving forces. First, it is well known that the concentration of H in interstitial lattice sites is increased proportional to an exponential dependence on hydrostatic stress that dilates the lattice (Li,

Oriani and Darken, 1966; Zhang and Hack, 1999). The exact magnitude of the crack tip σ_H is critically important to this H accumulation, be it ~$3\sigma_{YS}$ from conventional J_2 plasticity theory or ~$8\sigma_{YS}$ from strain gradient or dislocation-shielding based models.

Hydrogen also accumulates at a crack tip due to trapping associated with the high density of dislocations present from plastic deformation. This contribution was modeled and shown to be dominant provided that crack tip blunting is significant, as is typical of lower strength alloys with limited gradient plasticity enhancement of the hydrostatic stress (Krom, 1999; Taha and Sofronis, 2001). Modeling of IHAC and HEAC in high strength alloys has emphasized hydrostatic stress enhancement of H accumulation. This approach is particularly compelling if crack tip stresses are of order $8\sigma_{YS}$.

Hydrogen trapping at microstructural features within and about the FPZ is important to micromechanical-chemical modeling of K_{TH} and da/dt_{II}. The details of this behavior were summarized in 6.03.6.3.1, and H enhancement is controlled by the lattice H concentration and an exponential temperature dependence including the H-trap binding energy, E_B.

6.03.8.3 Threshold Stress Intensity Modeling

6.03.8.3.1 HEAC

The first quantitative model aimed at predicting the threshold stress intensity for HEAC was put forth by Oriani and Josephic based on the HEDE mechanism (Oriani and Josephic, 1974). Here, K_{TH} is the equilibrium threshold condition where the crack tip tensile stress is just sufficient to exceed the cohesive strength of atomic bonding, lowered by local H that accumulates in response to σ_H acting on the lattice concentration in equilibrium with the

surrounding H_2 pressure. Sievert's law related lattice H concentration to P_{H2} and T, trapping was allowed through a multiplying constant, stress-induced solute accumulation was defined by σ_H from an elastic expression, and the critical distance for H damage was avoided by relating crack tip stress to tip radius proportional to a power law function of K. These mechanics assumptions predicted high σ_H (18-26 GPa) and were judged to be inadequate in not dealing with plasticity (Rice, 1977). HEDE was modeled by assuming that H reduced the maximum cohesive force linearly. While these assumptions resulted in several unknown-adjustable parameters, the model reasonably predicted the relationship between K_{TH} and P_{H2} for high strength steel, as well as the very fast response time of changes in K_{TH} to changing H_2 pressure expected for the very-near surface location of H-damage sites dictated by the assumed stress distribution (Oriani and Josephic, 1974, 1977). This model also predicted the measured shift in the H_2 *vs.* D_2 pressure dependencies of K_{TH}.

Gerberich as well as Akhurst and Baker coupled the decohesion model with a continuum mechanics description of the crack tip stress field considering elastic-plastic behavior (Gerberich, 1974; Gerberich and Wright, 1981; Akhurst and Baker, 1981). The latter model defined the threshold as the equilibrium condition where the crack tip tensile stress exceeded the H-reduced cohesive strength over a critical distance into the FPZ, χ_{CRIT}, as dictated by the elastic-plastic fracture mechanics result that maximum σ_{YY} and σ_H are independent of K, but the breadth of the peak shown schematically in Fig. 44 increases as K rises (Rice, 1977). This χ_{CRIT} was hypothesized to be a material constant. The equation describing the H-reduced cohesive strength, σ^*, is:

$$\sigma^* = \sigma_O^* - A\sqrt{P_{H2}}\exp\left[V_H\left(2.6\sigma_{YY} - 1.3\sigma_{YS}\right)/3RT\right] \quad (8)$$

where σ_o^* is the cohesive strength of the H-free metal lattice, A is a group of adjustable constants, V_H is the partial molar volume of H in the metal, and R is the gas constant. The crack tip stress distribution, just beyond the peak in Fig. 44, was approximated by (Schwalbe, 1977):

$$\sigma_{YY}/\sigma_{YS} = \left[0.3/(X+1)\right]\left[0.04/X\right]^{\frac{1}{n+1}} \qquad \text{for } 0.04 < X < 0.073 \quad (9)$$

where n is the exponent in the constitutive relationship $\sigma \alpha \varepsilon^n$ and is ~0.1 for high strength alloys that exhibit limited work hardening, and the normalized parameter X is:

$$X = \frac{x}{\left(K/\sigma_{YS}\right)^2} \quad (10)$$

K equals K_{TH} when x equals χ_{CRIT} and numerical solutions to Eqs. 9 and 10 predict K_{TH} as a function of P_{H2}, T, and σ_{YS} for a microstructurally meaningful χ_{CRIT}. Such predictions are reasonable, as illustrated by the modeled trends in Fig. 45 (Akhurst and Baker, 1981). Similar trends were predicted for HEAC in austenitic superalloys (Stoltz, et al., 1983). This model is extended to HEAC in electrolytes, provided that permeation or crack chemistry based descriptions of the crack surface H concentration exist, paralleling Sievert's law (Gangloff, 1986).

The σ_o^* and A are difficult to define and were selected to provide reasonable values of K_{TH} for the pressures and yield strengths in Fig. 45. Alternately, Moody and coworkers related fracture stress to values from uniaxial tensile experiments (Moody et al., 1986; Somerday and Moody, 2001). The critical distance was selected to span the range of

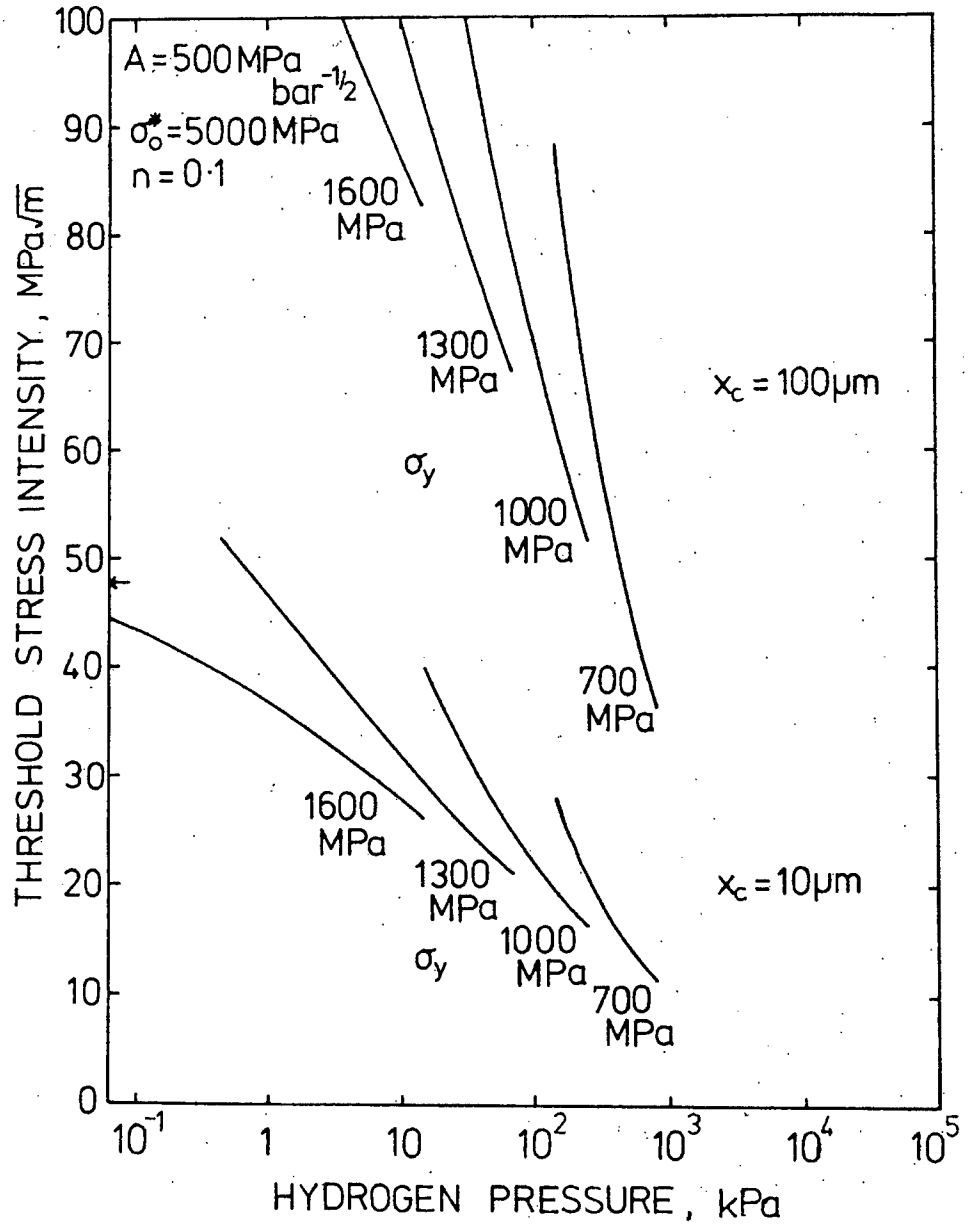

Figure 45. The model-predicted dependencies of the threshold stress intensity for HEAC on alloy yield strength and hydrogen gas pressure for two assumed values of the critical distance (x_C is referred to as χ_{CRIT} in the text). (Akhurst and Baker, 1981: Copyright The Minerals, Metals and Materials Society, reprinted with permission.)

austenite grain sizes typical of high strength steels, but there was no physical basis for this assumption. Finally, the crack tip stresses were based on conventional J_2 plasticity (Fig. 44), relevant to a blunted crack tip. The validity of critical distances in the range of 10 to 100 μm for threshold HEAC is questioned for two reasons. First, very high tensile stresses near the sharp H-crack tip (Fig. 44) could result in small χ_{CRIT}. Second, very high levels of crack tip surface H, unexpected from the simple permeation concept and Sievert's law for unstressed specimens, could override the dominant role of stress and lattice dilation in concentrating the critical H content. High levels of surface H were reported for a 7000-series aluminum alloy in NaCl solution (Cooper et al., 2000). These concepts have not been incorporated into a model of the threshold stress intensity for HEAC; however, this approach was employed recently to model da/dt_{II} for HEAC and the threshold for IHAC.

6.03.8.3.2 IHAC

The models of HEAC threshold are extendable to describe IHAC in high strength alloys. Mobile H dissolved in both the surrounding lattice and at lower binding energy trap sites feeds the crack tip FPZ due to stress enhancement, and there promotes cracking in conjunction with a critical stress and distance concept (Gerberich, 1974; van Leeuwen, 1979). The equations that describe the yield strength, temperature and bulk concentration dependencies of K_{TH} are similar to those presented for HEAC. Unknown values for σ_o^*, A and χ_{CRIT} limit the predictive capability of this modeling.

A dislocation description of crack tip mechanics (Huang and Gerberich, 1992; Katz et al., 2001) was employed to develop a new formulation of the threshold for HEAC and IHAC

(Gerberich et al., 1991). This approach was first developed to predict the temperature dependence of the macroscopic fracture toughness for cleavage, then extended to predict the yield strength, temperature and H concentration dependencies of K_{TH} (Gerberich, Marsh and Hoehn, 1996). Crack tip fracture is governed by the intrinsic Griffith toughness, k_{IG}, for cleavage fracture without H ($G_C \sim \gamma_S \sim k_{IG}^2/E$), where E is elastic modulus and γ_S is the energy required to produce unit crack surface. The local toughness is assumed to be reduced by accumulated H, yielding a Griffith-type threshold stress intensity for hydrogen embrittlement, k_{IH}, that equals (k_{IG} - $\alpha C_{H\sigma,T}$) where α is a coefficient in units of MPa$\sqrt{m}$/atom-fraction H and $C_{H\sigma,T}$ is the concentration of H localized at the embrittlement site due to the combined effects of hydrostatic stress and microstructural trapping unique to the FPZ. Local k_{IG} and k_{IH} were connected to macroscopic K_{IC} and K_{TH} for Mode I loading using the discrete dislocation simulation of the crack tip shown in Fig. 44 including emission from the crack and a standoff distance to the first dislocation. The resulting model prediction is:

$$K_{TH} = \frac{1}{\beta'} \exp\left[\frac{\left(k_{IG} - \alpha C_{H\sigma,T}\right)^2}{\alpha'' \sigma_{YS}}\right] \qquad (11)$$

where β' and α'' are constants determined by computer simulation of this dislocation structure about the crack tip. While developed for TG cleavage due to H, this formulation is likely relevant to H-assisted IG cracking.

This model explains the measured hydrogen concentration dependence of K_{TH} for transgranular IHAC in ultra-high strength AerMet®100 shown in Fig. 23. In Fig. 46 these K_{TH} are plotted *vs.* the $C_{H\sigma,T}$ dependent reduction in k_{IG} (Thomas, Li, Scully and Gangloff,

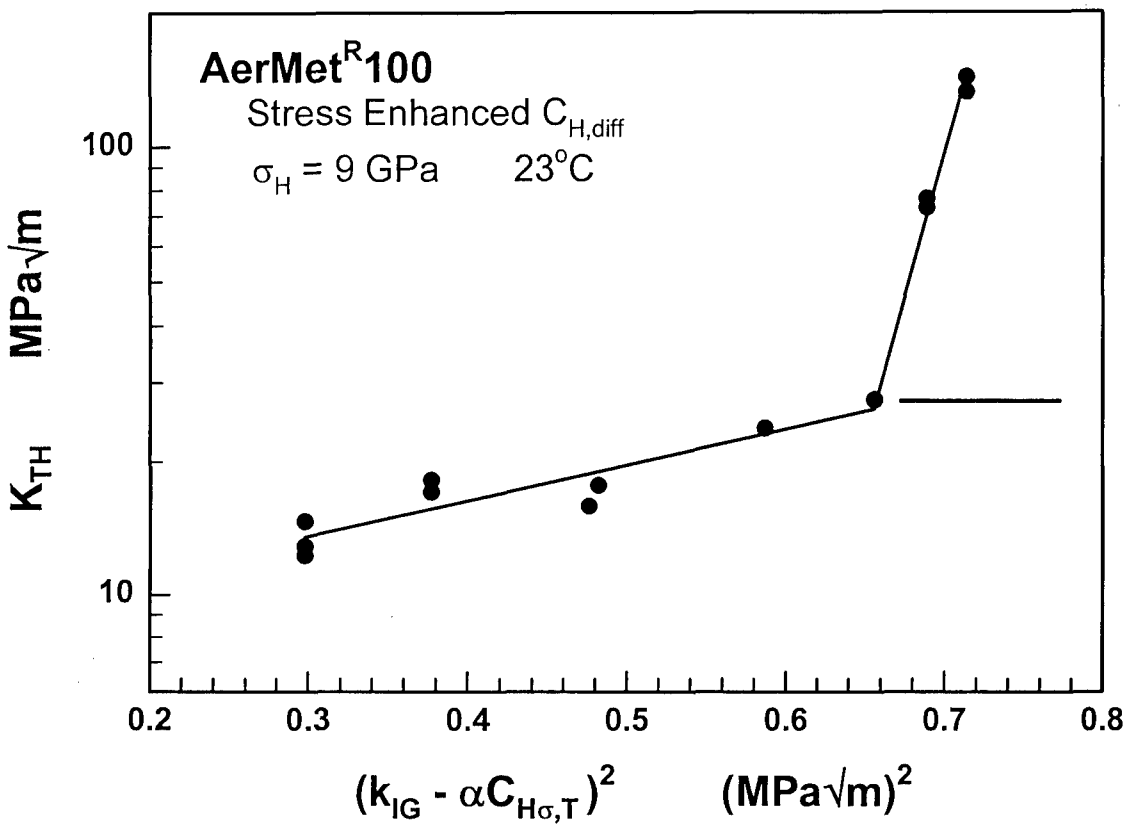

Figure 46. The measured and model-predicted effects of hydrostatic-stress enhanced H concentration, $C_{H\sigma,T}$ on the threshold for IHAC of AerMet®100. All measured K_{TH} values less than 30 MPa$\sqrt{m}$ relate to brittle-transgranular H cracking and the associated regression line is log $K_{TH} = 0.90 + 0.80 (k_{IG} - \alpha C_{H\sigma,T})^2$ with $r^2 = 0.85$. Cracking at higher K_{TH} involved some MVC. (Thomas et al., 2003)

2003). The $C_{H\sigma,T}$ was calculated from the measured-calibration value of precharged C_H for each K_{TH} and increased to include hydrostatic stress enhancement using a high value of σ_H = 9 GPa suggested by dislocation and strain gradient plasticity arguments. The parameters reported for Fe-Si (k_{IG} = 0.85 MPa$\sqrt{m}$ and α = 0.5 MPa$\sqrt{m}$/atom fraction H (Gerberich et al., 1996)) were used to calculate the concentration term in Fig. 46. The K_{TH} values less than 30 MPa$\sqrt{m}$ represent H charged specimens that failed by brittle TG cracking and are well described with the regression line; the slope yields $\alpha'' = 3 \times 10^{-4}$ MPa·m and β'_{IHE} = 0.13 $(MPa\sqrt{m})^{-1}$. Gerberich reported good fits between modeled and experimental measurements of K_{TH} *vs.* H_2 pressure and temperature for HEAC of a high strength steel using $\alpha'' = 2 \times 10^{-4}$ MPa·m and β'_{IHE} = 0.2 $(MPa\sqrt{m})^{-1}$ (Gerberich et al., 1996). The good fit between model predictions and measurements of K_{TH} supports the argument that IHE at low K_{TH} is due to the large amount of H that localizes in the highly stressed and trap laden FPZ, and validates this new model approach.

Kameda proposed a microscopic model for K_{IIHAC} based on the notion that the growth of an atomically sharp grain boundary microcrack is induced by H segregated to both grain interface and crack surfaces (Kameda, 1986a, 1986b). Crack sharpness was maintained by a dislocation free zone, with associated high near-tip stresses (6.03.8.1 and Fig. 44). Hydrogen promoted crack growth by reducing energies associated with the grain boundary and crack surfaces in local equilibrium with segregated H. Fracture was modeled by a Griffith-type energy balance between released-stored elastic energy and the H-sensitive energies associated with crack tip plasticity and surface creation. This thermodynamic approach was first recognized by Petch and Stables (Petch and Stables, 1952; Petch, 1956);

but was criticized by Oriani as not providing a mechanistic description of H damage, as well as based on the fact that adsorbed oxygen reduces substantially the surface energy of iron, but does not promote embrittlement under quasi-static loading (Oriani, 1990). While Sieradzki argues that a surface adsorption mechanism is valid (Pasco et al., 1984), and the Kameda formulation is intriguing, the point is moot since this formulation contains unknown-adjustable parameters and does not provide a confirmed-predictive capability that in any way exceeds the models based on crack tip stress plus decohesion. None-the-less, this modeling demonstrates that substantial levels of H accumulate in a zone very near to the crack tip surface due to stress and trapping.

6.03.8.3.3 Temperature Dependence

The data in Fig. 33 show that K_{TH} for HEAC rises sharply with increasing temperature just above ambient. The models summarized in the previous two sections suggest that this effect is due to reduced H accumulation at damage sites within the FPZ. There are two contributions to this reduction in H content with increasing T. First, H accumulation due to lattice dilation from hydrostatic stress declines proportionate to $\exp[\sigma_H V_H/RT]$. Second, the amount of microstructurally trapped hydrogen decreases with increasing temperature, proportionate to $\exp[E_B/RT]$. These important and beneficial effects of temperature on HEAC and IHAC are amplified by crack growth rate modeling.

6.03.8.4 Crack Growth Rate Modeling

The subcritical crack growth rates for IHAC and HEAC have been modeled extensively,

particularly the K-independent Stage II level. This da/dt_{II} is assumed proportional to the rate of H supply to the FPZ, limited by one or more slow steps in the mass transport and reaction sequence illustrated in Fig. 2 (Wei, 1981). Existing models emphasize the temperature, electrochemical or gas environment, H trapping, and time dependencies of each step in the embrittlement sequence. Uncertainties arise since damage is not described explicitly, χ_{CRIT} is unknown, transport/reaction kinetics are complex, and processes are highly gradated about the crack tip. None-the-less, existing models provide important guidance on incorporating the effects of key variables into structural integrity modeling.

Model predictions of the important effect of temperature on da/dt_{II} are highlighted to illustrate the capability of mechanism-based modeling. Both IHAC and HEAC are eliminated above a critical temperature, as shown in Figs. 31 to 36 (but not for the 7000 series aluminum alloy in Fig. 41). The explanations for this beneficial effect are worthy of particular consideration, as this temperature dependence provides a means to shield high strength alloys from hydrogen embrittlement. Several models have been advanced, with each focused on either thermally stimulated elimination of absorbed H on the reacting crack surface in HEAC, or elimination of H trapping accumulation at microstructural features that constitute the brittle-crack path for both HEAC and IHAC.

6.03.8.4.1 IHAC

6.03.8.4.1.1 H Diffusion and Trapping Control

The kinetics of internal hydrogen assisted cracking from H predissolved prior to loading have been modeled as governed by H diffusion to the crack tip FPZ (van Leeuwen, 1974,

1979; Gerberich, 1974; Gerberich et al., 1988, 1996; Moody et al., 1996; Toribio and Kharin, 1997; Moody et al., 2001; Symon, 2001). Diffusion-based models for IHAC include three important parameters: the critical distance ahead of the crack tip surface where H damage nucleates (χ_{CRIT}), the trap-sensitive diffusivity of H in the metal (the effective H diffusivity, D_{Heff}), and the concentration of H trapped at damage sites in the FPZ.

Gerberich and coworkers developed a detailed model to predict the da/dt_{II} for IHAC in high strength tempered martensitic steels (Gerberich, Chen and St. John, 1975; Gerberich, Livne and Chen, 1986; Gerberich et al., 1988). Hydrogen was partitioned at trap and lattice sites in the steel microstructure at time zero, and attracted to the crack tip by hydrostatic stress on load application. The crack path was typically along prior austenite grain boundaries, with H trapping at these boundaries as well as adjacent lath martensite interfaces. The point of maximum H accumulation was taken to be χ_{CRIT} ahead of the crack tip governed by the J_2 plasticity result in Fig. 44. The crack tip stress field was defined consistent with a blunt crack analysis ($\sigma_H \sim 3\sigma_{YS}$), and the intrinsic fracture strength (σ_o^*) was assumed to be reduced linearly by accumulated H according to HEDE. Trap sites in close proximity to this stressed zone were occupied by this diffused H and served as the preferred path for H damage. Hydrogen diffusion into the crack tip process zone, from the surrounding microstructure to a point χ_{CRIT} from the crack tip, was modeled by a transient solution to the diffusion equation including the hydrostatic stress term and H trapping described approximately by D_{Heff}. The crack growth rate was inferred from χ_{CRIT} and the time (t_i) required accumulating a critical amount of H to affect HEDE. For $da/dt_{II} = \chi_{CRIT}/t_i$:

$$\left(\frac{da}{dt}\right)_{II} = \frac{4D_{Heff}}{\chi_{CRIT}}\left\{1-\exp\left[\frac{\xi\left(T-T_o\right)}{R\,T\,T_o}\right]\right\}^2 \qquad (12)$$

where ξ is the sum of the binding energy for the trap state that is the dominant H-damage site plus the lattice dilation effect ($\sigma_H V_H$), and T_o is the temperature where da/dt_{II} falls to 0. In a later version of this model, $1/\chi_{CRIT}$ was represented as the ratio of crack advance distance ($\chi_A = \chi_{CRIT}$) to diffusion distance $(\chi_D)^2$ (Chen and Gerberich, 1991). These two distances are different for IHAC, but equal for HEAC since the source of H varies from the surrounding microstructure for the former to the crack tip surface for the latter.

Moody and coworkers developed a model for H-diffusion limited da/dt_{II} pertinent to transgranular IHAC in precipitation hardened austenitic superalloys (Moody, Robinson, Angelo and Perra, 1996; Moody, Baskes, Robinson and Perra, 2001). Cracking nucleated as microvoids at slip band intersections that strongly trapped H, located in the FPZ and ahead of cracked carbide particles. The da/dt_{II} was limited by short-range diffusion of H from normal lattice sites to these slip band interactions and equaled a critical distance, given by the slip band spacing, over the time required for this local H diffusion. The time for H accumulation between progressive crack nucleation events was modeled by a transient solution to the diffusion problem that was solved to yield quantitative predictions of da/dt_{II}.

6.03.8.4.1.2 Predicted Temperature Dependence

The H diffusion/trapping models by Gerberich, Moody and coworkers reasonably describe the temperature dependence of da/dt_{II} for IHAC. The Gerberich model fits the

experimental measurements of da/dt_{II} for intergranular IHAC in H precharged AISI 4340 steel, as shown by the solid line *vs.* data points in Fig. 32. This fit was achieved by assuming a reasonable binding energy for H trapped at martensite lath interfaces adjacent to the prior austenite grain boundary crack path, D_{Heff} of 1 x 10^{-8} cm^2/s for a trap-rich high strength steel, χ_{CRIT} of 1 μm based on both the spacing of martensite laths and the maximum stress point at $2\delta_T$ (Table 2), and T_o of 400K. Similar good agreement is obtained with other combinations of these parameters, but the values selected are reasonable and the approach of this modeling is validated. The major improvement needed is to incorporate higher levels of crack tip stress and a smaller critical distance, consistent with the dislocation and gradient plasticity perspectives in Fig. 44.

The model explanation for the temperature dependence in Fig. 32 is based on the opposing effects of thermally activated H diffusion control, dominant in the low temperature regime, and thermally stimulated H detrapping control at higher temperatures. As T rises from low temperatures, D_{Heff} increases as given by standard Arrhenius behavior with activation energy for H diffusion that is trapping dependent. The exponential term involving T_o dominates the high temperature reduction in da/dt_{II}. Physically, da/dt_{II} declines because the amount of H accumulated at sites of damage nucleation ($C_{H\text{-}FPZ\ trap}$) in the FPZ is lowered according to:

$$\left(C_{H-FPZ\ trap}\right) = C_l\ exp\left(\frac{E_B + \left(\sigma_H V_H\right)}{RT}\right) \qquad (13)$$

For the example shown in Fig. 32, $C_{H\text{-}FPZ\ trap}$ at the experimentally defined T_o (127°C) is 25 times less than the trapped H concentration at 25°C for ($E_B + \sigma_H V_H$) of 6.7 kJ/mol for a σ_{YS}

of 1600 MPa and H trapping at martensite lath interfaces that constitute the sites of H damage. When the equilibrium amount of H partitioned at damage sites decreases, the time required achieving the critical level for embrittlement increases and da/dt_{II} falls. Decreasing H requires increased local stress at damage sites, but maximum crack tip FPZ stresses are relatively independent of K and subcritical H cracking is effectively eliminated.

The model by Moody and coworkers predicts the measured temperature dependence of da/dt_{II} for H precharged IN 903 (Fig. 31), using a measured slip length of 0.6 μm and lattice-H diffusivity from the literature. The explanation is based on partitioning of H between various microstructural sites, and how this trapping affects H diffusivity that in turn controls crack growth rate. For $T < 25^{\circ}C$, H diffuses from lattice sites to slip band intersection traps to control da/dt_{II} that increases with increasing T and H mobility. For higher temperatures, the interdiffusion distance increases and a significant amount of dislocation-sheared γ' strengthening precipitate is encountered as well as multiple slip band intersections. These additional trap states reduce the relatively rapid lattice H diffusivity to a trap affected D_{Heff} and da/dt_{II} declines. Additionally, trap site occupancy decreases with increasing temperature, for a given lattice solubility of H, to further decrease H damage and H-enhanced crack growth rate (Pressouyre and Bernstein, 1978, 1979; Hirth, 1980; Moody et al., 2001). The decline in da/dt_{II} with increasing T for IN 903 (Fig. 31) was predicted quantitatively assuming additional H trap states with a specific volume percentage that increased with increasing temperature (diffusion distance) and constant binding energy. Several combinations of trap density and E_B fit the crack growth data.

6.03.8.4.2 HEAC

6.03.8.4.2.1 Framework

Modeling da/dt_{II} for HEAC is complicated since H production and uptake at the crack tip are each time dependent. Wei and coworkers modeled da/dt_{II} as proportional to the rate of supply of H to the FPZ; enabled by environment-mass transport, surface reaction to produce H, and H diffusion to competing fracture sites in the FPZ (Wei, 1981; Wei and Gao, 1985; Wei and Gangloff, 1989). A major aim of this work was to develop model predictions of the effects of gas pressure, electrochemical potential, solution composition, and temperature on da/dt_{II} in high strength alloys.

Model predictions were developed for each rate limiting step (Wei, 1981; Wei and Gao, 1985). When transport of a reactant in the crack environment is slow, the near-tip chemical activity is reduced and surface reaction rate is lowered, as expected for gaseous environments at low-bulk pressure and low concentration components in an electrolyte. The resulting da/dt_{II} prediction is:

$$\left(\frac{da}{dt}\right)_{II} = C_T P_O / \sqrt{T} \tag{14}$$

When mass transport to reaction sites at the crack tip is rapid, then surface reaction rate limits da/dt_{II}, as expected for high pressure gases or electrolytes:

$$\left(\frac{da}{dt}\right)_{II} = C_S P_O^m \exp\left(\frac{-E_S}{RT}\right) \tag{15}$$

When H production on the crack tip surface is rapid, and in equilibrium with the bulk and local environments, H diffusion in the crack tip FPZ limits da/dt according to:

$$\left(\frac{da}{dt}\right)_{II} = C_D\sqrt{P_O}\exp\left(\frac{-E_D}{2RT}\right) \qquad (16)$$

In these equations P_o is bulk pressure for a gas environment or pH-electrode potential dependent H fugacity for an electrolyte, T is temperature, E_D and E_S are activation energies for diffusion and surface reaction, respectively, and the C_I constants reflect (electro)chemical kinetics and boundary conditions. The C_I can depend on temperature, pH, electrode potential and gas pressure. This constant also reflects the local failure criterion, but this aspect of the models has not been well developed. When multiple steps limit da/dt_{II}, for example in a transition temperature or pressure regime, then more complex formulations of these equations are required as illustrated by the schematic in Fig. 47 (Wei, 1981). Here, da/dt_{II} is governed by surface reaction rate for H production at lower temperatures and hydrogen fugacities, and by H diffusion in the FPZ at higher temperatures or for more active H producing environments. The transition function (a-a) is easily derived. More than one microscopic crack path may exist, depending on H partitioning to trap sites within the FPZ, and can affect da/dt_{II} (Gao and Wei, 1985).

6.03.8.4.2.2 Rate Limiting Step Identification

The majority of the work to predict da/dt_{II} has focused on HEAC in high strength steels. The rate limiting step identifications established to date are not absolute because of modeling assumptions and unknown material-environment parameters. Modeling is complicated by uncertainties in chemical reaction kinetics pertinent to the crack tip, location of H damage between surface and bulk sites, and H diffusion in the midst of trapping.

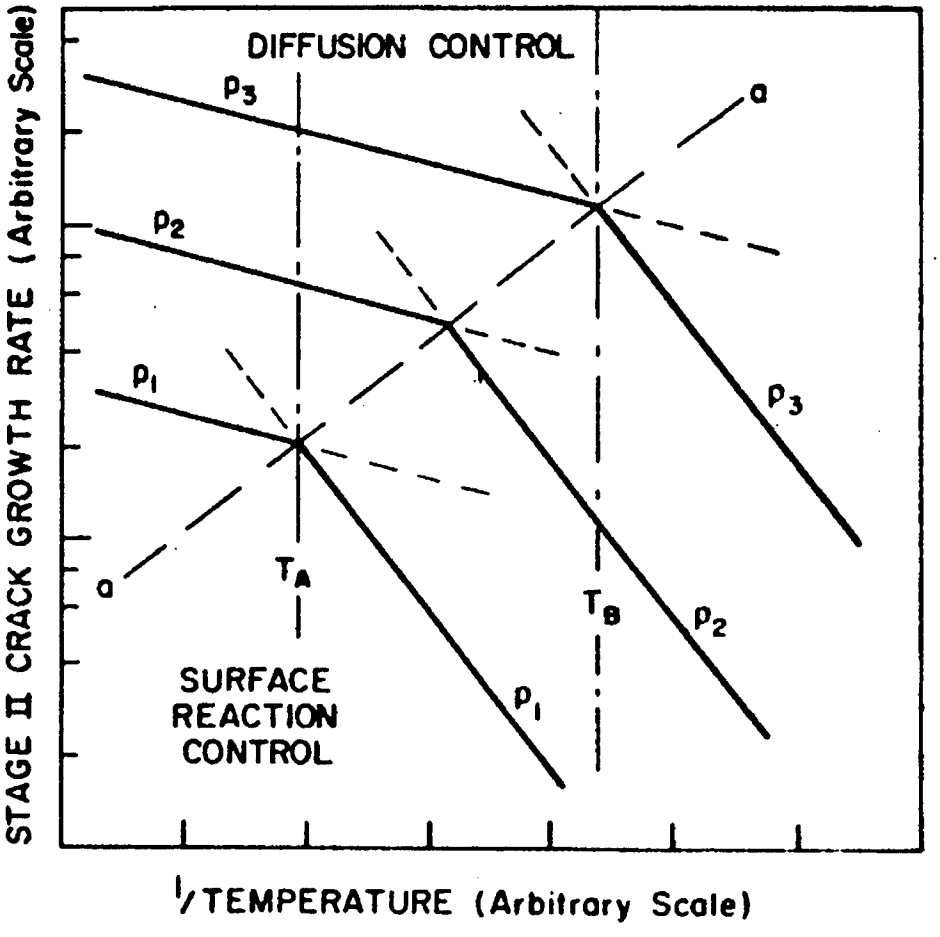

Figure 47. Schematic of the temperature and environment pressure or H fugacity dependencies of the Stage II crack growth rate for HEAC in high strength alloys, illustrating the transition from rate control by surface reaction limited H production to H diffusion in the crack tip FPZ. (Wei, 1981: Copyright The Minerals, Metals and Materials Society, reprinted with permission.)

Surface reaction has not been well integrated with H diffusion in the FPZ (Turnbull, Ferriss and Anzai, 1996). None-the-less, semiquantitative results are useful to understand variable effects and guide structural integrity analysis.

The measured temperature dependencies of da/dt_{II} in Fig. 35 and activation energies calculated from the crack growth rate data, illustrate the approach to determining the rate limiting step (Wei, 1981; Wei and Gao, 1985). These results suggest that da/dt_{II} is limited by: (a) surface reaction producing H for HEAC in distilled water, water vapor, and H_2 (curves *c* and *d*) (Simmons et al., 1978; Gao et al., 1984); (b) gas-phase transport of reactants for low pressure H_2S (curve *b*) (Lu et al., 1981; Gao et al., 1984), and (c) H diffusion in the FPZ for higher-pressure H_2S (curve *a*) (Lu et al., 1981; Gao, et al., 1984).

Substantial research focused on HEAC in H_2 and identifications of the rate limiting processes are contradictory. Several groups argue that da/dt_{II} in the thermally-activated low temperature regime is limited by surface reaction to produce H (Williams and Nelson, 1970, 1970a; Oriani et al., 1971; Nelson and Williams, 1977; Sieradzki and Ficalora, 1979a; Pasco et al., 1982, 1984; Pasco and Ficalora, 1983). Alternately, Vehoff and coworkers argue that crack tip H is in equilibrium with the surrounding H_2, with da/dt_{II} limited by short range diffusion of H from surface sites into the FPZ (Vehoff and Rothe, 1983; Vehoff and Neumann, 1985). A similar scenario was suggested to explain the low temperature behavior of 18Ni Maraging steels in Fig. 34 (Gangloff and Wei, 1977).

6.03.8.4.2.3 Surface Reaction Rate Control and Temperature Dependence

For HEAC in H_2, surface reaction and production processes for H were purported to

control da/dt_{II} (Williams and Nelson, 1970, 1970a; Oriani et al., 1971; Nelson and Williams, 1977; Sieradzki and Ficalora, 1979a; Pasco and Ficalora, 1983; Pasco et al., 1982, 1984). The low temperature thermally-activated behavior of da/dt_{II} was limited by dissociative chemisorption of H_2 to produce H on crack tip surfaces. Thermal desorption of H, as H_2, controlled the high temperature decline in da/dt_{II}; this decrease appears to be eliminated when H_2 was predissociated by a hot filament near the cracked specimen, supporting the importance of surface processes (Nelson, Williams and Tetelman, 1971). Pasco et al. modeled da/dt_{II} as proportional to the rate of surface-H production from this reaction sequence to yield (Pasco and Ficalora, 1983):

$$\left(\frac{da}{dt}\right)_{II} = k_1\sqrt{P_{H2}}\,exp\left[-E_E/RT\right] - k_2\,exp\left[-E_D/RT\right] \qquad (17)$$

where the activation energy in the first exponential term defines the kinetics of dissociation of H_2 to H, surface migration of H, and adsorption; while the second term defines the rate of H desorption to H_2. Reasonable values of constants and energies yielded predictions of both the high and low temperature HEAC kinetics for the maraging steels (e.g., Fig. 34), but not the more shallow reduction in da/dt_{II} for AISI 4340 (e.g., Fig. 36) and other steels (Williams and Nelson, 1970; Nelson and Williams, 1977; Simmons et al., 1978).

An alternate explanation was put forth for elimination of HEAC in 18Ni Maraging steel (Fig. 34), where da/dt_{II} decreased by orders of magnitude in response to a 2-4°C temperature increase, and increased by a like amount with the same temperature decrease (Gangloff and Wei, 1977). The P_{H2} dependence of this critical temperature (T_C) lead to the speculation that H was adsorbed as a 2-dimensional phase that transitioned through T_C, and crack growth

rate followed the presence or absence of this H source (Gangloff and Wei, 1977; Chan et al., 1978). These models each suggest that the high temperature reduction in HEAC in H_2 is due to the dominance of H desorption to reduce hydrogen supply to the FPZ.

Hydrogen uptake to the FPZ should be reduced by increased H recombination at increasing temperature for HEAC in electrolytes, but the detailed kinetics are not established. The data for distilled water (Fig. 35), as well as other results discussed in 6.03.6.3.3 do not show this reduction in da/dt_{II} for temperatures up to about 100°C (Johnson and Willner, 1965; Van der Sluys, 1969; Speidel, 1974; McIntyre et al., 1972a), but experiments with pressurized water environments at yet higher temperatures may show this effect. An example of this behavior is shown in Fig. 36 where the Ni superalloy exhibited declining da/dt_{II} in the range from 100 to 150°C in pressurized-pure water (Hall and Symons, 2001). There is; however, another explanation for the decline in da/dt_{II} at these high temperatures; reduced H trapping.

6.03.8.4.2.4 Diffusion-Trapping Control and Temperature Dependence

As an alternative to surface reaction control, diffusion of H from the crack tip surface to damage sites within the FPZ has been proposed to explain temperature dependent da/dt_{II} for high strength alloys, including martensitic steels. Chen and Gerberich modeled HEAC in ferrous alloys by modifying the IHAC model described in 6.03.8.4.1.1 to include the temperature dependence of H uptake from the gas (Chen and Gerberich, 1991). The resulting expression for da/dt_{II} is:

$$\left(\frac{da}{dt}\right)_{II} = \frac{4D_{Heff}}{\chi_{CRIT}}\left\{1 - \frac{\theta_O}{\theta_T}\exp\left[\frac{\xi\left(T - T_o\right)}{R\,T\,T_o}\right]\right\}^2 \qquad (18)$$

The parameter, ξ, equals ($E_B + \sigma_H V_H + H_S$) where H_S is the heat of solution for H in the lattice in equilibrium with the surrounding H_2. The term, θ_o/θ_T is the ratio of surface coverage of H at T_o and any T. This surface coverage ratio is given by a complex function of temperature involving the activation energy for desorption and H_2 pressure. This version of the model used the discrete dislocation estimate of σ_H (22 GPa for Fe-Si), while the earlier model for IHAC employed $\sigma_H \sim 2\text{-}3\sigma_{YS}$, a much lower stress (3,000 to 5,000 MPa).

Using reasonable values of the energies, Chen and Gerberich explained the two-dominant features of temperature dependent HEAC illustrated in Figs. 34 and 35. First, rising da/dt_{II} in the low temperature regime is consistent with H diffusion control and thermally activated D_{Heff}. Second, thermal detrapping of H from damage sites explains the reduction in da/dt_{II} at elevated temperatures, analogous to the temperature dependence of IHAC. This important role for thermal detrapping of H is not necessarily general as different combinations of the adsorption, solution, trapping and stress enhancement energies change the dominant term in this analysis. Clearly; however, thermal detrapping of H from damage sites is a key mechanism for elimination of both HEAC and IHAC at elevated temperatures.

Hall and Symons developed a similar model for intergranular Stage II crack growth rate in high strength austenitic superalloys stressed in high purity water (Hall and Symons, 2001). The da/dt_{II} was limited by H diffusion in the FPZ, as supplied by water oxidation of

the Ni rich crack surfaces:

$$\left(\frac{da}{dt}\right)_{II} = \frac{4D_{Heff}}{\chi_{CRIT}}\left[erf^{-1}\left(\frac{C_S - C^*(K,T)}{C_S - C_\infty}\right)\right] \approx \frac{4D_o}{\chi_{CRIT}}\left(1-\frac{c^*_{gb}}{c_{gb}}\right)^2 \exp\left[\frac{-\Delta H_D}{RT}\right] \qquad (19)$$

where $D_{Heff} = D_o \exp(-H_D/RT))$, χ_{CRIT} is the critical distance ahead of the crack tip where H damage nucleates, C_S is the amount of H produced by the oxide-metal equilibrium-H fugacity and enhanced by both σ_H and trapping, C_∞ is the H content far from the crack tip, $C^*(K,T)$ is the critical H concentration needed for grain boundary fracture, c_{gb} and c_{gb}^* are the grain boundary H contents corresponding to K levels of K_{IC} and K_{IHEAC}, respectively. The fit between measured da/dt_{II} in the low temperature regime and the predictions of this model is shown in Fig. 36. The parameters in the crack growth rate equation were taken from experimental and literature results, and the χ_{CRIT} was a fitting parameter as amplified in 6.03.8.4.2.7. The importance of H diffusivity at low temperatures and H detrapping at higher temperatures is apparent.

6.03.8.4.2.5 Rate Limitation, Trapped-H Partition and Temperature Dependence

Wei and Gao formalized the concept that, in addition to the rates of surface-H production and H diffusion in the FPZ, temperature affects H partitioning to various embrittlement (trap) sites in the microstructure (Gao and Wei, 1985). This partitioning of H is manifest by a changing crack path. In essence this model combines thermally stimulated detrapping of H with temperature dependent rate of H supply. Specifically:

$$\left(\frac{da}{dt}\right)_{II} = \left(\sum_i \alpha_i f_i \kappa_i\right)\frac{dQ}{dt} \tag{20}$$

where dQ/dt is the total rate of H supply set by the rate limiting step and supporting chemical quantities, α_i is the constant in the assumed proportionality between H supply rate and crack growth rate specific to the i^{th} microscopic crack path, f_i is the area fraction of the i^{th} crack path, and κ_i gives the fraction of dQ/dt that is provided to the i^{th} microscopic feature as governed by H trapping at this feature. The dQ/dt follows from any of the previous equations for a specific rate limiting processes.

This model explained the temperature dependence of da/dt_{II} in high strength AISI 4340-steel as shown in Fig. 35. For this case, the total dQ/dt partitions to three sites; prior austenite grain boundaries, lath martensite interfaces, and the martensite lattice. However, the amount of lath martensite H cracking was small for the data in Fig. 35. Assuming that da/dt_{II} is limited by a surface reaction for this tempered martensitic steel and low pressure H_2 environment:

$$\left(\frac{da}{dt}\right)_{II} = \left\{\frac{\alpha_{IG} f_{IG} \tau\delta\left(a^3/n\right)N_x \exp\left(E_B/RT\right)}{1+\tau\delta\left(a^3/n\right)N_x \exp\left(E_B/RT\right)} + \frac{\alpha_l\left(1-f_{IG}\right)}{1+\tau\delta\left(a^3/n\right)N_x \exp\left(E_B/RT\right)}\right\} C_S P_O^m \exp\left(-E_S/RT\right) \tag{21}$$

where δ is the volume fraction of prior austenite grain boundary, a is metal lattice parameter, N_x is density of trap sites on austenite grain surfaces, n is number of atoms per metal-unit cell, and τ is a parameter that describes a nonequilibrium situation in the Fermi-Dirac description of the temperature and coverage dependence of H trap occupancy. This cracking in AISI 4340 steel in H_2 was purely IG at all low temperatures where da/dt_{II} increased with

increasing temperature according to an Arrhenius relationship. Here, $da/dt_{II} = \alpha_{IG}(dQ/dt)$ and the H supply rate was controlled by surface reaction (or perhaps short range H diffusion). At higher temperatures, where da/dt_{II} deviates from Arrhenius behavior and declines from a maximum, an increasing proportion of TG microvoid cracking occurs. Here, $da/dt_{II} = (\kappa_{IG}\alpha_{IG} + \kappa_{TG}\alpha_{TG})(dQ/dt)$, where κ_i gives the fraction of dQ/dt supplied to either IG or TG embrittlement sites. These H distribution coefficients are given by:

$$\kappa_{IG} = \frac{\delta C_{IG}/C_l}{1+\delta C_{IG}/C_l} \qquad \kappa_{TG} = \frac{1}{1+\delta C_{IG}/C_l} \tag{22}$$

where C_{IG} is the concentration of H trapped at prior austenite grain boundaries and C_l is the concentration of H in martensite lattice sites. The equilibrium partitioning of H between austenite boundary and lattice sites is governed by the binding energy for trapping at the austenite boundary:

$$C_{IG}/C_l = \frac{\alpha_1 \exp\left(\frac{E_B}{RT}\right)}{1+\alpha_2 \exp\left(\frac{E_B}{RT}\right)} \tag{23}$$

where α_1 and α_2 are known constants. For a typical binding energy of H to a prior austenite grain boundary ($E_B \sim 75$ kJ/mol), C_{IG}/C_l decreases substantially with increasing temperature; κ_{TG} approaches 1 and κ_{IG} tends to 0 as C_{IG} tends to 0 due to thermal desorption. The amount of IG H cracking diminishes and TG microvoid damage is enhanced due to increasing temperature. The crack growth rate due to H embrittlement declines since the microvoid damage is presumed to be unaffected by H and α_{TG} is small to fit measured da/dt_{II}.

6.03.8.4.2.6 Vacancy-Diffusion Control and Temperature Dependence

Vogt and Speidel implemented a surface-process model of crack growth first advanced by Gavele to predict the temperature dependence of da/dt_{II} for intergranular HEAC in a 7000 series aluminum alloy stressed in aqueous chloride solution (Galvele, 1987; Vogt and Speidel, 1998). Crack advance is controlled by vacancy diffusion along the crack surface to a captured state at the tip where tension lowers the free energy of vacancy formation. Vacancies are produced by anodic corrosion and, critically for HEAC, the rate of vacancy migration is enhanced by surface-adsorbed H from cathodic reaction. The resulting prediction of growth rate is:

$$\left(\frac{da}{dt}\right)_{II} = \frac{D_S}{L}\left[\exp\frac{\left(\sigma a^3 + \alpha E_B\right)}{kT} - 1\right] \qquad (24)$$

where D_S is surface diffusivity, L is distance between unstressed and stressed lattice, σ is the elastic stress at the crack-tip surface, a is Al atom diameter, and α is a stress dependent parameter that describes the trapping of H at vacancies with a binding energy, E_B. These parameters are uncertain for 7000 series aluminum alloys and the surface-vacancy diffusion model is generally controversial (Parkins, 1990).

The prediction of this model in Fig. 37 was fit with the experimental measurements using reasonable values for these parameters, including a crack tip stress of 500 MPa. This stress equals σ_{YS} for this alloy and is substantially lower than the elastic stress generally associated with the crack tip FPZ, but not a free surface (Fig. 44). Thermally activated D_S and increased vacancy mobility govern the general increase in da/dt_{II} with increasing temperature. The exponential term, describing the effect of stress in attracting vacancies to

the crack tip, declines as T increases. The discontinuity in the plot, and general reduction in da/dt_{II} at all higher temperatures, is due to proportionately reduced H binding to vacancies between 30 and 50°C, or decreasing α, with full detrapping ($\alpha = 0$) of H from vacancies at higher temperatures.

6.03.8.4.2.7 Broad-based Growth Rate Correlation and Diffusion Control

Part of the controversy in defining the correct rate limiting step for HEAC in high strength alloys is due to the limited range of data typically examined when testing a model. A recent analysis of HEAC in a wide range of alloys stressed in electrolytes and gases provides a basis to identify the specific material and environment chemistry variables that favor H diffusion *vs.* surface reaction control of da/dt_{II} (Gangloff, 2003).

The fastest rates of HEAC were obtained from recent experiments at the University of Virginia, using a common experimental method, and from literature results for high strength alloys stressed during exposure in chloride solutions. As shown in Fig. 48, these da/dt_{II} are directly proportional to the best available estimate of trap affected D_{Heff} based on permeation experiments. This correlation is particularly strong for the alloy steels where declining D_{Heff}, from 10^{-7} cm^2/s for conventional tempered martensitic steels to 10^{-8} cm^2/s for precipitation hardened AerMet®100 and 10^{-9} cm^2/s for 18Ni Maraging steels, resulted in a 2 order of magnitude reduction in da/dt_{II}. There are two outliers. The ASTM A723 steel (σ_{YS} = 1310 MPa) exhibits unexpectedly high da/dt_{II} of 600 μm/s when stressed in pure H_2SO_4 (Troiano et al., 2002). AA7079-T6 is the only aluminum alloy that exhibits growth rates in chloride solution that exceed 0.1 μm/s, as shown in Fig. 12 (Holroyd, 1990). The causes of

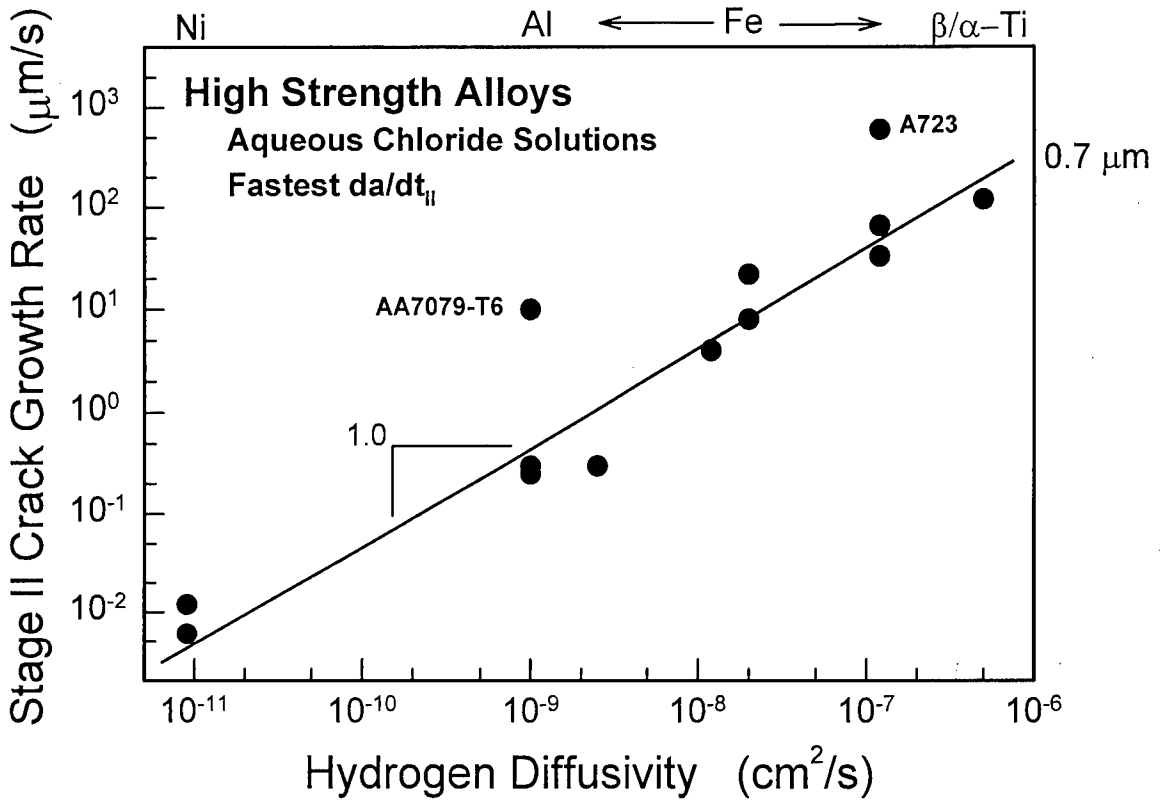

Figure 48. The dependence of the fastest-measured da/dt_{II} on effective hydrogen diffusivity, D_{Heff}, from permeation measurements for high strength alloys that exhibit HEAC in aqueous chloride solutions at 25°C. The Ni-based superalloy was cracked in NaCl that was either acidified (pH 0.3–1) or contained a H recombination poison (As_2O_3) with cathodic polarization; aluminum alloys in acidified chromate-chloride solution; steels in neutral NaCl, H_2S-bearing acidified chloride (NACE), or concentrated H_2SO_4/H_3PO_4 acid; and Ti alloys in neutral chloride solution. (Gangloff, 2003; containing references to specific data.)

these high crack growth rates are not understood.

Diffusion-based models were developed to describe da/dt_{II} for HEAC based on FPZ supply from the concentration of H on the crack tip surface and in equilibrium with the local environment (C_S) (Johnson, 1974; van Leeuwen, 1975, 1979; Doig and Jones, 1977; Chen and Gerberich, 1991; Gerberich et al., 1996; Toribio and Kharin, 1997; Krom et al., 1999; Hall and Symons, 2001; Taha and Sofronis, 2001; Yokobori et al., 2002). The da/dt_{II} is modeled as equaling the ratio of χ_{CRIT} to the time required for H to diffuse from C_S and over this distance to reach C_{CRIT}. Specific da/dt_{II} predictions from two of these models are represented by Eqs. 18 and 19 in 6.03.8.4.2.4. In general models of this type are of varying complexity depending on whether the H-diffusion field is: (a) concentration and/or stress driven, (b) transient or steady state, (c) ahead of a stationary or moving crack, (d) modeled in one or two dimensions (e) emanating from environment-sensitive C_S, (f) microstructure-trap affected, (g) plastic strain-trap affected, and (h) coupled with a H-failure criterion.

The results of diffusion modeling are of the general form:

$$\frac{da}{dt_{II}} = \frac{D_{Heff}}{\chi_{CRIT}} \left[\xi \left(\frac{C_S}{C_{CRIT}}, D_{Heff}, \chi_{CRIT}, \sigma_{YS}, t \right) \right] \quad (25)$$

where ξ is a function of the indicated variables and equals between 4.0 (Chen and Gerberich, 1991; Gerberich et al., 1996), 2.9 (Gerberich, 1974; Gerberich et al., 1975), 2.8 (van Leeuwen, 1979), 0.4 to 2.3 (Toribio and Kharin, 1997), and 0.01 to 0.3 (Johnson, 1974).

The observed and predicted proportionality between Stage II crack growth rate and D_{Heff} in Fig. 48 supports H-diffusion control of HEAC. An upper bound χ_{CRIT} can be determined

from these data. The highest-reasonable value of ξ is 3 and constant, provided that the da/dt_{II} are not sensitive to C_S for the various chloride solutions and if cracking is governed by constant C_{CRIT}/C_S of order 0.5. These assumptions result in χ_{CRIT} = 0.7 μm for the trend line in Fig. 48, independent of alloy. The smallest possible ξ is 0.03, yielding a lower bound on χ_{CRIT} of 70 nm. The low temperature dependence of da/dt_{II} for Ni superalloy X-750 illustrated in Fig. 36 and fit with the diffusion model in Eq. 19, agrees well with the trend line in Fig. 48, with D_H in the range from 4×10^{-11} to 2×10^{-9} cm^2/s as temperature increased from 30 to 130°C. Equivalently, Mills and coworkers, as well as Hall and Symons noted that the activation energy descriptive of this low temperature cracking (47.2 kJ/mol) essentially equals the activation energy for trapping sensitive diffusion of H in X-750 (48.1 kJ/mol) (Mills et. al., 1999; Hall and Symons, 2001; Symons, 2001). This limited set of data lead to an estimated χ_{CRIT} of 0.6 μm, and perhaps as low as 0.1 μm (Hall and Symons, 2001), consistent with the broad correlation shown in Fig. 48.

The complexity of modeling crack growth rate data for HEAC is illustrated by a correlation of all available da/dt_{II} with D_{Heff} in Fig. 49 (Gangloff, 2003). The da/dt_{II} can be 1-3 orders of magnitude less than the upper-bound trend from Fig. 48. With ξ = 3, larger apparent χ_{CRIT} (5 to 850 μm) are associated with the dashed lines for $da/dt_{II} \alpha D_{Heff}$, but these diffusion-based fits are incorrect due to three situations that reduce da/dt_{II} below the fastest levels. These include: (1) reduced-equilibrium C_S due to environment chemistry factors, (2) strength or metallurgy effects on C_{CRIT}, and (3) the intervention of environmental mass transport or surface reaction rate control that reduces H concentration to below the

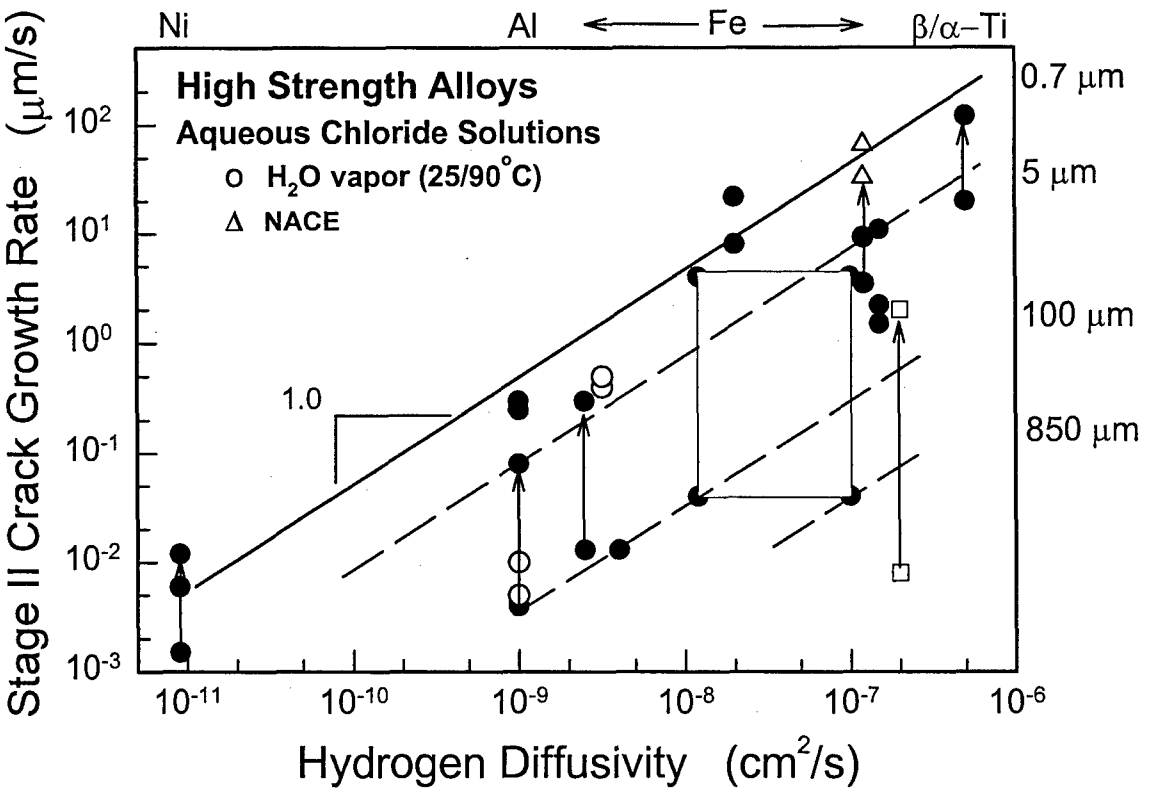

Figure 49. The dependence of da/dt_{II} on D_{Heff} for high strength alloys that exhibit HEAC in various chloride solutions at 25°C. The vertical arrows represent the range of growth rates reported for a given material and in response to electrochemical or metallurgical variables. The increases in da/dt_{II} for IN718 ($D_{Heff} \sim 10^{-11}$ cm^2/s) and AA7050 (1-4 x 10^{-9} cm^2/s) were produced by changing-applied electrode potential; for the 18Ni Maraging steel (2-5 x 10^{-9} cm^2/s) due to steel composition and strength change from the 250 to 350 grades; for 4340-type steels (10^{-8} to 10^{-7} cm^2/s) due to chemistry and metallurgical changes (boxed area) or sulfide addition to the chloride solution (Δ), for Ni-Cr-Mo ASTM A723 steel (10^{-7} cm^2/s) due to increasing σ_{YS} from 1150 to 1380 MPa (□), and for β-Ti alloys (5 x 10^{-7} cm^2/s) due to crack tip strain rate increase. (Gangloff, 2003; containing references to specific data)

equilibrium C_S. Essentially, ξ depends on C_S and C_{CRIT}, and is reduced below 3.

As an example, consider the large amount of data for steels ($10^{-8} < D_{Heff} < 10^{-7}$ cm^2/s) cracked in neutral NaCl solution at the free corrosion potential. Electrochemical conditions (e.g., cathodic polarization) that increase C_S will increase da/dt_{II} toward the upper bound line. This is supported by data for high strength AISI 4340-type steel cracked in neutral NaCl solution (• at $D_{Heff} = 1.0\text{-}1.2 \times 10^{-7}$ cm^2/s) and H_2S-saturated acidified chloride (NACE solution, Δ). A second example is provided for ASTM A723 (□ in Fig. 49), where the vertical arrow shows increasing da/dt_{II} for σ_{YS} from 1150 to 1380 MPa and HEAC in NaCl solution. This adverse effect of strength on da/dt_{II} is due to increasing crack tip stress, proportionate to σ_{YS} for a given K and achieving the H-failure condition at reduced C_{CRIT}. Reduced C_{CRIT} results in increased ξ and da/dt_{II} at fixed C_S.

Hydrogen diffusion control of HEAC is further established by correlating D_{Heff} with da/dt_{II} for IG cracking of high strength alloys in gaseous H_2 and H_2S environments at 23°C, Fig. 50 (Gangloff, 2003). The fastest Stage II crack growth rates in H_2 and H_2S are proportional to D_{Heff}, paralleling the correlation from Fig. 48 for chloride solutions and suggesting that H diffusion limits crack growth. The results for AISI 4340-type steels at high D_{Heff} (□, 1.5×10^{-7} cm^2/s), and 18Ni Maraging steels (□, 2.5×10^{-9} cm^2/s), are consistent with C_S reduced by low P_{H2} at equilibrium, or surface reaction limitation (Gangloff and Wei, 1977; Wei, 1981; Wei and Gao, 1985). The vertical arrows in Fig. 50 reflect increasing hydrogen pressure and hence C_S. While the alloy steels have not been studied in high pressure H_2, faster da/dt_{II} were reported for HEAC in H_2S (Δ in Fig. 50) where surface reaction is not likely to limit da/dt_{II} and efficient-H uptake leads to a high-

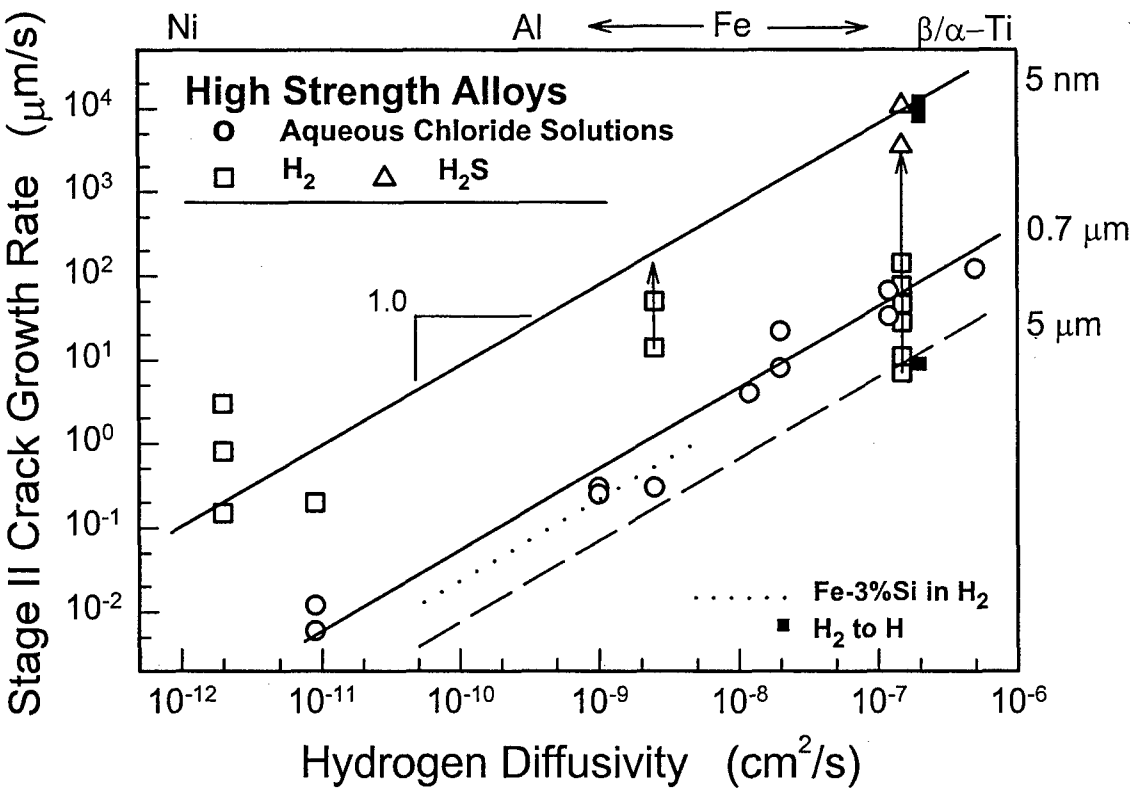

Figure 50 The dependence of da/dt_{II} on D_{Heff} for high strength alloys that exhibit HEAC in gases and electrolytes at 25°C. High strength austenitic stainless steel and nickel superalloys were cracked in high pressure (100–200 MPa) H_2, while maraging and tempered-martensitic steels were cracked in low pressure (~100 kPa) H_2. The dotted line represents TG cracking of Fe-3%Si single crystal in 100 kPa H_2 at 0°C to 125°C. Filled symbols (□) represent the transition from molecular to atomic hydrogen gas. (Gangloff, 2003; containing references to specific data)

equilibrium C_S. Support for this argument is provided by da/dt_{II} data reported for AISI 4130 steel tested in either low pressure H_2 (lowest □ at $D_{Heff} = 2.0 \times 10^{-7} cm^2/s$) or thermally dissociated H (highest two values of da/dt_{II}, □) (Nelson, Williams and Tetelman, 1971).

An extremely low critical distance, $\chi_{CRIT} = 5$ nm, is suggested for the H-producing gases based on the diffusion analysis of the trend line using $\xi = 3$. This distance is 150 times lower than the value calculated for the upper bound for the electrolytes, contradicting the notion that χ_{CRIT} should be independent of environment and C_S. The correlations in Fig. 50 suggest an intriguing possibility. Corrosion could produce a high concentration of vacancies localized to within a short distance of the crack-tip surface (Magnin et al., 1990; Jones et al., 1997). Highly mobile H is trapped at vacancies or vacancy clusters that are not annihilated by self-diffusion (Hirth, 1980; Pressouyre, 1980), suggesting that H transport in this near-surface layer is characterized by a reduced D_{Heff}. The correlations in Fig. 50 show that D_{Heff} must be reduced 200-fold to superpose the gas and electrolyte data.

6.03.8.4.3 Location of H Damage Sites in FPZ

A consensus is emerging that χ_{CRIT} is small for HEAC in high strength alloys. Supporting evidence includes: (1) H-diffusion correlations in Figs. 48-50 suggest χ_{CRIT} between 50 nm and 1 μm, (b) acoustic emission and crack-surface arrest markings suggest $\chi_{CRIT} < 1$ μm (Chen and Gerberich, 1991), (c) rapid changes in da/dt with changing H_2 pressure (Oriani and Josephic, 1974, 1977; Vehoff and Rothe, 1983) or temperature (Gangloff and Wei, 1977) suggest $\chi_{CRIT} < 0.1$ to 1 μm, (d) surface reaction-limiting models describe da/dt_{II} (Williams and Nelson, 1970, 1970a; Nelson, Williams and Tetelman, 1971;

Nelson and Williams, 1977; Pasco et al., 1982, 1984; Vehoff and Rothe, 1983; Pasco and Ficalora, 1983; Vehoff and Neumann, 1985), hence the process zone must be near to the crack tip to enable non-limiting H diffusion, (e) the temperature dependence of da/dt_{II} for HEAC of high strength steels cracked in H_2 is described by a H-diffusion model with χ_{CRIT} from 50 to 400 nm (Gerberich, Livne and Chen, 1986), and (f) the independence of K_{IH} on applied dK/dt is consistent with $\chi_{CRIT} < 1$ μm for X-750 in H_2 (Symons, 2001) and two β/α-Ti alloys cracked in NaCl (Fig. 6) (Somerday, Young and Gangloff, 2000).

A sub-μm process zone is consistent with three aspects of the crack tip FPZ that are only recently appreciated. First, crack chemistry considerations and direct measurements by nuclear reaction analysis and thermal desorption spectroscopy demonstrate that H is concentrated to unexpectedly high levels (0.01 to 0.1 atom pct) on the crack tip surface in contact with the occluded crack electrolyte, at least for a 7000 series aluminum alloy in chloride solution (L.M. Young, 1999; Cooper et al., 2000; Cooper and Kelly, 2001). This H accumulation may be stabilized by near-surface vacancies from dissolution and degrade the fracture resistance of the alloy in this region within 1 μm of the crack surface. Unfortunately, such measurements are complex and limited; this perspective is presently speculative.

Second, modern dislocation and strain gradient plasticity models of the crack tip demonstrate that extremely high stresses are localized within 20 nm to several micrometers of the crack tip surface (Fig. 44 and 6.03.8.1). The existence of these high stresses is consistent with experimental observations of very sharp and small-opening crack tips produced under H-embrittlement conditions, as opposed to crack blunting considerations

(Vehoff and Rothe, 1983; Vehoff and Neumann; Somerday et al., 2000). High crack tip stress exacerbates HEAC by promoting high levels of H accumulation through lattice dilation and associated H trapping (Thomas et al., 2003) and results in damage at lower C_{CRIT}. Finally, modeling shows that H is trapped by the high density of dislocations that are produced by plastic deformation immediately adjacent to the crack tip surface (Krom et al., 1999; Taha and Sofronis, 2001). If this H participates in damage and crack extension, then a small χ_{CRIT} is reasonable.

Lynch argued that fast crack growth rates can only be explained by AIDE focused on the crack surface (Lynch, 1988, 1997, 2003). HEDE-based models reasonably describe da/dt_{II} levels up to 10,000 μm/s (Fig. 50), given the evidence that χ_{CRIT} is small. Unexpectedly large levels of H accumulated in this region provide a compelling reason to accept HEDE.

6.03.9 UNCERTAINTIES AND NEEDS

Substantial successes have been recorded in developing the fracture mechanics framework, laboratory data on the properties of materials, and fundamental-mechanistic understanding necessary to quantitatively describe subcritical H-cracking in structural integrity modeling involving high strength alloys. However, substantial uncertainties exist.

6.03.9.1 Fracture Mechanics Issues

6.03.9.1.1 Specimen Constraint

Specimen size, particularly thickness for a Mode I through crack, is a variable that affects hydrogen cracking by both mechanical constraint and chemical mechanisms. Constraint results in increased crack tip opening-direction and hydrostatic stresses for a

crack tip plastic zone and FPZ governed by either conventional J_2 plasticity or length-scale dominant plasticity (Fig. 44) (Anderson, 1995; Needleman and Sevillano, 2003). This higher crack tip stress environment exacerbates H cracking, in terms of lowered K_{TH} and increased da/dt_{II}, as suggested by each of the micromechanical models summarized in 6.03.8.

Specimen size and geometry can affect crack tip H concentration, and hence K_{TH} and da/dt. For IHAC, a through-thickness gradient in H concentration from insufficient precharging exposure results in raised threshold and lowered crack growth rate (Thomas, et al., 2003). For HEAC, K_{IHEAC} decreases with decreasing thickness, counter to a constraint effect and traced to increasing amount of H distributed about the crack tip FPZ from environmental reaction (Fujii, 1976; Kobayashi and Takeshi, 1985). This effect depends on the relative amounts of H provided by reactions at boldly exposed surfaces *vs.* the crack tip, as governed by the electrochemical considerations detailed in 6.03.6.3.2 and 6.03.7.1.2 (Turnbull and Saenz de Santa Maria, 1990); generalization is not possible.

Only limited guidance is available to guarantee small-scale yielding and quantify mechanical constraint for laboratory testing that yields K_{IHEAC} and da/dt under quasi-static loading (ASTM, 2000). This standard requires that the plane strain thickness criterion determined empirically from fracture toughness experiments be satisfied so that the environmental cracking threshold is certified as a plane strain value. There are no data to support that this criterion ensures a specimen-thickness independent and lower-bound threshold for hydrogen cracking (Barsom and Rolfe, 1987). Furthermore, the geometry necessary for size independent measurement of K_{IH} under rising load is not known. Crack

tip constraint is high in laboratory specimens of high strength alloys at the low K levels that cause IHAC and HEAC. As such, size dependent chemical effects on H distribution about the crack tip are likely to be most important in structural integrity modeling.

6.03.9.1.2 Small Crack Size

Small crack size could invalidate stress intensity similitude due to mechanical or chemical mechanisms (Clark, 1976). The hypothesis that the threshold for H cracking depends on crack size was demonstrated experimentally for high strength AISI 4130 steel stressed in NaCl solution. The measured K_{TH} was constant at 20 $\pm$ 5 MPa$\sqrt{m}$ for crack depths between 1 and 20 mm, but declined to 8 MPa$\sqrt{m}$ for short cracks sized below 1 mm, as shown in Fig. 39 (Gangloff, 1985; Gangloff and Turnbull, 1986). This effect was explained based on a 10-fold increase in the H production rate at the crack tip, as crack size declined from 20 to 0.3 mm, and modeled based on the role of crack geometry in setting the occluded crack tip electrochemistry that established the level of H production. Similar effects were reported for other high strength alloys, but data and crack chemistry modeling are limited (Gangloff and Wei, 1986).

6.03.9.1.3 Precrack Path

Precrack path could affect subsequent H cracking kinetics, but data showing this behavior are limited. Conceptually, a precrack tip located apart from the H-susceptible crack path in the microstructure could exhibit a different K_{TH} and early growth kinetics compared to a starting crack located along the H-sensitive path. A recent study of HEAC in

high strength β-Ti showed that cracking during fixed-CMOD loading in chloride solution occurred when the precrack was transgranular, as produced by fatigue (Somerday, et al., 2000). Hydrogen cracking did not occur for the same solution and applied K level when the precrack was intergranular, produced by prior HEAC. This behavior was ascribed speculatively to the effect of crack tip path and morphology on crack tip strain and strain rate, that in turn influenced the stability of a crack tip passive film that blocked the uptake of H. Similar studies have not been reported for steels and aluminum alloys.

6.03.9.1.4 Mixed Mode Hydrogen Assisted Cracking

Mixed mode hydrogen cracking in high strength alloys has received substantially less attention than the Mode I case. Several studies showed that HEAC was substantial for high strength steel, aluminum and α-based titanium alloys under Mode I, but not resolved under pure Mode III loading (Hayden and Floreen, 1971; St. John et al., 1973; Swanson, et al., 1981; Pickens et al., 1983). In contrast other studies showed that H promoted subcritical crack growth for IHAC and HEAC in high strength steels under simple Mode III loading (Chu et al., 1986; Gao and Cao, 1998), as well as pure Mode II loading (McGuinn and Aballe, 1982; Gao and Cao, 1998). In these cases the threshold for H cracking was equal to the low level measured for Mode I. Results for mixed mode cracking typically show that the addition of a Mode II component to Mode I loading reduces the severity of IHAC and HEAC (Gao and Xue, 1989; Ohsaki et al., 1997; Gao and Cao, 1998). A specific example of these trends is presented in Fig. 51 for both IHAC and HEAC of martensitic steel.

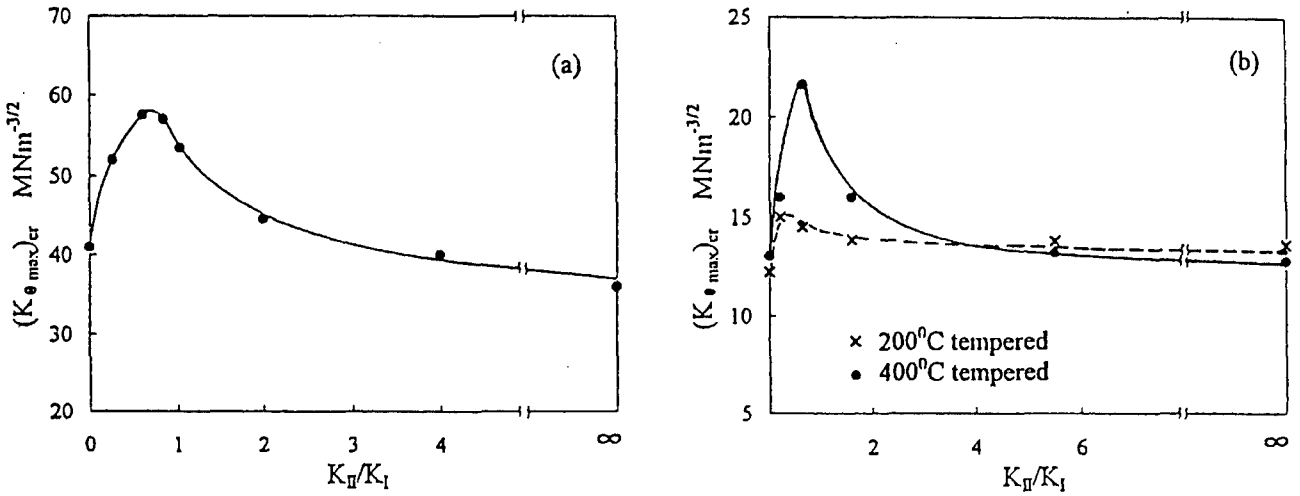

Figure 51. The effect of loading mode, represented as the ratio of applied K_{II}/K_I, on the threshold stress intensity for: (a) IHAC and (b) HEAC of high strength low alloy steel ($1300 < \sigma_{YS} < 1600$ MPa) in H_2SO_4. $K_{\theta max}$ represents a trigonometric combination of K_I and K_{II}, and H cracking was always in the plane normal to the maximum crack tip tensile stress from elastic analysis. (Gao and Cao, 1998: Copyright *Fatigue and Fracture of Engineering Materials and Structures*, reprinted with permission.)

These complex effects of loading mode are explained qualitatively by the interaction of H in the FPZ with two aspects of crack tip mechanics that depend on loading mode; hydrostatic tensile stress and plastic strain/dislocation density as summarized in 6.03.8.1. Hydrostatic stress enhanced H accumulation and damage is optimized for pure Mode I, but is none-the-less present at reduced levels for Modes II and III (Nichols, 1983; Zang and Hack, 1999; Jones et al., 2000). The detrimental plasticity effect on H accumulation increases with increasing amounts of Mode II or III loading over Mode I. Additionally, plastic flow is localized by Mode III loading and can in some instances exacerbate H damage (Kumar et al., 1993). To further complicate the situation, theory and experiment suggest that the effect of Mode II addition to Mode I depends on the loading format, be it constant load or rising CMOD (Gao and Cao, 1998). The implication to structural integrity modeling is clear; Mode I cannot be assumed to be the most damaging from the hydrogen cracking perspective and mixed-mode loading must be considered. New laboratory experimentation will be required to support such life prediction.

6.03.9.1.5 Transient Exposure

Transient mechanical and chemical effects are likely present in component service, and present a formidable challenge to structural integrity modeling. Reduced H cracking due to prestressing or overloading of a precracked specimen, as well as prolonged incubation prior to crack propagation at K levels above K_{TH}, were demonstrated for laboratory specimens as discussed in 6.03.3.5.1 (Wei et al., 1972; Jonas, 1973; Hudak and Wei, 1981). Of equal importance, alternating environmental exposure likely affects crack chemistry and the

resulting H production plus uptake. An example is atmospheric exposure involving a thin-layer electrolyte where ohmic voltage drop within the crack should be increased while occluded chemistry changes may be muted. For this case, as well as alternate immersion in an electrolyte, anodic and cathodic reactions are forced to occur largely within the crack. Lack of separation of anode and cathode sites should reduce acidification, and thus affect H uptake at the crack tip. Finally, drying could form condensed and concentrated corrosion products that rehydrate into a more aggressive state when rewet. There have been no systematic laboratory studies of these speculative effects on HEAC.

6.03.9.1.6 Interacting Cracks

A distribution of interacting cracks confounds structural integrity modeling (Parkins, 1990). Research to date on hydrogen cracking has almost exclusively examined the behavior of a single Mode I crack in high strength alloys, following the classic fracture mechanics approach. Studies in the peripheral areas of environment-sensitive fatigue in precipitation hardened aluminum alloys (Harlow and Wei, 2001, 2001a, 2002), stress corrosion cracking in low strength pipeline steels (Parkins, 1991; Leis and Parkins, 1998), and hydrogen induced stepwise cracking in low strength C-Mn steels in sour-environment service (Iino, 1979; Suarez, et al., 2000) demonstrate the challenges associated with understanding the formation and coalescence of multiple cracks. Unique crack electrochemistry effects, accurate stress intensity solutions, and reexamination of K as the proper crack tip driving force are challenging issues.

6.03.9.1.7 Distribution of Material Cracking Properties

Distribution of material properties and the associated statistical description are essential to structural integrity modeling, particularly with probabilistic analysis. Variability in the threshold and kinetics of IHAC and HEAC results from measurement errors in laboratory experiments (Wei and Novak, 1987) as well as the distribution of intrinsic variables such as grain boundary purity.

The complexity and duration of hydrogen cracking experiments has limited determinations of distributions of K_{TH} and da/dt measurements for a specific material-environment situation. The many possible variables (6.03.6) and measurement issues are too numerous to permit either precise definition of laboratory precision or intrinsic material variability (ASTM, 2000). Two interlaboratory studies indicate the magnitude of variability for two lots of high strength steel in chloride solution. The K_{IHEAC} of 34.5 MPa$\sqrt{m}$ varied by $\pm$17% for 4000 h duration experiments conducted by 8 laboratories (Wei and Novak, 1987), and the K_{IHEAC} of 28.9 MPa$\sqrt{m}$ varied by $\pm$19% based on data from 6 laboratories, all employing a similar experimental protocol (Yokobori, et al., 1988). This level of uncertainty should be viewed as typical of best effort by an experienced laboratory, with larger errors possible given the difficulty of long term chemical environment control. No study has reported on heat-to-heat threshold variability for a given alloy. Variations in crack growth rates have not been reported and are likely to be substantial, a factor of 2 to10. Figure 12 provides an example of multiple specimen variability in da/dt that likely represents the best-achievable agreement between experiments.

6.03.9.2 Research Needs

The discussions of fundamental H cracking mechanisms in 6.03.7 and micromechanical-chemical models of H cracking thresholds and kinetics in 6.03.8 demonstrate substantial uncertainties in the understanding of HEAC and IHAC. The majority of these issues are traced to the complexity and highly localized character of H production, uptake and damage about the very small crack tip process zone. Advances in each of the following four areas will improve the capability for next generation structural integrity modeling.

6.03.9.2.1 Hydrogen Damage Mechanism

While the decohesion mechanism is favored by many to explain H cracking in high strength alloys, this effect has never been demonstrated directly. The last review of HEDE by Oriani is timely, with no substantial results or approaches recorded in the interim (Oriani, 1990; McMahon, 2001; Katz et al., 2001). First principles modeling of the effect of H on bond cohesion, as well as the implications for both sequential (slip) and sympathetic (fracture) bond breaking, continues to be an obvious need. Additionally, micromechanical-chemical models of macroscopic cracking properties must be formulated, stemming from the H-enhanced plasticity mechanisms, AIDE and HELP, when operative.

6.03.9.2.2 Crack Chemistry and H Production

While the framework exists for modeling occluded-crack chemistry and electrochemistry (Wei, 1981; Wei and Gangloff, 1989; Turnbull, 2001), specific information on transport and reaction rates is lacking. For example, it is important to determine H production kinetics for

multi-component and multi-phase metal surfaces exposed to hydrogen bearing gases and aqueous electrolytes while under stress and plastic deformation (Pasco and Ficalora, 1983). The compositions of these environments must be selected carefully to simulate the actual conditions affecting crack tip reaction sites. Second, it is important to integrate recent crack mass transport and reaction models with a quantitative description of H diffusion in the crack tip FPZ (Turnbull, 1996).

To calibrate and validate crack chemistry modeling, it is necessary to measure H content local to the crack tip FPZ. While a suite of methods exists to measure H in metals (e.g., Sakurai and Pickering, 1982; Birnbaum et al., 1982; Myers et al., 1985), local H contents are elusive due to the small and gradated scale of the FPZ and mobility of H. Success with thermal desorption spectroscopy (Fig. 40) and neutron reaction analysis of crack wake specimens should be confirmed and developed (Young, 1999; Cooper, et al., 2000).

6.03.9.2.3 Crack Tip Mechanics

The discussion in 6.03.8.1 establishes substantial progress in modeling crack tip stress and strain. Conventional plasticity theory that enabled ductile fracture modeling (Anderson, 1995), must be modified to properly reflect the steep gradient and small-process zone size typical of H cracking in high strength alloys (Hutchinson, 2000; Needleman and Sevillano, 2003). The resulting constitutive description should be incorporated into a high resolution finite element analysis of the crack tip region. The characteristic-material length should be defined and explained physically for high strength microstructures). Following this work, crack tip strain rate should be better quantified, particularly for the crack surface where film

destabilization by plastic strain is a critical aspect of HEAC (Somerday, et al., 2000).

Experimental results are required to calibrate and confirm crack mechanics modeling. For example, transmission electron microscope determination of crack tip dislocation structures is limited due to the small size of the FPZ and complex microstructures typical of high strength alloys. Results are necessary to guide formulations of dislocation-based descriptions of crack tip stress (Kameda, 1986a; Gerberich et al., 1991; Gerberich et al., 1996; Katz et al., 2001), and confirm the validity of AIDE and HELP (Lynch, 2003). Measurement of crack tip strain has been limited for H cracking in high strength alloys compared to the extensive *in situ* scanning electron microscope studies of fatigue crack tips in a variety of alloys (Davidson and Lankford, 1983, 1992). Application of this method used the environmental scanning electron microscope to examine the effect of H_2 and H_20 on crack-tip opening in AISI 4340 steel (σ_{YS} = 1670 MPa) with a fine (3-5 μm) prior austenite grain size (Kinaev et al., 1999, 1999a, 1999b). Measured crack tip strains were increased by H from each environment, compared to those recorded for loading to the same remote K level (15-35 MPa$\sqrt{m}$) in vacuum. Additionally, creep at 23°C was stimulated and the plastic zone shape was altered by environment compared to vacuum. These results were interpreted to support the HELP mechanism (6.03.7.2.2). The resolution of this method was ~1 μm, sufficient to detect environment-sensitive changes in crack tip opening and plastic zone size on the specimen surface, but large compared to the sub-micrometer critical distance that likely controls HEAC in high strength alloys (6.03.8.4.3). It is important to extend this experimental approach to improve resolution and include other materials and environments.

6.03.9.2.4 Hydrogen Trapping

Hydrogen trapping is centrally important to cracking in high strength alloys (6.03.6.3.1). The need is to better determine H-binding energies for each of the trap states encountered in a high strength alloy microstructure. This identification is complex and often non-unique due to uncertainties in trap characteristics (Thomas, et al., 2002). Modeling of temperature-dependent H diffusion through a forest of multiple trap states, surrounding and included within the crack tip FPZ, is needed. Much of the work to date, including the modeling and correlations in 6.03.8.4, was based on effective-H diffusivity. A fundamental treatment employs lattice-H diffusivity coupled with Fick's laws modified to include rates of trapping and detrapping from multiple binding-energy states (Oriani, 1970; Griffiths and Turnbull, 1995; Krom et al., 1999; Taha and Sofronis, 2001; Moody et al., 2001).

6.03.10 CONCLUSIONS

- Hydrogen from a variety of sources substantially degrades the subcritical crack growth resistance of most advanced high strength metallic alloys at threshold stress intensity levels as low as 5 to 25% of the plane strain fracture toughness and crack growth rates as high as 10,000 μm/s. Hydrogen assisted cracking is either intergranular or transgranular, with each sufficiently distinct to enable failure analysis.

- While metallurgical advances have resulted in high performance materials with outstanding strength and fracture toughness, the lack of H-cracking immune alloys in the iron, nickel, titanium and aluminum classes requires that structural integrity modeling of fracture critical components consider subcritical hydrogen embrittlement.

- Modern fracture mechanics methods provide the framework for structural integrity modeling to combat H-assisted cracking, following the damage tolerant procedures developed broadly for fatigue crack propagation-life prediction.

- Effective laboratory methods exist to determine the threshold and kinetics properties for both Internal Hydrogen Assisted Cracking and Hydrogen Environment Assisted Cracking in high strength alloys. These methods are complex and often require prolonged environmental exposure, but have been employed successfully to develop substantial K_{TH} and da/dt data relevant to structural integrity modeling.

- A wide range of metallurgical, mechanical, and environment chemistry variables affect IHAC and HEAC in high strength alloys. Alloy strength, grain size, purity, and 2^{nd} phase characteristics; stress intensity level and application rate, small crack size, constraint, loading mode, and load transients; predissolved hydrogen content, surrounding gas pressure, electrode potential, solution pH, environment composition, and temperature; interact to affect K_{TH} and da/dt. The effects of these variables must be considered in structural integrity modeling.

- IHAC and HEAC are eliminated by decreasing and increasing temperature from near-ambient levels. The temperature range where H-cracking is severe depends on alloy strength and crack tip H concentration. This temperature dependence is traced to limited H diffusion to the FPZ at low temperature and reduced H supply at elevated temperature. Regarding supply, thermally stimulated desorption of H from the adsorbed state on the crack surface is important for HEAC. Thermal detrapping of H from low-binding energy traps that constitute the embrittlement path is important for IHAC and HEAC.

- Important albeit circumstantial evidence establishes that HEAC provides the dominant contribution to stress corrosion cracking in high strength alloys stressed in moist gases

and aqueous electrolytes near ambient temperature. Extensive threshold and Stage II crack growth rate data are correlated with the amount of H absorbed on the crack tip surface and transported into the fracture process zone, as established semi-quantitatively by crack electrochemistry measurements and modeling.

- The consensus is emerging that hydrogen enhanced decohesion is the basic damage mechanism for IHAC and HEAC in high strength alloys. This view is dictated by the high accumulation of H, local to the crack tip FPZ and driven by the concentrating effects of high tensile stress coupled with H trapping at microstructural features. Between the competing H-enhanced decohesion and H-localized plasticity concepts, only decohesion has been developed into models capable of predicting macroscopic hydrogen cracking properties relevant to structural integrity modeling.

- Micromechanical-chemical models have been developed to predict the quasi-equilibrium threshold stress intensity, as well as Stage II subcritical crack growth rate for both IHAC and HEAC in high strength alloys. These models contain adjustable constants that hinder quantitative predictions, but are useful to guide extrapolations of limited laboratory data and explain the influences of important variables.

- Fundamental understanding of H cracking is limited by the highly localized and gradated nature of crack tip H production and trapping, tensile stress and plastic strain, and H damage in high strength alloys. Nano-scale atomistic processes dominate material degradation within a micrometer-scale fracture process zone, leading to millimeter-scale crack growth. Future research on IHAC and HEAC must better integrate such behavior across these length scales.

- Uncertainties confound implementation of the capability to manage H cracking in a comprehensive structural integrity plan. Descriptions of interacting cracks, mixed mode loading, transient load and environment exposure, and the statistics of cracking

properties are in an infant state. Mechanistic understanding and associated micromechanical models are insufficient to predict quantitative algorithms for K_{TH} and da/dt_{II}.

6.03.11 ACKNOWLEDGEMENT

Preparation of this review was enabled by sustained support from the Office of Naval Research (Grant N00014-91-J-4164), with Dr. A. John Sedriks as Scientific Monitor, as well as the Alcoa Technical Center with Dr. James T. Staley as Program Manager. Much of the research was conducted by graduate students in the Environmental Fracture Group at the University of Virginia; including Drs. Lisa M. Young, Brian P. Somerday, Jennifer G. Lillard, Edward Richey, III and Sean P. Hayes, as well as Ms. Lisa Hartman and Mr. Richard L.S. Thomas. The NASA-Langley Research Center, as well as Alcoa, ONR, and McDonnell-Douglas/Boeing provided the support for these research studies. Professors John R. Scully and Robert G. Kelly provided important insights and collaborations throughout this work. These contributions are gratefully acknowledged, as are the pioneering works of many over the past decades.

6.03.12 REFERENCES

K.N. Akhurst and T.J. Baker, The threshold stress intensity for hydrogen induced crack growth. *Metall. Trans. A*, **12A**, 1981, 1059-1070.

J. Albrecht, B.J. McTiernan, I.M. Bernstein and A.W. Thompson, Hydrogen embrittlement in a high-strength Al alloy. *Scripta Metall.*, **11**, 1977, 893-897.

J. Albrecht, A.W. Thompson and I.M. Bernstein, The role of microstructure in hydrogen-assisted fracture of 7075 aluminum. *Metall. Trans. A*, **10A**, 1979, 1759-1766.

J. Albrecht, A.W. Thompson and I.M. Bernstein, Evidence for dislocation transport of hydrogen in aluminum. *Metall. Trans. A*, **13A**, 1982, 811-820.

G. Alefeld and J. Völkl. Eds., "Hydrogen in Metals," Springer-Verlag, Berlin, Germany, 1978.

G. Alefeld and J. Völkl, Eds., "Hydrogen in Metals III: Properties and Applications," Springer-Verlag, Berlin, Germany, 1997.

T.L. Anderson, "Fracture Mechanics: Fundamentals and Applications," 2nd Ed., CRC Press, Boca Raton, FL, 1995, pp. 117-181.

ASM International, "Metals Handbook Ninth Edition: Vol.8, Mechanical Testing", Materials Park, OH, 1985.

ASTM, "Standard Test Method for Determining a Threshold Stress Intensity Factor for Environment-Assisted Cracking of Metallic Materials," Designation E1681-99, *Standards on Disc*, Vol. 03.01, ASTM International, West Conshohocken, PA, 2000.

P. Azou, Ed., "Third International Congress on Hydrogen and Materials," Pergamon Press, New York, NY, 1982.

Robert Baboian, Ed., "Corrosion Tests and Standards," ASTM International, West Conshohocken, PA, 1995.

R.G. Baggerly, Hydrogen-assisted stress cracking of high-strength wheel bolts. *Engr. Fail. Anal.*, **3**, 1996, 231-240.

N. Bandyopadhyay, J. Kameda, and C.J. McMahon, Jr., Hydrogen-induced cracking in 4340-type steel: Effects of composition, yield strength and hydrogen pressure. *Metall. Trans. A*, **14A**, 1983, 881-888.

J.M. Barsom and S.T. Rolfe, "Fracture and Fatigue Control in Structures," 2nd Ed., Prentice-Hall, Englewood Cliffs, NJ, 1987.

J.M. Barsoin, "Fracture Mechanics Retrospective: *Early Classic Papers (1913-1965)*," ASTM International, West Conshohocken, PA, 1987.

C.E. Barth and E.A. Steigerwald, Evaluation of hydrogen embrittlement mechanisms. *Metall. Trans.*, **1**, 1970, 3451-3455.

B.A. Bayles, P.S. Pao, S.J. Gill and G.R. Yoder, in: "Systems Engineering Approach to Mechanical Failure Prevention," Eds., H.C. Pusey and S.C. Pusey, Vibration Institute, Willowbrook, IL, 1993, 167-176.

C.D. Beachem, A new model for hydrogen-assisted cracking (hydrogen embrittlement). *Metall. Trans.*, **3**, 1972, 437-451.

I.M. Bernstein and A.W. Thompson, Eds., "Hydrogen in Metals", ASM International, Materials Park, OH, 1974.

I.M Bernstein and A.W. Thompson, Effect of metallurgical variables on environmental fracture of steels. *Intl. Metall. Rev.*, **21**, 1976, 269-287.

I.M. Bernstein and A.W. Thompson, Eds., "Hydrogen Effects in Metals," The Minerals, Metals & Materials Society, Warrendale, PA, 1981.

H.K. Birnbaum, H. Fukushima and J. Baker, in: "Advanced Techniques for Characterizing Hydrogen in Metals," The Minerals, Metals & Materials Society, Warrendale, PA, 1982, pp. 149-154.

H.K. Birnbaum, in: "Environment Induced Cracking of Metals", Eds., R.P. Gangloff and M.B. Ives, NACE, Houston, TX, 1990, pp. 21-29.

H.K. Birnbaum, I.M. Robertson, P. Sofronis and D. Teter, in: "Second International Conference on Corrosion-Deformation Interactions," Ed., T. Magnin, The Institute of Materials, London, UK, 1997, pp. 172-195.

H.K. Birnbaum and P. Sofronis, Hydrogen-enhanced plasticity—a mechanism for hydrogen related fracture. *Mater. Sci. Engr.*, **A176**, 1993, 191-202.

M.J. Blackburn, J.A. Feeney and T.R. Beck, in: "Advances in Corrosion Science and Technology," Vol. 3, Eds., M.G. Fontana and R.W. Staehle, Plenum Publishing, New York, NY, 1972, pp. 67-292.

B.M. Bond, I.M. Robertson and H.K. Birnbaum, The influence of hydrogen on deformation and fracture processes in high-strength aluminum alloys. *Acta Metall.*, **35**, 1987, 2289-2296.

R.R. Boyer, in "Beta Titanium Alloys in the 1990s," eds., D. Eylon, R.R. Boyer and D.A. Koss, The Minerals, Metals & Materials Society, Warrendale, PA, 1993, 335-346.

C.L. Briant and S.K. Banerji, Intergranular failure in steel: The role of grain boundary composition. *Intl. Metall. Rev.*, **23**, 1978, 164-199.

C.L. Briant and S.K. Banerji, in: "Treatise on Materials Science and Technology: Embrittlement of Engineering Alloys," Eds., C.L. Briant and S.K. Banerji, Vol. 25, Academic Press, New York, NY, 1983, pp. 21-58.

B.F. Brown and C.D. Beachem, A study of the stress factor in corrosion cracking by use of the precracked cantilever-beam specimen. *Corros. Sci.*, **5**, 1965, 745-750.

B.F. Brown and C.D. Beachem, "Specimens for Evaluating the Susceptibility of High Strength Steels to Stress Corrosion Cracking," Naval Research Laboratory Report, Washington, DC, 1966.

B.F. Brown, in: "The Theory of Stress Corrosion Cracking," Ed., J.C. Scully, NATO Scientific Affairs Division, Brussels, Belgium, 1971, pp. 186-204.

B.F. Brown, in: "Stress Corrosion Cracking and Hydrogen Embrittlement of Iron Base Alloys," Eds., R.W. Staehle, et al., NACE, Houston, TX, 1977, pp. 747-751.

P.F. Buckley, R. Brown, G.H. Graves, E.U. Lee, C.E. Neu and J. Kozol, in: "Metallic Materials for Lightweight Applications, 40th Sagamore Army Materials Research Conference," Eds., M.G.H. Wells, E.B. Kula and J.H Beatty, US Army Laboratory Command, Watertown, MA, 1993, 377-388.

P. Buckley, B. Placzankis, J. Beatty and R. Brown, "Characterization of the Hydrogen Embrittlement Behavior of High Strength Steels for Army Applications," *Corrosion/94*, Paper No. 547, NACE, Houston, TX, 1994.

T.D. Burleigh, The postulated mechanisms for stress corrosion cracking of aluminum alloys. *Corrosion*, **47**, 1991, 89-98.

C.S. Carter, "Stress Corrosion Cracking and Corrosion Fatigue of Medium-Strength and High Strength Steels," Boeing Commercial Airplane Company report, Seattle, WA, unpublished,

C.S. Carter, The effect of silicon on the stress corrosion resistance of low alloy high strength steels. *Corrosion*, **25**, 1969, 423-431.

T.J. Carter and L.A. Cornish, Hydrogen in metals. *Engr. Fail. Anal.*, **8**, 2001, 113-121.

N.H. Chan, K. Klier and R.P. Wei, A preliminary investigation of Hart's model in hydrogen embrittlement in maraging steels. *Scripta Metall.*, **12**, 1978, 1043-1046.

J.C. Charbonnier and H. Margot-Marette, in: "Current Solutions to Hydrogen Problems in Steels," Eds., C.G. Interrante and G.M. Pressouyre, ASM International, Materials Park, OH, 1982, pp. 462-466.

P.S. Chen, B. Panda and B.N Bhat, in: "Hydrogen Effects in Materials", Eds., A.W. Thompson and N.R. Moody, The Minerals, Metals & Materials Society, Warrendale, PA, 1996, pp. 1011-1019.

X. Chen and W.W. Gerberich, The kinetics and micromechanics of hydrogen assisted cracking in Fe-3 pct Si single crystals. *Metall. Trans. A*, **22A**, 1991, 59-70.

L. Christodoulou and H.M. Flower, Hydrogen embrittlement and trapping in Al-6%Zn-3%Mg. *Acta Metall.*, **28**, 1980, 481-487.

W.Y. Chu, C.M. Hsiao and B.J. Xu, Stress corrosion cracking in high strength steel under Mode III loading. *Metall. Trans. A.*, **17A**, 1986, 711-716.

W.G. Clark, Jr. and J.D. Landes, in: "Stress Corrosion Cracking—New Approaches, ASTM STP 610", Ed., H.L. Craig, Jr., ASTM International, West Conshohocken, PA, 1976, pp. 108-127.

W.G. Clark, Jr., in: "Cracks and Fracture, ASTM STP 601," ASTM International, West Conshohocken, PA, 1976, pp. 138-153.

W.G. Clark, Jr., Effect of temperature and pressure on hydrogen cracking in high strength type 4340 steel. *J. Matls. Energy Sys.*, **1**, 1979, 33-40.

K.R. Cooper, L.M. Young, R.P. Gangloff, and R.G. Kelly, The electrode potential dependence of environment-assisted cracking of AA7050. *Matls. Sci. For.*, **331-337**, 2000, 1625-1634.

K.R. Cooper and R.G. Kelly, in: "Chemistry and Electrochemistry of Stress Corrosion Cracking: A Symposium Honoring the Contributions of R.W. Staehle," Ed., R.H. Jones, The Minerals, Metals & Materials Society, Warrendale, PA, 2001, pp. 523-542.

L. Coudreuse and P. Bocquet, in: "Hydrogen Transport and Cracking in Metals," Ed., A. Turnbull, University Press, Cambridge, UK, 1995, 227-252.

W.R. Crumly, in: "Hydrogen Embrittlement: Prevention and Control, ASTM STP 962," Ed., L. Raymond, ASTM International, West Conshohocken, PA, 1988, pp. 173-178.

D.P. Dautovich and S. Floreen, The stress intensities for slow crack growth in steels containing hydrogen. *Metall. Trans.*, **4**, 1973, 2627-2630.

D.P. Dautovich and S. Floreen, in: "Stress Corrosion Cracking and Hydrogen Embrittlement of Iron Base Alloys," Eds., R.W. Staehle, et al., NACE, Houston, TX, 1977, pp. 798-815.

D.L. Davidson and J. Lankford, Fatigue crack growth in metals and alloys: mechanisms and micromechanics. *Intl. Metall. Rev.*, **37**, 1992, 45-76.

D.L. Davidson and J. Lankford, in: "Fatigue Mechanisms: Advances in Quantitative Measurement of Physical Damage," ASTM International, West Conshohocken, PA, 1983, pp. 371-399.

M.S. Daw and M.I. Baskes, in: "Chemistry and Physics of Fracture," Eds., R.M. Latanision and R.H. Jones, Martinus Nijhoff Publishers BV, Netherlands, 1987, pp. 196-218.

W. Dietzel and K. Ghosal, Effect of displacement rates on EAC of AISI 4340 steel. *Fatg. Fract. Engr. Matls. Struct.*, **21**, 1998, 1279-1286.

W. Dietzel and J. Mueller-Roos, Experience with rising load/rising displacement stress corrosion cracking testing. *Materials Science (Russia)*, **37**, 2001, 264-271.

W. Dietzel, K.-H. Schwalbe and D. Wu, Application of fracture mechanics techniques to the environmentally assisted cracking of aluminum 2024. *Fatg. Fract. Engr. Matls. Struct.*, **12**, 1989, 495-510.

P. Doig and G.T. Jones, Model for the initiation of H embrittlement cracking at notches in gaseous H environments. *Metall. Trans. A*, **8A**, 1977, 1993-1998.

R.A.H. Edwards, in: "Predictive Capabilities in Environmentally Assisted Cracking," American Society of Mechanical Engineers, New York, NY, 1985, pp. 153-175.

N. Eliaz, A. Shachar, B. Tal and D. Eliezer, Characteristics of hydrogen embrittlement, stress corrosion cracking and tempered martensite embrittlement in high strength steels. *Engr. Fail. Anal.*, **9**, 2002, 167-184.

J. A. Feeney and M. J. Blackburn, Effect of microstructure on the strength, toughness and stress-corrosion cracking susceptibility of a metastable beta titanium alloy. *Metall. Trans*, 1, 1970, 3309-3323.

N.A. Fleck and J.W. Hutchinson, A reformulation of strain gradient plasticity. *J. Mech. Phys. Sol.*, **49**, 2001, 2245-2271.

L.G. Fritzemeier, R.J. Walter, A.P. Meisels and R.P. Jewett, in: "Hydrogen Effects on Material Behavior", Eds., N.R. Moody and A.W. Thompson, The Minerals, Metals & Materials Society, Warrendale, PA, 1990, pp. 941-954.

R.P. Frohmberg, W.J. Barnett and A.R. Troiano, Delayed failure and hydrogen embrittlement in steel. *Trans. ASM*, **47**, 1955, 892-925.

C.T. Fujii, in "Stress Corrosion-New Approaches, ASTM STP 610," Ed., H.L. Craig, Jr., ASTM International, West Conshohocken, PA, 1976, pp. 213-225.

J.R. Galvele, A stress corrosion cracking mechanism based on surface mobility. *Corros. Sci.*, **27**, 1987, 1-33.

R.P. Gangloff and R.P. Wei, Gaseous hydrogen embrittlement of high strength steels. *Metall. Trans., A*, 1977, **8A**, 1043-1053.

R.P. Gangloff and R.P. Wei, in: "Fractography in Failure Analysis, ASTM STP 645," eds., B.M. Strauss and W.H. Cullen, Jr., ASTM International, West Conshohocken, PA, 1978, pp. 87-106.

R.P. Gangloff, Ed., "Embrittlement by the Localized Crack Environment," The Minerals, Metals & Materials Society, Warrendale, PA, 1984.

R.P. Gangloff, Crack size effects on the chemical driving force for aqueous corrosion fatigue. *Metall. Trans., A*, **16A**, 1985, 953-969.

R.P. Gangloff, in: "Corrosion Prevention and Control," 33rd Sagamore Army Materials Research Conference, Eds., M. Levy and S. Isserow, US Army Laboratory Command, Watertown, MA, 1986, pp. 64-111.

R.P. Gangloff and R.P. Wei, in "Small Fatigue Cracks," Eds., R.O. Ritchie and J. Lankford, The Minerals, Metals & Materials Society, Warrendale, PA, 1986, pp. 239-264.

R.P. Gangloff and A. Turnbull, in: "Modeling Environmental Effects on Crack Initiation and Propagation," Eds., R.H. Jones and W.W. Gerberich, The Minerals, Metals & Materials Society, Warrendale, PA, 1986, pp. 55-81.

R.P. Gangloff, Crack tip models of hydrogen environment embrittlement: applications to fracture mechanics life prediction. *Matls. Sci. Engr.*, **A103**, 1988, 157-166.

R.P. Gangloff, in: "Basic Questions in Fatigue, Vol. 2, ASTM STP 924," Eds., R.P. Wei and R.P. Gangloff, ASTM International, West Conshohocken, PA, 1988, pp. 230-251.

R.P. Gangloff, in: "Environment Induced Cracking of Metals", Eds., R.P. Gangloff and M.B. Ives, NACE, Houston, 1990, TX, pp. 55-109.

R.P. Gangloff and M.B. Ives, Eds., "Environment-Induced Cracking of Metals," NACE, Houston, TX, 1990.

R.P. Gangloff, in: "Advanced Earth-To-Orbit Propulsion Technology", Eds., R.J. Richmond and S.T. Wu, NASA CP 3092, Vol. III, 1990a, Washington, DC, pp. 483-510.

R.P. Gangloff, B.P. Somerday and D.L. Cooke, in: "Life Prediction of Structures Subject to Environmental Degradation," Eds., P.L. Andresen and R.N. Parkins, NACE, Houston, TX, 1996, pp. 161-175.

R.P. Gangloff, Fracture mechanics characterization of hydrogen embrittlement in Cr-Mo Steel. in: "Present Situation on Steels for Hydrogen Pressure Vessels," Creusot-Loire Industrie, Le Creusot, France, 1998.

R.P. Gangloff, Embrittlement of high strength β-Ti alloys. In: "Advances in Fracture Research, Proceedings of ICF10," Eds. K. Ravi-Chandar, et al., Paper No. ICF108920R, CD version, Elsevier Science, Oxford, UK, 2001.

R.P. Gangloff, in: "Fatigue '02", Ed., Anders Blom, Engineering Materials Advisory Services, West Midlands, UK, 2002, pp. 3401-3433.

R.P. Gangloff, Diffusion control of hydrogen environment embrittlement in high strength alloys. in "Hydrogen Effects in Materials," Eds., N.R. Moody and A.W. Thompson, The Minerals, Metals & Materials Society, Warrendale, PA, 2002, in press.

R.P. Gangloff and K. George, unpublished research, University of Virginia, Charlottesville, VA, 2002a.

H. Gao and W. Cao, Effects of stress-strain conditions on hydrogen-induced fracture. *Fatg. Fract. Engr. Matls. Struct.*, 1998, **21**, 1351-1360.

M. Gao and R.P. Wei, Quasi-cleavage and martensite habit plane. *Acta metall.*, **32**, 1984, 2115-2124.

M. Gao, M. Lu and R.P Wei. Crack paths and hydrogen-assisted crack growth response in AISI 4340 steel. *Metall. Trans. A*, **15A**, 1984, 735-746.

M. Gao and R.P. Wei, A hydrogen partitioning model for hydrogen assisted crack growth. *Metall. Trans. A*, **16A**, 1985, 2039-2050.

H. Gao and L. Xue, (I + II) mixed mode hydrogen induced cracking. *Acta Metall. Sin.*, **25**, 1989, A48-A52.

W.M. Garrison, Jr., Ultrahigh-strength steels for aerospace applications. *J. Metals*, May, 1990, 20-24.

M.A. Gaudett and J.R. Scully, The effects of pre-dissolved hydrogen on cleavage and grain boundary fracture initiation in metastable beta Ti-3Al-8V-6Cr-4Mo-4Zr. *Metall. Mater. Trans. A*, **30A**, 1999, 65-79.

M.A. Gaudett and J.R. Scully, Metallurgical factors governing the H-assisted intergranular cracking of peak-aged Ti-3Al-8V-6Cr-4Mo-4Zr (Beta-C). *Metall. Mater. Trans. A*, **31A**, 2000, 81-92.

W.W. Gerberich, in: "Hydrogen in Metals", Eds., I.M. Bernstein and A.W. Thompson, ASM International, Materials Park, OH, 1974, pp. 115-147.

W.W. Gerberich, Y.T. Chen and C. St. John, A short-time diffusion correlation for hydrogen induced crack growth kinetics. *Metall. Trans. A*, **6A**, 1975, 1485-1498.

W.W. Gerberich and A.G. Wright, in: "Environmental Degradation of Engineering Materials in Hydrogen," Eds., M.R. Louthan, R.P. McNitt and R.D. Sisson, VPI Press, Blacksburg, VA, 1981, pp. 183-205.

W.W. Gerberich, T. Livne, and X.-F. Chen, in: "Modeling Environmental Effects on Crack Initiation and Propagation," Eds., R.H. Jones and W.W. Gerberich, The Minerals, Metals & Materials Society, Warrendale, PA, 1986, pp. 243-257.

W.W. Gerberich, T. Livne, X.-F. Chen and M. Kaczorowski, Crack growth from internal hydrogen-temperature and microstructure effects in 4340 steel. *Metall. Trans. A*, **19A**, 1988, 1319-1344.

W.W. Gerberich, R.A. Oriani, M.-J. Lii, X. Chen and T. Foecke, The necessity of both plasticity and brittleness in the fracture thresholds of iron. *Phil. Mag. A*, **63**, 1991, 363-376.

W.W. Gerberich, P.G. Marsh and J.W. Hoehn, in: "Hydrogen Effects in Materials," Eds., A.W. Thompson and N.R. Moody, The Minerals, Metals & Materials Society, Warrendale, PA, 1996, pp. 539-553.

R.J. Gest and A.R. Troiano, Stress corrosion and hydrogen embrittlement in an aluminum alloy. *Corrosion*, **30**, 1974, 274-279.

J.A. Grandle, B.P. Somerday and R.P. Gangloff, in: "Proceedings of the Tri-Service Conference on Corrosion," Ed., T. Naguy, USAF Wright-Patterson Air Force Base, OH, 1994, pp. 375-392.

A.J. Griffiths and A. Turnbull, On the effective diffusivity of hydrogen in low alloys steels. *Corros. Sci.*, **37**, 1995. 1879-1881.

W. Gruhl, Stress corrosion cracking of high strength aluminum alloys. *Z. Metallkd.*, **75**, 1984, 819-826.

E.M. Hackett, P.J. Moran and J.P. Gudas, in: "Fracture Mechanics: 17th Volume, ASTM STP 905," Eds., R. Chait, et al., ASTM International, West Conshohocken, PA, 1986, pp. 512-541.

M.M. Hall, Jr. and D.M. Symons, in: "Chemistry and Electrochemistry of Stress Corrosion Cracking," Ed., R.H. Jones, The Minerals, Metals & Materials Society, Warrendale, PA, 2001, pp. 447-466.

G.G. Hancock and H.H. Johnson, Hydrogen, oxygen, and subcritical crack growth in a high-strength steel. *Trans. Met. Soc. AIME*, **236**, 1966, 513-516.

D.G. Harlow and R.P. Wei, Probability modeling and statistical analysis of damage in the lower wing skins of two retired B-707 aircraft. *Fatg. Fract. Engr. Matls. Struct.*, **24**, 2001, 523-535.

D.G. Harlow and R.P. Wei, Life prediction—the need for a mechanistically based probability approach. *Key Engineering Materials*, **200**, 2001a, 119-138.

D.G. Harlow and R.P. Wei, A critical comparision between mechanistically based probability and statistically based modeling for materials aging. *Matls. Sci. Engr. A*, **323**, 2002, 278-284.

H.W. Hayden and S. Floreen, Effects of various modes of loading on the stress corrosion cracking of a maraging steel. *Corrosion*, **27**, 1971, 429-433.

S.P. Hayes, "Internal Hydrogen Embrittlement of High-Strength Beta-Alpha Titanium Alloys," PhD Dissertation, University of Virginia, Charlottesville, VA, 2000.

R.W. Hertzberg, "Deformation and Fracture of Engineering Materials," 4th Ed., John Wiley & Sons, New York, NY, 1996.

P.D. Hicks and C.J. Altstetter, Hydrogen-enhanced cracking of superalloys. *Metall. Trans. A*, **23A**, 1992, 237-249.

K. Hirano, S. Ishizaki, H. Kobayashi and H. Nakazawa, Determination of threshold stress corrosion cracking characteristics using rising load K_{ISCC} testing based on ultrasonic method. *J. Test. Eval.*, **13**, 1985, 162-168.

J.P. Hirth, Effects of hydrogen on the properties of iron and steel. *Metall. Trans. A*, **11A**, 1980, 861-890.

J.P Hirth, in: "Hydrogen Effects in Metals," Eds., A.W. Thompson and N.R. Moody, The Minerals, Metals & Materials Society, Warrendale, PA, 1996, pp. 507-522.

N.J.H. Holroyd and D. Hardie, Strain-rate effects in the environmentally assisted fracture of a commercial high-strength aluminium alloy (7049). *Corros. Sci.*, **21**, 1981, 129-144.

N.J.H. Holroyd, in: "Environment-Induced Cracking of Metals," Eds., R.P. Gangloff and M.B. Ives, NACE, Houston, TX, 1990, pp. 311-345.

M. Horstmann and J.K. Gregory, Observations on the ripple-loading effect. *Scripta Metall. Mater.*, **25**, 1991, 2503-2506.

H. Huang and W.W. Gerberich, Crack-tip dislocation emission arrangements for equilibrium-II: Comparisons to analytical and computer simulation models. *Acta metall. mater.*, **40**, 1992, 2873-2881.

S.J. Hudak, Jr. and R.P. Wei, Consideration of nonsteady-state crack growth in materials evaluation and design. *Intl. J. Pressure Vessels*, **9**, 1981, 63-74.

J.W. Hutchinson, Plasticity at the micron scale. *Intl. J. Sol. Struc.*, **37**, 2000, 225-238.

M. Iino, Influence of sulfur content on the hydrogen-induced fracture in linepipe steels. *Metall. Trans. A*, **10A**, 1979, 1691-1698.

C.G. Interrante and G.M. Pressouyre, Eds., "Current Solutions to Hydrogen Problems in Steels," ASM International, Materials Park, OH, 1982.

C.G. Interrante and L. Raymond, in: "Corrosion Tests and Standards: Application and Interpretation," R. Baboian, Ed., ASTM International, West Conshohocken, PA, 1995, pp. 272-286.

G.R. Irwin and A.A. Wells, in: "Selected Papers on Foundations of Linear Elastic Fracture Mechanics," Vol. MS 137, SPIE Milestone Series, SEM, Bethel, CT, 1997, 215-266.

R.P. Jewett, R.J. Walter, W.T. Chandler and R.P. Fromberg, "H Environment Embrittlement of Metals," NASA CR-2163, NASA, Washington, DC, 1973.

H. Jiang, Y. Huang, Z. Zhuang and K.C. Hwang, Fracture in mechanism-based strain gradient plasticity. *J. Mech. Phys. Solids*, **49**, 2001, 979-993.

H.H. Johnson, J.G. Morlet and A.R. Troiano, Hydrogen, crack initiation, and delayed failure in steel. *Trans. AIME*, **212**, 1958, 528-535.

H.H. Johnson and A.M. Willner, Moisture and stable crack growth in a high strength steel. *App. Matls. Res.*, **4**, 1965, 34-43.

H.H. Johnson, in: "Hydrogen in Metals," Eds., I.M. Bernstein and A.W. Thompson, ASM International, Materials Park, OH, 1974, pp. 35-49.

O. Jonas, Influence of preloading on the sustained load cracking behavior of maraging steels in hydrogen. *Corrosion*, **29**, 1973, 299-304.

D.A. Jones, A.F. Jankowski and G.A. Davidson, "Diffusion of Anodically Induced Vacancies in Cu/Ag Thin-Film Couples", Paper No. 188, *Corrosion 97*, NACE International, Houston, TX, 1997.

R.H. Jones and W.W. Gerberich, Eds., "Modeling Environmental Effects on Crack Initiation and Propagation," The Minerals, Metals & Materials Society, Warrendale, PA, 1986.

R.H. Jones, H. Li, and J.P. Hirth, 2000, "Effects of Mixed Mode I/III Loading on Environment-Induced Cracking," Paper No. 00360, *Corrosion 2000*, NACE International, Houston, TX, 2000.

J. Kameda, Equilibrium and growth characteristics of hydrogen-induced intergranular cracking in phosphorus-doped and high purity steels. *Acta Metall.*, **34**, 1986, 1721-1735.

J. Kameda, A microscopic model of H-induced intergranular cracking—I. Equilibrium crack growth. *Acta Metall.*, **34**, 1986a, 867-882.

J. Kameda, A microscopic model of H-induced intergranular cracking—II. Steady state crack growth. *Acta Metall.*, **34**, 1986b, 883-889.

Y. Katz, N. Tymiak and W.W. Gerberich, Nanomechanical probes as new approaches to hydrogen/deformation interaction studies. *Engr. Frac. Mech.*, **68**, 2001, 619-646.

G.E. Kerns, M.T. Wang and R.W. Staehle, in: "Stress Corrosion Cracking and Hydrogen Embrittlement of Iron Base Alloys," Eds., R.W. Staehle, et al., NACE, Houston, TX, 1977, pp. 700-735.

N.N. Kinaev, D.R. Cousens and A. Atrens, The crack tip strain field of AISI 4340: Part I Measurement Technique. *J. Matls. Sci.*, **34**, 1999, 4909-4920.

N.N. Kinaev, D.R. Cousens and A. Atrens, The crack tip strain field of AISI 4340: Part II Experimental measurements. *J. Matls. Sci.*, **34**, 1999a, 4921-4929.

N.N. Kinaev, D.R. Cousens and A. Atrens, The crack tip strain field of AISI 4340: Part III Hydrogen Influence. *J. Matls. Sci.*, **34**, 1999b, 4931-4936.

A.S. Kobayashi and Y. Takeshi, in: "Predictive Capabilities in Environmentally Assisted Cracking," PVP-Vol. 99, ASME, New York, NY, 1985, pp. 223-234.

G.H. Koch, Hydrogen induced fracture of a high strength aluminum alloy. *Corrosion*, **35**, 1979, 73-78.

D.G. Kolman and J.R. Scully, Understanding the potential and pH dependency of high-strength beta -titanium alloy environmental crack initiation. *Metall. Mater. Trans. A*, **28A**, 1997, 2645-2656.

D.G. Kolman and J.R. Scully, in: "Effects of the Environment on the Initiation of Crack Growth, ASTM STP 1298," Eds., W.A. Van der Sluys, R.S. Piascik and R. Zawierucha, ASTM International, West Conshohocken, PA, 1998, pp. 61-73.

D.G. Kolman and J.R. Scully, Continuum mechanics characterization of plastic deformation-induced oxide film rupture. *Phil. Mag. A*, **79**, 1999, 2313-2338.

D.G. Kolman and J.R. Scully, An assessment of the crack tip potential of beta-titanium alloys during hydrogen environmentally assisted crack propagation based on crack tip and passive surface electrochemical measurements. *Corros. Sci.*, **42**, 2000, 1863-1879.

J. Kolts, in: "Corrosion Resistant Alloys in Oil and Gas Production," Vol. II, eds., J. Kolts and S.M. Corey, NACE, Houston, TX, 1996, 733-748.

A.H.M. Krom, R.W.J. Koers, and A. Bakker, Hydrogen transport near a blunting crack tip. *J. Mech. Phys. Solids*, **47**, 1999, 971-992.

A.H.M. Krom and A. Bakker, Hydrogen trapping models in steel. *Metall. Trans. B*, **31B**, 2000, 1475-1482B.

J.M. Kumar, J.P. Hirth, N.R. Moody, Jr. and J.A. Gordon, Effects of hydrogen on the mixed Mode I/III toughness of a high-purity rotor steel. *Metall. Trans. A*, **24A**, 1993, 1450-1451.

A.J. Kumnick and H.H. Johnson, Deep trapping states for hydrogen in deformed iron. *Acta Metall.*, **28**, 1980, 33-39.

J.B. Leblond and D. Dubois, A general mathematical description of hydrogen diffusion in steels---II: Numerical study of permeation and determination of trapping parameters. *Acta Metall.*, **31**, 1983, 1471-1478.

S.M. Lee, S.I. Pyun and Y.G. Chun, Critical evaluation of the stress-corrosion cracking mechanism in high-strength aluminum alloys. *Metall. Trans. A*, **22A**, 1991, 2407-2414.

E.U. Lee, H. Sanders and B. Sarkar, Stress corrosion cracking of high strength steels. CD file s08p2a.pdf, in: "Proceedings of the Tri-Service Conference on Corrosion," Eds., J.V. Kelley and B. Placzankis, US Army Research Laboratory, Aberdeen, MD, 2000.

B.N. Leis and R.N. Parkins, Mechanics and materials aspects in predicting serviceability limited by stress-corrosion cracking. *Fatg. Fract. Engr. Matls. Struct.*, **21** 1998, 583-601.

J.F. Lessar and W.W. Gerberich, Grain size effects in hydrogen-assisted cracking. *Metall. Trans. A*, **7A**, 1976, 953-960.

J.C.M. Li, R.A. Oriani and L.S Darken, The thermodynamics of stressed solids. *Z. Physik. Chem.*, **49**, 1966, 271-290.

J.A. Lillard, R.G. Kelly and R.P. Gangloff, "Effect of Electrode Potential on Stress Corrosion Cracking and Crack Chemistry of a Nickel-Base Superalloy", Paper No. 197, *Corrosion '97*, NACE, Houston, TX, 1997.

J.A. Lillard, "Environment Assisted Cracking of a Nickel-Based Superalloy in Hydrogen-Producing Solutions," PhD Dissertation, University of Virginia, Charlottesville, VA, 1998.

W.B. Lisagor, T.W. Crooker and B.N. Leis, Eds., "Environmentally Assisted Cracking: Science and Engineering, ASTM STP 1049," ASTM International, West Conshohocken, PA, 1990.

M.R. Louthan and R.P. NcNitt, Eds., "Environmental Degradation of Engineering Materials," VPI Press, Blacksburg, VA, 1977.

M.R. Louthan, Jr., G.R. Caskey, J.A. Donovan and D.E. Rawl, Jr., Hydrogen embrittlement of metals. *Matls. Sci. Engr.*, **10**, 1972, 357-368.

M.R. Louthan, R.P. McNitt and R.D. Sisson, Eds., "Environmental Degradation of Engineering Materials in Hydrogen," Eds., VPI Press, Blacksburg, VA, 1981.

M. Lu, P.S. Pao, T.W. Weir, G.W. Simmons and R.P. Wei, Rate controlling processes for crack growth in hydrogen sulfide for an AISI 4340 steel. *Metall. Trans. A*, **12A**, 1981, 805-811.

S.P. Lynch, in: "Mechanisms of Environment Sensitive Fracture of Materials," Eds., P.R. Swann, F.P. Ford, and A.R.C. Westwood, The Metals Society, London, UK, 1977, pp. 201-212.

S.P. Lynch, Environmentally assisted cracking: Overview of evidence for an adsorption-induced localized slip process. *Acta Metall.*, **36**, 1988, 2639-2661.

S.P. Lynch, Failures of structures and components by environmentally assisted cracking. *Engr. Fail. Anal.*, **1**, 1994, 77-90.

S.P. Lynch, in: "Second International Conference on Corrosion-Deformation Interactions," Ed., T. Magnin, The Institute of Materials, London, UK, 1997, pp 206-219.

S.P. Lynch, Mechanisms of hydrogen assisted cracking—A review. in "Hydrogen Effects in Materials," Eds., N.R. Moody and A.W. Thompson, The Minerals, Metals & Materials Society, Warrendale, PA, 2003, in press.

T. Magnin, R. Chieragatti, and R. Oltra, Mechanism of brittle fracture in a ductile 316 alloy during stress corrosion. *Acta Metall.*, **38**, 1990, 1313-1319.

P. Martin, J.I. Dickson and J.-P. Bailon, Stress corrosion cracking in aluminum alloy 7075-T651 by discrete crack jumps as indicated by fractography and acoustic emission. *Mater. Sci. Engr.*, **69**, 1985, L9-13.

M.E. Mason and R.P. Gangloff, in: "Advanced Structural Integrity Methods for Airframe Durability and Damage Tolerance," Ed., C.E. Harris, NASA Conference Publication 3274, Part 1, NASA-Langley Research Center, Hampton, VA, 1994, pp. 441-462.

A.J. McEvily, "Atlas of Stress-Corrosion and Corrosion Fatigue Curves," ASM International, Materials Park, OH, 1990.

K.F. McGuinn and M. Aballe, Hydrogen embrittlement in Mode II, *Brit. Corros. J.*, **17**, 1982, 18-20.

P. McIntyre and A.H. Priest, "Accelerated Test Technique for the Determination of K_{ISCC} in Steels," British Steel Corporation Report MG/31/72, London, England, 1972.

P. McIntyre, A.H. Priest and C.E. Nicholson, "Hydrogen Induced Subcritical Flaw Growth in Steels Under Static and Cyclic Loading," British Steel Corporation Report No. MG/38/72, London, UK, 1972a.

P. McIntyre, in: "Hydrogen Degradation of Ferrous Alloys," Eds., R.A. Oriani, J.P. Hirth and S. Smialowska, Noyes Publications, Park Ridge, NJ, 1985, pp. 763-798.

C.J. McMahon, Jr., Hydrogen-induced intergranular fracture of steels. *Engr. Frac. Mech.*, **68**, 2001, 773-788.

R.A. Mayville, T.J. Warren and P.D. Hilton, in "Fracture Mechanics: Perspectives and Directions, ASTM STP 1020", Eds., R.P. Wei and R.P. Gangloff, ASTM International, West Conshohocken, PA, 1989, pp. 605-614.

P.G. Marsh and W.W. Gerberich, in: "Stress Corrosion Cracking," Ed., R.H. Jones, ASM International, Materials Park, OH, 1992, pp. 63-90.

W.J. Mills, M.R. Lebo and J.J. Kearns, Hydrogen embrittlement, grain boundary segregation and stress corrosion cracking of alloy X-750 in low and high-temperature water. *Metall. and Matls. Trans. A*, **30A**, 1999, 1579-1596.

N.R. Moody, R.E. Stoltz and M.W. Perra, in: "Corrosion Cracking," Ed., V.S. Goel, ASM International, Materials Park, OH, 1986, pp. 43-53.

N.R. Moody, S.L. Robinson and M.W. Perra, The effect of hydrogen on fracture toughness of the Fe-Ni-Co superalloy IN903. *Metall. Trans. A*, **18A**, 1987, 1469-1482.

N.R. Moody, M.W. Perra and S.L. Robinson, Hydrogen pressure and crack tip stress effects on slow crack growth thresholds in an iron-based superalloy. *Scripta Metall.*, **22**, 1988, 1261-1266.

N.R. Moody, S.L. Robinson, S.M. Myers and F.A. Greulich, Deuterium concentration profiles in Fe-Ni-Co alloys electrochemically charged at room temperature. *Acta Metall.*, **37**, 1989, 281-290.

N.R. Moody, S.L. Robinson and W.M. Garrison, Jr., Hydrogen effects on the properties and fracture modes of iron-based alloys. *Res. Mech.*, **30**, 1990, 143-206.

N.R. Moody and A.W. Thompson, Eds., "Hydrogen Effects on Material Behavior," The Minerals, Metals & Materials Society, Warrendale, PA, 1990a.

N.R. Moody, M.W. Perra and S.L. Robinson, in: "Hydrogen Effects on Material Behavior," Eds., N.R. Moody and A.W. Thompson, The Minerals, Metals & Materials Society, Warrendale, PA, 1990b, pp. 625-635.

N.R. Moody, S.L. Robinson and M.W. Perra, Internal hydrogen effects on thresholds for crack growth in the iron-based superalloy IN903. *Engr. Frac. Mech.*, **39**, 1991, 941-954.

N.R. Moody, S.L. Robinson, J.E. Angelo and M.W. Perra, in: "Hydrogen Effects in Materials," Eds., A.W. Thompson and N.R. Moody, The Minerals, Metals & Materials Society, Warrendale, PA, 1996, pp. 967-977.

N.R. Moody, M.I Baskes, S.L Robinson and M.W. Perra, Temperature effects on hydrogen-induced crack growth susceptibility of iron-based superalloys. *Engr. Frac. Mech.*, **68**, 2001, 731-750.

N.R. Moody and A.W. Thompson, Eds., "Hydrogen Effects on Material Behavior," The Minerals, Metals & Materials Society, Warrendale, PA, 2003, in press.

L. Montgrain and P.R. Swann, in: "Hydrogen in Metals", Eds., I.M. Bernstein and A.W. Thompson, ASM International, Materials Park, OH, 1974, pp. 575-584.

M.J. Morgan and C.J. McMahon, Jr., in: "Hydrogen Degradation of Ferrous Alloys," Eds., R.A. Oriani, J.P. Hirth, and M. Smialowski, Noyes Publications, Park Ridge, NJ, 1985, 608-40.

N.K. Mukhopadhyay, G. Sridhar, N. Parida, S. Tarafder and V.R. Ranganath, Hydrogen embrittlement failure of hot dip galvanized high tensile wires. *Engr. Fail. Anal.*, **6**, 1999, 253-265.

S.M. Myers, W.R. Wampler, F. Besenbacher, S.L. Robinson and N.R. Moody, Ion beam studies of hydrogen in metals. *Mater. Sci. Engr.*, **69**, 1985, 397-409.

National Materials Advisory Board, "Characterization of Environmentally Assisted Cracking for Design: State of the Art," NMAB-386, Washington, DC, 1982.

A. Needleman and J.G. Sevillano, Preface to the viewpoint set on geometrically necessary dislocations and size dependent plasticity. *Scripta Mater.*, **48**, 2003, 109-111.

H.G. Nelson, D.P. Williams and A.S. Tetelman, Embrittlement of a ferrous alloy in a partially dissociated hydrogen environment. *Metall. Trans.*, **2**, 1971, 953-959.

H.G. Nelson and D.P. Williams, in: "Stress Corrosion Cracking and Hydrogen Embrittlement of Iron Base Alloys," Eds., R.W. Staehle, et al., NACE, Houston, TX, 1977, pp. 390-404.

H.G. Nelson, in: "Treatise on Materials Science and Technology: Embrittlement of Engineering Alloys," Eds., C.L. Briant and S.K. Banerji, Vol. 25, Academic Press, New York, NY, 1983, pp. 275-359.

D. Nguyen, A.W. Thompson and I.M. Bernstein, Microstructural effects on hydrogen embrittlement in a high purity 7075 aluminum alloy. *Acta. Metall.*, **35**, 1987, 2417-2425.

F.A. Nichols, 1983, Loading mode and stress corrosion cracking mechanisms. *Corrosion*, **39**, 449-451.

S.R. Novak and S.T. Rolfe, Comparison of fracture mechanics and nominal stress analysis in stress corrosion cracking. *Corrosion*, **26**, 1970, 121-130.

S.R. Novak and S.T. Rolfe, Modified WOL specimen for K_{ISCC} environmental testing. *J. Matls.*, **4**, 1969, 701-728.

A. Oehlert and A. Atrens, Stress corrosion crack propagation in AerMet®100. *J. Matls. Sci.*, **33**, 1998, 775-781.

S.H. Ohsaki, M. Iino and M. Utsue, SCC extension of 7075 series aluminum alloys under mixed-mode I-II loading. *J. Japan Inst. Light Metals*, **47**, 1997, 370-377.

G.B. Olson, in: "Innovations in Ultrahigh Strength Steel Technology, 34th Sagamore Army Materials Research Conference," Eds., G.B. Olson, M. Azrin, and E.S. Wright, US Army Laboratory Command, Watertown, MA, 1987, pp. 549-593.

G.B. Olson, Brains of steel: Designing metallurgists. *Advanced Matls. Proc.*, July, 1997, 72-79.

J. Opoku and W.G. Clarke, Jr., The effects of various hydrogen bearing environments on the K_{ISCC} of AISI type 4340 and 3.5%NiCrMoV steels. *Corrosion*, **36**, 1980, 251-258.

R.A. Oriani, Diffusion and trapping of hydrogen in steel. *Acta Metall.*, **18**, 1970, 147-157.

R.A. Oriani, D.P. Williams and H.G. Nelson, Discussion of evaluation of hydrogen embrittlement mechanisms. *Metall. Trans.*, **2**, 1971, 1987-1988.

R.A. Oriani, The mechanistic theory of hydrogen embrittlement of steels. *Berichte Bunsen Gesellschaft fur Physik Chem.*, **76**, 1972, 848-857.

R.A. Oriani and P.H. Josephic, Equilibrium aspects of H-induced cracking of steels. *Acta Metall.*, **22**, 1974, 1065-1074.

R.A. Oriani, in: "Stress Corrosion Cracking and Hydrogen Embrittlement of Iron Base Alloys," R.W. Staehle, et al., Eds., NACE, Houston, TX, 1977, pp. 32-50.

R.A. Oriani and P.H. Josephic, Equilibrium and kinetic studies of the H-assisted cracking of steel. *Acta Metall.*, **25**, 1977, 979-988.

R.A. Oriani, Hydrogen embrittlement of steels. *Annual Reviews in Materials Science*, 1978, **8**, 327-357.

R.A. Oriani, J.P. Hirth and S. Smialowska, Eds., "Hydrogen Degradation of Ferrous Alloys," Noyes Publications, Park Ridge, NJ, 1985.

R.A. Oriani, Hydrogen-the versatile embrittler. *Corrosion*, **43**, 1987, 390-397.

R.A. Oriani, in: "Environment Induced Cracking of Metals", Eds., R.P. Gangloff and M.B. Ives, NACE, Houston, 1990, TX, pp. 439-448.

R.A. Page and W.W. Gerberich, The effect of hydrogen source on crack initiation in 4340 steel. *Metall. Trans.* A, **13A**, 1982, 305-311.

R.N. Parkins, in: "Environment Induced Cracking of Metals," Eds., R.P. Gangloff and M.B. Ives, NACE, Houston, 1990, TX, pp. 1-119.

R.N. Parkins, in: "Life Prediction of Corrodible Structures," Vol. 1, Ed., R.N. Parkins, NACE, Houston, TX, 1991, pp. 97-119.

P.S. Pao, R.A. Bayles and G.R. Yoder, Effect of ripple load on stress corrosion cracking in structural steels. *J. Engr. Matls. Tech.*, **113**, 1991, 125-129.

P.S. Pao, S.J. Gill and R.A. Bayles, Effect of ripple loads on stress-corrosion cracking in AA7075 Al alloys. *Scripta Metall. Mater.*, **25**, 1991a, 2085-2089.

P.S. Pao, C.R. Feng, R.A. Bayles, D.A. Meyn and G.R. Yoder, in: "Titanium '95: Science and Technology," Eds., P.A. Blenkinsop, W.J. Evans and H.M.Flower, The Institute of Materials, London, UK, 1996, pp. 1219-1226.

P.C. Paris, Fracture mechanics and fatigue: A historical perspective. *Fatg. Fract. Engr. Matls. Struct.*, 1998, **21**, 535-540.

R.W. Pasco, K. Sieradzki and P.J. Ficalora, Surface chemistry kinetic model of gaseous hydrogen embrittlement. *Scripta Metall.*, **16**, 1982, 881-883.

R.W. Pasco and P.J. Ficalora, A work function-chemisorption study of hydrogen on iron-kinetics and strain effects. *Acta Metall.*, **31**, 1983, 541-558.

R.W. Pasco, K. Sieradzki and P.J. Ficalora, in: "Embrittlement by the Localized Crack Environment," Ed., R.P. Gangloff, The Minerals, Metals & Materials Society, Warrendale, PA, 1984, pp. 375-381.

M.W. Perra and R.E. Stoltz, in: "Hydrogen Effects in Metals," Eds., I.M. Bernstein and A.W. Thompson, The Minerals, Metals & Materials Society, Warrendale, PA, 1981, pp. 645-653.

N.J. Petch, Lowering of fracture stress due to surface adsorption. *Phil. Mag.*, **1**, 1956, 331-337.

N.J. Petch and P. Stables, Delayed fracture of metals under static load. *Nature*, **169**, 1952, 842-851.

J.R. Pickens, J.R. Gordon and J.A.S. Green, The effect of loading mode on the stress corrosion cracking of aluminum alloy 5083. *Metall. Trans. A*, **14A**, 1983, 925-930.

J.R. Pickens, T.J. Langan and J.A.S. Green, in: "Environment Sensitive Fracture of Metals and Alloys," eds., R.P. Wei, D.J. Duquette, T.W. Crooker, and A.J. Sedriks, Office of Naval Research, Arlington, VA, 1987, pp. 115-131.

Martin Prager, Ed., "Interaction of Steels with Hydrogen in Petroleum Industry Pressure Vessel Service," Materials Properties Council, New York, NY, 1989.

Martin Prager, Ed., "Second International Conference on Interaction of Steels with Hydrogen in Petroleum Industry Pressure Vessel and Pipeline Service," Materials Property Council, New York, NY. 1994.

G.M. Pressouyre and I.M. Bernstein, A quantitative analysis of hydrogen trapping. *Metall. Trans. A*, **9A**, 1978, 1571-1580.

G.M. Pressouyre, A classification of hydrogen traps in steel. *Metall. Trans. A*, **10A**, 1979, 1571-1573

G.M. Pressouyre and I.M. Bernstein, A kinetic trapping model for hydrogen-induced cracking. *Acta Metall.*, **27**, 1979, 89-100.

G.M. Pressouyre, Trap theory of hydrogen embrittlement. *Acta Metall.*, **28**, 1980, 895-911.

G.M. Pressouyre and I.M. Bernstein, An example of the effect of hydrogen trapping on hydrogen embrittlement. *Metall. Trans. A*, **12A**, 1981, 835-844.

G.M. Pressouyre, Hydrogen traps, repellers, and obstacles in steel: Consequences on hydrogen diffusion, solubility and embrittlement. *Metall. Trans. A.*, **14A**, 1983, 2189-2193.

R.P.M. Procter and H.W. Paxton, The effect of prior austenite grain size on the stress corrosion cracking susceptibility of AISI 4340 steel. *Trans. ASM*, **62**, 1962, 989-999.

V.L. Ratke and W. Gruhl, Model experiments concerning the mechanisms of stress corrosion cracking of Al-Zn-Mg alloys. *Werkst. Korros.*, **31**, 1980, 768-773.

L. Raymond, Ed., "Hydrogen Embrittlement Testing, ASTM STP 543," ASTM International, West Conshohocken, PA, 1972.

L. Raymond, Ed., "Hydrogen Embrittlement: Prevention and Control, ASTM STP 962," ASTM International, West Conshohocken, PA, 1988.

K.G. Reedy, A.K. Jha and V. Diwakar, Failure of cadmium plated maraging steel tension bolt. *Engr. Fail. Anal.*, **8**, 2001, 263-269.

I.M. Robertson and H.K. Birnbaum, HVEM study of hydrogen effects on the deformation of nickel. *Acta Metall.*, **34**, 1986, 353-366.

I.M. Robertson, The effect of hydrogen on dislocation dynamics. *Engr. Frac. Mech.*, **68**, 2001, 671-692.

P. Rozenak, I.M. Robertson and H.K. Birnbaum, HVEM studies of the effects of hydrogen on the deformation and fracture of AISI type 316 austenitic stainless steel. *Acta metall. Mater.*, **38**, 1990, 2031-2040.

J.R. Rice, in: "Stress Corrosion Cracking and Hydrogen Embrittlement of Iron Base Alloys," Eds., R.W. Staehle, et al., NACE, Houston, TX, 1977, pp. 11-15.

T. Sakai, T. Takahashi, M. Yamada, S. Nose and M. Katsumata, in "High Pressure Technology, PVP-Vol. 344," ASME, New York, NY, 1997, pp. 79-98.

T. Sakurai and H.W. Pickering, in: "Advanced Techniques for Characterizing Hydrogen in Metals," The Minerals, Metals & Materials Society, Warrendale, PA, 1982, pp. 171-181.

G. Sandoz, C.T. Fujii and B.F. Brown, Solution Chemistry within stress corrosion cracks in alloy steels. *Corros. Sci.*, **10**, 1970, 839-845.

G. Sandoz, in: "Second International Congress on Hydrogen and Materials," Ed., P. Azou, l'Ecole Centrale des Arts et Manufactures, Paris, FR, 1977, pp. 335-341.

B. Sarkar, M. Marek and E.A. Starke, Jr., The effect of copper content and heat treatment on the stress corrosion characteristics of Al-6Zn-2Mg-xCu alloys. *Metall. Trans. A*, **12A**, 1981, 1939-1943.

V.R. Sawicki, "Hydrogen Induced Cracking in a High Strength Steel," PhD Dissertation, Cornell University, Ithaca, NY, 1971.

G.M. Scamans, R. Alani and P.R. Swann, Pre-exposure embrittlement and stress corrosion failure in Al-Zn-Mg alloys. *Corros. Sci.*, **16**, 1976, 443-459.

G.M. Scamans, Evidence for crack arrest markings on intergranular stress corrosion cracks in Al-Zn-Mg alloys. *Metall. Trans. A.*, **11A**, 1980, 846-850.

J.H. Schmidt, R.B. Meade and L. Raymond, Process management to control risk of hydrogen embrittlement. *Plating and Surface Finishing*, **87**, 2000, 53-55.

H. Schmiedel and W. Gruhl, The influence of the zinc, magnesium and copper concentrations at the grain boundaries on the stress corrosion susceptibility of AlZnMg alloys. *Z. Metallkd.*, **74**, 1983, 777-783.

K.-H. Schwalbe, Finite element solutions of crack tip behavior in small scale yielding. *J. Engr. Matl. Tech.*, **99**, 1977, 186-188.

J.C. Scully, Ed., "The Theory of Stress Corrosion Cracking," NATO Scientific Affairs Division, Brussels, Belgium, 1971.

J.R. Scully and P.J. Moran, The influence of strain on hydrogen entry and transport in a high strength steel in sodium chloride solution. *J. Electrochem. Soc.*, **135**, 1988, 1337-1348.

J.R. Scully, J.A. Van Den Avyle, M.J. Cieslak, A.D. Romig and C.R. Hills, The influence of Pd on the hydrogen-assisted cracking resistance of PH 13-8 Mo stainless steel. *Metall. Trans. A*, **22A**, 1991, 2429-2443.

J.R. Scully, G.A. Young, Jr. and S.W. Smith, Hydrogen solubility, diffusivity and trapping in high purity aluminum and selected Al-base alloys. *Matls. Sci. Forum*, **331-337**, 2000, 1583-1600.

J.R. Scully, unpublished research, University of Virginia, Charlottesville, VA, 2002.

A.J. Sedriks, "Stress Corrosion Cracking Test Methods", NACE, Houston, TX, 1990.

Y. Shen and P.G. Shewmon, IGSCC crack growth of Alloy 600 and X-750 in steam. *Corrosion*, **47**, 1991, 712-718.

D.S. Shih, I.M. Robertson and H.K. Birnbaum, Hydrogen embrittlement of alpha titanium: in situ TEM studies. *Acta Metall.*, **36**, 1988, 111-124.

R.J. Shipley and W.T. Becker, Eds., "Failure Analysis and Prevention", *Metals Handbook*, Vol. 11, ASM International, Materials Park, OH, 2002, in press.

K. Sieradzki and P. Ficalora, The dependence of the fracture toughness of 4340 steel on an external chlorine gas environment. *Scripta Metall.*, **13**, 1979, 535-536.

K. Sieradzki and P.J. Ficalora, Kinetic aspects of slow crack growth in the gaseous hydrogen embrittlment of steels. *J. Mater. Sci.*, **14**, 1979a, 2703-2708.

G.W. Simmons, P.S. Pao, and R.P. Wei, Fracture mechanics and surface chemistry studies of subcritical crack growth in AISI 4340 steel. *Metall. Trans. A*, **9A**, 1978, 1147-1158.

H.R. Smith, D.E. Piper and F.K. Downey, A study of stress corrosion cracking by wedge-force loading. *Engr. Frac. Mech.*, **1**, 1968, 123-128.

J.A. Smith, M.H. Peterson and B.F. Brown, Electrochemical conditions at the tip of an advancing stress corrosion crack in AISI 4340 steel. *Corrosion*, **26**, 1970, 539-542.

B.P. Somerday and R.P. Gangloff, Effect of strength on environment-assisted cracking of Ti-8V-6Cr-4Mo-4Zr-3Al in aqueous chloride: age hardening *vs.* work hardening. *Matls. Sci. Engr. A*, **A254**, 1998, 166-178.

B.P. Somerday and R.P. Gangloff, Effect of strength on environment-assisted cracking of Ti-8V-6Cr-4Mo-4Zr-3Al in aqueous chloride: crack tip strain rate. *Matls. Sci. Engr. A*, **A254**, 1998a, 179-188.

B.P Somerday, "Metallurgical and Crack-Tip Mechanics Effects on Environment-Assisted Cracking of Beta-Titanium Alloys in Aqueous Chloride," PhD Dissertation, University of Virginia, Charlottesville, VA, 1998b.

B.P. Somerday, L.M. Young and R.P. Gangloff, Crack tip mechanics effects on environment-assisted cracking of beta-titanium alloys in aqueous NaCl. *Fatg. Fract. Engr. Matls. Struct.*, **23**, 2000, 39-58.

B.P. Somerday and N.R. Moody, Micromechanical modeling of hydrogen-induced fracture modes in IN903. in "Advances in Fracture Research, Proceedings of ICF10," Eds., K. Ravi-Chandar, et al., Paper No. ICF108920R, CD version, Elsevier Science, Oxford, UK, 2001.

B.P. Somerday, A.W. Wilson, J.M. Howe, and R.P. Gangloff, Microstructural cause of intergranular hydrogen environment embrittlement of aged beta-titanium alloys. *Metall. Mater. Trans., A*, in review, 2003.

M.O. Speidel and M.V. Hyatt, in: "Advances in Corrosion Science and Technology," Vol. 2, Eds., M.G. Fontana and R.W. Staehle, Plenum Press, New York, NY, 1972, pp. 115-335.

M.O. Speidel, in: "Hydrogen in Metals", Eds., I.M. Bernstein and A.W. Thompson, ASM International, Materials Park, OH, 1974, pp. 249-276.

M.O. Speidel, Stress corrosion cracking of aluminum alloys. *Metall. Trans. A*, **6A**, 1975, 631-651.

M.O. Speidel and P.M. Fourt, in: "Stress Corrosion Cracking and Hydrogen Embrittlement of Iron Base Alloys," Eds., R.W. Staehle, et al., NACE, Houston, TX, 1977, pp. 57-60.

R.W. Staehle, et al., Eds., "Stress Corrosion Cracking and Hydrogen Embrittlement of Iron Base Alloys," NACE, Houston, TX, 1977.

E.A. Starke, Jr. and J.T. Staley, Application of modern aluminum alloys to aircraft. *Prog. Aerospace Sci.*, 1995, **32**, 131-172.

C. St. John and W.W. Gerberich, The effect of loading mode on hydrogen embrittlement. *Metall. Trans.*, **4**, 1973, 589-598.

E.A. Steigerwal, F.W. Schaller and A.R. Troiano, The role of stress in hydrogen induced delayed failure. *Trans. AIME*, **218**, 1960, 832-841.

M.F. Stevens and I.M. Bernstein, The role of aging reactions in the hydrogen embrittlement susceptibility of an HSLA steel. *Metall. Trans. A*, **16A**, 1985, 1879-1886.

R.E. Stoltz N.R. Moody, and M.W. Perra, Microfracture model for hydrogen embrittlement of austenitic steels. *Metall. Trans. A*, **14A**, 1983, 1528-1531.

C. Suarez, G. Velazquez, G. Lopez and R. Robles, in "ECF 13—Fracture Mechanics: Applications and Challenges," Elsevier Science Publishing Co., New York, NY, 2000, pp. 163-181.

P.R. Swann et al., Eds., "Mechanisms of Environment Sensitive Fracture of Materials," The Metals Society, London, UK, 1977.

R.E. Swanson, A.W. Thompson, I.M. Bernstein and J.L. Maloney, in: "Hydrogen Effects in Metals", Eds., I.M. Bernstein and A.W. Thompson, The Minerals, Metals & Materials Society, Warrendale, PA, 1981, pp. 459-466.

D.M. Symons and A.W. Thompson, The effect of hydrogen on the fracture toughness of alloy X-750. *Metall. Trans. A*, **28A**, 1997, 817-824.

D.M. Symons, The effect of hydrogen on the fracture toughness of alloy X-750 at elevated temperatures. *J. Nucl. Matls.*, **265**, 1998, 225-231.

D.M. Symons, A comparison of internal hydrogen embrittlement and hydrogen environment embrittlement of X-750. *Engr. Frac. Mech.*, **68**, 2001, 751-771.

T. Tabata and H.K. Birnbaum, Direct observations of hydrogen enhanced crack propagation in iron. *Scripta Metall.*, **18**, 1984, 231-236.

A. Taha and P. Sofronis, A micromechanics approach to the study of hydrogen transport and embrittlement. *Engr. Frac. Mech.*, **68**, 2001, 803-837.

D.F. Teter, I.M. Robertson and H.K. Birnbaum, The effects of hydrogen on the deformation and fracture of beta–titanium. *Acta Mater.*, **49**, 2001, 4313-4323.

R.L.S. Thomas, "Internal Hydrogen Embrittlement of a Trap-Rich Ultrahigh-Strength Steel, AerMet®100," MS Thesis, University of Virginia, Charlottesville, VA, 2000.

R.L.S. Thomas, J.R. Scully and R.P. Gangloff, Internal hydrogen embrittlement of ultrahigh-strength AerMet®100 Steel. *Metall. Trans., A*, **34A**, 2003, 327-344.

R.L.S. Thomas, D. Li, R.P. Gangloff and J.R. Scully, Trap-governed hydrogen diffusivity and uptake capacity in ultrahigh-strength AerMet® 100 steel. *Metall. Mater. Trans. A*, **33A**, 2002, 1991-2004.

A.W. Thompson, in: "Fracture 1977, Advances in Research on the Strength and Fracture of Materials," Vol. II, Pergamon, New York, NY, 1978, pp. 237-242.

A.W. Thompson and I.M. Bernstein, in: "Advances in Corrosion Science and Technology," Eds., M.G. Fontana and R.W. Staehle, Plenum Publishing Company, New York, NY, 1980, pp. 53-175.

A.W. Thompson and I.M. Bernstein, in: "Hydrogen Effects in Metals," Eds., I.M. Bernstein and A.W. Thompson, The Minerals, Metals & Materials Society, Warrendale, PA, 1981, pp. 291-308.

A.W. Thompson and J.A. Brooks, Hydrogen performance of precipitation-strengthened stainless steels based on A-286. *Metall. Trans. A*, 6**A**, 1975, 1431-1442.

A.W. Thompson and N.R. Moody, Eds., "Hydrogen Effects in Metals," The Minerals, Metals & Materials Society, Warrendale, PA, 1996.

J.J. Thompson, E.S. Tankins and V.S. Agarwala, A heat treatment for reducing corrosion and stress corrosion cracking susceptibilities in 7xxx aluminum alloys. *Matls. Perf.*, **26**, 1987, 45-52.

R.M. Thomson, Brittle fracture in a ductile material with application to H embrittlement. *J. Mater. Sci.*, **13**, 1978, 128-142.

G.P. Tiwari, A. Bose, J.K. Chakravartty, S.L. Wadekar, M.K. Totlani, R.N. Arya and R.K. Fotedar, A study of internal hydrogen embrittlement of steels. *Matls. Sci. Engr. A*, **A286**, 2000, 269-281.

J. Toribio and V. Kharin, The effect of history on hydrogen assisted cracking. *Intl. J. Frac.*, **88**, 1997, 233-258.

A.R. Troiano, The role of hydrogen and other interstitials in the mechanical behavior of metals. *Trans.* ASM, **52**, 1960, 54-80.

A.R. Troiano, in: "Hydrogen in Metals," Eds., I.M. Bernstein and A.W. Thompson, ASM International, Materials Park, OH, 1974, pp. 3-15.

E. Troiano, G.N. Vigilante and J.H. Underwood, in: "Fatigue and Fracture Mechanics: 33rd Volume, ASTM STP 1417," Eds., W.G. Reuter and R.S. Piascik, ASTM International, West Conshohocken, PA, 2002, pp. 116-128.

C.D.S. Tuck, The embrittlement of Al-Zn-Mg and Al-Mg alloys by water vapor. *Metall. Trans. A*, **16A**, 1985, 1503-1514.

A. Turnbull, in: "Embrittlement by the Localized Crack Environment," Ed., R.P. Gangloff, The Minerals, Metals & Materials Society, Warrendale, PA, 1984, pp. 3-31.

A. Turnbull and D.H. Ferriss in: "Corrosion Chemistry Within Pits, Crevices and Cracks," ed., A. Turnbull, HMSO Books, London, UK 1987, pp. 357-396.

A. Turnbull and D.H. Ferriss, Mathematical modeling of the electrochemistry in corrosion fatigue cracks in steel corroding in marine environments. *Corros. Sci.*, **27**, 1987a, 1323-1350.

A. Turnbull and M.S. Saenz de Santa Maria, in "Environment-Induced Cracking of Metals," Eds., R.P. Gangloff and M.B. Ives, NACE, Houston, TX, 1990, pp. 193-196.

A. Turnbull, Ed., "Hydrogen Transport and Cracking in Metals," Institute of Materials, London, UK, 1995.

A. Turnbull, D.H. Ferriss, and H. Anzai, Modeling of the hydrogen distribution at a crack tip. *Matls. Sci. Engr.*, **A206**, 1996, 1-13.

A. Turnbull, Modeling of the chemistry and electrochemistry in cracks--a review. *Corrosion*, **57**, 2001, 175-189.

A. Turnbull, in: "Aging Studies and Lifetime Extension of Materials," Kluwer Academic/Plenum Publishers, New York, NY, 2001a, pp. 397-414.

P.S. Tyler, M. Levy and L. Raymond, Investigation of the conditions for crack propagation and arrest under cathodic polarization by rising step load bend testing. *Corros.*, **47**, 1991, 82-87.

W.A. Van der Sluys, Mechanisms of environment induced subcritical flaw growth in AISI 4340 steel. *Engr. Frac. Mech.*, **1**, 1969, 447-462.

H.P. van Leeuwen, The kinetics of hydrogen embrittlement: A quantitative diffusion model. *Engr. Frac. Mech.*, **6**, 1974, 141-161

H.P. van Leeuwen, Plateau velocity of high strength steel in SCC- A quantitative treatment. *Corrosion*, **31**, 1975, 42-50.

H.P. van Leeuwen, Quantitative models of hydrogen-induced cracking in high strength steels. *Review on Coatings and Corrosion*," **4**, 1979, 5-93.

H. Vehoff and W. Rothe, Gaseous hydrogen embrittlement in Fe-Si and Ni-single crystals. *Acta Metall.*, **31**, 1983, 1781-1793.

H. Vehoff and P. Neumann, in: "Hydrogen Degradation of Ferrous Alloys," Eds., R.A. Oriani, J.P. Hirth and S. Smialowska, Noyes Publications, Park Ridge, NJ, 1985, pp. 686-711.

H. Vehoff, in: "Hydrogen in Metals III: Properties and Applications," Eds., G. Alefeld and J. Völkl, Spinger-Verlag, Berlin, Germany, 1997, pp. 215-278.

L. Vehovar, Hydrogen-assisted stress corrosion of prestressing wires in a motorway viaduct. *Engr. Fail. Anal.*, **5**, 1998, 21-27.

G.N. Vigilante, J.H. Underwood, D. Crayton, S. Tauscher, T. Sage and E. Troiano, in: "Fatigue and Fracture Mechanics: 28th Volume, ASTM STP 1321," Eds., J.H. Underwood, B.D. MacDonald and M.R. Mitchell, ASTM International, West Conshohocken, PA, 1997, pp. 602-616.

G.N. Vigilante, J.H. Underwood and D. Crayton, in: "Fatigue and Fracture Mechanics: 30th Volume, ASTM STP 1390," Eds., P.C. Paris and K.L. Jerina, ASTM International, West Conshohocken, PA, 2000, pp. 377-387.

R. Viswanathan and S.J. Hudak, Jr., The effect of impurities and strength level on hydrogen induced cracking in a low alloy turbine steel. *Metall. Trans. A*, **8A**, 1977, 1633-1637.

H. Vogt and M.O. Speidel, Stress corrosion cracking of two aluminium alloys: a comparison between experimental observations and data based on modeling. *Corros. Sci.*, **40**, 1998, 251-270.

R.J. Walter, R.P. Jewett and W.T. Chandler, On the mechanism of hydrogen-environment embrittlement of iron- and nickel-based alloys. *Matls. Sci. Engr.*, **5**, 1969/70, 99-110.

R.J. Walter and W.T. Chandler, in: "Hydrogen in Metals," Eds., I.M. Bernstein and A.W. Thompson, ASM International, Materials Park, OH, 1974, pp. 515-525.

R.J. Walter and W.T. Chandler, in: "Environmental Degradation of Engineering Materials," Eds., M.R. Louthan and R.P. McNitt, VPI Press, Blacksburg, VA, 1977, pp. 513-522.

R.J.H. Wanhill, Aqueous stress corrosion in Ti alloys. *Brit. Corros. J.*, **10**, 1975, 69-78.

R.P. Wei, S.R. Novak and D.P. Williams, Some important considerations in the development of stress corrosion cracking test methods. *Matls. Res. Stds.*, **12**, 1972, 25-30.

R.P. Wei, in: "Hydrogen Effects in Metals," Eds., I.M. Bernstein and A.W. Thompson, The Minerals, Metals & Materials Society, Warrendale, PA, 1981, pp. 677-689.

R.P. Wei and M. Gao, in: "Hydrogen Degradation of Ferrous Alloys," Eds., R.A. Oriani, J.P. Hirth and S. Smialowska, Noyes Publications, Park Ridge, NJ, 1985, pp. 579-607.

R.P. Wei and S.R. Novak, Interlaboratory evaluation of K_{ISCC} and da/dt measurement procedures for high-strength steels. *J. Test. Eval.*, **15**, 1987, 38-75.

R.P. Wei and R.P. Gangloff, in: "Fracture Mechanics: Perspectives and Directions, ASTM STP 1020," Eds., R.P. Wei and R.P. Gangloff, ASTM International, West Conshohocken, PA, 1989, pp. 233-264.

Y. Wei and J.W. Hutchinson, Steady state crack growth and work of fracture for solids characterized by strain gradient plasticity. *J. Mech. Phys. Sol.*, **45**, 1997, 1253-1273.

M.G.H. Wells, Advances in steels for aerospace applications. *Key Engr. Matls.*, 1993, **77-78**, 71-80.

E.P. Whelen, in: "Hydrogen Effects in Metals," Eds., I.M. Bernstein and A.W. Thompson, The Minerals, Metals & Materials Society, Warrendale, PA, 1981, pp. 979-986.

D.P. Williams and H.G. Nelson, Embrittlement of 4130 steel by low pressure gaseous hydrogen. *Metall. Trans.*, **1**, 1970, 63-68.

D.P. Williams and H.G. Nelson, Discussion of embrittlement of 4130 steel by low-pressure gaseous hydrogen. *Metall. Trans.*, **1**, 1970a, 2346-2357.

J. Woodtli and R. Kieselbach, Damage due to hydrogen embrittlement and stress corrosion cracking. *Engr. Fail. Anal.*, **7**, 2000, 427-450.

Y. Yamaguchi, H. Nonaka and K. Yamakawa, Effect of H content on threshold stress intensity factor in carbon steel in hydrogen-assisted cracking environments. *Corrosion*, **53**, 1997, 147-155.

K. Yamakawa, S. Yonezawa and S. Yoshizawa, in: "International Congress on Metallic Corrosion," National Research Council, Toronto, Canada, 1984, pp. 254-261.

K. Yamakawa, H. Tsubakino and S. Yoshizawa, in: "Critical Issues in Reducing the Corrosion of Steels," Eds., H. Keidheiser Jr. and S. Haruyama, NACE, Houston, TX, 1986, pp. 348-358.

G.R. Yoder, P.S. Pao and R.A. Bayles, Ripple load cracking in a titanium alloy. *Scripta Metall. Mater.*, **24**, 1990, 2285-2289.

T. Yokobori, J. Watanabe, T. Aoki and T. Iwadate, in: "Fracture Mechanics, 18th Symposium, ASTM STP 945," ASTM International, West Conshohocken, PA, 1988, pp. 843-866.

A.T. Yokobori, Jr., Y. Chinda, T. Nemoto, K. Satoh and T. Yamada, The characteristics of hydrogen diffusion and concentration around a crack tip concerned with hydrogen embrittlement. *Corros. Sci.*, **44**, 2002, 407-424.

K. Yoshino and C.J. McMahon, Jr., Cooperative relation between temper embrittlement and H embrittlement in a high-strength steel. *Metall. Trans.*, **5**, 1974, 363-370.

G.A. Young, Jr. and J.R. Scully, Hydrogen embrittlement of solution treated and aged β-titanium alloys Ti-15%V-3%Cr-3%Al-3%Sn and Ti-15%Mo-3%Nb-3%Al. *Corrosion*, **50**, 1994, 919-933.

G.A. Young, Jr. and J.R. Scully, The effects of test temperature, temper and alloyed copper on the hydrogen-controlled crack growth rate of an Al-Zn-Mg-Cu alloy. *Metall. Mater. Trans.A*, **33A**, 2002, 1167-1181.

L.M. Young, M.R. Eggleston, H.D. Solomon and L.R. Kaisand, Hydrogen-assisted cracking in a precipitation-hardened stainless steel: Effects of heat treatment and displacement rate. *Matls. Sci. Engr.*, **A203**, 1995, 377-387.

L.M. Young, G.A. Young, Jr., J.R. Scully, and R.P. Gangloff, Aqueous environment enhanced crack propagation in high strength beta titanium alloys. *Metall. Mater. Trans., A*, **26A**, 1995, 1257-1271.

L.M. Young, "Microstructural Dependence of Aqueous-Environment Assisted Crack Growth and Hydrogen Uptake in AA7050," PhD Dissertation, University of Virginia, Charlottesville, VA, 1999.

L.M. Young and R.P. Gangloff, in: "Advances in the Metallurgy of Aluminum Alloys," Ed., M. Tiryakioglu, ASM International, Materials Park, OH, 2001, pp. 135-140.

Tong-Yi Zhang and J.E. Hack, The equilibrium concentration of hydrogen atoms ahead of a mixed Mode I-Mode III crack tip in single crystal iron. *Metall. Mater. Trans. A*, **30A**, 1999, 155-159.